UNIVERSITY OF CAPE TOWN

Dissertation submitted in partial fulfilment of the requirements for the degree of
Master of Science in Engineering in Civil Engineering (MSc Eng)
Department of Civil Engineering
University of Cape Town, Private Bag Rondebosch, 7700
South Africa

STUDENT:	**Grant Tarwirei Kucherera,** *Pr Eng, BSc (Eng), MSAICE*
STUDENT NUMBER:	KCHGRA002
SUPERVISOR:	**Prof. Alphose Zingoni,** *Pr Eng, CEng, PhD, FSAAE, FIABSE, FIStructE*
COURSE:	**CIV5000Z:** MASTERS DISSERTATION: CIVIL ENGINEERING

Stability behaviour and dynamic response of cooling towers subjected to wind loading

14 MAY 2016

PLAGIARISM DECLARATION:

I, **Grant Tarwirei Kucherera**, hereby declare that:

i. I am presenting this dissertation in PARTIAL fulfilment of the requirements for my degree.
ii. I know the meaning of plagiarism and declare that all of the work in this dissertation, save for that which is properly acknowledged, is my own;
iii. I have used the Harvard Anglia (Author Date) referencing system as the convention for citation and referencing. Each significant contribution to, and quotation in, this proposal from the work, or works of other people has been attributed and has been cited and referenced;
iv. I have not allowed, and will not allow, anyone to copy my work with the intention of passing it off as their own work;
v. I hereby grant the University of Cape Town free licence to reproduce for the purpose of research either the whole or any portion of the contents in any manner whatsoever of the this dissertation.

Signature: Signed by candidate Date: **14 May 2016**

Signature Removed

Stability behaviour and dynamic response of cooling towers subjected to wind loading

Grant Tarwirei Kucherera, *PrEng, BSc (Eng), MSAICE,*
Address: *No. 22 Sluysken Avenue, Fernglen 6045, Port Elizabeth, South Africa*
Telephone: 041 363 0189, Email: gkucherera@keon.co.za
Date: *25 November 2015*

ABSTRACT:

In this study, a linear eigenvalue buckling parametric analysis is presented for various cooling tower shell geometries. The shells are subjected to increasing wind pressures (speeds) to observe the trends in the critical buckling pressures/speeds at which the shell first buckles and the corresponding buckling modes. The cooling tower's geometry is changed in a systematic manner to obtain the relationship between critical wind speeds associated with the first mode of buckling and the cooling tower's geometry. Geometrical parameter ratios of the cooling tower's dimensions are considered in order to cover a wider spectrum of the cooling tower's geometry. The critical wind speed versus height curve is observed to be similar to the Euler buckling curve. There appears to be a certain optimum throat height to total height ratio of about 0.75 for any cooling tower at which the critical wind speed is maximum. The critical wind speed varies linearly with the cooling tower thickness and non-linearly with all diameter ratios. A linear eigenvalue vibration parametric analysis is presented for various cooling tower shell geometries to observe trends in the free vibration response (natural frequencies and mode shapes). The forced response of the cooling tower to various forcing frequencies of wind gusts is analysed using the mode superposition method. The shells are subjected to increasing wind gust periods of the same speed to obtain the trends in the forced vibration response (response frequencies and modes). The cooling tower's geometry is changed in a systematic manner to obtain the free and forced vibration behaviour. The natural frequencies and their corresponding bandwidths for the first ten different modes reduce with increasing height. They are generally invariant with the height to top diameter ratio, but the bandwidth increases with increasing height to top diameter ratio. The response frequencies and their corresponding bandwidths generally decrease with increasing height as well as the height to top diameter ratios. The response frequency generally decreases with decreasing forcing frequency, but not for all the cooling tower geometries. The findings can be used as a basis for further research and establishment of conceptual design guidelines when considering stability, free and forced vibration cooling tower behaviour.

KEY WORDS: *hyperbolic cooling tower, stability, buckling, modes, critical wind pressure, speed/velocity, free/forced vibration, dynamic response, natural frequency, mode shape*.

TABLE OF CONTENTS

GLOSSARY:

USA: United States of America
m/s: Metres per second
mm: Millimetre
%: Percentage
σ_c: Circumferential stress
σ_m: Meridional stress
3-D: Three dimensional

ASCE:	American society of civil engineers
DOF:	Degrees of freedom
2-D:	Two dimensional
m:	Metre
SRSS:	Square root sum of sums
COV:	Coefficient of variance
CFD:	Computational fluid dynamics
FEM:	Finite element method
RCGA:	Real coded genetic algorithm
BSF:	Buckling safety factor
GDQ:	Generalised differential quadrature method
ESWL:	Equivalent static wind load
CCM:	Consistent coupling method

LIST OF TABLES AND FIGURES:

1 INTRODUCTION

Cooling towers, usually referred to as hyperbolic natural draft towers, are large, thin, reinforced concrete shell structures used for cooling large quantities of water in thermal or atomic power stations and other industrial plants like steel plants and refineries. The cooling operation inside the tower is by air flow through the tower. The rising air flow is produced by the difference in air density that exists between the less dense heated air inside the tower and the more dense cooler ambient air outside.

Owing to the huge amounts of heated water through the power stations, the height and diameter of the cooling tower are generally huge. It is normal practice to have diameters of cooling towers up to 100m and heights of up to 200m. The thickness of the shell is generally very small compared to the principal radii of curvature of the shell. The cooling tower shell is therefore generally very tall, thin, with a large base diameter, and therefore possesses a huge surface area and a very low mass to surface area ratio. A pictorial representation of cooling towers is shown in *Figure 1*.

***Figure 1**: Picture of hyperbolic cooling towers adopted from* (httk://en-wikipedia.org/wiki/Ferrybridge-power stations, n.d.)

It is with no doubt that this type of shell is susceptible to significant dynamic excitation under wind loading. This is sometimes coupled with buckling of the shell under compression due to its own weight and the wind load.

A lot of studies have been done on the static analysis, dynamic analysis and stability behaviour of the cooling tower shell. However, with the advent of powerful computers and software, coupled with the need for more capacity in power generating plants and increases in the size of cooling towers, it has become more important to understand the dynamic response and stability.

In this thesis, a parametric study is performed to interrogate the relationship between the critical wind speeds, buckling modes, natural frequencies, vibration mode shapes and vibration response frequencies of a hyperbolic cooling tower with its geometrical parameters of height, bottom and top edge diameters, throat diameter, thickness and curvature. The various geometrical parameters are represented as parametric ratios in order to cover a wider range of cooling tower geometries. The same relationship is investigated for the cooling tower's forced vibration response due to wind loading. Some interesting trends are observed when the results are plotted against the various geometrical parameters and their ratios.

1.1 HISTORICAL DEVELOPMENT OF COOLING TOWERS

Cooling towers originated out of the development of condensers in the 19th century for use with the steam engine. In the beginning of the 20th century, cooling ponds, where land was available, and cooling towers, where land was scarce, were developed as alternatives. The hyperboloid cooling tower was patented by the Dutch engineers Frederick van Herson and Gerard Kuypers in 1918 and the first hyperboloid cooling towers were completed in 1914 near Heerlen (Lang & Straus, n.d.). An overview of the historical development of the hyperboloid cooling tower is shown in *Figure 2* below.

A number of structural failures and collapses of cooling towers have been recorded, the most notable of these being the collapse of the Ferrybridge cooling towers. On 1 November 1965, three of the eight 114m high cooling towers at the Ferrybridge power plant reportedly collapsed due to vibrations in 136 km/h gale force winds. It was reported that the cooling towers had been designed to withstand high wind speeds, but the design had only considered average wind speeds over one minute and neglected shorter wind gusts (Orosz, 1980). In addition, the grouping of the towers resulted in the funnelling of westerly winds into the towers thereby creating a vortex. Pictures of the collapsed towers are shown in *Figure 3*.

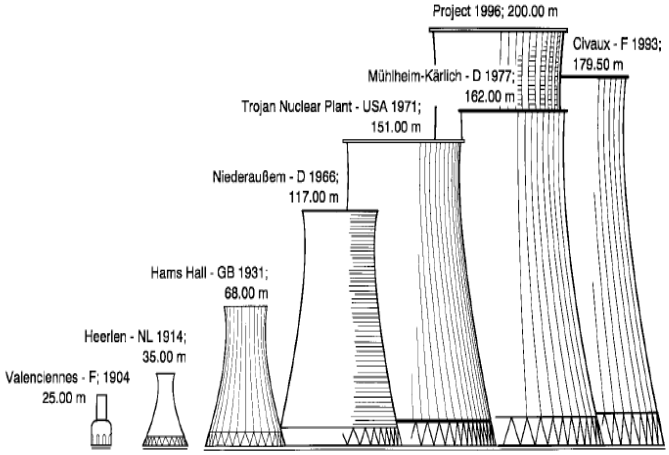

***Figure 2**: An overview of the historical development of the hyperboloid cooling tower* (Lang & Straus, n.d.)

***Figure 3**: Collapse of the Ferrybridge cooling towers in 1965* (Orosz, 1980)

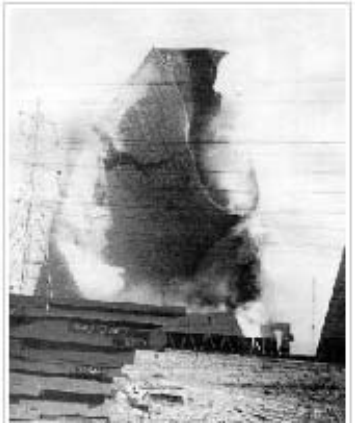

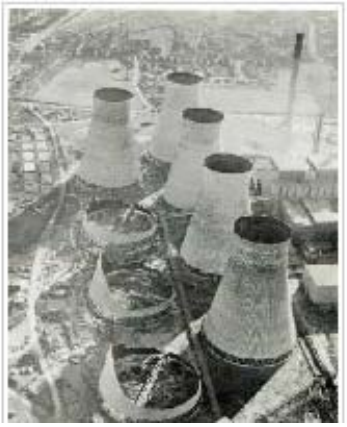

1.2 GEOMETRY AND LOADING OF COOLING TOWERS

Cooling towers are shells that have the shape and geometry of a hollow single-cavity hyperboloid of revolution. The cooling tower internal and external surfaces are generated by rotating through 360° a hyperbola curve about a straight imaginary vertical axis of revolution. It follows that the middle surface is formed by rotating an imaginary hyperbola about the same axis of revolution. The generated surface is termed an *axi-symmetric hyperbolic shell of revolution*.

The *middle surface* of the shell is a locus of all points within the thickness of the shell that are equi-distant from the shell internal and external surfaces. Planes normal to the axis of revolution intersect the middle surface in curves called *latitudes.* Planes that contain the axis intersect the middle surface in curves called *meridians*. The latitude and meridians are lines of principal curvature on the middle surface. Points on the middle surface are referred to by polar coordinates Φ and θ, where

Φ denotes the angle between the axis of revolution and a normal to the shell mid-surface at the point in question and

θ denotes a circumferential coordinate.

The equation of the *meridian* is usually represented as follows:

$$\frac{x^2}{a^2} - \frac{y^2}{b^2} = 1, \text{ where } x \geq a \quad \text{.....[1]}$$

(Prabhakar, 1990) summarised the structural features and practices generally adopted in the structural design of hyperbolic cooling towers in India. He highlighted brief structural design aspects obtained from the British and Indian codes of practices, example cooling towers as well as design practices of that time. Geometric and key structural salient features were described, applied loadings were reviewed and special problems were highlighted.

The salient geometric and key structural features can be described as follows:

- the cooling tower height to base diameter ratios generally ranges from 1.15 to 1.48. The ratio decreases with increasing tower height;
- the ratio of the cooling tower throat height from the top to the overall height generally ranges from 0.15 to 0.30;
- the slope of the shell at the bottom is usually limited to 17° from the vertical for practical construction purposes;
- the cooling tower is normally supported on reinforced concrete raker columns on pedestals which are integral with a peripheral cooling water basin retaining wall. The raker columns and wall are normally aligned to the same meridional plane of the shell to enhance direct force transfer. The pedestals are replaced with raker piles in poor bearing capacity ground conditions. A general arrangement of a cooling tower is shown in *Figure 4*.

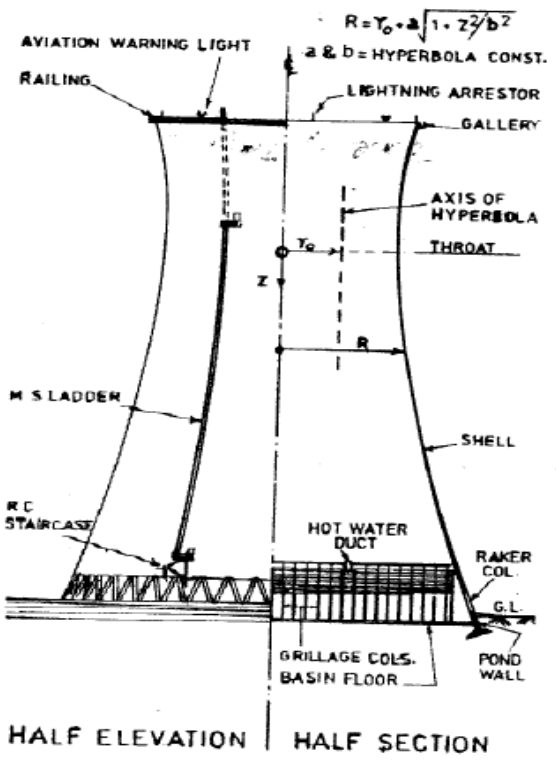

***Figure 4**: General cooling tower arrangement* (Prabhakar, 1990)

The external applied loads applied on a cooling tower can be summarised as follows:

Wind: The vertical wind pressure distribution is area dependent, and is guided by specific code of practices for various countries/regions. The circumferential distribution of wind pressures around the shell can be represented by a Fourier series as shown in the equation below.

$$H = \sum A_n \cos n\theta \quad \text{.....[2]}$$

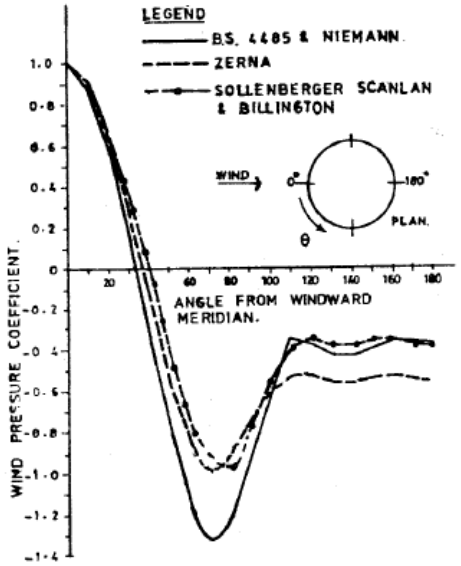

***Figure 5**: Circumferential wind pressure distribution excluding internal suction* (Prabhakar, 1990)

A comparison of the wind pressure distribution by Niemann (British code) and Zerna (Indian Code) is shown in *Figure 5*. The flow of air through the cooling tower creates internal negative pressure (suction) ranging from 0.4 to 0.5kN/m2. The internal suction can result in an increase in the circumferential compressive stress of up to 40% of the wind forces and a corresponding reduction in the circumferential tensile stresses. When cooling towers are grouped, a clear spacing of 0.5 times the base diameter is allowed for between the cooling towers and pressures are increased by 10% to 40% to account for aero-dynamic interference effects. Table 1 shows the wind load factors variation with wind speed obtained by (Prabhakar, 1990).

Earthquake: The earthquake ground motion is generally represented by 3 orthogonal components (two horizontal and one vertical). The natural frequency that corresponds to the lowest mode generally ranges from 2Hz to 3Hz. The response spectrum method allows the designer to consider the maximum response of each mode calculated by the square root of the sum of squares (SRSS) of the values contributing to each mode. A critical damping factor of 5% is normally considered.

Temperature Effects: The temperature gradients (between inside and outside faces of the cooling tower) do not cause excessive tensile stresses in the shell. They can increase the meridional reinforcement in the shell by about 10%. The structural design aspects of a cooling tower can be briefly summarised as follows (Prabhakar, 1990):

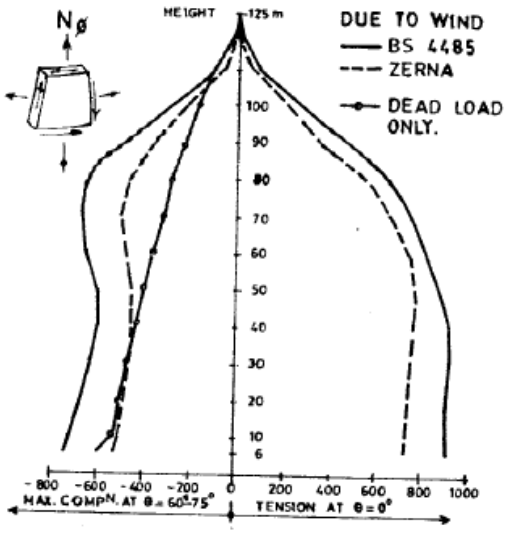

***Figure 6**: Meridional stress resultants adopted from* (Prabhakar, 1990)

Structural Analysis: The membrane analysis of the shell provides a satisfactory design tool for design purposes provided that the top and bottom of the shell are thickened to account for boundary local bending moments. The FEM methods accuracy is dependent on the size of elements adopted. 5m to 10m high elements result in wind load stresses that are less by about 10% to 15% than those of 1.4m high elements. Meridional shell moments are generally of the order of +/- $0.0015pR^2$ where p = wind pressure, R = radius of shell at point of consideration. Circumferential bending moments are generally of the order of +/- $0.005pR^2$. *Figure 6* shows a comparison of the stress resultants for the two cooling tower cases.

Shell Buckling: A factor of safety of buckling of 5 is generally applied. The buckling safety is derived from the Der and Fidler equation (BS: 4485-4). The tensile stress in the concrete is limited to 3MPa.

Geometrical Imperfections: The following permissible tolerances were noted +/- 15mm in a horizontal chord of 3m, +/-10mm rotation for a height of 1m in the meridional plane, -5mm to +10mm for the thickness and +/- 40m radially from the certain line of the shell base.

Shell Reinforcement: The shells are reinforced with two layers of deformed bars in the meridional and circumferential directions with a minimum reinforcement density of 0.3%. The circumferential reinforcement is usually nominal. With a minimum concrete cover of 40mm and two layers of reinforcement, the minimum shell thickness is usually 175mm.

The shell reinforcement is sensitive to wind loads. The wind load factor significantly reduces with an increase in wind speed. A proper assessment of the wind speed is therefore a critical aspect of the design process.

Vibration Effects: The cooling tower natural frequency is inversely proportional to its size and also drops rapidly with increased thickness of the shell. For 160m or more high cooling towers, the natural frequency is normally below 1Hz.

As noted by Prabhakar, there is ample scope for instrumentation of full scale structures in order to establish design confidence. The observations made in Prabhakar's studies can be very useful for a geometric parametric study of hyperbolic cooling towers in which certain parameters of the cooling tower's geometry can be changed to investigate the stability behaviour and dynamic response of the cooling tower.

Wind speed (m/sec)	Wind load Factor
39	1.400
40	1.331
42	1.207
44	1.100
46	1.006

***Table 1**: Wind load factors for various wind speeds* (Prabhakar, 1990)

1.3 COOLING TOWER SHELL MECHANICS

1.3.1 Static analysis of hyperbolic shells of revolution

Shells are generally defined as three dimensional curved structures bounded by two arbitrary curved surfaces whose distance between them is relatively small compared to their radius of curvature. In order to approximately reduce the three-dimensional problem of deformation of the shell body to a two dimensional problem, shell theory attempts to make use of the smallness in the dimension normal to the shell surface. The essence of the theory is that the displacement of any point inside the shell wall is expressed in terms of the displacement components of a corresponding point on the middle surface (Don, *et al*., 1975).

All shell theories available today that include bending are based on the assumption that the strains in the shell are small enough to be discarded in comparison with unity. It is assumed that the shell is thin enough that quantities such as the thickness/radius ratio may be discarded in comparison with unity. Two basic theories on shells are in existence: the linear shell theory and the non-linear shell theory. The linear shell theories can adequately predict stresses and deformations for shells exhibiting small elastic deformations. The non-linear shell theory generally forms the basis for the finite-deflection and stability shell theories. The non-linear shell theory equations are more complex and therefore difficult to solve. This has resulted in the more limited use of the non-linear shell theory.

1.3.2 Membrane theory

Shells of revolution generally find their application in the design of roof domes, pressure vessels and cooling towers. By general inspection of the shape of these structures, it can be observed that their surface is generated by rotating through a complete cycle (360°) a plane curve about a straight line (axis of revolution). The generated surface is called the surface of revolution.

The membrane theory of these shells is based on the Love-Kirchoff assumptions (Zingoni, 1997). These are stated below as follows:

- The shell thickness is negligibly small in comparison with the least radius of curvature of the shell middle surface;
- Strains and displacements that arise within the shell are small;
- Straight lines that are normal to the middle surface prior to deformation remain straight and normal to the middle surface during deformation, and experience no change in the length;
- The direct stress acting in the direction normal to the shell middle surface is negligible.

The membrane theory of shells assumes that a convenient and satisfactory approximation to the actual state of stresses in a shell can be arrived at by assuming that the state of stress in the shell is momentless. That is, the shell has got a negligible bending stiffness and that the bending moments developed will be very small that they can be neglected if the general conditions below are satisfied.

The above is famously referred to as the *membrane hypothesis*. The membrane theory is applicable to shells of revolution when the following conditions are met:

- The shell wall should be thin compared to the smallest principal radius;
- The shell meridian should be smooth with no discontinuities in the middle surface profile;
- The principal ratio of curvature and the shell thickness should be constant, or vary continuously and smoothly with no rapid change and

- The surface-loading components in both the meridional direction and the direction of the normal to the middle surface should vary continuously and smoothly along the meridian.

General equilibrium equations

The general governing equations for shell of revolutions were presented and are repeated below (Zingoni, 1997)

$\frac{N_\Phi}{r_1} + \frac{N_\theta}{r_2} = p_r$ and ……[3]

$N_\Phi = \frac{1}{r_2 sin^2\Phi} \int [\, r_1 r_2 (p_r cos\Phi - p_\Phi sin\Phi) sin\Phi \, d\Phi + k \,]$ ……[4]

where:

N_Φ = direct force per unit length in the meridional direction, see *Figure 7*;
N_θ = direct force per unit length in the hoop direction;
r_1 = principal radius of curvature of the shell mid-surface as seen in the meridional plane;
r_2 = principal radius of curvature of the shell mid-surface given by the distance between the shell mid-surface point in question and the intercept of the normal to the shell mid-surface at that point and the axis of revolution of the shell;
p_r = external loading component per unit area in the direction normal to the shell mid-surface;
p_Φ = external loading component per unit area in the meridional direction;
Φ =the angle measured from the axis of revolution of the shell to the normal to the shell mid-surface at the point in question;
θ = the angle measured in the horizontal plane of a circle of latitude, defining the position of a given meridional plane relative to some reference meridional plane;
k = a constant of integration that can be obtained from an appropriate boundary condition.

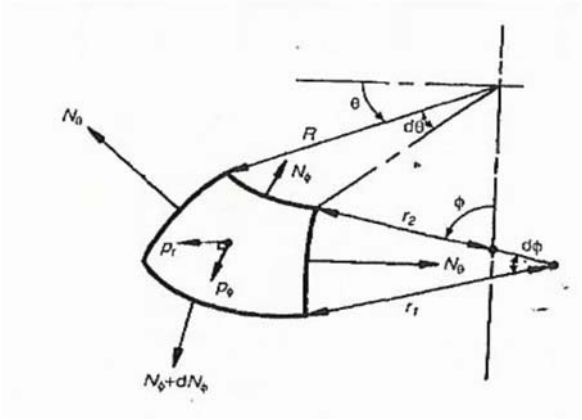

***Figure 7**: Shell properties* (Zingoni, 1997)

The most common shell of revolution is the circular cylindrical shell. This is formed by rotating a straight line through a complete circle (360°) about a central axis of revolution. Many investigations have been devoted to this type of shells of revolution. In addition, a lot of advances were made in the analysis of circular cylindrical as well as spherical shells. These advances were made by Reissner and later generalised to apply to symmetrical deformations of shells of revolution of any arbitrary shape and variable thickness by Meissner (Novozhilov, 1970). Therefore, the analysis of shells of revolution of arbitrary shape and variable thickness has been studied in adequate detail. The complex transformation of equations reducing the order of differential equations of these shell problems has played an important role.

However, the analysis of shells of revolution under un-symmetrical "wind" loading is undoubtedly more complex. The solution for spherical shells under "wind" loading was obtained by Schwerin (Novozhilov, 1970) who transformed the differential equations in the manner the equations for the symmetrical loading had been obtained. Schwerin's solution was in the form of a badly converging hyper-geometric series. Novozhilov then discovered two quadrature and the possibility of a complex transformation in order to reduce the analysis of spherical shells under "wind" loading to the integration of a single second order differential equation. This result was generalized to the work of shells of revolution of arbitrary shape and thickness.

In summary the analysis of shells of revolution under arbitrary loading is done conveniently in the complex form. The corresponding differential equations are transformed in a similar way to those in the membrane theory. Consequently, the analysis reduces to a solution of two fourth order differential equations. The solution of this problem may be reduced to the integration of a single second order differential equation to obtain results for symmetrical deformations; similar results can also be obtained from this problem for the "wind" loading.

1.3.3 Hyperbolic shells of revolution subjected to an axisymmetric load

The general governing equations for cooling towers under axisymmetric loading were presented and are as follows: (Zingoni, 1997)

$$N_\theta = |r_2|\left(p_r + \frac{N_\Phi}{|r_1|}\right) \quad \text{.....[5]}$$

$$N_\Phi = \frac{qb^2}{4a(a^2+b^2)^{\frac{1}{2}}}\frac{(a^2sin^2\Phi - b^2cos^2\Phi)^{\frac{1}{2}}}{sin^2\Phi}\left[\left\{\left(\frac{2a^2(a^2+b^2)^{\frac{1}{2}}cos\Phi_1}{a^2-(a^2+b^2)\,cos^2\Phi_1}\right) + ln\left(\frac{a+\left(a^2+b^2\right)^{\frac{1}{2}}cos\Phi_1}{a-\left(a^2+b^2\right)^{\frac{1}{2}}cos\Phi_1}\right)\right\} - \left\{\left(\frac{2a(a^2+b^2)^{\frac{1}{2}}cos\Phi}{a^2-(a^2+b^2)\,cos^2\Phi}\right) + ln\left(\frac{a+\left(a^2+b^2\right)^{\frac{1}{2}}cos\Phi}{a-\left(a^2+b^2\right)^{\frac{1}{2}}cos\Phi}\right)\right\}\right] \quad \text{.....[6]}$$

where

Φ_1 = the angle measured from the axis of revolution of the shell to the normal to the shell mid-surface at the top of the cooling tower;
q = loading per unit area of the shell mid-surface.

It is worth to note at this juncture that wind loading on a cooling tower cannot be symmetric about the axis of revolution. It is therefore not an axisymmetric load. The deformations arising from the wind loading can therefore not be symmetric. Equations 5 and 6 therefore cannot be applied to wind loading on a cooling tower.

1.3.4 Hyperbolic shells of revolution subjected to a "wind" load

The general solution for shells of revolution subjected to "wind" loading is tabled below. The loading system for general loading, also referred to as "wind" loading is obtained from the formula:

$$q_1 = q_{1,1}\,cos\theta \quad \text{.....[7]}$$

$$q_2 = q_{2,1}\,sin\theta \quad \text{.....[8]}$$

$$q_n = q_{n,1}\,cos\theta \quad \text{.....[9]}$$

where: $q_{1,1}$, $q_{2,1}$, $q_{n,1}$ are functions of θ

The analysis of shells of revolution of arbitrary shape subjected to wind loading can be reduced to the integration of the following second order differential equation (Novozhilov, 1970).

$$\frac{d^2\,\tilde{T}^{(1)}}{d\theta^2} + \left[\left(2\frac{R_1}{R_2} - 1\right)cotan\theta - \frac{1}{R_1}\frac{dR_1}{d\theta}\right]\frac{d\tilde{T}^{(1)}}{d\theta} + \frac{R_1}{R_2}\left(1 - 2\frac{R_1}{R_2}\right)\frac{1}{sin^2\theta}\,\tilde{T}^{(1)} + \frac{i{R_1}^2}{R_2 c}\tilde{T}^{(1)} = \frac{i{R_1}^2}{R_2 c}F_1(\theta)$$

.....[10]

where:

$$F_1(\theta) = R_2 q_{n,1} - \left(\frac{1}{R_1} - \frac{1}{R_2}\right)\frac{1}{R_2 sin^3\theta}\left[C_1 + C_2\int_{\theta^u}^{\theta} R_1 sin\theta\, d\theta + \int_{\theta^u}^{\theta} \Phi R_1 sin\theta\, d\theta\right] \quad \text{.....[11]}$$

1.3.5 Stability behaviour of cooling towers

The cooling tower shell is generally thin-walled. It is very often subjected to compressive stresses due to its own self weight and in some cases due to wind loading. It is therefore important to understand the buckling phenomena of the cooling tower shell.

If the cooling tower shell (or an element of it) is considered to carry a certain compression load, called the basic load, the load will produce basic stresses and basic displacements and deformations. If the same cooling tower shell (or element of it) is disturbed by imposing a small additional displacement or deformation, the additional displacement/deformation is coupled with strains and stresses. It is expected that external forces are required to produce these stresses. If the whole

disturbance and additional displacements/deformations vanishes when the external forces are removed, the shell/element of it is said to be in an elastic equilibrium state under the disturbances.

Should the basic load be gradually increased, less and less external disturbing forces will be required to produce the same disturbance effect and the same displacements and deformations (Flugge, 1973). Finally, certain displacements and deformations become possible without any further application of the external disturbing forces. In this case, the shell/element of it is said to be in a neutral elastic equilibrium state with respect to the disturbance. Any further increase in the basic load will cause instability of the shell/element of it. This phenomenon is called *shell buckling*. The smallest value of the basic load necessary to achieve the neutral elastic equilibrium state of the shell or element of it is termed the *critical* or *buckling load*.

The stability equations for any shell of revolution were presented and are indicated as follows (Don, *et al*., 1975):

$(rN_{\Phi 1})_{,\Phi} + r_{\Phi}N_{\Phi\theta 1,\theta} - r_{\Phi}N_{\theta 1}cos\Phi = 0;$

$(rN_{\Phi 1})_{,\Phi} + r_{\Phi}N_{\theta 1,\theta} + r_{\Phi}N_{\Phi\theta 1}cos\Phi = 0;$

$\left[\frac{1}{r_{\Phi}}(rM_{\Phi 1})_{,\Phi}\right]_{,\Phi} + 2\left(M_{\Phi\theta 1,\Phi\theta} + \frac{r_{\Phi}}{r}M_{\Phi\theta 1,\theta}cos\Phi\right) + \left[\frac{r_{\Phi}}{r}M_{\theta 1,\theta 0} - (M_{\theta 1}cos\Phi)_{,\Phi}\right] - (rN_{\Phi 1} + r_{\Phi}N_{\theta 1}sin\Phi) - [(rN_{\Phi 0}\beta_{\Phi 1} + rN_{\Phi\theta 0}\beta_{\theta 1})_{,\Phi} + (r\beta_{\Phi 0}N_{\Phi 1} + r\beta_{\theta 0}N_{\Phi\theta 1})_{,\Phi} + r_{\Phi}(N_{\Phi 0}\beta_{\Phi 1} + N_{\Phi\theta 0}\beta_{\Phi 1})_{,\theta} + r_{\Phi}(\beta_{\theta 0}N_{\theta 1} + \beta_{\Phi 0}N_{\Phi\theta 1})_{,\theta}] = 0$.....[12]

where the force and moment intensities and the displacement variables are given by the following equations:

$N_{\Phi 1} = C[(e_{\Phi\Phi 1} + \beta_{\Phi 0}\beta_{\Phi 1}) + v(e_{\theta\theta 1} + \beta_{\theta 0}\beta_{\theta 1})]$

$N_{\theta 1} = C[(e_{\theta\theta 1} + \beta_{\theta 0}\beta_{\theta 1}) + v(e_{\Phi\Phi 1} + \beta_{\Phi 0}\beta_{\Phi 1})]$

$N_{\Phi\theta 1} = C\frac{1-v}{2}(e_{\Phi\theta 1} + \beta_{\Phi 0}\beta_{\theta 1} + \beta_{\theta 0}\beta_{\Phi 1})$

$M_{\Phi 1} = D\left[\frac{\beta_{\Phi 1,\Phi}}{r_{\Phi}} + \frac{v}{r}\beta_{\theta 1,\theta} + \beta_{\Phi 1}cos\Phi\right]$

$M_{\theta 1} = D\left[\frac{1}{r}(\beta_{\theta 1,\theta} + \beta_{\Phi 1}cos\Phi) + \frac{v}{r_{\Phi}}(\beta_{\Phi 1,\Phi})\right]$

$M_{\Phi\theta 1} = D\frac{1-v}{2}\left[\frac{r}{r_{\Phi}}\left(\frac{\beta_{\theta 1}}{r}\right)_{,\Phi} + \frac{\beta_{\Phi 1}}{r}\right]$

$e_{\Phi\Phi 1} = \frac{1}{r_{\Phi}}(u_{1,\Phi} + w_1)$

$e_{\theta\theta 1} = \frac{r}{r_{\Phi}}\left(\frac{v_1}{r}\right)_{,\Phi} + \frac{U_{1,\theta}}{r}$

$e_{\Phi\theta 1} = \frac{1}{r}(v_{1,\theta} + u_1cos\Phi + w_1sin\Phi)$

$\beta_{\Phi 1} = -\frac{w_{1,\Phi}}{r_{\Phi}}$

$\beta_{\theta 1} = -\frac{w_{1,\theta}}{r}$ .....[13]

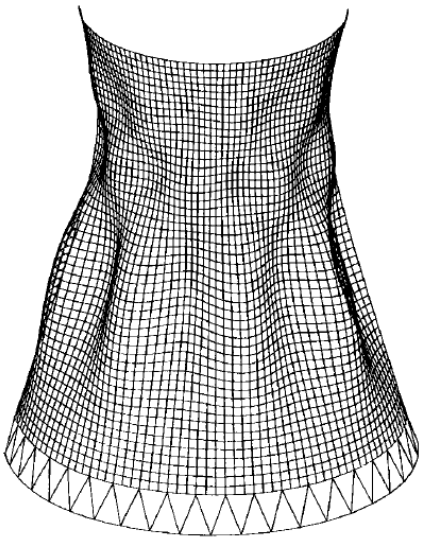

***Figure 8**: Buckling of the hyperbolic shell under wind loading* **(Gould & Kratzig, 1999)**

An example of one of the buckling modes of the hyperbolic shell is shown in *Figure 8* above.

1.3.6 Dynamic analysis of hyperbolic shells of revolution

In the dynamic analysis of structures, the distinction is made between the dynamic and the static analysis on the basis of whether the applied action has enough acceleration in comparison to the structure's natural frequency. For a load that is applied sufficiently slowly, the inertia forces (Newton's second law of motion) can be ignored and the analysis can be simplified as a static analysis or a quasi-static analysis. Therefore, structural dynamics is a section of structural analysis which covers the behaviour of structures subjected to dynamic loading (actions having high accelerations). In addition, the dynamic analysis is also related to inertia forces developed by a structure when it is excited by means of dynamic loads applied suddenly (e.g., wind blasts, explosions and earthquakes). Dynamic analysis for simple structures can generally be carried out manually.

Displacements: The effects of a dynamic load can be significantly larger than those of a static load of the same magnitude due to the structure's inability to respond quickly to the loading. The increase in the effect of a dynamic load is measured by the dynamic amplification factor (DAF):

$$DAF = \frac{U_{max}}{U_{static}} \text{.....[14]}$$

where u is the structure's deflection caused by the applied load. A time history analysis shows graphs of the DAF versus the non-dimensional rise in time for standard loading functions.

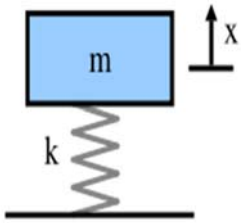

Figure 9: *Single DOF mass-stiffness system*

Time history analysis: A time history gives the response of a structure over a time period during and after the application of the load. The time history of a structure's response is obtained by solving the structure's equation(s) of motion. The equation of motion of a simple single degree of freedom system (SDOF) is shown in the equation below.

$$M\ddot{x} + kx = F(t)$$

.....[15]

where $\ddot{x}$ is the acceleration and x is the displacement of the system, M and k are the system mass and stiffness respectively whilst $F(t)$ is the applied force as a function of time. For a suddenly applied load, the above equation of motion is solved as

$$x = \frac{F_0}{k}[1 - \cos(\omega t)], \text{ where } \omega = \sqrt{\frac{k}{M}} \text{ .....[16]}$$

The static deflection of a single degree of freedom system is

$$x_{static} = \frac{F_0}{k} \text{ which follows that } x = x_{static}\,[1 - \cos(\omega t)] \text{.....[17]}$$

This is a theoretical time history of the SDOF system falsely assuming that damping does not affect the system. This is a simplistic approach. In reality, loads are never normally applied instantaneously as assumed above. In addition, the assumed SDOF system is theoretical and most structures display various modes of vibration and therefore have multiple degrees of freedom (MDOF systems). As the number of degrees of freedom increases, it becomes rapidly increasingly difficult to solve the equation(s) of motion and the time history manually. Non-liner finite element analysis software becomes the primary method of solution in this situation.

Modal Analysis: In order to find the natural frequencies of a structural dynamic system, a modal analysis is performed. The natural frequency of the system depends only on the stiffness of the structure and the mass (including self-weight) which participates with the structure. It does not depend on the load function. The modal frequencies are an important property of any dynamic system. It allows the engineer to ensure that the frequency of any applied periodic loading will not coincide with a modal frequency in order to avoid causing resonance (large oscillations and displacements).

Energy method: Rayleigh's principle states that "the frequency ω of an arbitrary mode of vibration as calculated by the energy method is always greater than or equal to the fundamental frequency, ω_n." The energy method allows for the calculation of the frequency of different mode shape of a system manually. An "equivalent" single degree of freedom mass, stiffness or applied force can be obtained by the energy method for a multiple degree of freedom system.

Equivalent mass: $M_{eq} = \int M\bar{u}^2 du$ .....[18]

Equivalent stiffness: $k_{eq} = \int EI \left(\frac{d^2\bar{u}}{dx^2}\right)^2 dx$ .....[19]

Equivalent force: $F_{eq} = \int F\bar{u}dx$ .....[20]

from which $\omega = \sqrt{\frac{k_{eq}}{M_{eq}}}$ .....[21]

The vibration response of shells is considerably more complex than that of beams and plates. The complexity is primarily due to the effects of the curvature on the shell equations and on the dynamic behaviour. For beams and plates, the flexural and extensional vibrations are considered separately, and are only combined when it is necessary to combine them for complex problems. On the other hand, shell membrane deformations are coupled with flexural deformations. Hence, any shell vibration theory must consider both the membrane and flexural effects simultaneously (Warburton, 1976).

The dynamic response of a shell element is derived using Hamilton's Variational Principle which states that the actual path taken by a dynamic system is such that

$$\int_{t_0}^{t_1} (\prod - K_E)dt = 0 \text{ .....[22]}$$

where

$\prod$ = the total potential energy of the system, and

K_E = the kinetic energy of the system.

The potential energy of the shell element that can be projected onto a Cartesian base is represented as follows

$$\prod = \int\int_{A_e}\int_{-h/2}^{h/2}\{\varepsilon\}^T[\boldsymbol{D}]\{\varepsilon\}dt\,dx\,dy \quad \text{.....[23]}$$

where

h = thickness of shell

$[\boldsymbol{D}]$ = matrix of shell material constants

$\{\varepsilon\} = \begin{bmatrix}\varepsilon_x \\ \varepsilon_y \\ \varepsilon_{xy}\end{bmatrix}$ = matrix of strain-displacement relationships

x, y = Cartesian coordinated in the base plane

t = thickness coordinate normal to the middle surface

The strain-displacement relationships of the shell element are represented as follows

$$\varepsilon_x = \frac{\partial u}{\partial x} - k_{xx}\omega - t\frac{\partial^2\omega}{\partial x^2} \quad \text{..... [24]}$$

$$\varepsilon_y = \frac{\partial v}{\partial x} - k_{yy}\omega - t\frac{\partial^2\omega}{\partial y^2} \quad \text{..... [25]}$$

$$\gamma_{xy} = \frac{\partial u}{\partial y} + \frac{\partial v}{\partial x} - 2k_{xy}\omega - 2t\frac{\partial^2\omega}{\partial x\partial y} \quad \text{..... [26]}$$

where

k_{xx}, k_{yy} and k_{xy} are curvatures and twists of the middle surface;

ω = displacement normal to the middle surface and

u, v = tangential displacements of a point on the middle surface.

The kinetic energy of the shell element is represented as follows

$$K_E = \iint_{A_e}\rho h(\dot{u}^2 + \dot{v}^2 + \dot{w}^2)dx\,dy \quad \text{..... [27]}$$

where ρ = material density

$\dot{u}$, $\dot{v}$ and $\dot{\omega}$ = displacement derivatives with respect to the Cartesian coordinates.

1.3.7 Wind loading and effects on cooling towers

There is a fundamental difference between the wind pressure distribution on round structures such as cooling towers and sharp-edged buildings. The wind pressure distribution in sharp-edged structure is influenced by gusts and air-flow direction variation. The flow always separates at the corner of the structure. In contrast, the separation point and the whole pressure distribution on a cooling tower (or any round structure) will sway to and fro with the variation of the air flow direction. This is the reason why strong pressure fluctuations have a dynamic action on cooling towers. The above phenomenon is illustrated in *Figure 10* and *Figure 11* below.

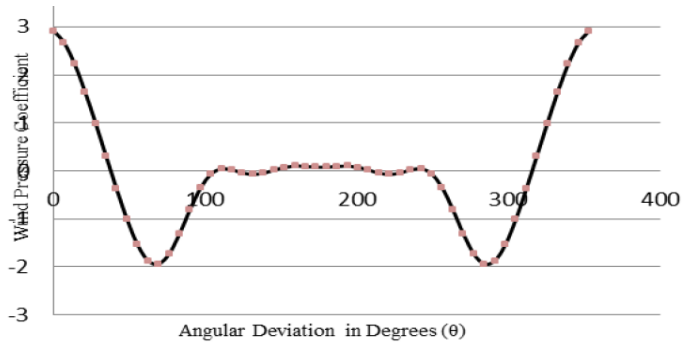

Figure 11: *Wind pressure variations with shell geometry* (Gaikwad, *et al*., 2014)

The above phenomenon was confirmed by Ebner during his wind pressure measurements on a cooling tower as well as during wind tunnel tests on model cooling towers (University of Toronto, 1967).

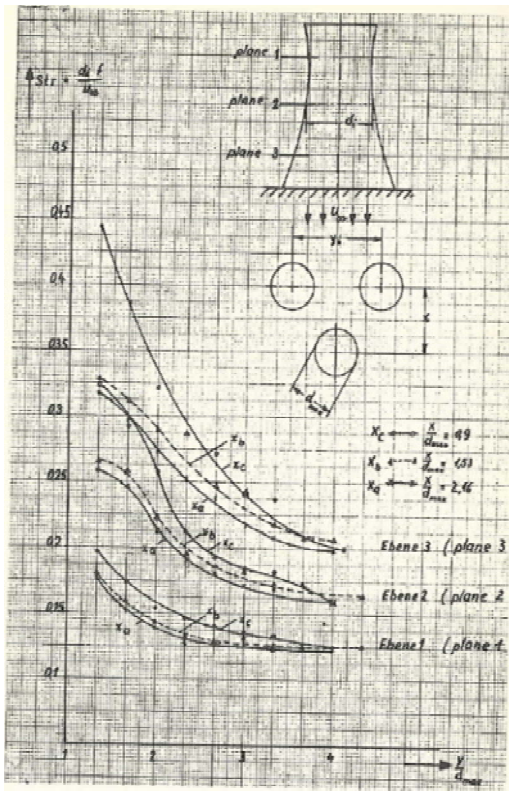

Figure 10: *Wind pressure measurements around the cooling tower and pressure variations with shell geometry* (University of Toronto, 1967)

2 LITERATURE REVIEW

2.1 A SUMMARY OF LITERATURE SURVEYS UP TO THE YEAR 2014

In their paper, (Bamu & Zingoni, 2005) summarised the research developments on concrete hyperbolic cooling tower damage, deterioration and long-term structural performance. A trace of the developments in the research on concrete hyperbolic cooling tower shells with particular attention to the issues of concrete deterioration, durability, long-term performance, condition surveys and strengthening, collapse and the lack of proper collapse documentation was performed. They confirmed research by others for the period from 1961 to 2005.

Their survey revealed that steady wind only had been considered in an exact calculation method for membrane stresses arising from the hyperbolic cooling tower self-weight and wind loading by Martin and Seriven (1961). The finite difference method and model testing was used as a calculation method for the natural frequencies of the hyperbolic cooling tower by Gardner (1969). This method was also used to calculate turbulent wind peak deformations. Quasi-steady and resonant stress predictions were to be calculated based on a model test based procedure developed by Hashish and Abu-Sitta (1974). The dynamic and stability problem for the wind-loaded hyperbolic cooling tower was investigated by Cole et al (1975). The site experiments done by Sollenberger et al (1980) to measure wind pressures on the hyperbolic cooling tower had concluded that the values used in the design generally are higher than the actual measurements. During the same year, experimental tests done by Niemann and Ruhwedel (1980) had confirmed that dynamic stresses are not always correctly assessed by assuming a static design wind.

In addition, the literature survey by Bamu and Zingoni recorded the various research done on the historical collapses of hyperbolic cooling towers and the lessons learnt from these collapses. The 1965 Ferrybridge Power station failure had been recorded by Pope (1994) who concluded that the cooling towers had collapsed due to tension failure of the meridional reinforcement after a gross underestimation of the wind loading coupled with a limited knowledge of the adverse effects of turbulence and cooling tower group effects. The 1973 Adeer Nylon Works power plant failure was noted to be due to meridional curvature imperfections which led to high circumferential stresses causing yielding of horizontal steel, cracking and collapse. The 1979 Bouchain failure was noted to be due to serious construction dimensional and progressive deterioration whilst the 1984 Fiddlers Ferry power station failure had been due to an axisymmetric external bulge imperfection built into the shell just above the lower ring.

On the other hand, the literature survey by Bamu and Zingoni (2005) highlights that a record number of hyperbolic cooling towers had been demolished due to progressive deterioration and high risk of collapse. Structural surveys of existing concrete hyperbolic cooling towers had been performed in the United Kingdom and in South Africa. In South Africa, only 2 cooling towers at Kelvin Power Station had considerable vertical cracking and were to be strengthened by 1986 with cast-in-situ concrete stiffening rings. A similar exercise was to be performed at two of the Athlone Power Station cooling towers in 1993.

Investigations and research into the damage and deterioration phenomena of concrete hyperbolic cooling towers as summarised by Bamu and Zingoni (2005) recorded that studies by Soare (1967) of a concrete cooling tower under construction in Romania showed that small constructional changes in the radius of the latitude circles of the shell of revolution could cause significant changes in the meridional radius of curvature and in-turn cause large changes in hoop stresses. They further recorded that Kemp and Croll (1976) had analysed a cooling tower shell similar to the Adeer Nylon power station cooling tower that had collapsed and demonstrated that moderate imperfections induced hoop stresses in the area of the imperfection. The induced hoop stresses were of the same order of magnitude as the meridional stresses. Their research was credited for leading to the development of a rational set of guidelines on construction tolerances in the United Kingdom.

By studying a number of damaged cooling towers, Aflak et al (1991) were to conclude that the development of modal deformations, accompanied by cracking, is the most dominant phenomena that characterises concrete deterioration of hyperbolic cooling tower shells. A non-linear model that represented wind loading stochastically, was capable of accounting for gradual deterioration as well as loss of stiffness and changes in the dynamic behaviour was proposed by Zahlten and Borri (1998). Jurkiewiez et al (1999) developed a numerical scheme based on the theory of linear viscoelasticity to prove that the distributions of both stresses and displacements can vary considerably over 30 years. The need for models that account for the gradual variation of imperfections with time for use on long term programme assessment of the hyperbolic cooling tower shell was recorded by Bamu and Zingoni (2005). They concluded that durability and long term performance criteria should be incorporated in the design of the cooling towers in order to limit progression of structural deterioration.

A comprehensive review of studies done on modelling analysis, design, theoretical and practical investigations on cooling towers between 2005 and 2014 was performed by (Asadzadeh & Alam, 2014). They recorded that the world's tallest cooling tower had been built in 2002 at Niederaussen power station in Germany at a height of 200m. This had now been replaced in 2012 by the construction of two cooling towers at the Kalisindh thermal energy plant in Rajasthan (India) which were built to a height of 202 meters. A picture of the two towers under construction is shown in *Figure 12*.

Their survey concluded that a huge amount of research had gone into investigating the geometry and shape optimisation of the cooling tower. This development had started as early as in 1967 when the first cooling tower shell was analysed using the shell bending theory (Krivoshapko, 2002). The Finite Element Method (FEM) had begun to be used as a tool for analysis of the hyperbolic cooling tower shell in the 1970's (Asadzadeh and Alam, 2014). Followed by this was an era of research into numerical solutions of symmetrical and asymmetrical problems of the hyperbolic shell. According to Asadzadeh and Alam (2014), the latest research done from 2005 to 2014 is mostly related to the FEM and analysis of the hyperbolic cooling tower considering material nonlinearity and formation of cracks, large displacements and the use of multilevel elements in the FEM methods. The comprehensive investigations into the non-linearity and ultimate load capacity of the hyperbolic cooling tower were summarised by Asadzadeh and Alam.

***Figure 12**: Construction of the Kalisindh cooling towers in Rajasthan (India) adopted from* (Asadzadeh & Alam, 2014)

The research into this area started four decades ago with tensile cracking in the concrete being employed in the finite element analysis of the RC structures. The main objective of studies in this area had been to determine the ultimate strength of the cooling towers in the non-linear static analysis when subjected to the quasi-static severe wind loads. The sources of non-linearity that had been considered up to this time were noted to be material non-linearity in concrete and reinforcement, tensile cracking, effects of bond between concrete and reinforcement in cracked concrete (tension stiffening) and large displacement effects (Asadzadeh & Alam, 2014).

The FEM had been extensively used to perform comprehensive numerical investigations of the RC hyperbolic cooling tower ultimate load capacity considering the above mentioned non-linearities. The ultimate load factors obtained by non-linear analysis was reported to be considerably lower than that obtained by the buckling analysis (Asadzadeh & Alam, 2014). They reported the load factors obtained in various studies as **2.1** (Milford and Schnobrich, 1984), **1.73** (Mahmoud and Gupta, 1995) and **2.34** (Noh, 2006) after repeating the same work. This research has led to the successful use of FEM analysis for the designing process. According to Harte and Wittek (2009), two different concepts have subsequently been developed for designing purposes. These are basically a general cross-section design procedure in accordance with EC2 and an ultimate load design procedure in accordance with German standard DIN 1045-1.

Asadzadeh and Alam (2014) summarised research done on the response of the hyperbolic cooling tower to earthquake and wind forces. They also summarised research done on the effect of stiffening rings, interference effects of cooling tower groups exposed to wind loading and the soil structure interaction of cooling towers. Their survey tracked the latest theoretical and experimental research improvements in the analysis and design of the natural draft hyperbolic cooling towers.

Amongst other findings recorded in their research paper, (Asadzadeh & Alam, 2014) recorded that the overall buckling of the hyperbolic cooling tower shell may be caused by a combination of its self-weight and wind load. This normally takes place with large displacements. They noted that there are different approaches to the buckling theory that has led to a considerable difference between design codes. The **snap-through** approach by Der and Fidler (1968) is used in the British, Indian and German codes whilst the **local or buckling stress states** approach by Mungan (1976) is used in the German code. The **global buckling** approach requires a full non-linear buckling analysis of the hyperbolic cooling tower shell and is used in the USA code as recorded by Bamu and Zingoni (2005). In addition, the literature survey recorded that under seismic excitation, stiffening rings on a hyperbolic cooling tower may not help to increase the resistance of the structure because they have no effect on the model characteristics of the cooling tower under such excitations as had been recorded by Bhimaraddi *et al* (1991). However, it had been concluded that the stiffening rings help to increase the load-carrying capacity of the hyperbolic cooling tower under wind excitations. Furthermore, it was recorded that the total hyperbolic cooling tower structural response to seismic loading depends on the supporting column systems. The response of the tower when supported by I-column supports and V-column supports was found to be different from the response of the tower when supported by conventional pin-supports as concluded by Hara (2002). Afterwards, Asadzadeh *et al* (2012) observed that the I-column supports create more flexibility at the tower base than the V-column support. They also found out that the hyperbolic cooling tower structure can be optimized by finding the optimum inclination angle of the supporting columns.

Parallel studies investigated the effect of stiffening rings on the dynamic properties of the hyperbolic cooling tower. (Asadzadeh & Alam, 2014) summarised the findings of these investigations. The stiffening rings effect was noted to be related to its location for any specific mode of vibration, and the eigen-frequency of that mode will be increased mostly

if the stiffing ring is located at the point of maximum displacement for that specific mode of vibration. It was shown by Form (1986) that by adding 2, 3 or 4 stiffening rings to the hyperbolic cooling tower, the buckling safety factor of the shell increases by **1.65**, **2.32** and **2.80** respectively.

After Bhimaradi's (1991) investigations on whether stiffening rings affect the earthquake resistance of the hyperbolic cooling tower, Sabouri-Ghomi *et al* (2006) did investigations on the stability of the hyperbolic cooling tower supported by X-shaped columns. They considered the number, dimensions and location of the stiffening rings and concluded that adding stiffening rings increases the buckling stability of the hyperbolic cooling tower. They discovered that the stiffening rings behaved either flexibly or rigidly. As such, they found that there was a higher number of flexible stiffening rings required to maximise the buckling safety factor than the number of rigid stiffening rings required to do the same. Similar investigations were performed by Zhang *et al* (2014). They concluded that the stiffness in the latitude direction of the hyperbolic cooling tower contributes more to the structure than the stiffness in the meridional direction. They also concluded that the point of maximum modal displacement of an unstiffened hyperbolic cooling tower will not always be the most effective place for a stiffening ring unless the mode shapes of the unstiffened and stiffened hyperbolic cooling tower are similar.

The paper by (Asadzadeh & Alam, 2014) presented a complete collection of theoretical, numerical and experimental studies done on the hyperbolic cooling tower after 2005. It provides design engineers and researchers with updated literature material for use in the design and maintenance of cooling towers.

2.2 STATIC AND QUASI-STATIC BEHAVIOUR

2.2.1 Theoretical studies

About three decades ago, studies on thermal loading and effects on cooling towers had already started. Particular emphasis of the stress states due to thermal loading is required at the base of the hyperbolic cooling tower where the solar heating generates non-linear thermal variation across the wall thickness in the region close to the base of the hyperbolic cooling tower. (Blocki, 1988) recorded that very little research had been done in full scale measurements of the temperature field or numerical solutions for thermal stresses in hyperbolic cooling towers. He conducted experimental measurements of the temperature field on a hyperbolic cooling tower. Thereafter, numerical calculations of the magnitudes of thermal stresses were performed to investigate aspects of the thermal stresses in the hyperbolic cooling tower. Finally, he investigated whether the circumferential variation of the temperature field observed on a hyperbolic cooling tower in the experimental measurements has an influence on the stress field.

The study concluded that the thermal stresses generated by the variation of the average temperature are small and can be neglected. In addition, the circumferential variation of the thermal difference was found to be smooth enough to generate bending moments which depend only on the value of the thermal difference. The thermal distribution across the wall thickness in the region close to the base of the hyperbolic cooling tower for the sun thermal load is non-linear. The total stress state consists of two parts: the stress defined by the means of shell theory and the self-equilibrated stress state. Finally, the study concluded that the overall uniform cooling leads to appreciable stresses only in the region close to the base of the hyperbolic cooling tower shell. These results proved to be useful in structural design calculations when considering stress states due to thermal loading of hyperbolic cooling towers.

Exactly four years later, studies on geometric imperfections were to be re-visited. (Alexandridis & Gardner, 1992) observed that the tolerance limits for geometric imperfections in hyperbolic cooling towers proposed by Croll and Kemp (1979), and by Dabbagh and Gupta (1979), had assumed the cooling tower shell to behave isotropically upto the instant that local failure occurs. In assuming a failure mechanism, neither of the two studies' approaches had accounted for the presence of meridional cracks in the region of the particular geometrical imperfection under consideration. In contrast, hyperbolic cooling tower shells may undergo meridional cracking which lowers the membrane stiffness in the circumferential directions. This renders the shell *orthotropic*. To solve this dilemma, (Alexandridis & Gardner, 1992) performed a theoretical derivation of tolerable imperfections at any point in a hyperbolic cooling tower shell. In their study, they derived the following proposed equations to calculate the tolerable imperfection at any point in a hyperbolic cooling tower shell.

$$\xi_{max} = \frac{p_\theta t L^2 f_y}{N_\Phi^P R \Gamma}, \qquad \xi_{max} = \frac{0.4\eta t}{\beta}, \qquad \xi_{max} = \frac{4}{3}\frac{p_\theta t L^2 f_y}{N_\Phi^P R \Gamma} \qquad \xi_{max} = \frac{2}{5}\frac{0.4\eta t}{\beta} \quad \text{..... [28]}$$

The proposed calculation method includes the effects due to vertical cracking and circumferential yield. The derived tolerance limits relate the size of the imperfection to the reinforcement provided as well as the stress that exists in the orthotropic shell due to vertical cracking with and without the yield of the hoop reinforcement. The tolerance limits obtained are shown in *Figure 14* and *Figure 13*. These proposed tolerance limits are useful to both the design and construction engineer.

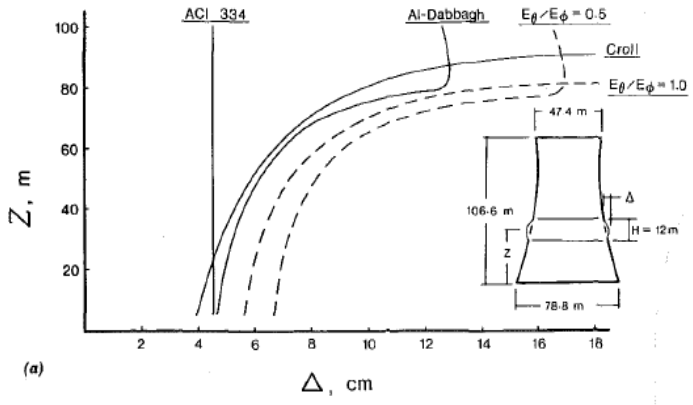

***Figure 14**: Maximum tolerable radial deviation at various levels of cooling tower shell* (Alexandridis & Gardner, 1992))

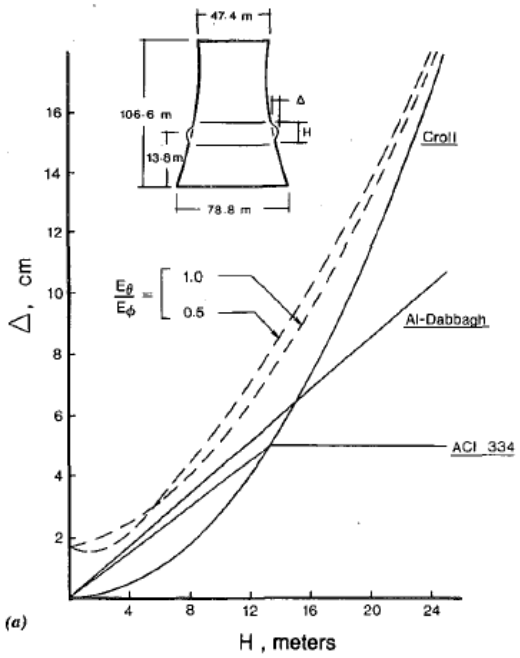

***Figure 13**: Maximum imperfection tolerable radial deviation near base of cooling tower adopted from* (Alexandridis & Gardner, 1992)

Another four years later, the coincidence of wind and thermal loads acting at the same time with dead loads were to be investigated. The fundamental loads in hyperbolic cooling tower static analysis dead loads (g), wind loads (w) and thermal loads (t) are considered to act in three combinations: *g+w*, *g+t* and *g+w+t*. In the first two combinations, the extreme values of g, w and t are considered. However, in the case of the combination g+w+t, the coefficients of coincidence of these loads should be applied because the loads never act simultaneously at their extreme values. (Bosak & Flaga, 1996) investigated the coefficients of the load coincidence by analysing static calculations of the hyperbolic cooling tower loads in their different pairs or combinations.

They summarised results from a numerical calculation on a hyperbolic cooling tower based on a finite element and finite difference computer displacement based programme. Thereafter, they created probability density distributions for wind velocity and air temperature in winter for the Polish climate. From these results, coefficients of coincidence for the load combinations at the level of the characteristic loads were determined.

For the Polish climate, (Bosak & Flaga, 1996) used the probability density distributions to create wind velocity and temperature measurement results of different probability levels (p) of exceeding the load combinations (V_{max}, T) or (T_{min}, V). The probability levels (p) were set at a = 0.05, b = 0.01, c = 0.005, d = 0.0025, e = 0.001, f = 0.0005.

On analysing all the various combinations, they found out that the dead and wind load combination is a representative combination of characteristic loads for establishing maximum and minimum values in the case of the meridional force. When all combinations were analysed, small differences in the values of the meridional force for the combinations *g+w* and *g+t* loads indicated the negligibly small participation of the thermal load. The maximum and minimum circumferential force was connected with the *g+w+t* load combination. The maximum meridional force occurs in the *g+w* load combination where the dead load is determined with a combination factor of 0.9 (under-loading). The minimum meridional force occurs in the *g+w* load combination where the dead load is determined with a 1.1 combination factor. The thermal load significantly influences the bending moments increase in the hyperbolic cooling tower shell. This can have a decisive influence in the distribution of the reinforcement in the shell.

By the turn of the 21st century, complete iterative computational algorithms had been developed by Min (1999) and Cho and Min (2000) to design a plate and shell element subjected to combined membrane forces and bending moments. The algorithm was based on Gupta's (1986) derivation of equations. The equations had been derived for only the case of reinforcement required in the top and bottom layers simultaneously. There was a need for three more cases for reinforcement in the bottom layer only, top layer only and for no reinforcement required at all. (Jang & Min, 2001) developed an iterative numerical computational algorithm to check the design strength of the Grand Gulf Nuclear Power station (Mississippi) hyperbolic cooling tower.

According to (Jang & Min, 2001), the Grand Gulf power station hyperbolic cooling tower constructed in 1977 (shown in

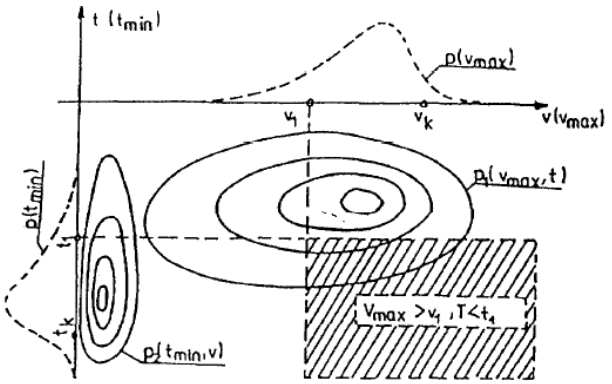

***Figure 15**: Probability density distribution of wind speed and temperature in winter* (Bosak & Flaga, 1996)

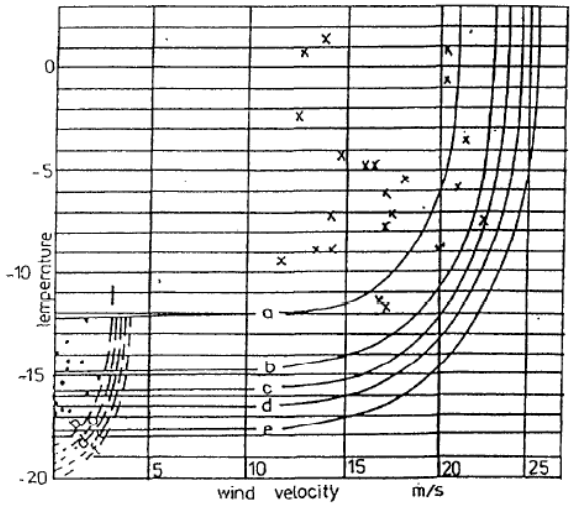

***Figure 16**: Different probability levels p of exceeding the load combination (V_{max}, T) or (T_{min}, V)* (Bosak & Flaga, 1996)

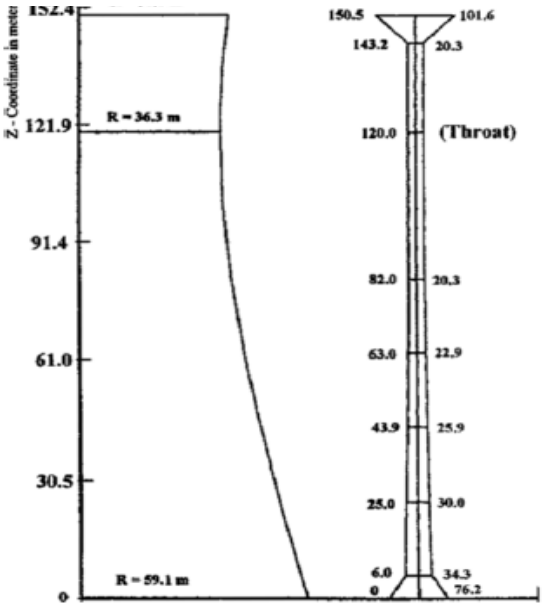

***Figure 17**: Grand Gulf cooling tower geometry and wall profile* (Jang & Min, 2001)

Figure 17), had been studied by many researches including (Mang, *et al.*, 1983), Milford and Schnobrich (1984, 1986), Gupta and Maestrini (1986), (Min & Gupta, 1993), (Mahmoud & Gupta, 1995) and (Choi & Noh, 2000). The results of the studies had been compared by (Mahmoud & Gupta, 1995) who found considerable variations in the results. The variations were attributed to differences in the crack model, mesh sizes, type of finite element, tension stiffening effect and geometric non-linearities used on the various studies.

The analytically calculated load exceeded the design ultimate load from 26% to 63% for an analysis with tension stiffening. The design reinforcement obtained from this was considerably lower than the Grand Gulf tower reinforcement. Although the ultimate loads are dependent on the tensile properties of the concrete, the calculated ultimate loads were higher than the design ultimate load for the study by Jang and Min (2001). Therefore, their design algorithm gave a lower bound solution. Their design algorithm for combined membrane and bending forces on a hyperbolic cooling tower can be evolved into a general design algorithm for reinforced concrete plates and shells by further studies using different shell configurations and environmental conditions. The reinforcement results and comparison obtained from this study is shown in *Table 2*.

	Design methods	Total amount of reinforcement capacity required (unit=MN/m)			
		Circumferential dir.		Meridional dir.	
		Outer layer	Inner layer	Outer layer	Inner layer
Zurn Ind. design (1977)	• Elastic finite element analysis • Use Nx, Ny and Nxy only • Limit state design method	4.07		6.35	
Present study	• Elastic finite element analysis • Use membrane-flexural forces • Design algorithm developed	1.21 (30%)*	1.38 (34%)	4.35 (69%)	3.86 (61%)

*Percentage of the layer compared to the capacity of Zurn's original design

Table 2: Comparison of total reinforcement required for original cooling tower versus that for the study (Jang & Min, 2001)

Research and studies into ring elements had started as early as in the 1960's. Popov *et al* (1964) had proposed simple conical ring elements with a constant wall thickness. Over the years, several researches had extended the idea of ring elements into arbitrary wall thickness and arbitrary curvature of the element's shape in the meridional direction. In their paper, (Lang, *et al*., 2002) proposed to extend the ring element that had been proposed by Eckstein *et al* (1980) to take into account general non-linear material response in the circumferential direction of a shell of revolution of arbitrary shape exposed to arbitrary distributed loads. In their study, (Lang, *et al*., 2002) modelled two shells of revolution (a cylindrical shell and a hyperbolic cooling tower shell) with ring elements. Their study started with a systematic derivation of element matrices for the non-linear ring element. The proposed concept was then transferred to the formulation of an arbitrary ring element on any shell of revolution. The validity of the proposed ring element was then demonstrated using an example that illustrated the stress re-distribution due to cracking in a hyperbolic cooling tower under wind loading.

Their matrix derivation results of the ring element of a shell of revolution were compared to the Boxberg hyperbolic cooling tower in Germany. They modelled the shell with ring elements and material and reinforcement data shown in *Figure 18* and *Figure 20*. They observed that the results of the ring element model at the axis of symmetry could be validated with the approximate calculations from the derived equations. In addition to this, they concluded that the ring elements have several advantages when compared to commonly used shell elements. That is:

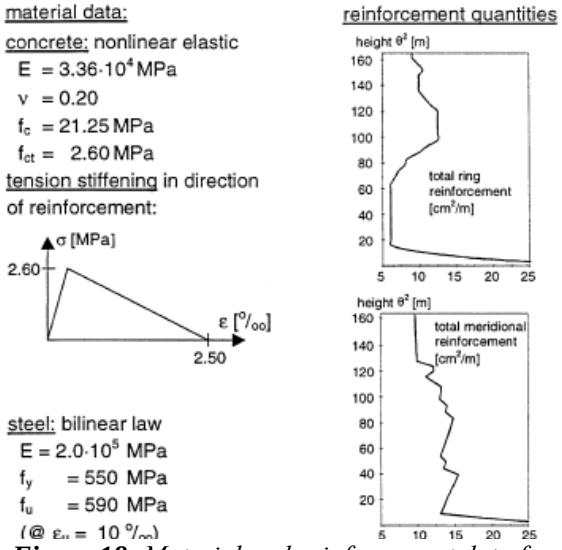

***Figure 18**: Material and reinforcement data for the Boxberg cooling tower* (Lang, *et al.*, 2002)

- There is no requirement to discretize the elements in the circumferential direction;
- The accuracy of the results in the circumferential direction is dependent on the adopted Fourier series terms;
- The displacement field can be continuously differentiated in the circumferential direction without any requirement to reduce the order of the trial functions, hence a better strain and stress approximation;
- The computation effort required is substantially reduced due to the smaller number of global degrees of freedom.

On the other hand, they observed that the ring elements have a major disadvantage when applied to shells of revolutions with cut-outs. Such shells cannot be modelled using this approach.

They concluded that their proposed algorithm was attractive due to the super-diagonal nature of the derived mass matrix which dominates the stiffness matrix for small time steps. Hence the proposed ring element could be used for the seismic response analysis of shells of revolution and more certainly the hyperbolic cooling tower shell. They also concluded that the ring element could be extended to other types of structural elements like axi-symmetric shell stiffeners, dynamic analysis of shell revolution or the uplift of the shell base from the foundation.

Three years later, (Sudret, *et al*., 2005) investigated the durability of hyperbolic cooling towers subjected to reinforcement corrosion induced by carbonation of the concrete. The problem was investigated as a time-variant finite element reliability analysis and later converted to a time-invariant finite element reliability analysis at a specific time for the hyperbolic cooling tower. They then developed a response-surface approach using the linearity of the finite element problem to come up with an exact expression under certain conditions. The application of this analysis was finally exposed to a representative hyperbolic cooling tower by firstly describing a deterministic model (geometrical, material and loading properties) and then secondly random variables and the design criteria. The results obtained where in terms of the initial probability of failure and its evolution with time as well as a sensitivity analysis. Only the circumferential reinforcement was considered for corrosion because of its closeness to the outside surfaces. Their study found out that the random variables describing the thermal load effect (dilatation coefficient and intensity of thermal gradient) are the most important during the initiation of corrosion. The results obtained can be used for further studies to evaluate the evolution of time of the probability of failure by using enough samples of the variables.

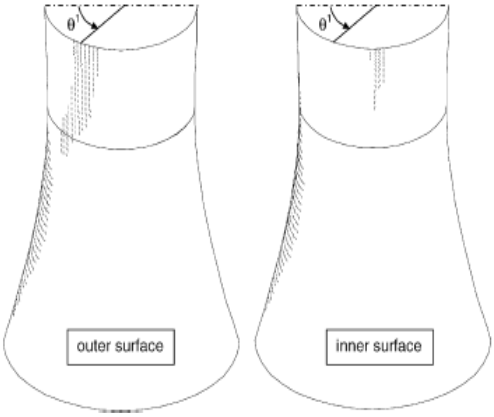

***Figure 20**: Crack distributions due to dead and wind loads* (Lang, *et al*., 2002)

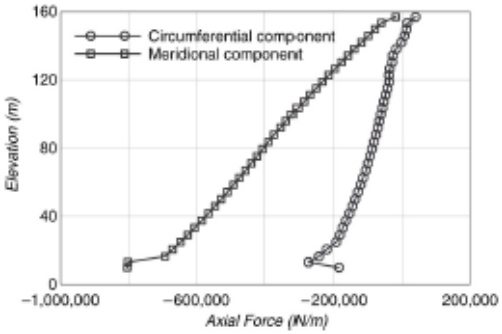

***Figure 19**: Axial windward meridional forces due to gravity* (Noh, 2006)

Another four years later, (Noh, 2006) was to study the ultimate behaviour of a reinforced concrete hyperbolic cooling tower taking into account geometric non-linearity by considering the Green-Lagrange strain tensor, and material non-linearities (tensile cracking, tension stiffening and non-linear stress-strain relationship in compressed concrete). The study considered the various non-linearities (geometric and material) that influence the static response of a hyperbolic cooling tower. A work-hardening plasticity model was employed to depict the bi-axial behaviour of the concrete. The effects of large displacements were considered by including second order non-linear strain terms in the Green-Lagrange strain tensor. By assuming the tensile cracks in concrete as smeared into the finite elements domain, the tension stiffening was modelled using gradual linear strain-softening. The analysis was done on the Port Gibson Tower (USA).

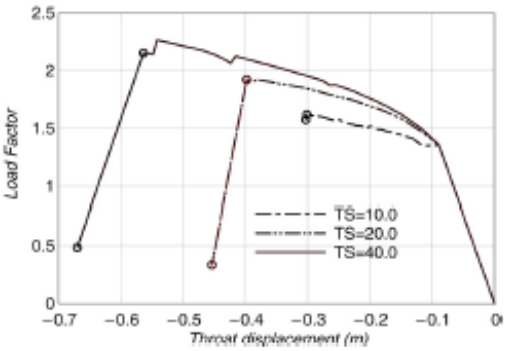

***Figure 21**: Load displacement path* (Noh, 2006)

The study concluded that the ultimate load bearing capacity of the hyperbolic cooling tower shell was 1.925 times that of the quasi-static design wind pressure that corresponds to a wind velocity of 40.2 m/s and corresponding to a tension strain of 20 and a throat displacement of 328mm. The non-linear behaviour started by the formation of horizontal tension cracks in the windward meridian at about 43% of the height of the hyperbolic cooling tower shell. As the load increased, cracks spread along meridional and circumferential directions and at failure, the windward meridional reinforcement yielded resulting in a sudden increase in the along-wind displacement. The maximum crack width was found to be above 3.0mm at failure in the part where the reinforcement had yielded. The cracks caused by bending along the line of large curvature on the outside were noted to be two orders lower than that of the maximum. For compressive stress in the concrete, yielding was noted to be along the windward meridian in the circumferential component (σ_c) as well as in the meridional component (σ_m) at the lower part of the hyperbolic cooling tower shell. The force variations were plotted as shown in *Figure 21*, the load displacement curve in *Figure 19* and the stress distributions in *Figure 22*.

The studies by (Noh, 2006) managed to provide an understanding of the failure mechanism of a hyperbolic cooling tower when subjected to a quasi-static wind load when the geometric and material non-linearities of the shell are taken into account. The study perfected the outcomes of the studies that had been done in the same area without considering these non-linearities.

In the same year, (Noorzaei, *et al.*, 2006) recorded that the studies that had been done by this time had paid very little attention on the interactive analysis of the hyperbolic cooling tower-foundation-soil system by considering them as a single compatible unit. In addition, the effect of soil non-linearity on the structural interactive response of the hyperbolic cooling tower-foundation system had not been widely reported in literature. To solve this challenge, they developed a 3-D non-linear finite element computer code to model a hyperbolic cooling tower under unsymmetrical wind loading with the shell, annular foundation raft and soil mass considered as a compatible single unit. They also explored the effect of the non-linearity of the soil on the response of the hyperbolic cooling tower shell. The wind loading was modelled as an unsymmetrical pressure distribution in the form of a Fourier series:

$$c(\Phi) = \sum_0^8 a_n \cos n\Phi + \sum_{n=0}^8 b_n \sin n\Phi \text{.....[29]}$$

in the circumferential direction and in accordance with the ASCE Committee 334 commentary (1984) in the vertical profile. Their research established the following key findings:

- An unsymmetrical wind pressure distribution represented by seven harmonic terms each of a Fourier sine-cosine series produced satisfactory results;
- The non-linear interactive analysis produced higher radial deformations compared to the non-interactive and the linear interactive analysis;
- A significant release in the principal stress (σ_3) values was observed when the effect of the non-linear interactive analysis was considered compared to that of the non-interactive analysis as shown in *Figure 23*.

These findings can be used by design engineers to determine the stress-strain effects in the hyperbolic cooling tower shell due to the shell-foundation-soil system interaction.

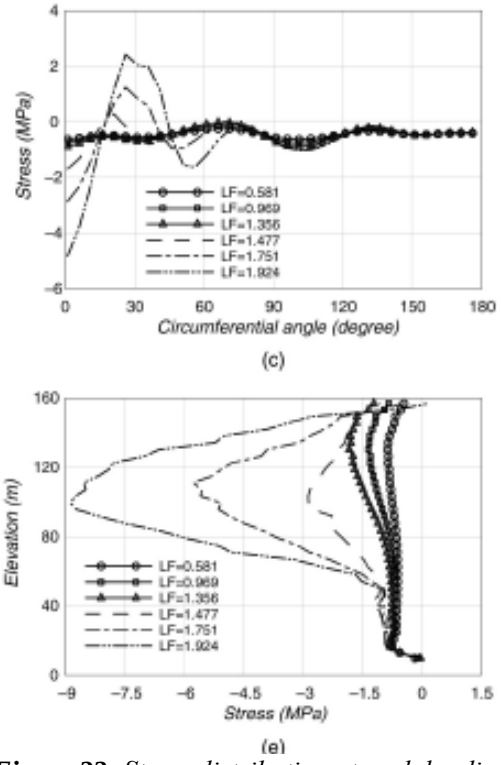

***Figure 22**: Stress distribution at each loading steps in the circumferential and meridional array of elements* (Noh, 2006)

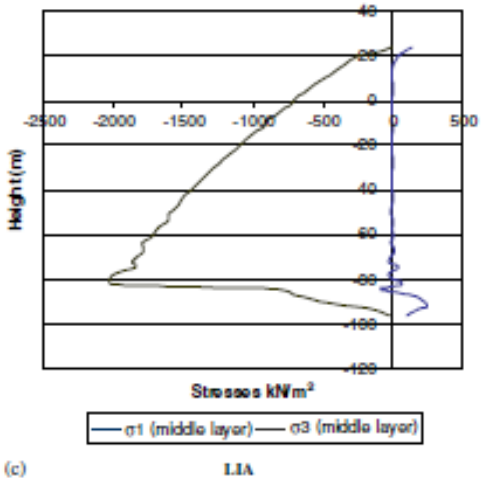

***Figure 23**: Variation of the principal stresses along the cooling tower height* (Noh, 2006)

2.2.2 Numerical studies

By the time of their study, (Viladkar, *et al.*, 1997), observed that earlier research related to the static analysis of hyperbolic cooling towers under dead or wind loads had considered only the tower shell in the analysis with a continuous boundary condition in the form of a fixity of the base of the shell. In contrast, the shell is usually supported by A-frame columns. Their study considered the hyperbolic cooling tower as represented by semi-loof shell elements and the supporting columns by semi-loof beam elements. The unconstrained version of the semi-loof element was configured as follows:

- four corner nodes and four mid-side nodes with three degrees of freedom along the x, y, z directions;
- eight loof nodes: two on each side located at the Gaussian quadrature positions $(+1/\sqrt{3};\ -1/\sqrt{3})$ with two rotational degrees of freedom along the perpendicular edge;
- The central node with five degrees of freedom (three displacements and two rotations).

Therefore, the loof element had a total of 17 nodes and 45 degrees of freedom and is shown in *Figure 24* and *Figure 28*. The study considered the column supported hyperbolic cooling tower shell under dead loads that had earlier been analysed by Gould (1984). The results obtained were to be compared to those obtained by Gould (1984) and Iyer and Appa Rao (1990).

Their study concluded that there was a significant difference in the membrane forces observed in the 1/9th portion of the tower above the top of the columns for the hyperbolic cooling tower under dead loads particularly for the hoop forces. The membrane forces away from the bottom of the tower were not affected by the different boundary conditions. The results obtained matched to those that had been obtained by Gould (1984) and Iyer and Appa Rao (1990). This research work gave a better physical representation of the column supported hyperbolic cooling tower shell.

In the same year, (Gould, *et al*., 1998) developed a local-global finite element analysis to perform non-linear analysis of column-supported general shells of revolution, of which the hyperbolic cooling tower shell certainly falls under this category. Their intention was to achieve a computationally simple and judicious model that makes use of rotational and general shell elements as well as beam-elements for the supporting columns. They employed rotational (axisymmetric) shell elements to accommodate geometric non-linearities in the axisymmetric portion of the shell. Appropriate Fourier harmonics were used to account for the non-axisymmetric loading behaviour and

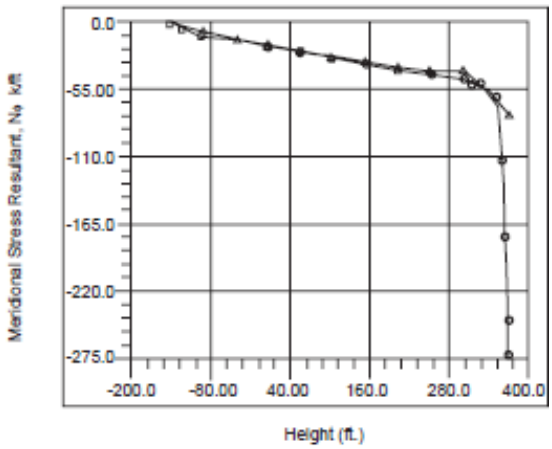

Figure 26: *Meridional stress resultants (Gould, et al., 1998)*

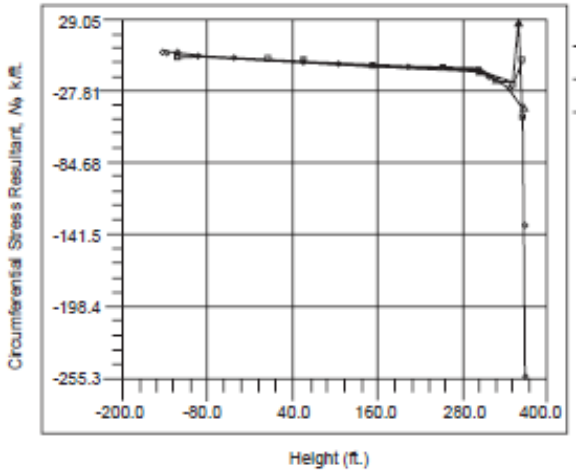

Figure 27: *Circumferential stress resultants* (Gould, *et al*., 1998)

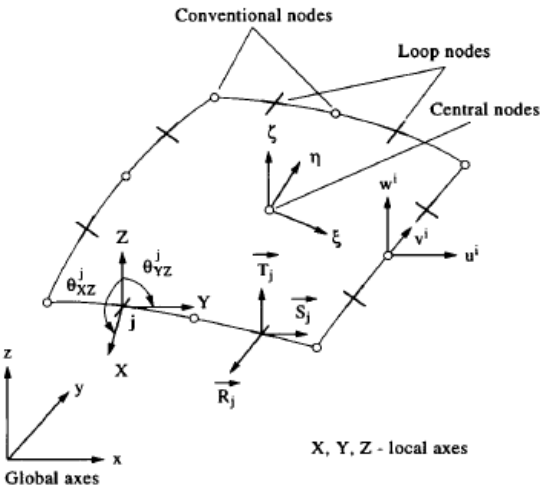

Figure 24: *Semi-loof shell element* (Viladkar, et al., 1997)

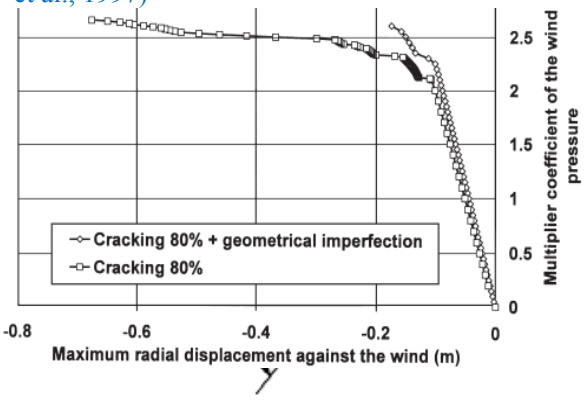

Figure 28: *Final node configuration adopted from* (Viladkar, *et al*., 1997)

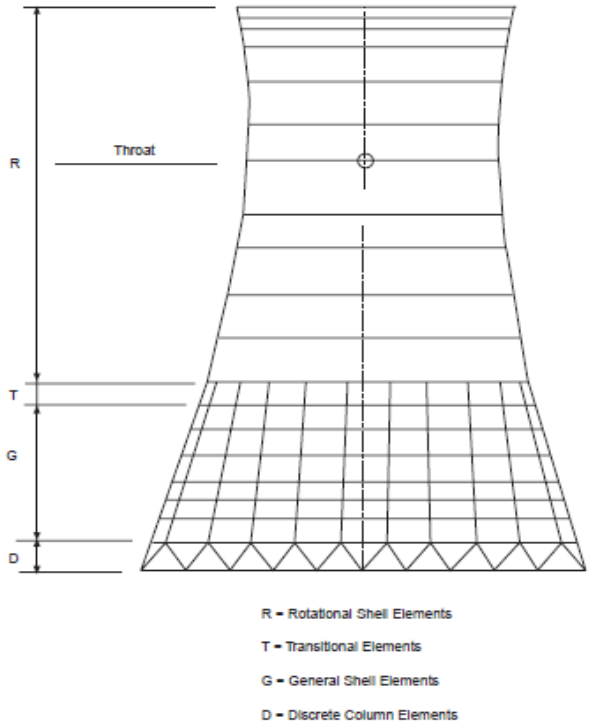

Figure 25: *Local-global finite element model* (Gould, *et al*., 1998)

deformation in this region. The supporting columns were modelled using individual beam elements and the results of the model were compared to those produced during earlier studies. The hyperbolic cooling tower analytical model was divided into an axisymmetrical zone, a local zone and the column elements as shown in *Figure 25*. The beam element (6 DOF per node) for the supporting column was connected to the general shell element (5 DOF) for the lower part of the shell by transforming the stiffness matrix of the column element into a five degree-of-freedom system before assembly. After this, numerical examples for a cylindrical and a hyperbolic cooling tower shell were performed.

The meridional and circumferential stress results obtained by (Gould, *et al*., 1998) for the hyperbolic cooling tower shell compared very well with those by Gould (1984) and by Iyer and Appa Rao (1990). The model they developed presented a single-stage, robust finite element analysis procedure of column-supported general shells of revolution.

Two years later, (Baillis, *et al*., 2000) developed an accurate model that takes into account the reinforced concrete behaviour, crack distribution and geometric imperfections for a static numerical analysis of the behaviour of the hyperbolic cooling tower shell. Their analysis also considered the influence of the material and geometric non-linearities on the stability phenomenon of the thin shell of revolution.

The study performed a parametrical analysis of the influence of the different damages on the strength of the structure. The authors performed a 2-D axisymmetric analysis with the Fourier series around the circumference taking into account non-axisymmetric imperfections and loading. Their model allowed for the introduction of initial cracks into the structure by way of initial plastic strains. Afterwards, a buckling analysis was undertaken. The effects of differential settlement of the foundation was also analysed.

They concluded that the initial regularly distributed meridional cracking greatly reduces the safety coefficient of the hyperbolic cooling tower shell against buckling proportionally to the depth of the cracks under dead loads. However, under wind loading, they noted that the initial cracks do not significantly affect the strength because the shell works mainly in the meridional direction. The results confirmed that the failure is a collapse (and not buckling) because they did not find a safety coefficient against buckling that was inferior to unity.

In the same year, (Waszczyszyn, *et al*., 2000) considered the static analysis of non-linear deformation and ultimate load of an existing hyperbolic cooling tower with large geometrical imperfections and a cut out that had been made for gas discharge. Their study performed numerical analyses dealing with:

- a perfect hyperbolic cooling tower shell;
- the actual shell with measured geometrical imperfections of the shell mid surface;
- an imperfect shell with a cut-out.

The geometric imperfections of the actual shell were obtained from iso-lines of the imperfections obtained from photogrammetric measurements as shown in Figure 30. The analysis results on the three cases of the hyperbolic cooling tower were compared and are shown in *Figure 31*, *Figure 33* and *Figure 34*.

***Figure 29**: Load displacement curves considering effect of geometrical imperfections combined with meridional cracks* (Baillis, *et al*., 2000)

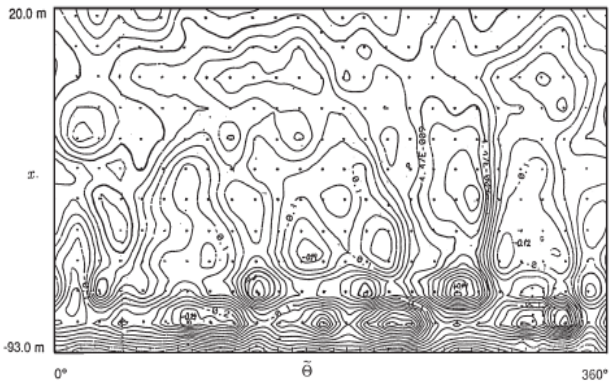

***Figure 30**: Radial imperfections isolines* (Waszczyszyn, *et al*., 2000)

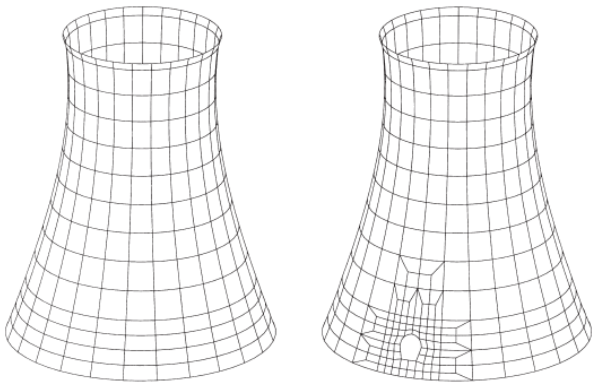

***Figure 31**: Finite element shell model with and without cut-out* (Waszczyszyn, *et al*., 2000)

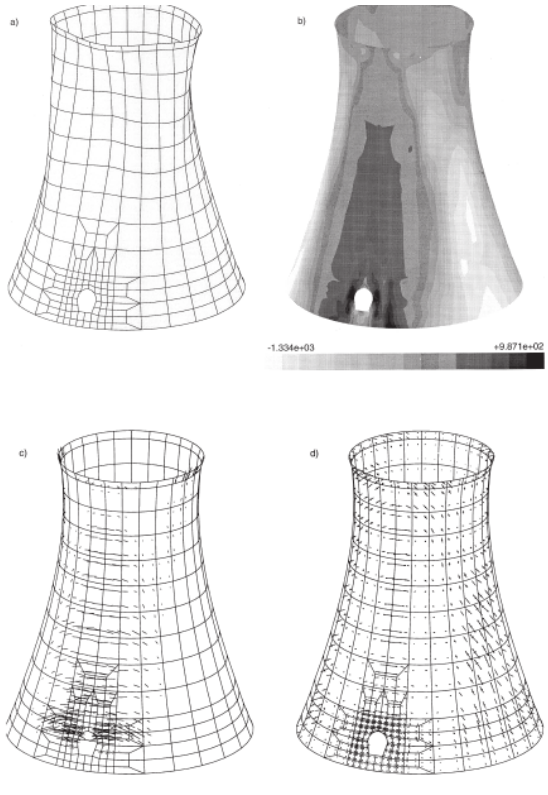

***Figure 33**: (a) Shell deformation, (b) Meridional distribution for the outer concrete layer, (c) Crack pattern, (d) Principal stresses for the outer concrete layer* (Waszczyszyn, *et al*., 2000)

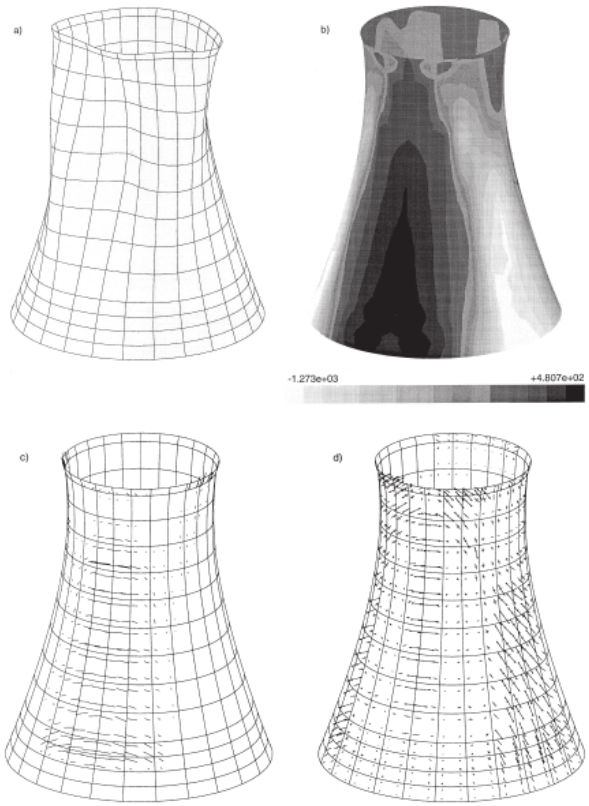

***Figure 34**: (a) Shell deformation, (b) Meridional force distribution, (c) Vector plot representing smeared crack directions and the "cracking" strain at Gauss points for outer concrete layer, (d) Vector plot of principal stresses for outer concrete layer* (Waszczyszyn, *et al*., 2000)

The non-linear analysis produced limit load factors that are much lower than the critical load factors obtained from a linear buckling analysis of an elastic hyperbolic cooling tower shell obtained by (Mang, *et al*., 1983). As had been confirmed in earlier research, the load level at which cracking begins was noticeable on the plotted curves. The cracking process dominates the non-linear behaviour of the shell. Extensive cracking is accompanied by a stress redistribution to the reinforcement until the reinforcement yield limit point is observed. Additional reduction of the shell stiffness and load carrying capacity was observed due to the interaction of material and geometrical non-linearities. However, insignificant effects of the geometrical imperfection and local weakness of the shell due to the cut out was noted during the time of loading. The study noted strengthening of the shell around the cut-out played its role. Although the cut-out had a slight influence on the global response of the hyperbolic cooling tower, local stress redistributions and concentrations were noted. Because the study determined the load level at which the first cracking was observed, predicted the deformation process, the limit load and the redistribution of internal forces, it can be used for a "checking-design" process and applied to practical instances where shell linearity is abandoned (for example, cooling towers facing collapse).

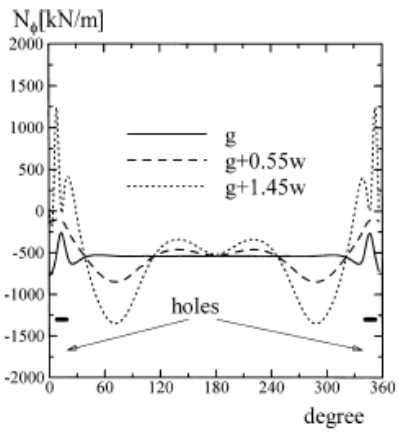

***Figure 32**: Meridional stress resultants (Wind A)* (Hara & Gould, 2002))

Two years later, (Hara & Gould, 2002) were to extend the local-global analysis method to the non-linear analysis of a column supported hyperbolic cooling tower shell with imperfections in the form of two openings. They conceded that since the openings introduce non-axisymmetry in the shell, the use of a general shell finite element method produces a large number of degrees of freedom when the elements are discretised. Such a solution will be laborious to solve.

Their study was based on the Boxberg IV cooling tower that had been earlier studied by Eckstein and Nunier (1998). They were particularly interested with the influence of the existing small equal sized tunnel type openings for flue gas pipes on the whole shell. They studied the three types of wind pressures:

- with windward direction coinciding with a meridian equi-distant from the centres of the openings (WIND A);
- with windward direction coinciding with a meridian on the centre of one of the openings (WIND B);
- with maximum suction coinciding with a meridian on the centre of one of the openings (WIND C).

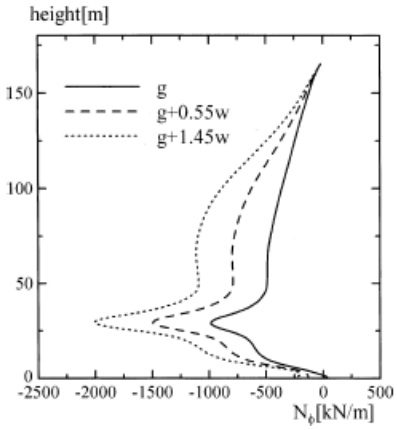

***Figure 37**: Meridional stress resultants (Wind C)* (Hara & Gould, 2002)

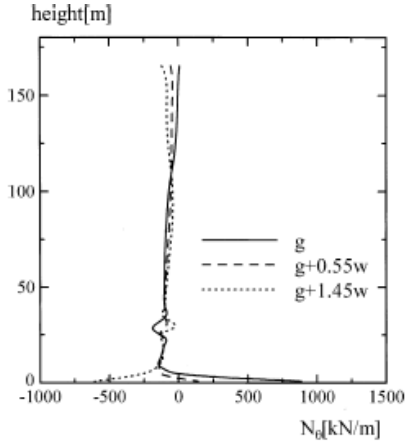

***Figure 36**: Hoop stress resultants (Wind A)* (Hara & Gould, 2002)

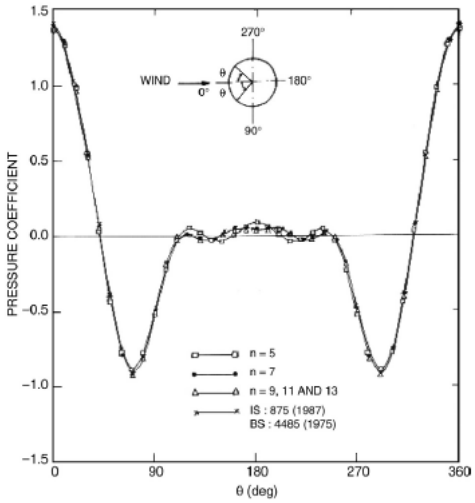

***Figure 35**: Circumferential pressure distribution on cooling tower* (Viladkar, *et al*., 2006)

Part of the stress resultants obtained for the different winds are shown in *Figure 32*, *Figure 37* and *Figure 36*.

The study confirmed that the openings have an influence on the stress distribution of the cooling tower and that there was a stark change in the stress distribution around the opening. The combination of openings and the wind direction strongly influences the stress state in the hyperbolic cooling tower. Maximum tension and maximum compression was observed from the stress concentration under wind pressures A and C respectively. The findings of this study can be used by design engineers when planning for openings or cut-outs on hyperbolic cooling towers.

Four years later, (Viladkar, *et al*., 2006) studied the soil structure interaction of the column-supported hyperbolic cooling tower and it's supporting annular raft-soil system when subjected to a symmetrical wind load. The study considered numeric modelling of the soil-structure system by using semi-loof shell elements and semi-loof beam elements.

The entire system was considered as an integral compatible unit in order to estimate differential settlements of the annular raft, contact pressure distribution under the annular raft and their combined effect on the shell deformation pattern, redistribution of membrane forces and bending moments in the hyperbolic cooling tower shell as well as forces and moments in the column. The wind pressure was represented by the first eight harmonics of a Fourier cosine series only in order to reduce unnecessary computational effort and is shown graphically in *Figure 35*. A parametric study was done to consider the soil-structure interaction for the following cases:

- NIA - Non interactive Analysis;
- SSI - Case I - Soil-Structure Interaction Analysis Case I;
- SSI - Case II - Soil-Structure Interaction Analysis, Case – II;
- SSI - Case III - Soil-Structure Interaction Analysis, Case – III.

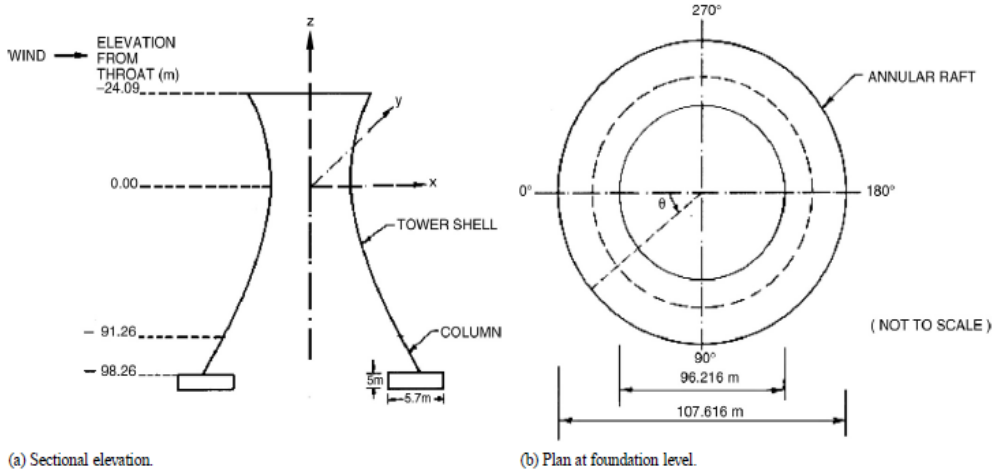

***Figure 38**: Cooling tower foundation details* (Viladkar, *et al*., 2006)

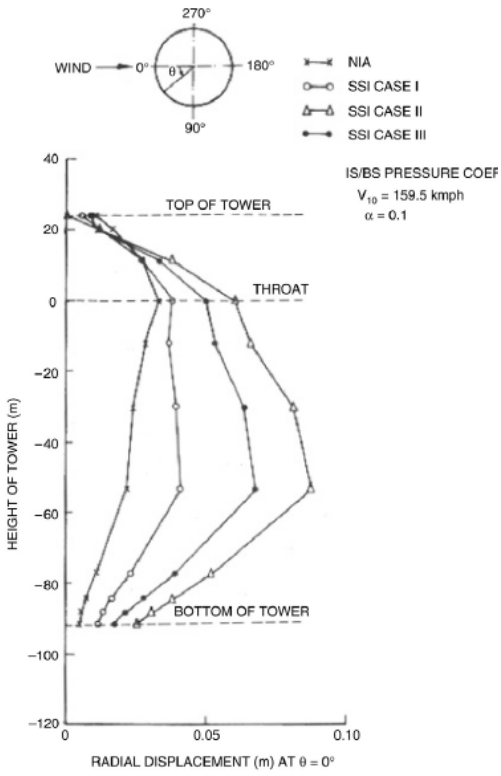

***Figure 39**: Radial displacements along $\theta=0^0$ meridian* (Viladkar, *et al*., 2006)

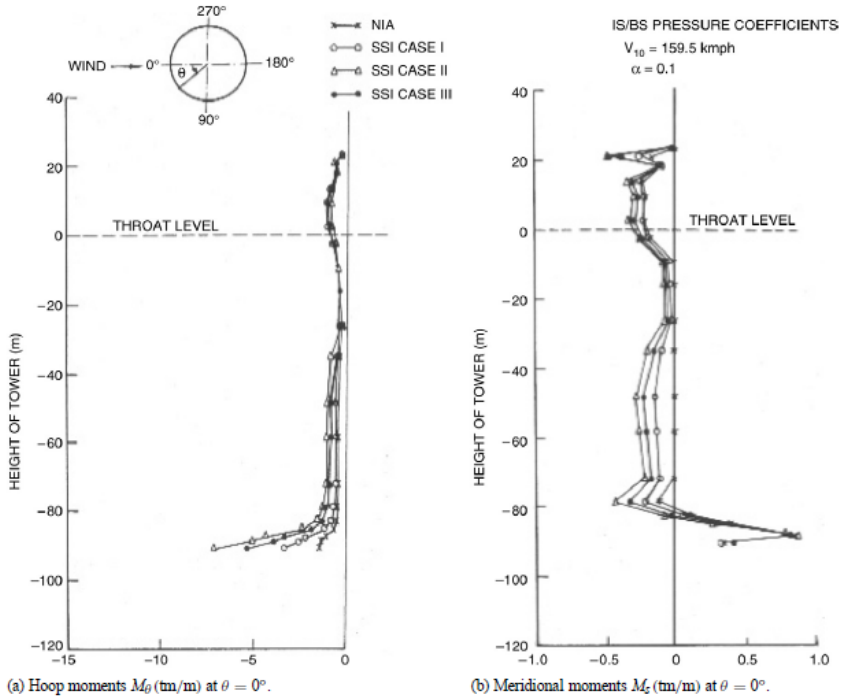

***Figure 40**: Bending moments along $\theta=0^0$ meridian* (Viladkar, *et al*., 2006)

They concluded that the hyperbolic cooling tower shell-column supports-annular raft-soil system is a more realistic three-dimensional finite element model than any individualistic model. Redistribution of forces and moments was observed in the entire hyperbolic cooling tower shell, column supports and annular raft due to their considered interactive behaviour. Significant increases in radial displacements along the $\theta = 0°$ meridian, meridional forces and bending moments were observed due to the interaction effect. A 15% to 29% reduction in the columns tensile and compressive forces was noted when the interaction was considered. A 5.0m thick annular raft behaved as a flexible foundation and experienced a maximum differential settlement of 14.57mm at the meridian $\theta = 73.64°$. The findings of the study provides design engineers with tools to estimate the interactive behaviour of the hyperbolic cooling tower shell-column supports-annular raft-soil global system.

Six years later, (Murali, *et al*., 2012) considered the finite element analysis of two hyperbolic cooling tower shells of 122m (CTI) and 200m (CT2) height above ground subjected to a symmetrical wind load and fixed at the base. Their intention was to obtain non-dimensional values of the membrane forces ($N_\emptyset$ and N_θ) and bending moments ($M_\emptyset$ and M_θ) by normalizing the forces and moments using reference values at the base or at meridian $\theta = 0°$.

The finite element analysis of the two cooling towers was performed to evaluate:

- meridional forces $N_\emptyset$;
- hoop forces N_θ;
- meridional bending moments $M_\emptyset$;
- and hoop bending moments M_θ.

The study attempted to generalise the distribution of these membrane forces and bending moments in a non-dimensional form along the circumference at the top, throat and base of the cooling tower as well as along the vertical for the two meridians $\theta = 0°$ and 70°. The non-dimensional values were obtained by normalising the actual values with reference values at the following reference locations:

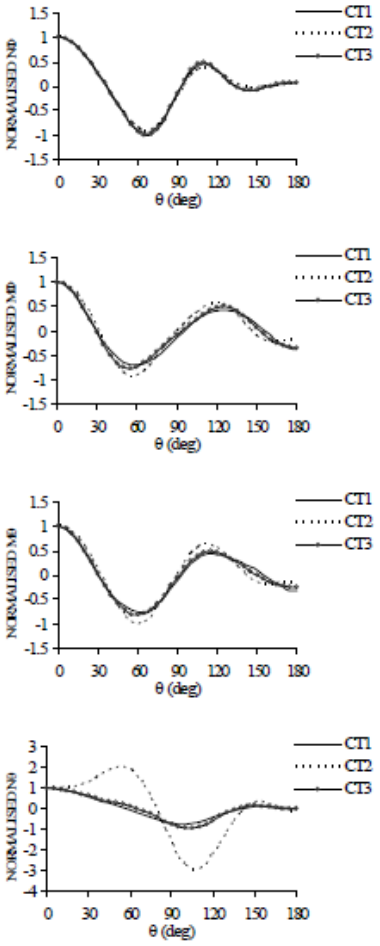

***Figure 41**: Circumferential distribution of normalised membrane forces and bending moments at throat level* (Murali, *et al*., 2012)

- Meridian θ = 0° for the circumferential distribution;
- Base for the vertical distribution.

In addition, the authors considered a third additional cooling tower (CT3) with the same height as CT2 (200m) but with the throat height/total height (H_{thr}/H) and throat diameter/base diameter (D_{thr}/D) ratios as the same as for the CTI cooling tower. Their intention was to observe any dependence of the normalised curves on the above mentioned ratios. The wind load was applied as a symmetrically distributed pressure represented by an 8 harmonic Fourier cosine series.

$$P' = \sum_{n=0}^{7} F_n \cos n\theta = F_0 + F_1 \cos\theta + F_2 \cos 2\theta + \ldots\ldots + F_7 \cos 7\theta \quad \text{[30]}$$

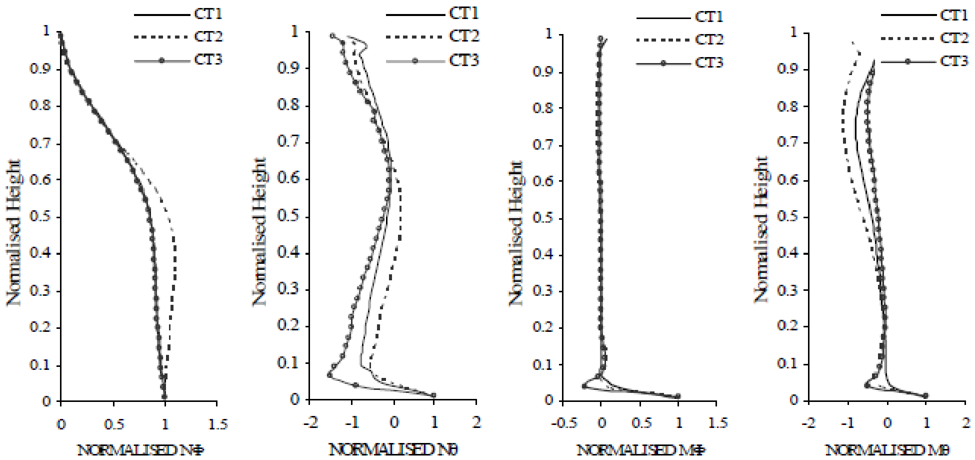

***Figure 42**: Vertical distribution of normalised membrane forces and bending moments at θ=0⁰ meridian* (Murali, *et al.*, 2012)

For the circumferential distribution at the base, throat and top levels all the normalised curves (shown in *Figure 41* and *Figure 42*) compared well with each other except for the N_θ curve at throat level, $M_\emptyset$ and M_θ at the top level. The well compared curves can therefore be generalised independent of the ratios (H_{thr}/H) and (D_{thr}/D). For the vertical distribution at meridian θ = 0° and 70°, $M_\emptyset$ curves compared very well with each other and can be generalised independent of the height and depth ratios. The obtained normalised curves can be used by the design engineer to evaluate membrane forces and bending moments in a hyperbolic cooling tower without performing a detailed finite element analysis. The authors confirmed that further study is required in this particular area.

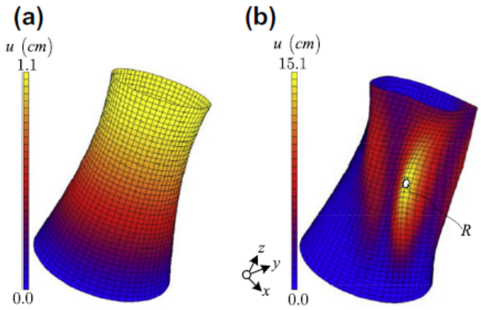

***Figure 43**: Cooling tower shell deformation subject to (a) dead load, (b) dead load and wind load* (Jia, 2013)

A year later, (Jia, 2013) re-analysed the Port Gibson hyperbolic cooling tower that had been analysed by Mang *et al* exactly 30 years before. The study was meant to investigate whether the argument presented by (Mang, *et al*., 1983) and many others that followed (Hara *et al* (1994), Min (2004), Noh (2005)), that failure of the hyperbolic cooling tower shell under static and quasi-static loads would be initiated by propagation of cracks in the tensile zones followed by an increased activation of the load-carrying capacity of the shell and finally yielding of the reinforcement (not buckling of the shell) would still be applicable if the original design were to be changed to include:

- Ultra-High Strength Fibre Concrete (UHSFC);
- A reduction of the shell thickness;
- Geometric imperfections.

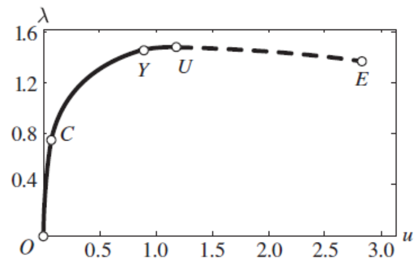

***Figure 44**: Typical Load displacement curve* (Jia, 2013)

The Port Gibson cooling tower was re-analysed with a finite element computer programme similar to the one that had been used by (Mang, *et al.*, 1983). A parametric study was performed using finite element modelling considering a change in the strength of the concrete from the one that Mang *et al* had used, a reduction in the shell thickness of the cooling tower and a change in the geometry by way of introducing imperfections. Before the design changes were introduced, the author confirmed the failure mode to be the same as that noted during previous studies (crack propagation, load carrying capacity increase, reinforcement yielding and failure). Results of the deformations and buckling modes are shown in *Figure 43*, *Figure 44* and *Figure 45*.

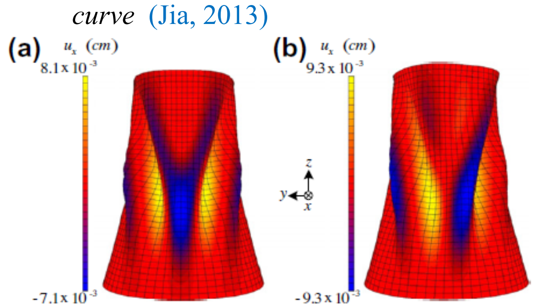

***Figure 45**: (a) Symmetric buckling mode, (b) Antisymmetric buckling mode of the cooling tower* (Jia, 2013)

When the strength of the concrete was increased to a 200MPa strength concrete (compared to the previous 35MPa), the failure mode was noted to be the same. The only difference was that zones of reinforcement plastic deformation spread faster than in the original case and hence reinforcement rupture occurred just after ultimate failure. When the shell thickness was reduced, the failure mode exhibited the same failure paths. Although yielding of reinforcement did not occur (as expected) before the ultimate load, the steel began to yield shortly after the ultimate load was reached. This proved that neither "snap-through-buckling" failure load-displacement nor bifurcation buckling does not exist in the hyperbolic cooling tower shell. When imperfect geometric shapes of the hyperbolic cooling tower were considered, a similar failure mode was observed: cracking of concrete-yielding of reinforcement-collapse. The author reiterated the thesis that buckling "in the classical sense of this term" does not occur in a hyperbolic cooling tower shell as had been confirmed with previous studies, this time even with changes in the concrete strength, shell thickness and geometric imperfections.

2.2.3 Experimental and field studies

(Meschke, *et al.*, 1991) investigated the limit of serviceability and residual safety against structural collapse of the Ptolemais - III (Greece) hyperbolic cooling tower that had been built in 1966. They were concerned with investigating numerically the safety coefficient of the cooling tower using finite element analysis. Concrete specimens where taken for testing for carbonation and any other cause of corrosion of the reinforcement. The influence of the thermal pre-loading on the limit of serviceability and on the ultimate load of the structure was investigated by use of several thermal load histories. In the finite element model, the load histories were summarised as shown in the equations below. The reduction in the stiffness of the cooling tower caused by existing cracks was assessed by performing an ultimate load analysis of the originally uncracked cooling tower shell.

Load case II: $g + \frac{\Delta T_w}{h} + \lambda w$.....[31]

Load case III: $g + \frac{\Delta T_w}{h} - \frac{\Delta T_w}{h} + \lambda w$.....[32]

$g + \frac{\Delta T_w}{h} - \frac{\Delta T_w}{h} + \frac{\Delta T_s}{h} - \frac{\Delta T_s}{h}\ \lambda w = g + \lambda w$.....[33]

A load displacement curve (shown in Figure 46) was plotted for all the load cases where:

λ_c corresponds to level of crack plateau;

λ_y corresponds to the starting of yielding and

λ_u corresponds to the level of ultimate collapse.

Corrosion of the reinforcement was considered by multiplying the diameter of the steel by a factor of 0.9.

For the load case when corrosion of the reinforcement was considered by multiplying its diameter by 0.9, the ratio of λ_u/λ_y was found to be equal to 1.22. This meant that the reduction of the reinforcement diameter can be regarded as a tolerable upper limit of the corrosion in view of the 1.22 residual safety factor. For the originally uncracked shell, the value of λ_u at collapse was found to be 1.56. For all the other load cases, the minimum value of λ_u for the cracked shell was 1.47 (load case representing weakening of structure due to winter-summer cycle of temperature changes). Therefore, the loss of strength of the cooling tower shell due to cracking caused by temperature gradients was found to be relatively small. The stress distribution obtained is shown in Figure 47.

***Figure 46**: Load-displacement diagrams for load cases I, II, III and IV* (Meschke, *et al*., 1991)

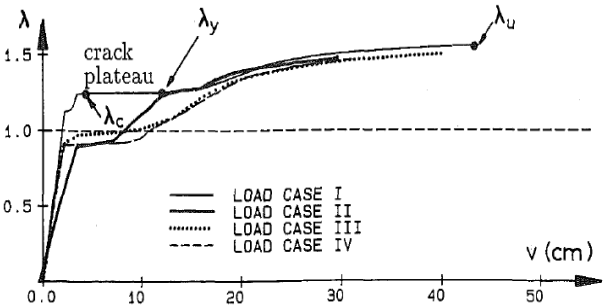

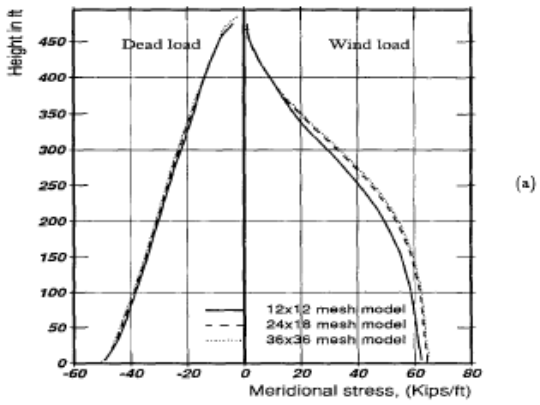

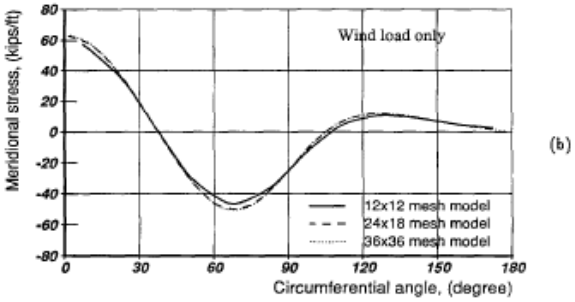

***Figure 47**: (a) Vertical distribution of meridional stress due to dead and wind loads at 3.17^0, 1.58^0, 1.06^0 from windward meridian; (b) Circumferential distribution of meridional stress due to wind load at 15.5m, 17.7m and 18m from shell bottom* (Meschke, *et al*., 1991)

The investigation concluded that the Ptolemais-III hyperbolic cooling tower was sufficiently safe against failure even without repairs, provided that the corrosion of the reinforcement does not exceed 10% of the original diameter for the remaining cooling tower's life. Detailed in-situ inspections of the cooling tower confirmed that the temperature gradient between the inside and outside of the cooling tower during winter was the most likely cause of the meridional cracks. The degree of corrosion controls the safety of the cooling tower. With respect to the sensitivity analysis, attaching stiffening rings to the cooling tower shell showed that three rings will

increase the safety against collapse by 61% compared to the unstiffened shell, at a height of 63% of shell. The ultimate load increased by 26%. The study confirmed methods that can be used when investigating existing cooling towers.

Two years later, (Min & Gupta, 1993) investigated the inelastic non-linear behaviour of the Grand Gulf Nuclear Power Station (Mississippi) hyperbolic cooling tower using a finite-element modelling program. In their study, they used a reinforced concrete shell finite-element modelling computer program to perform a mesh-convergence study. The same cooling tower had been studied by others before (Mang, *et al.*, 1983), (Milford and Schnobrich, 1984, 1986) and (Gupta and Maestrini, 1986). Wind and dead loads were first applied to the model and meridional stress variations due to these loads compared for three different finite element mesh models. In order to account for the effect of bending on the cracking of concrete and yielding of the steel, the study performed a "single-layer model" and a "multi-layer model" finite element analysis for the three different mesh models. The purpose of this approach was to investigate the membrane stresses at the middle surface (effect of bending on cracking and yielding of reinforcement ignored) for the single-layer model analysis and to simulate the membrane and bending effect on concrete cracking and reinforcement yielding for the multi-layer model analysis.

They recorded that there were several elements in all the three mesh models in which either only the outer layer or the inner layer of the circumferential reinforcement had yielded. This key finding indicated that bending plays an important role in the circumferential direction. The single-layer model analysis could not predict failure because the analysis had to be stopped when the models had gained relatively large horizontal throat displacements. Significant positive load-deflection gradients where observed. The investigations concluded that this meant that the hyperbolic cooling tower had a considerable capacity of circumferential re-distribution of meridional stresses. In the single-layer model analysis, the cooling tower shell continues to possess both circumferential bending stiffness and strength until the circumferential reinforcement has yielded. Only when the circumferential reinforcement had yielded due to the membrane stresses could the failure occur (this only happens at much higher applied loads).

On the other hand, the study concluded that the multi-layer model analysis accounted for the effects of bending on the yielding of the circumferential reinforcement. This analysis therefore could predict failure when the meridional stresses could no longer be re-distributed because of the loss of circumferential bending stiffness. The ultimate-wind-load factor was predicted at 2.46 for the multi-layered model analysis, whereas a 3.09 factor was predicted for the single-layered model analysis. These results confirmed that bending deformation plays an important role in the strength and deformation of the cooling tower shell.

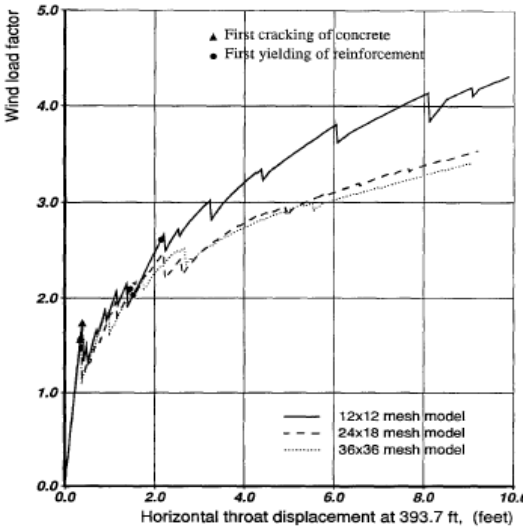

***Figure 48**: Load displacement curves for single layer models* (Min & Gupta, 1993)

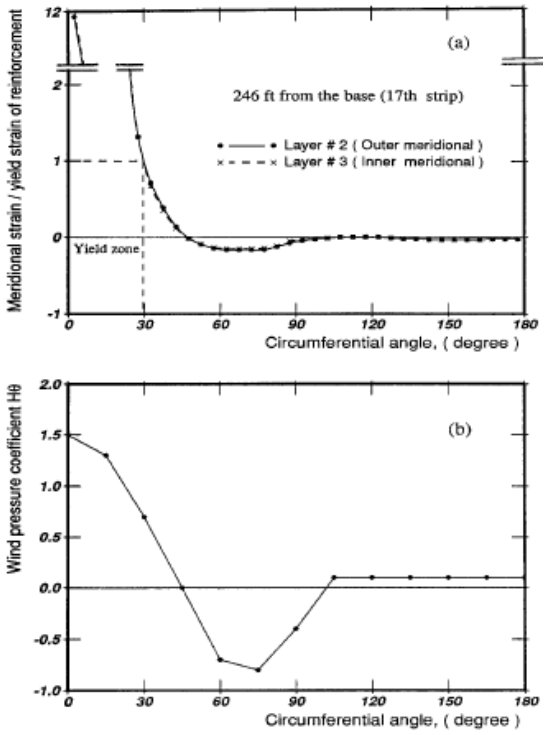

***Figure 49**: (a) Circumferential distribution of meridional strain; (b) Wind-pressure-coefficient distribution including internal suction* (Min & Gupta, 1993)

The circumferential distribution of meridional stresses was noted to follow the wind-pressure distribution. The strain distribution for the two layers were noted to be identical. This implied that the membrane forces control the deformations in the meridional direction. The differences between the ultimate-wind-load factor obtained from this study (1.66) and those from the other studies on the same cooling tower (1.66, 1.52 by (Mang, *et al.*, 1983), (Milford and Schnobrich, 1984) respectively) was attributed to differences in the three analysis related to computational and material factors. The load displacement, strain distribution as well as the wind pressure distribution is shown in Figures 48, 49(a) and 49(b) respectively.

The study confirmed that the failure of cooling towers occurs when the meridional reinforcement yields. This happens when the meridional stresses can no longer redistribute because the circumferential reinforcement would have yielded in bending. (Min & Gupta, 1993)'s performance of a mesh convergence study led to them obtaining a higher shape factor (1.48) than obtained by (Mang, *et al.*, 1983) and Milford and Schnobrich (1986). The mesh convergence ensures an accurate prediction of the inelastic behaviour of the cooling tower. A higher shape factor indicates significant

redistribution of meridional stresses. The study re-established the findings by previous investigations and improved on showing the need for considering the mesh-convergence studies when running finite element model analysis of hyperbolic cooling towers.

Seven years later, (Choi & Noh, 2000) where interested in establishing the variations in the response of a reinforced concrete hyperbolic cooling tower due to geometric imperfections by using a statistical stochastic analysis. They conceded that although general analysis of cooling towers considers them as ideal shapes (axisymmetric hyperbolic), this kind of idealisation does not well represent the real shape imperfections in the actual shell.

The shape imperfection of the cooling tower was modelled with two uncertain geometrical parameters (radius and thickness of the cooling tower shell). The model assumed the imperfections to be a globally distributed stochastic field with the spatially varying stochastic fields with predetermined statistical terms. The imperfections were modelled as shown on the stochastic configurations in *Figure 50*. Four numerical analyses of the model were performed with the following parameters varied:

- Only the radius deviation included as a random parameter;
- Only the thickness deviation included as a random parameter;
- The radius and thickness deviation assumed to be independent with no correlation existing between them and
- The spatial randomness of the elastic modulus considered in order to compare the variation in response of the first three cases.

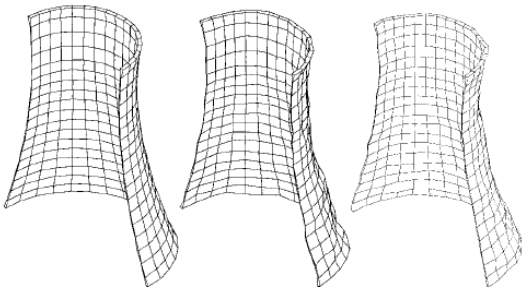

***Figure 50**: Perfect and sample stochastic cooling tower shell configurations* (Choi & Noh, 2000)

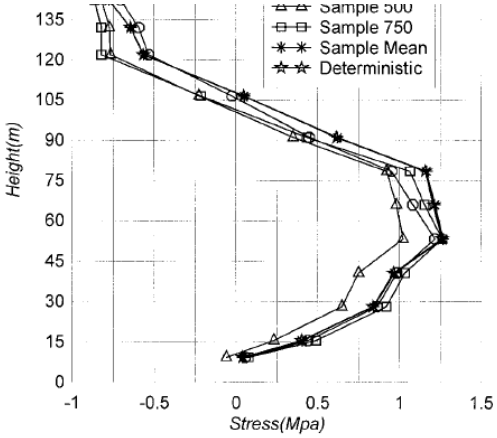

***Figure 51**: Stresses along windward meridian* (Choi & Noh, 2000)

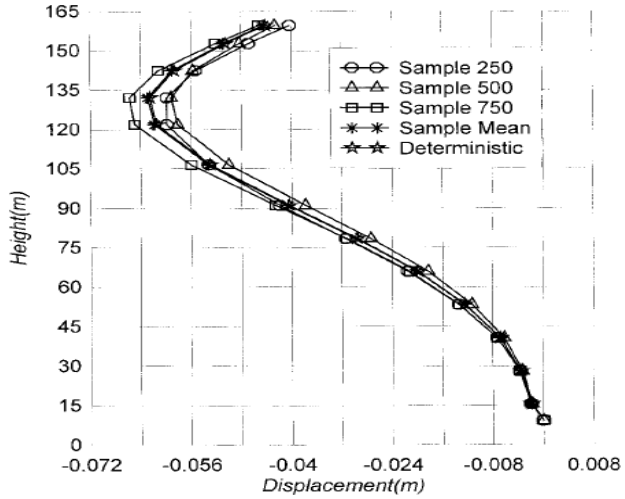

***Figure 52**: Displacements along windward meridian* (Choi & Noh, 2000)

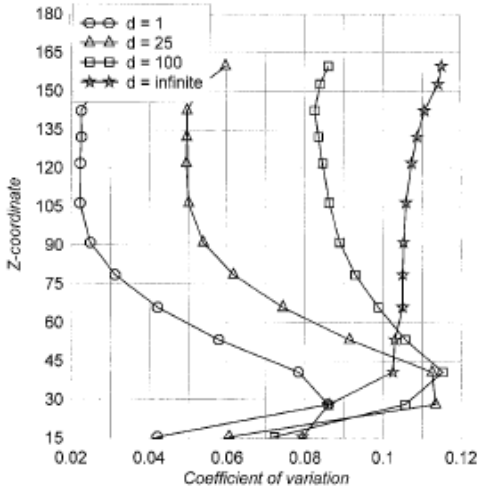

***Figure 53**: Trend of coefficient of variation (COV) along windward meridian of displacement (thickness)* (Choi & Noh, 2000)

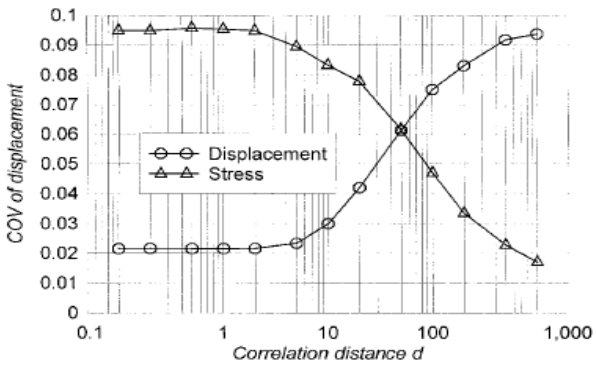

***Figure 54**: Coefficient of variation (COV) trend of displacement and stresses due to material randomness* (Choi & Noh, 2000)

The intent was to be able to observe any salient properties/features of each random parameter's influence on the variation of the response. *Figure 51*, *Figure 52*, *Figure 54* and *Figure 53* show the stress, displacement, coefficient of displacement variation for the various shell parameters.

They concluded that response variability due to radius deviations was found to be significantly larger than that due to the randomness of the shell thickness. The mixed effect of the two random parameters (obtained through their Square Root Sum of Square, SRSS) showed a difference in trend influence. The thickness deviation resulted in a reduction in the response variability, whereas the radius deviation resulted in an increase in the response variability, thereby causing an additional response. The value of the additional response revealed that the coefficient of variation (COV) of stresses are larger than those of displacements. The additional response caused by the randomness of the radius was larger than that caused by the shell thickness deviation. The study found out that there was no direct relationship between the random parameters (radius randomness and shell thickness deviation) and the responses.

Six years later, (Ioannidis, *et al*., 2006) used state of the art time-of flight laser scanners to perform a quantitative assessment of the surfaces of an existing old hyperbolic cooling tower at Megalopolis (in Greece) in order to detect any shape imperfections and obtain a 3-D model for use in FEM structural analysis. They used scanners to obtain a 3-D model of the existing cooling tower. Detailed geometric recording of the inner and outer surface of the shell was performed. Concrete visual inspections and non-destructive tests and destructive test were performed in order to obtain the concrete properties. Local cracks were also measured. The knowledge of the in-situ cooling tower deviation was to be used in a structural analysis to determine the safety of the cooling tower against various loads. *Figure 55* shows a 3-D comparison of the actual shell versus the theoretical shell.

The study concluded that the terrestrial laser measurement was a success when the achieved model was compared to a theoretical (mathematical) model created from the same cooling tower dimensions. Deviations of +/- 30mm between the measured model and the theoretical model were noted. The obtained model was used to check the structural deformations. It was confirmed that the structure was still in good shape. The small deviations noticed were attributed to construction methods.

Seven years later, (Goudarzi, 2013) investigated the possibility of reducing the structural wind design load whilst enhancing the thermal performance of a hyperbolic cooling tower. The wind design load (being of such a dominant effect on the load cases acting on a cooling tower) should inherently reduce when the height of the tower is reduced. However, this may have adverse effects on the thermal performance of the cooling tower. Although the reduced cooling tower (RCT) can reduce the critical wind loads significantly, they might lead to an undesirable reduction of the thermal performance when compared to a whole cooling tower (WCT).

A whole cooling tower was considered for various analysis. The structural design wind load was calculated for the RCT and WCT using German guidelines: *WCT height = 135m, base diameter = 122m, RCT height = 70m, base diameter = 122m.* The computational fluid dynamic (CFD) model was then considered for the RCT and WCT for various cross winds to obtain and compare the thermal performance of the two cooling tower cases.

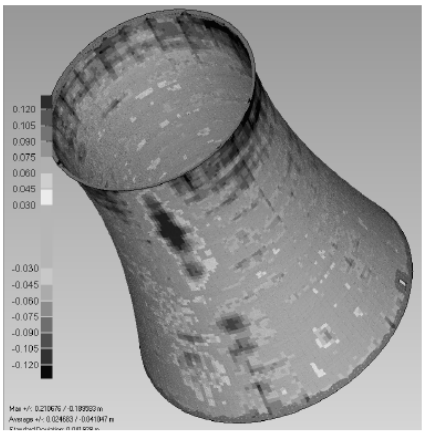

Figure 55*: 3D comparison of the actual cooling tower model and the theoretical (mathematical) surface* (Ioannidis, *et al.*, 2006)*)*

The study concluded that the reduction of the cooling tower height resulted in an approximate reduction of the structural design wind load by up to 25 times more for the RCT when compared to the WCT. The thermal performances of the RCT and WCT were found to be similar under high wind speeds. Hence, the reduction of the cooling tower under gusty wind conditions was noted to have no considerable adverse effect on the thermal performance of the cooling tower. Reducing the height of the cooling tower under high velocity winds would significantly reduce the structural wind loads whilst maintaining the same level of thermal performance of the cooling tower. The study's finding provides designers with tools to consider variations in the cooling tower height whilst enhancing its thermal performance.

2.3 STABILITY BEHAVIOUR

2.3.1 Theoretical studies

(Mang, *et al*., 1983) were concerned with proving sufficient safety against buckling of a hyperbolic cooling tower under wind load. By the time of their study, Abel *et al* (1982) had discussed several methods to determine buckling pressures by assuming a linear pre-buckling path and equivalent axisymmetric concepts. (Mang, *et al*., 1983) queried the application of axisymmetric buckling concepts to non-axisymmetric (wind loading) situations. In addition, they queried whether determining bifurcation points on a linearised load-displacement path was justified.

Their research was divided into two parts: a theoretical part dealing with a constitutive model and the basic equations for incremental-iterative ultimate load analysis and instability and a numerical part considering a finite element analysis of the Port Gibson (Mississippi) hyperbolic cooling tower. The second part contains buckling analysis results reported by Floegl (1981), Mang *et al* (1977) and Mang *et al* (1978). It also contains results from a linear and non-linear buckling analyses for wind load as well as for an "equivalent axisymmetric" wind load. Results from an ultimate load analysis are also included. The numerical analyses considered the following cases:

- geometric nonlinearity disregarded;
- tension stiffening effect neglected;
- reinforcement percentage varied.

In their treatment of the theoretical part, a consideration of the constitutive equations and incremental iterative finite element analysis were presented. The "equivalent uniaxial constitutive model" was employed because of the equivalent uniaxial stress-strain behaviour of concrete. The loss of stability was noted to be usually associated with an extreme value (bifurcation point) on the load-displacement path. The 150m high Port Gibson (Mississippi) cooling tower shell was analysed (see *Figure 56*) and the finite element mesh model shown in *Figure 57* was adopted. Instability points to the load-displacement path were compared for various cases. The behaviour of the cooling tower was studied from the un-cracked state through to final collapse. A wind load pressure with the function shown in equations below was applied on a 12x12x12 = 288 curved triangular finite element model.

$$p_S^{(R)} = 413.013 H_a\ (3.281\beta + 393.696)^{2/7} \text{.....[34]}$$

where $H_a = -0.5 + \sum_{n=0}^{12} A_n \cos(na)$.....[35]

Their study concluded that the buckling loads from both the linear and geometrically nonlinear analysis were found to be significantly larger than the ultimate load. This supported the conclusion that failure of wind loaded reinforced concrete cooling towers is initiated by rapid propagation of cracks in the tensile zones and not by buckling. The authors observed that had the instability of the shell been relevant, the computer program would have shown a bifurcation point or a limit point prior to cracking of concrete and yielding of the reinforcement. They concluded that there would be no need to prove sufficient safety against buckling modes of failure (bifurcation or limit-point buckling) because "they have little to do with the actual reason" why reinforced concrete cooling towers fail: cracking of concrete and yielding of reinforcement.

The results obtained from the equivalent axisymmetric load were noted to be on the unsafe side of the corresponding "actual" wind load results. The failure mechanism of wind loaded cooling towers was explained by means of an ultimate load analysis considering the non-linearity of concrete, fracture of concrete "smeared cracks," strain-hardening of the reinforcement, tension stiffening and geometric non-linearity.

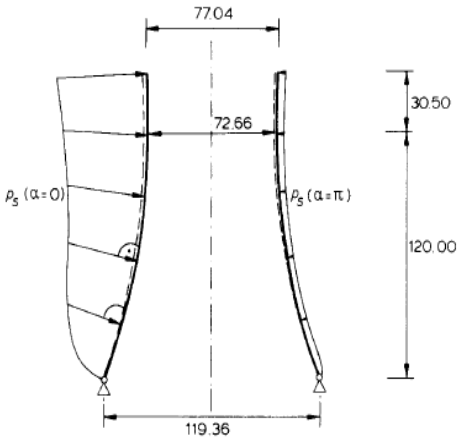

***Figure 56**: Wind profile for the windward and opposite meridian* (Mang, *et al*., 1983)

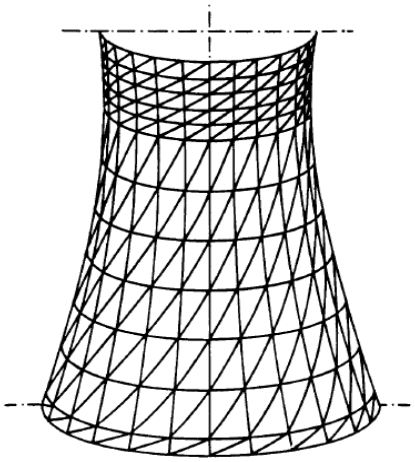

***Figure 57**: Finite element mesh model* (Mang, *et al*., 1983)

***Table 3**: Critical load intensities x_{CR}, disregarding material nonlinearity* (Mang, *et al.*, 1983)

Load	Critical load intensity x_{CR}: Linear buckling using eq. (26)	Nonlinear instability
x_{CR} X wind load	4.80	
Dead load + (x_{CR} X wind load)	4.80 (4.97[32])	≐20* (19.5[32])
x_{CR} X equivalent axisymmetric pressure	13.67	
Dead load + (x_{CR} X equivalent axisymmetric pressure)	12.85	≐33†

* Load increments $\Delta x = 2$. † Load increments $\Delta x = 3$.

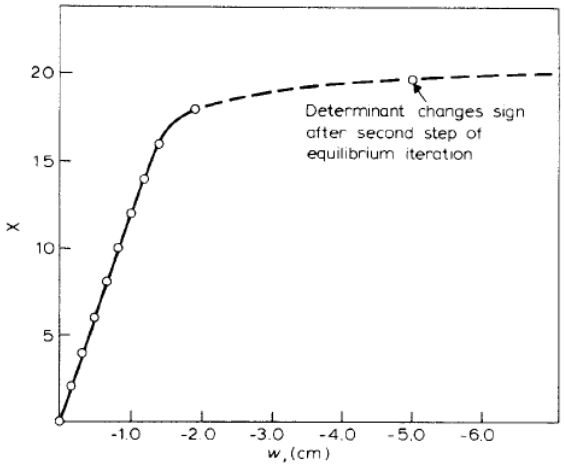

***Figure 59**: Transverse displacement w at windward meridian (throat point) versus load intensity factor* (Mang, *et al.*, 1983)

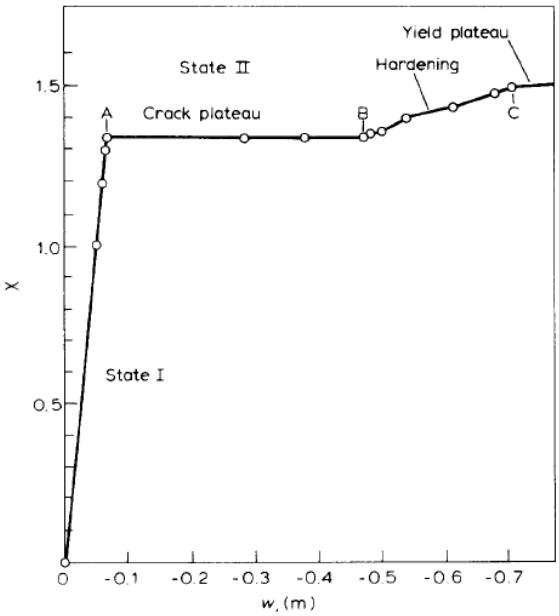

***Figure 58**: Transverse displacement w at $\theta = 37.9^0$ (throat point) versus load intensity* (Mang, *et al.*, 1983)

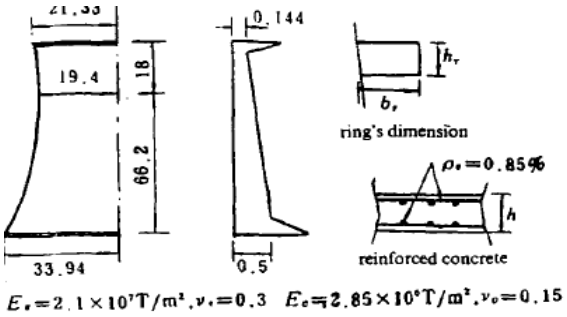

***Figure 60**: Cooling tower dimensions* (Long-yuan & Wen-da, 1987)*)*

The typical load-displacement path (*Figure 58* and *Figure 59*) was noted to consist of two points. One characterised by intact concrete (linear) and the other by fractured concrete (non-linear). The second part is divided into a crack plateau, hardening section, and yield plateau. It was shown, by varying the reinforcement percentages, that the ratio of the crack loads is approximately equal to the corresponding membrane stiffness. In addition, it was shown that the crack plateau length decreases with increasing reinforcement percentage and the ultimate-crack load difference increases with increasing reinforcement percentage. The authors noted that the tensile strength of concrete is crucial for the safety of cooling tower shells since their failure is by tension/cracking of the concrete first. They also noted that further experimental investigations should consider the influence of cracking of concrete and the non-axisymmetry of the load.

About six years later, (Long-yuan & Wen-da, 1987) were to study the post-buckling analysis of a hyperbolic cooling tower shell with discrete fixed supports when subjected to wind loads. They analysed a 90m high cooling tower (see *Figure 60*) using a developed numerical solution for hyperbolic cooling tower shells. A 250mm deep x 500mm wide ring stiffener at the throat of the cooling tower was assembled in the model. The influence of placing the ring stiffener on the instability loads was also studied. The results of the stiffened and the unstiffened cooling tower models were compared.

The influence of geometric non-linearities on pre-buckling of the hyperbolic cooling tower was observed to be very slight. The results obtained from the linear buckling analyses had good approximations. They concluded that by placing a ring stiffener (250mm x 500mm) at the cooling tower's throat, the instability critical load can be raised by about 30%.

Another six years later, (Radwanska & Waszczyszyn, 1995) had to perform a numerical buckling analysis of a hyperbolic cooling tower shell with measured and theoretically-modelled imperfections. In their study, geometrical imperfections were measured on a 20 year old reinforced concrete cooling tower (see *Figure 63*) using photogrammetric techniques. Three models of the shell geometry were analysed:

- A cooling tower with a perfect hyperbolic meridian (P);
- The measured shell with imperfections (M) and
- Theoretical imperfections corresponding to primary buckling modes of the perfect shell (T).

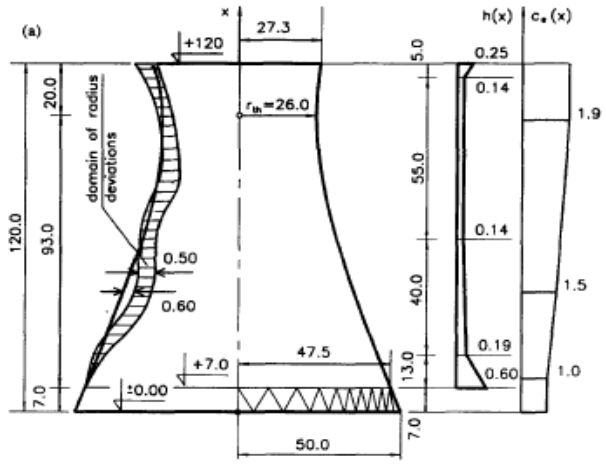

***Figure 63**: Cooling tower shell with measured radial deviations* (Radwanska & Waszczyszyn, 1995)

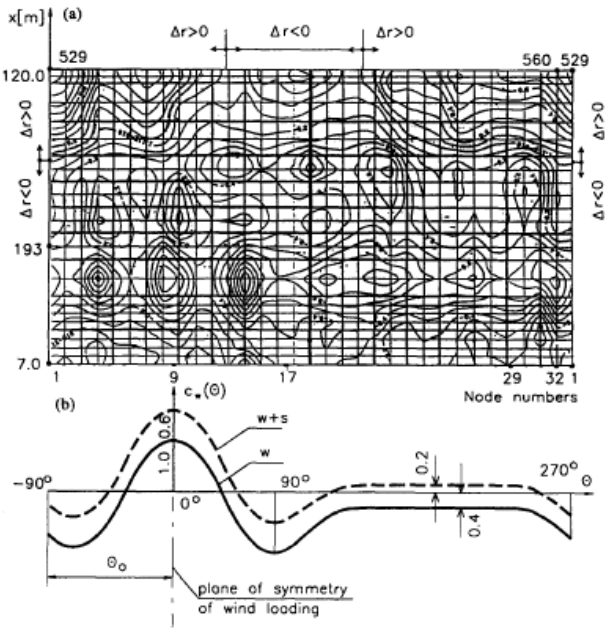

***Figure 64**: (a) Contour lines of radial imperfections; (b) Coefficient of wind load* (Radwanska & Waszczyszyn, 1995)

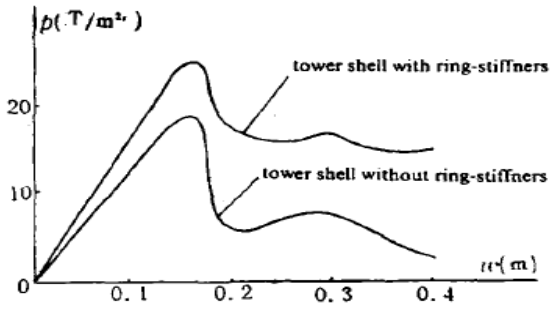

***Figure 61**: Nonlinear buckling results of cooling tower at cooling tower top against wind surface* (Radwanska & Waszczyszyn, 1995)

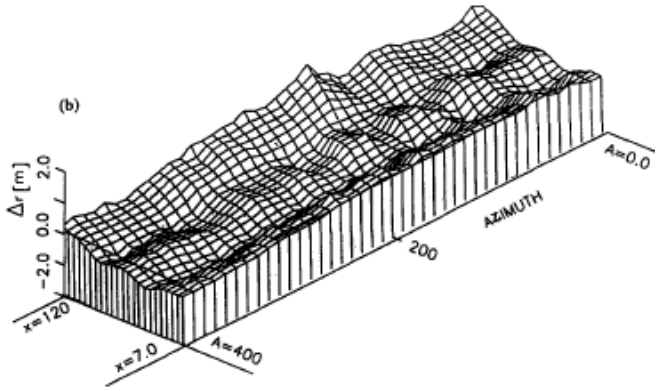

***Figure 62**: Isometric view of radial deviations* (Radwanska & Waszczyszyn, 1995)

The imperfections related to the radii of the real shell were considered as the input data to create the real cooling tower model and an imperfection contour surface created (see *Figure 62*). A non-linear analysis on the three shell models was performed. An evaluation of the most dangerous direction of the wind load was done and compared to the real shell imperfection contour surface.

They concluded that the study's assumption of a linear elastic material led to the cooling towers instability by bifurcation. When the measured radial imperfections were compared to the buckling mode of the perfect shell under dead load, some similarities were observed (see *Figure 61* and *Figure 64*). The study concluded that this partially confirmed the hypothesis that imperfections can be caused by dead loads during the construction of cooling towers. Buckling loads for the measured imperfections (M) case were found to be lower than the critical loads of the perfect shell (P) case by about 15% to 35%. The study confirmed that besides the material nonlinearity, more realistic models were required for geometric imperfections in order for cooling tower shell behaviour to be understood.

A decade later, in his paper dedicated to a well recorded research working relationship with Michael Thompson at the University College London, (Croll, 2006) elaborated the general theme of the development of the reduced stiffness method in the theory of the shell buckling. He was interested in tracking his own interest in the development of shell buckling theories.

(Croll, 2006) recognised the strong influence of membrane actions in controlling the critical eigenvalues of shells. The largely in-extensional critical buckling mode regains stiffness in the non-linear, post buckling, regime due to an increase in the contribution of membrane stiffness in a shell. The non-linearity is a result of changes in the membrane stiffness. Most design codes allow for an estimation of the safe load carrying capacity of the shell in the elastic range. The reduced stiffness method provides the designer with a rational basis for the prediction of a safe lower bound to buckling which is sensitive to imperfections for most shells, cooling towers included.

Half a decade later, (El Ansary, *et al*., 2011) developed a numerical tool that achieves an optimum shape and structural design of a hyperbolic cooling tower by combining non-linear finite element analysis, geometric modelling with a B-spline function and real coded genetic algorithm (RCGA) techniques. The investigation was divided into two parts:

- The optimum shape of the cooling tower was investigated to achieve minimum global weight assuming a constant shell thickness. The shell rings radii were taken as design variables. The shape optimisation was then formulated taking into account different constraints like strength requirements, buckling capacity, construction practicality (formwork) and thermal efficiency/functionality of the cooling tower;
- The same study was extended by introducing the cooling tower shell thickness as an extra design variable. This second part was meant to predict an optimum cooling tower shell and corresponding optimum shell thickness. The following numerical tools were combined in the study:

1) B-Spline curves adopted to generate finite element mesh (see *Figure 65*);
2) Finite element modelling (FEM) to study cooling tower response under loads;
3) Real coded genetic algorithm RCGA to optimise the shape and thickness of the tower;

Geometric B-spline modelling of cooling tower:
The surface of revolution was generated by rotating a B-spline curve (generatrix) as shown in *Figure 65*. The control points $P_{i,j}$ are generated by revolving this generatrix's control points along the path of a chosen circles control points, forming a mesh of points that create a surface.

Finite Element Formulation:
Sub parametric triangular shell elements (as shown in *Figure 66*) were used to develop a numeric model of the cooling tower. 24 elements along the horizontal direction and 20 elements along the vertical direction (480 total) were used to develop a finite element model of the cooling tower. The study assumed a simply supported base and a linear elastic behaviour of the shell material.

RCGA Optimisation technique:
The design variables were encoded in an algorithm as real numbers. Some parameters were first defined as design variables, design constraints and genetic operators. The structural design variables were considered to be the ring radii and the cooling tower shell thickness. The design constraints were considered to be as follows:

- thickness of cooling tower should be adequate to sustain design loads and avoid elastic buckling and instability;
- the maximum circumferential and meridional compressive stresses resulting from the loads should be less than the allowable stresses and;
- the same condition for tensile stresses was imposed in-order to avoid cracking of the cooling tower shell under wind loads.

A construction practicality constraint was imposed to restrain the slope of the shell surface from exceeding a certain value (20°) which is normally governed by the maximum slope that is feasible for form-work systems. A constraint related to the cooling tower functionality was imposed for the inner volume of the tower to have a specific capacity which is normally controlled by thermal capacity requirements. The genetic algorithm technique applied the selecting crossover and mutation operators. A random selection of a number of cooling towers with varying geometry and thickness was selected first (initial population). Crossover and mutation operators were applied to this initial population in order to generate a new population of cooling towers having geometrical shapes and thickness that lead to a reduction in the cooling tower weight. The initial "tower population" was replaced by the "new population" with better "fitness". The steps were repeated for a certain number of generations until a global optimum solution was obtained (40 generations were adopted in this study). *Figure 67* shows a flow chart of the algorithm steps. *Figure 68* shows a comparison of the reference and optimum cooling tower moments.

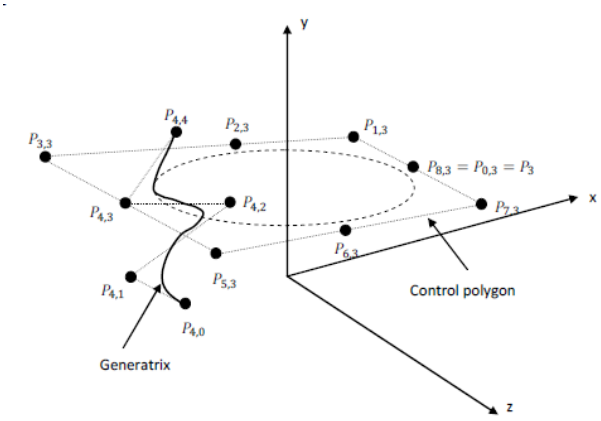

***Figure 65**: B-spline curve representing surface of revolution* (El Ansary, *et al.*, 2011)

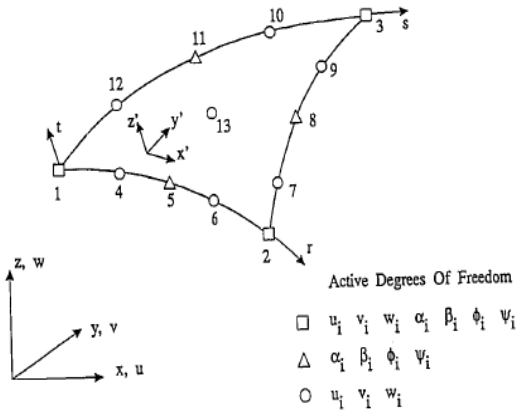

***Figure 66**: Consistent shell element coordinate systems and degrees of freedom* (El Ansary, *et al.*, 2011)

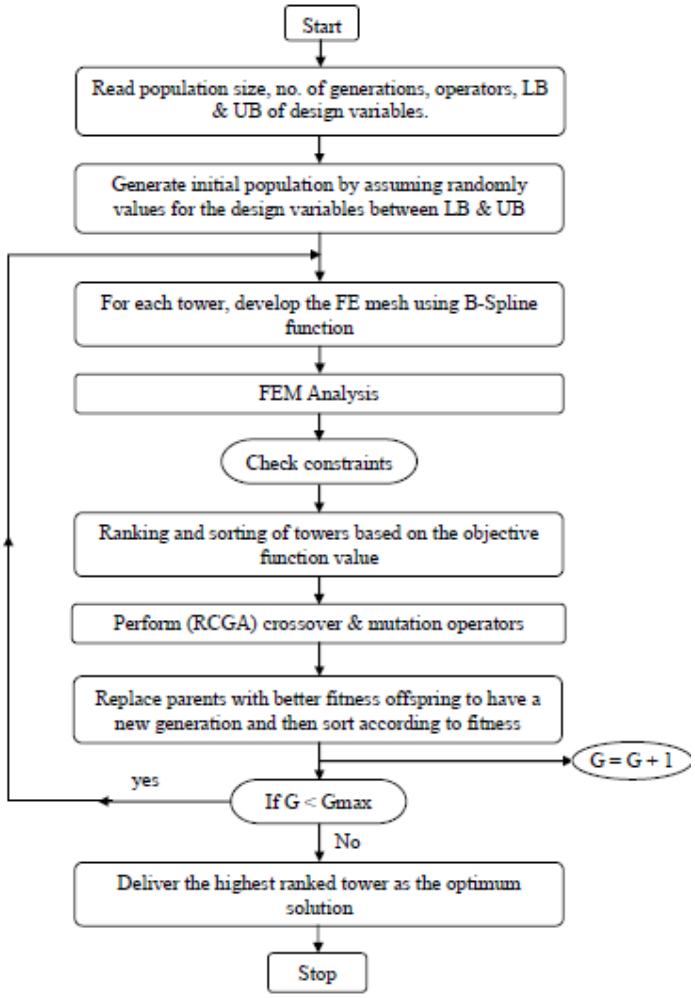

***Figure 67**: Flow chart for optimum shape and design of cooling towers* (El Ansary, *et al.*, 2011)

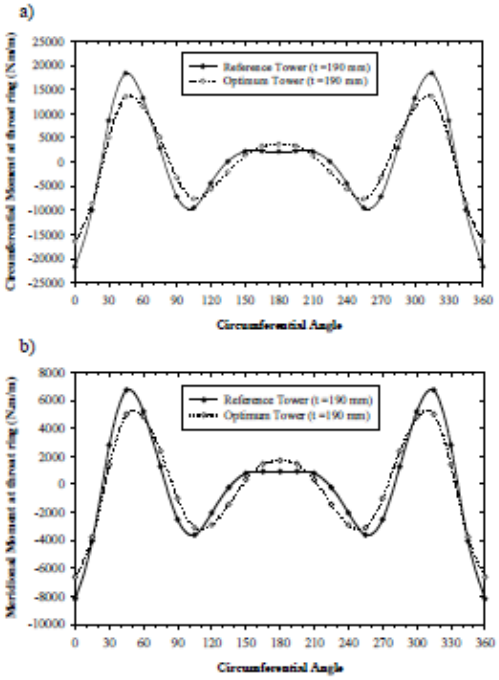

Fig. 9 Comparison between reference and optimum tower for case of moments
a) Circumferential moment b) Meridional Moment

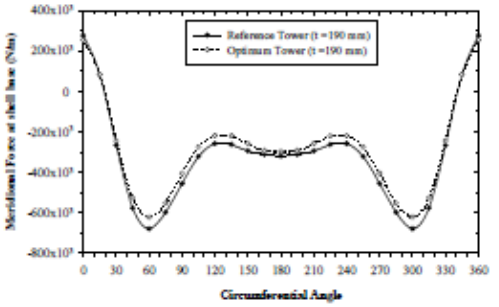

***Figure 68**: Comparison between reference and optimum cooling tower* (El Ansary, *et al.*, 2011) *r*

When the shell thickness was excluded from the set of design variables (first analysis), the hyperbolic shape of the reference cooling tower was considered to be close to optimum. The optimum shape of the cooling tower lead to a reduction of circumferential and meridional bending moment of up to 26% and 25% respectively. A minor 7% reduction in meridional forces was observed at the cooling tower base. When the cooling tower shell thickness was considered as one of the design variables, the optimum shell thickness lead to about 13% reduction in the cooling tower weight compared to the reference cooling tower with a reduction in thickness from 190mm to 165mm. Reductions of 40% and 22% in the maximum circumferential and meridional bending moments respectively were achieved. A 25% reduction in maximum axial stress at the base was achieved.

2.3.2 Numerical studies

(Zerna, *et al.*, 1983) solved the equations of the bending and stability theories for the orthotropic shell using the finite element method. By considering the bi-axial stress-strain relationship for concrete, reinforcing steel as well as a layered reinforced concrete shell element (see Figure 70), the study determined the variation of the load factor λ_B when the load is increased. The stability equation

$$(K_E + \lambda_B K_G)Y = 0 \quad \ldots\ldots [36]$$

was solved where: K_E = material stiffness matrix, K_G = geometric stiffness matrix Y = displacement vector. Two different height and diameter cooling towers were analysed.

They concluded that buckling was observed to be a local commencing phenomenon due to either unavoidable imperfections or the type of the loading. The global buckling safety factor can be reduced by more than half of its value near the ultimate load when the stress dependant tangent moduli under biaxial stress state are considered in the calculation. In both cooling towers, local buckling preceded failure due to the loss of material strength. This was because

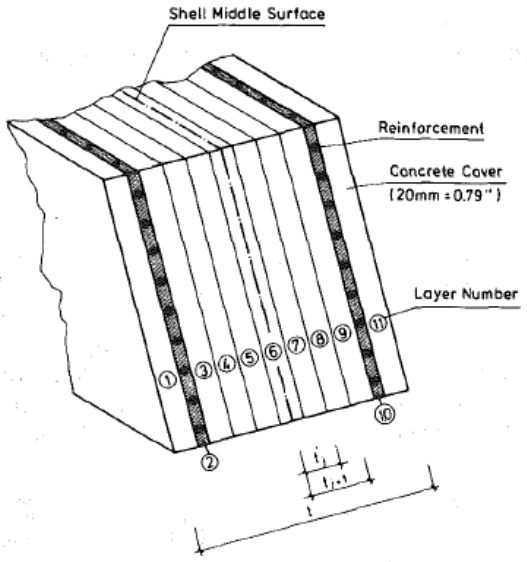

***Figure 69**: Layered RC shell element (Zerna, et al., 1983)*

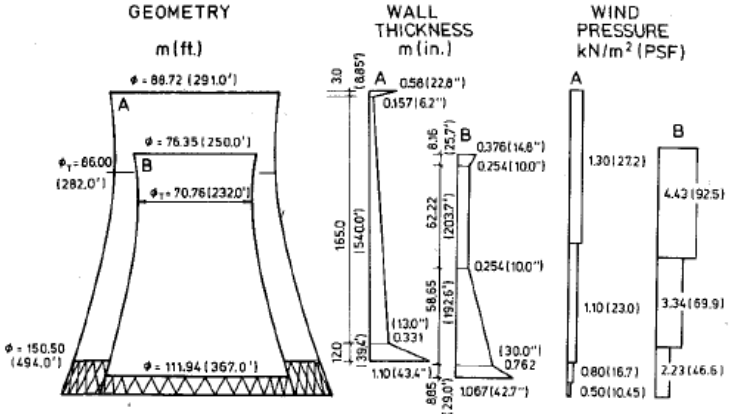

***Figure 70**: Investigated cooling tower shells (Zerna, et al., 1983)*

the local buckling safety factor was noted to be lower than the ultimate load factor. When the dead and wind loads were increased simultaneously lower buckling safety factors were observed compared to when only the wind load was increased independently of the dead load. The study observed that it is possible to design a **balanced** hyperbolic cooling tower (shell having nearly the same buckling safety at every region) regardless of the axisymmetry or non-axisymmetry of the wind loading. The discovery of the balanced cooling tower approach leads to economic material use that matches the local buckling safety factor everywhere in the cooling tower shell.

A decade later, (Rao & Ramanjaneyulu, 1993) observed that the Der and Fidler (1968) formula for checking the buckling safety of cooling towers under wind loading had been obtained from tests on models with uniform thickness, constant wind pressure coefficients along the height of the shell and without a ring stiffener at the top. They noted that this formula therefore had limitations. In their study, they considered the local enhancement of wind pressure coefficients at the cooling tower's top gradual thickening of the shell's thickness and addition of a top ring stiffener. A parametric study was undertaken to investigate the buckling behaviour of the cooling tower when the above parameters were changed.

The general circumferential wind pressure was expressed as a Fourier series and the vertical pressure distribution increased locally at the cooling tower top. A parametric study was carried out on the cooling tower shown in *Figure 71* and the influence of the following parameters in the buckling behaviour of the cooling tower shell under wind loading was investigated:

- Ring stiffener at the top of the cooling tower;
- Gradual thickening of the shell at the bottom;
- Vertical cracking due to the thermal gradient.

They performed a buckling analysis of the shell using different ratios of the ring stiffener to shell wall second moment of area I_r/I_s in order to arrive at a minimum size of the top ring stiffener. Gradual variations of the shell thickness at the bottom 20% to 70% of the total height were factored into the analysis and critical buckling factors obtained.

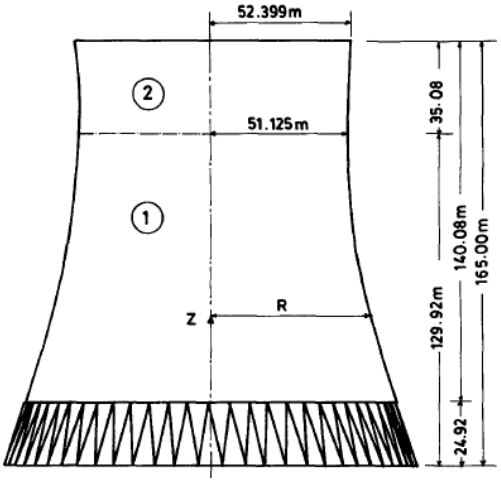

Figure 72: Geometry of cooling tower considered for parametric study (Rao & Ramanjaneyulu, 1993)

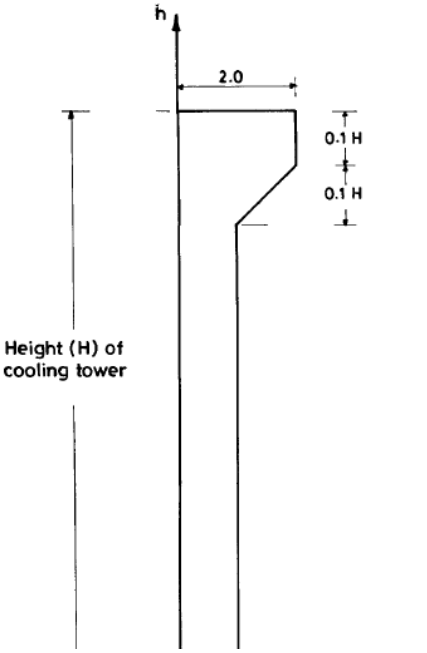

Figure 71: Assumed external pressure coefficient along cooling tower height (Rao & Ramanjaneyulu, 1993)

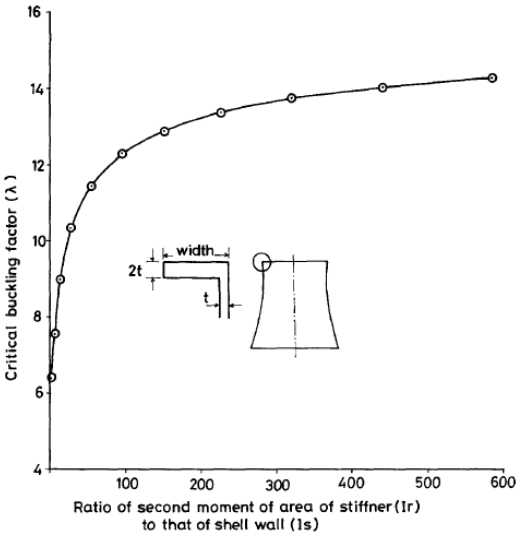

***Figure 73**: Influence of top ring stiffener on buckling resistance of cooling tower* (Rao & Ramanjaneyulu, 1993)

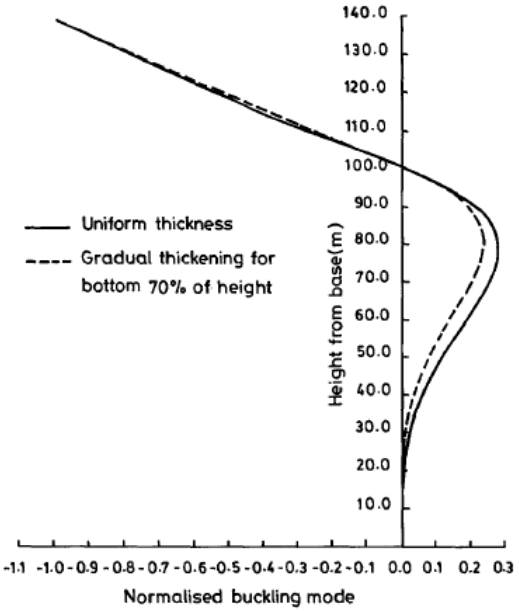

***Figure 75**: Influence of gradual thickening on pattern of buckling* (Rao & Ramanjaneyulu, 1993)

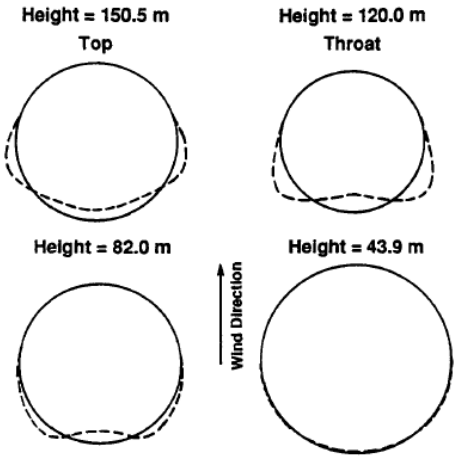

***Figure 76**: Deformed shapes* (Mahmoud & Gupta, 1995)

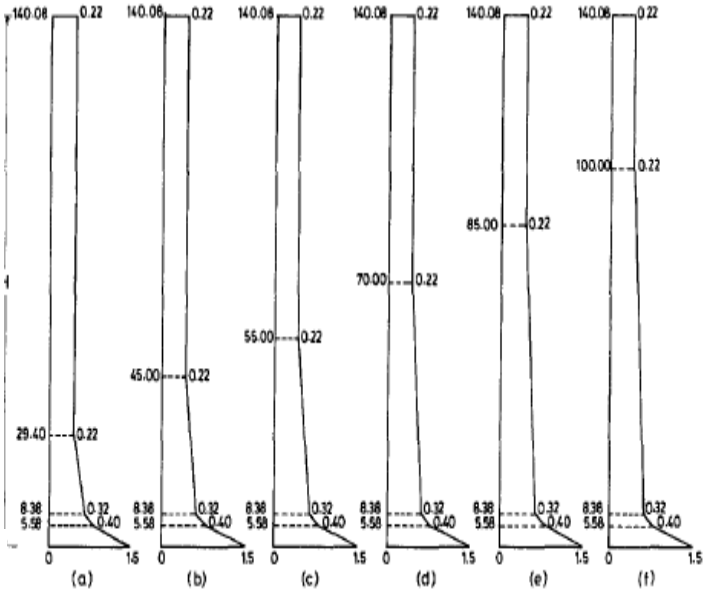

***Figure 74**: Different patterns of gradual thickening for (a) 20% of H; (b) 30% of H; (c) 40% of H; (d) 50% of H; (e) 60% of H and (f) 70% of H* (Rao & Ramanjaneyulu, 1993)

The authors concluded that the buckling behaviour obtained when wind pressure coefficients for the top 20% of the cooling tower height compared closely with the Der and Fidler's wind tunnel study results. Gradual thickening of the shell wall alone did not change the buckling strength significantly and there was no difference in the magnitude of the mode shapes. The top stiffener alone increased the buckling strength and the maximum buckling mode amplitude shifted from the top edge to the shell interior. The critical buckling factors were increased when the shell wall gradual thickening was provided in addition to the top ring stiffener. The results are represented in *Figure 73*, *Figure 75* and *Figure 74*.

The results of this study confirmed the findings of the preceding studies (Der and Fidler, 1968, Mungan *et al*, 1984). It also provided guidelines on the size of the top ring stiffener to obtain an optimum buckling strength.

The consideration of localised increased wind pressures at the cooling tower shell was a key development that reinforced the occurrence of the first buckling dimple at the top of the windward meridian of an unstiffened cooling tower shell.

Two years later, (Mahmoud & Gupta, 1995) investigated the inelastic large displacement behaviour of the Grand Gulf Nuclear Power Station (Mississippi) cooling tower that had been studied before by various other researchers (Mang, *et al.*, 1983), (Milford and Schnobrich, 1984), (Gupta and Maestrini, 1986), (Min & Gupta, 1993). They were interested in establishing the effects of large displacements on the cooling tower behaviour. The preceding studies had ignored the influence of large displacements in treating the behaviour of the cooling tower.

The Mahmoud and Gupta (1993) computer program was modified to include the effects of large displacements together with the effects of tension stiffening, concrete stress-strain curve non-linearity, and the chance of two orthogonal element cracks. A displacement based numerical analysis was performed taking into account effects of tension stiffening, concrete cracking strength and reinforcement yield stress. The study's results are shown in *Figure 76*, *Figure 77*, *Figure 78* and *Figure 79*.

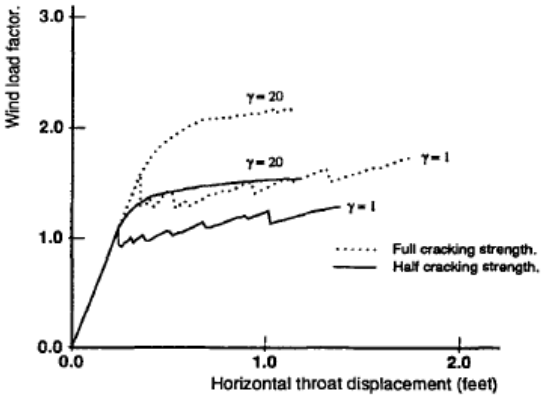

***Figure 77**: Load-deflection curves for full and half cracking strength* (Mahmoud & Gupta, 1995)

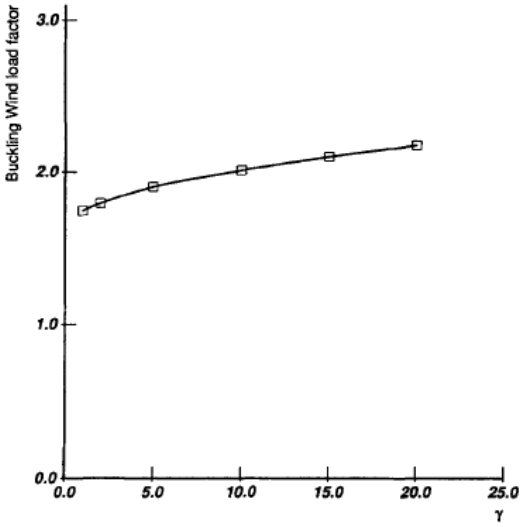

***Figure 78**: Variation in buckling wind load factor with cracking strength* (Mahmoud & Gupta, 1995)

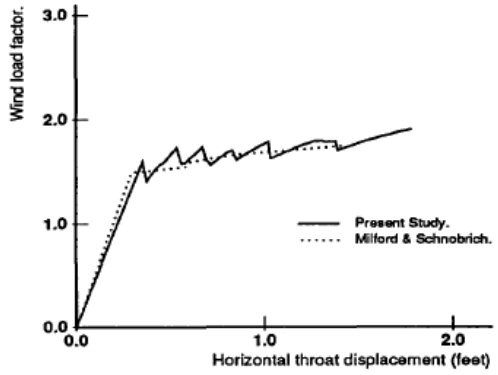

***Figure 79**: Load deflection curves Milford and Schnobrich(1984) and* (Mahmoud & Gupta, 1995)*)*

```
Procedure AG
begin
        generation t = 0
        create at random population P(t)
        evaluate P(t)
        while termination criterion is not valid
            begin
                generation t = t+1
                select P(t) from P(t−1)
                crossover P(t)
                mutate P(t)
                evaluate P(t)
        end
end
```

***Figure 80**: The structure of the genetic algorithm* (Pieczara, 1999)

Although the load-displacement characteristic were very similar to those by previous studies, it was found that the failure mode was not by yielding of meridional reinforcement obtained in the preceding studies but was rather by the circumferential buckling of the shell in the cooling tower throat region. The maximum displacements were observed to be at the throat level. The analysis output displayed large unbalanced forces in the vicinity of the throat. The buckling wind load factor increased with tension stiffening. It was also observed that the buckling wind load factor reduced significantly when the cracking strength of the concrete was reduced. On comparing the results of their study with those of the preceding studies, it was observed that when the large-displacement effect was neglected the failure of the cooling tower was due to yielding of the meridional reinforcement. It was also found that neither of the preceding studies had considered re-analysing the cooling tower using a higher yield stress for the reinforcement. In this particular study, when the reinforcement yield stress was increased to avoid yielding, there was no change in the behaviour of the cooling tower (failure was concluded to be circumferential buckling of the shell's throat region).

The design philosophy at the investigation time did not consider buckling as the intended mode of failure. On the other hand, there was no simple way of predicting the buckling wind load of a cooling tower other than performing a non-linear analysis. Further research is required to develop simple methods of predicting the buckling loads of cooling tower shells for use in designing.

Four years later, (Pieczara, 1999) investigated the optimisation of the cooling tower shell by using a genetic algorithm through considering the shell wall thickness at the nodal points of finite elements as the decision variables. The genetic algorithm approach was to create a population of members for every generation of wall thickness *(t)*. The evaluation of each members' performance assigns selection probabilities to each design member. A new generation of wall thickness *(t+1)* was created by the selection of designs for the processing. A crossover operator was created to exchange properties of each pair of designs. A mutation operator mutated some properties of the design. The genetic algorithm was then called iteratively. The structure of the genetic algorithm is shown in *Figure 80*. The hyperbolic cooling tower model was divided into seven exact finite elements (EFEs) and an axisymmetric wind pressure applied. An optimisation process was undertaken with vector decision variables (8 nodal wall thickness).

Results of the optimisation by applying the genetic algorithm (GA) were compared to those by formulation using the direct search (DS) method. It was also noted that the genetic algorithm obtained the minimum global cooling tower shell volume in 20 seconds. For the same mode, the direct search formulation method needed 5 minutes.

Half a decade later, (Min, 2004) developed an iterative numerical computational algorithm to design a plate or shell element subjected to membrane forces and bending moments. The algorithm was based on an equilibrium consideration for the limited ultimate state of reinforcement and cracked concrete. The algorithm was verified on an element level by running several experimental designs. On a global structural level, the author performed a design of a hyperbolic cooling tower by checking the design strength in order to verify the adequacy of the algorithm. The study performed the design of the reinforcement by considering both the combined membrane forces and bending moments obtained from the finite element analysis of the cooling tower

***Table 4**: Comparison of the results of optimisation* (Pieczara, 1999)

Decision variables x_i	Position of decision variables h_i [m]	Values of decision variables [m]			
		Eckstein *et al.* (1984)	Substitute Hartley model		Real model
			GA formulation (15)	DS formulation (10)	DS formulation (10)
x_1	140.08	0.90	0.6001	0.6000	0.6000
x_2	135.88	0.22	0.2041	0.2000	0.2018
x_3	105.88	0.22	0.2650	0.2652	0.2762
x_4	65.08	0.30	0.2878	0.2884	0.2855
x_5	33.58	0.30	0.2878	0.2884	0.2855
x_6	8.40	0.32	0.2878	0.2885	0.2855
x_7	5.60	0.40	0.2878	0.2886	0.2855
x_8	0.00	1.50	0.6003	0.6000	0.6000
Volume [m^3]		16 515.8	14 752.4	14 751.7	14 792.4
Critical load factor		6.35	6.35	6.35	6.35
Volume reduction [%]			11	11	10

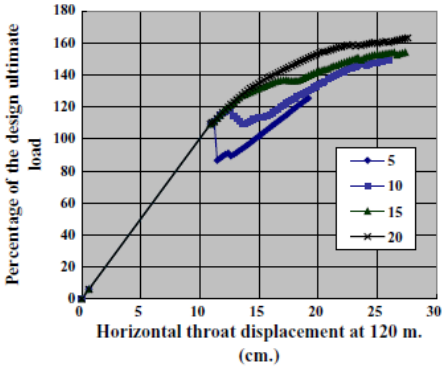

***Figure 82**: Load and throat displacement curves for the cooling tower with tension stiffening ranging from 5 to 20* (Min, 2004)

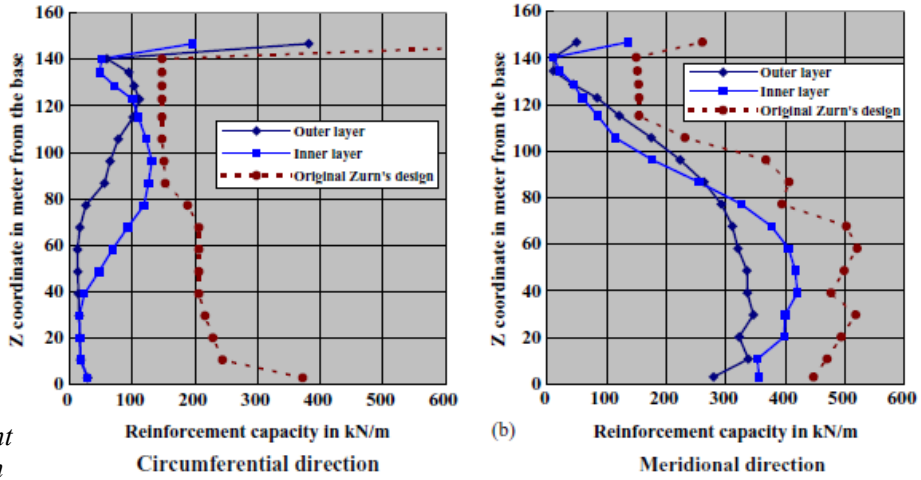

***Figure 81**: Reinforcement designs from original designs compared to that obtained by* (Min, 2004)

and applying the design ultimate load combinations. This approach was in contrast with conventional cooling tower design approach which is based only on the membrane stresses with the bending stresses ignored (ACI-ASCE, 1977, Gupta, 1978). The conventional approach of ignoring bending stresses is mainly because bending plays a secondary role. With this approach, the author's intention was that the cooling tower fails by yielding of the reinforcement and not by buckling or instability. The design was based on the Grand Gulf Nuclear Power Station (Mississippi) cooling tower that had been studied before by other researchers (Mang, *et al.*, 1983), Milford and Schnobrich 1984, 1986, Gupta and Maestrini, 1986, Min and Gupta, 1992, 1993, (Mahmoud & Gupta, 1995), Noh, 1999, (Choi & Noh, 2000). The cooling tower was designed for the load case *(0.9D +1.3W)/0.9* and the adequacy of the design method evaluated by performing a non-linear inelastic finite element analysis. The results of the analysis are shown in *Figure 81* and *Figure 82*.

The original design reinforcement was found to be well covered in capacity required by the Min (2004) design. A load factor of 1.11 and a throat displacement of 112mm was obtained when the nonlinear inelastic analysis, taking into account a tension stiffening parameter of 5, was performed. Yielding of the meridional reinforcement was observed in one of the windward element. After running a numerical experiment to prevent the steel yielding, it was observed that preventing steel yielding does not change the behaviour of the cooling tower. Neither was there any change in the calculated ultimate load for a tension stiffening parameter of 5. On observing the sliced deformed shapes of the cooling tower from the top, the maximum displacements were noted to be near the throat. The cooling tower displayed buckling considerably in the circumferential direction. Min concluded that it is this circumferential buckling of the cooling tower around the throat that leads to failure. The failure mode designed for the tower was circumferential buckling caused by loss of bending stiffness in this direction. Yielding of reinforcement was observed on one element in the wind ward meridional direction but this was noted to be of no effect on the ultimate behaviour of the tower. The design algorithm

using combined membrane and flexural stresses can be improved to be a general design method for reinforced concrete and plates. The author concluded that further studies in this area will be necessary.

Two years later, (Sabhouri-Ghomi, *et al.*, 2006) studied the relationship between the stiffening ring parameters (number, dimension and location of rings) on the maximum buckling stability of a hyperbolic cooling tower. The 92m high S. Montazer Qaem power plant (Iran) hyperbolic cooling tower was selected to be the basis of the study. Using finite element analysis, seven configurations were modelled with 400mm x 1000mm stiffening rings placed at different heights of the cooling tower (see *Figure 83*). The optimal positioning of these stiffening rings was determined by examining the cooling tower buckling modes and their associated buckling capacities. The stiffening ring thickness and quantity parameters were varied to obtain a relationship between these parameters and the buckling safety factor (BSF). In addition, the stiffening ring widths and quantity parameters were also varied to investigate their relationship with the BSF.

The maximum BSF was obtained with the stiffening ring located at 55m from the cooling tower bottom. The first-mode buckling deformation was also found close to this height. The BSF was found to increase proportionately with the increase in the stiffening ring thickness up to a thickness value of 400mm. For stiffening ring thickness greater than 400mm, too significant increases in the BSF were observed. On introducing more 300mm thick or higher stiffening rings, the buckling deformation shifted from the shell to the X-shaped columns. At 300mm, the stiffening rings were stiff enough to be considered rigid. Figure 84 shows results of the analysis performed.

The authors therefore noted that the stiffening rings could be divided into flexible stiffness (thickness less than 300mm) and rigid stiffness (thickness greater than 300mm). Additional 200mm (or less) thick stiffener rings were observed to not efficiently increase the BSF compared to 400mm thick rings.

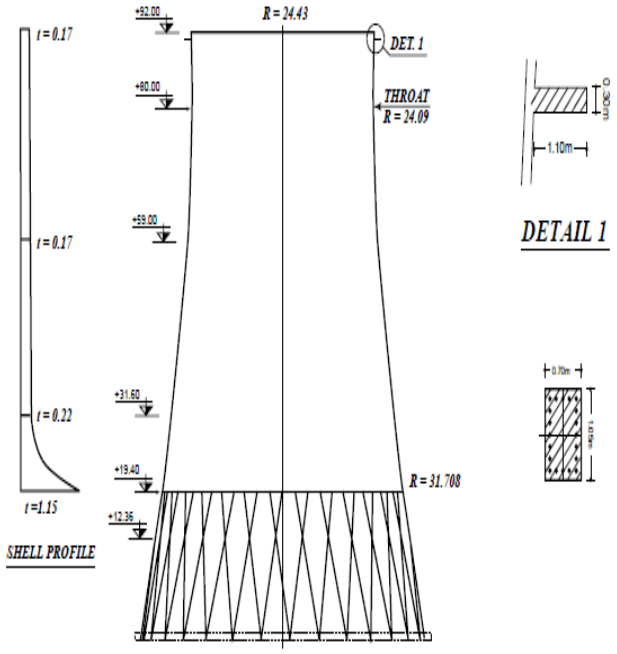

***Figure 83**: Elevation and details of the S. Montazer Qaem cooling tower* (Sabhouri-Ghomi, *et al.*, 2006)

They therefore encouraged increasing the additional stiffening rings thickness whilst discouraging the addition of extra stiffening rings in order to increase the buckling stability of a cooling tower. On increasing the stiffening rings width and quantity, the BSF was observed to increase in proportion to the stiffener ring width increase. The rate of the BSF increase was observed to significantly decrease once the ring width approached a value of **six times** the minimum shell thickness. The analysis method studied by the authors can be used as a benchmark in the designing of cooling towers.

In the same year, (Andres & Harte, 2006) reviewed preceding and new developments in the numerical simulation of the buckling phenomena of shells. They were interested in discussing in detail the algorithms for finite element methods in classical stability methods and their application to concrete shells. In their paper, they described an approach to find more realistic buckling loads for a number of shell structures, cooling towers included. In order to establish the multiple equilibrium states for buckling (pre- and post-buckling, the equations for neutral equilibrium were formulated and are shown.

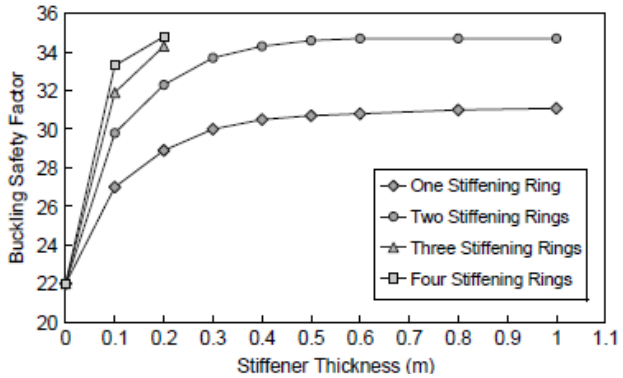

***Figure 84**: Buckling safety factor (BSF) of stiffening ring's thickness for the R.C cooling tower with different number of stiffening rings* (Sabhouri-Ghomi, *et al.*, 2006)

State of equilibrium	Stiffness-parameter	determinant $\mathbf{K}_T$	Diagonal values
stable	$S_p \neq 0$	$\det \mathbf{K}_{Td} > 0$	$\forall\, D_{ii} > 0$
neutral (snap-through point)	$S_p = 0$	$\det \mathbf{K}_{Td} = 0$	$\exists\, D_{ii} = 0$
neutral (bifurcation point)	$S_p \neq 0$	$\det \mathbf{K}_{Td} = 0$	$\exists\, D_{ii} = 0$
unstable	$S_p \neq 0$	$\det \mathbf{K}_{Td} \neq 0$	$\exists\, D_{ii} < 0$

***Table 5**: Parameters for identification of critical states of equilibrium* (Andres & Harte, 2006)

The stiffness parameter was presented as an observation parameter to signal a neutral equilibrium point (*Table 5*). The other is the determinant of the stiffness matrix as shown in the equations below. For snap-through behaviour, the stiffness parameter = 0. For bifurcation behaviour, the determinant of the stiffness matrix = 0.

$$K_T \,.V_{alt}^{+} = 0 \text{…..……[37]}$$

$$S_P = \left(\frac{\Delta\lambda_i}{\Delta\lambda_1}\right)^2 . \frac{V_1^T.K_{T1}.V_1}{V_i^T.K_{Ti}.V_i} \text{……..[38]}$$

A simple iterative approach was employed to calculate the buckling loads and modes of shell structures, cooling towers included. The Grand Gulf Nuclear Power Plant (Mississippi) cooling tower was used as an example. The analysis was first done using the same concrete and reinforcement material properties that had been used by other researches before (Mahmoud and Gupta, 1993); (Mang, *et al*., 1983); Min 1992). The same analysis were repeated using a high strength concrete. *Figure 86* and *Figure 87* show the analysis results.

They concluded that the classical linear buckling analysis of the cooling tower shell led to a buckling factor of 9.3 for normal concrete and 9.6 for the high strength concrete. There was no significant difference in the buckling modes for the two concrete materials. For the linear elastic analysis, the snap-through phenomenon was noticed on the load displacement curves. The mode of buckling was a single buckle in the highest compression region of the lower section of the tower. For the non-linear analysis, the behaviour was noticed to be different. A non-linear load displacement relation in the pre-buckling state due to concrete cracking in the windward meridian was observed. The snap through occurred at a load about 30% lower than that for the linear elastic analysis. The buckling behaviour for the high strength concrete was not very different although considerable smaller displacements until total failure were observed due to a reduced ductility of the high strength concrete.

The presented algorithm can allow a realistic approach of the expected stability phenomena. This was a significant development of a numerical tool that simulates non-linearity of concrete shells during the buckling phenomena. The algorithm provides the design engineer with tools to test the cooling tower shell against buckling failure in order to determine optimal shapes of the shell.

Six years later, (Tomas & Tovar, 2012) studied the influence of an initial geometric imperfection on the buckling load of various single and double curved concrete shells. They were interested in determining the imperfection sensitivity factor graphically for concrete shells of different geometries (spherical dome, barrel vault, hyperbolic paraboloid and hyperbolic rotational surface: cooling tower). The results were compared to those studied by the International Association for Shell and Spatial Structures (IASS). The geometric imperfection sensitivity factor is the ratio of the upper critical buckling load (calculated by a geometric non-linear analysis) to the buckling critical load for linear homogeneous material (calculated by a linear or eigenvalue analysis). Although the study focussed on several shell geometries, only the hyperbolic rotational surface (cooling tower) is of particular interest to this literature review.

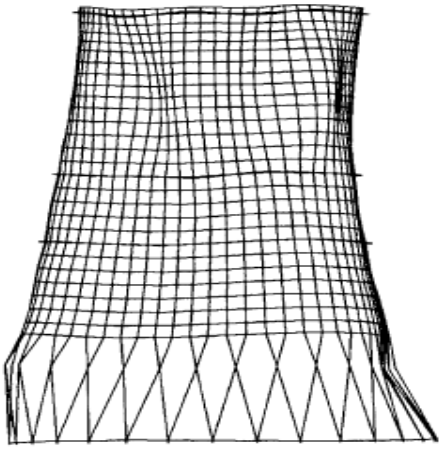

Figure 85*: Deformed shape of first buckling mode due to wind and dead loads of cooling tower with two stiffening rings at 44m and 55m height* (Andres & Harte, 2006)

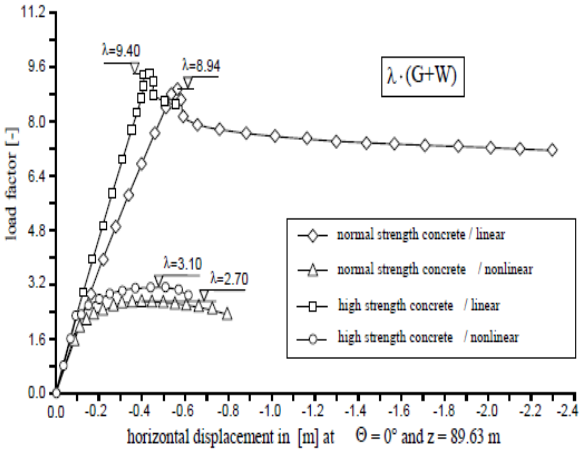

Figure 86*: Load-displacement-curve of different analysis of the cooling tower* (Andres & Harte, 2006)

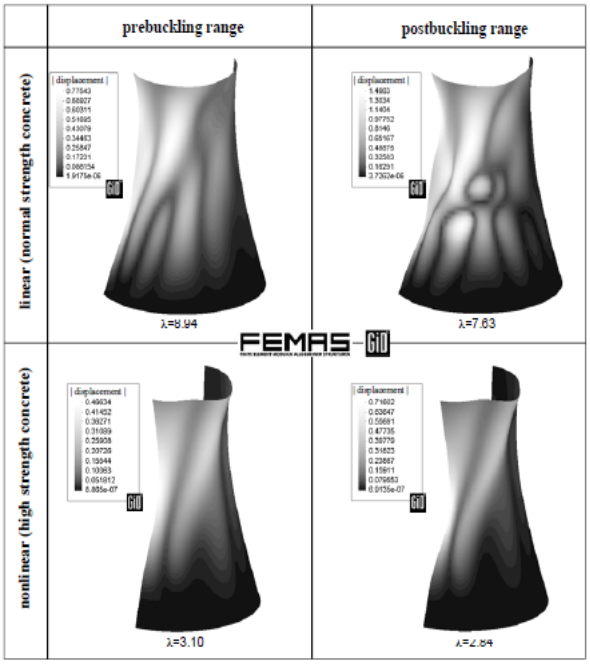

Figure 87*: Displacement patterns in the prebuckling and postbuckling state of a linear and nonlinear analysis* (Andres & Harte, 2006)

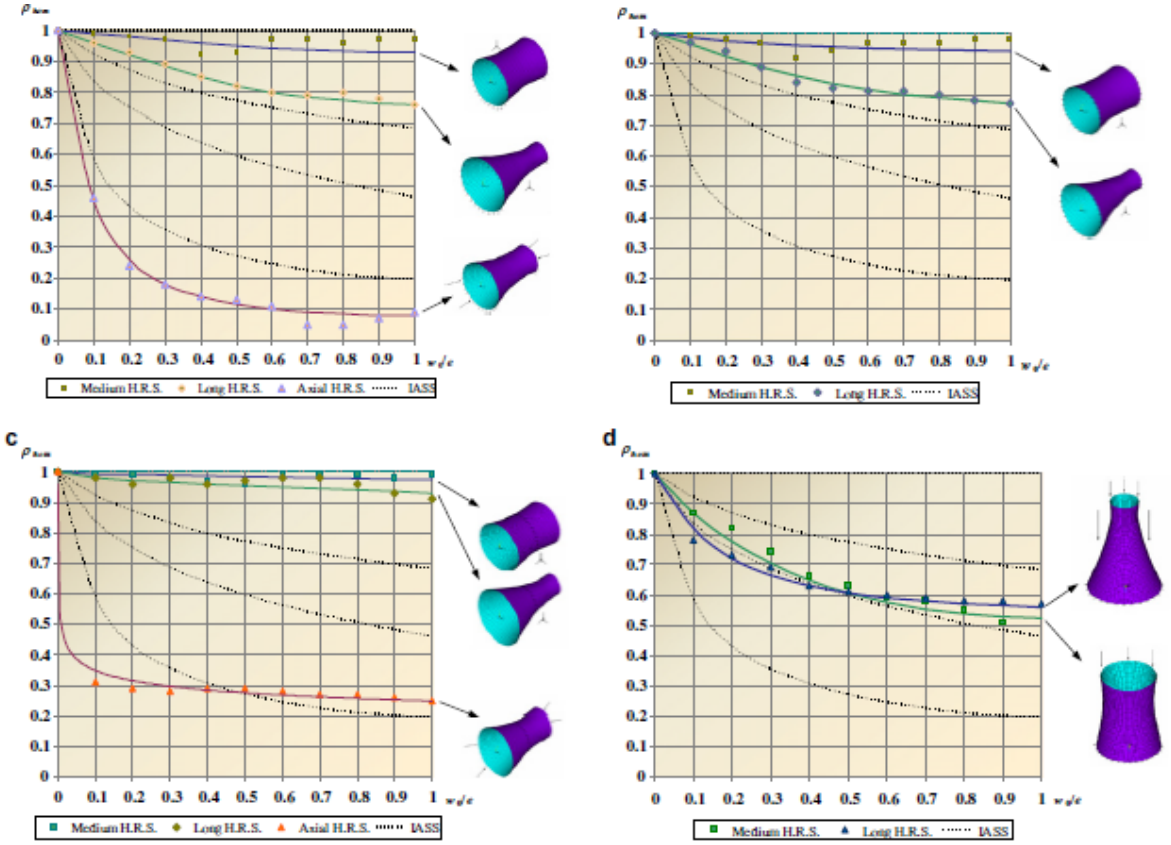

***Figure 88**: Imperfection sensitivity factors* (Tomas & Tovar, 2012)

Figure 88, *Figure 90* and *Figure 89* show the results obtained from the analysis.

The imperfection sensitivity factor obtained by the graphical method was found to be 0.58. The imperfection sensitivity factor obtained by the analytical method was found to be 0.55. The initial geometric imperfection sensitivity factor obtained using the IASS method was noted to be 0.52. The maximum displacement was noted to be 131.8mm. There was no significant differences in the behaviour of hinged and clamped supported shells.

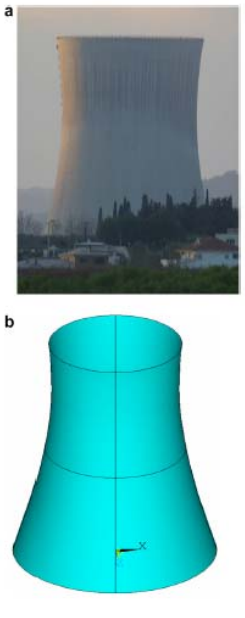

***Figure 90**: Asco cooling tower* (Tomas & Tovar, 2012)

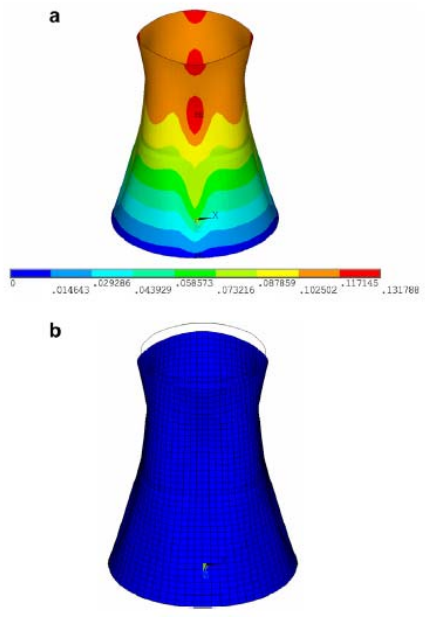

***Figure 89**: Cooling tower displacements and deformed shape* (Tomas & Tovar, 2012)

A year later, (Xu & Bai, 2013) performed an analysis of the random structural buckling problem by investigating the overall random buckling bearing capacity of a super large cooling tower (see *Figure 91*) using the probability density evolution method. The statistical properties of the random buckling bearing capacity were analysed by introducing random material properties and wind loads. Three random variables (elastic modulus of concrete, wind speed at 10m above ground and ground roughness) were introduced. The reliability for the super-large 250m high by 200m diameter cooling tower was evaluated. The authors derived a joint probability density evolution equation of the buckling bearing capacity using the probability preservation theory combined with the formal solution that governs buckling and the numerical scheme developed. The formulation is shown in the equations below.

$$|K_0 + \lambda K_\sigma| = 0 \quad \text{.....[39]}$$

$$P_\lambda(\lambda) = \int_{-\infty}^{\infty} p_{x\theta}(x, \theta, \tau = 1) d\theta \quad \text{.....[40]}$$

$$p_f(\alpha) = \int_{-\infty}^{\alpha} p(\lambda) d \quad \text{.....[41]}$$

A finite element model of the cooling tower was created and a mesh convergence undertaken to determine the optimum mesh grid. The following probability models of random parameters were considered:

- probability density distribution of the elastic modulus of concrete;
- probability density function of the ground roughness and
- probability density function of the wind speed.

Random buckling bearing capacity analysis for the super-large cooling tower was performed for three cases:

- Case A for random buckling bearing capacity with material randomness;
- Case B for random buckling bearing capacity with the random wind loads;
- Case C for random buckling bearing capacity with material and wind loads variation.

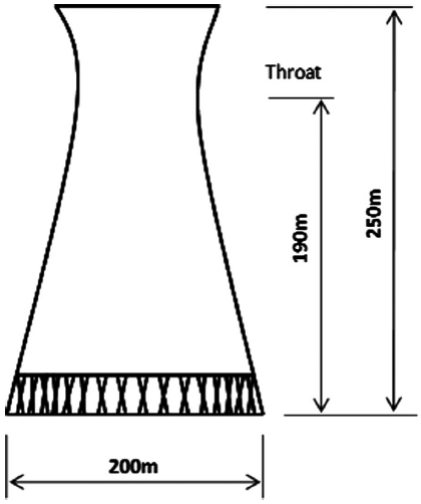

***Figure 91**: Cooling tower schematic* (Xu & Bai, 2013)

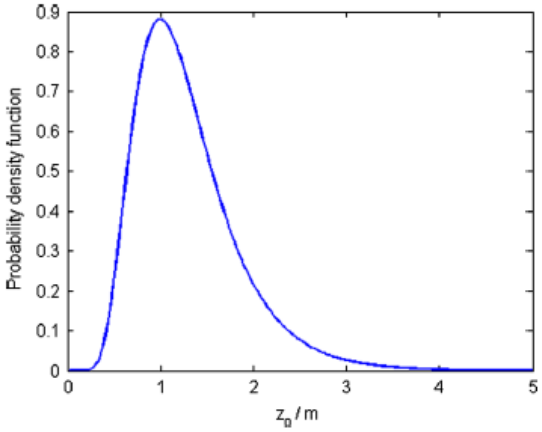

***Figure 92**: Probability density function* (Xu & Bai, 2013)

The adopted probability density function is shown in *Figure 94* whilst the selected points in standard normal space are shown in *Figure 92*. *Figure 93* and *Figure 95* show respectively the comparison of failure probability distribution functions and probability density functions of the buckling bearing capacity with different random factors.

After integrating the probability density function of the random buckling bearing capacity (with a failure limitation of 5) the calculated probability of failure was 0.0082 (0.82%), translating into a buckling reliability of 99.18%. For a specific failure boundary, the more random factors are considered, the lower the structural reliability. The variation of buckling bearing capacity was observed to be more sensitive to the wind loads than it was to the material property of concrete.

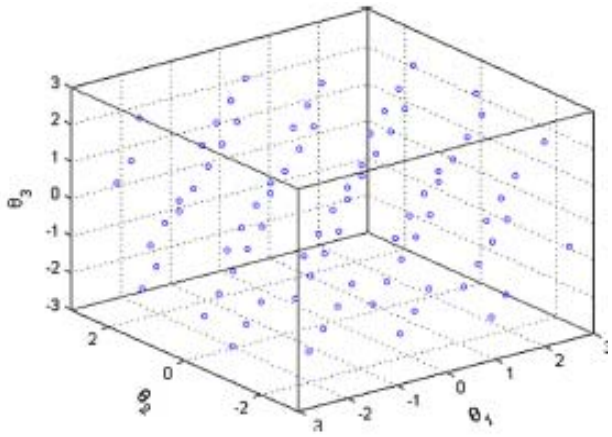

***Figure 94**: Selected points in standard normal space* (Xu & Bai, 2013)

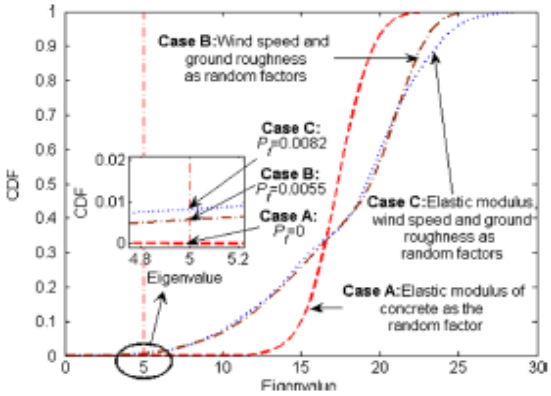

***Figure 93**: Comparison of failure probability and cumulative probability distribution functions of the buckling bearing capacity with different random factors space* (Xu & Bai, 2013)

A year later, as part of his post graduate studies, (Kulkarni & Kulkarni, 2014) investigated the wind and buckling analysis of two existing (143.5m and 175.5m high) cooling towers. The existing cooling towers were chosen from the Bellany thermal power station (India). By assuming a base fixity, the two towers were analysed using finite element analysis. The two towers geometry is shown in Figure 97 and Table 6. The analysis was performed on both shells with the thickness of the cooling tower varied as 200mm, 250mm, 300mm, 350mm, 400mm, 450mm and 500mm thick. Results of the analysis are shown in *Figure 96* and *Figure 98*.

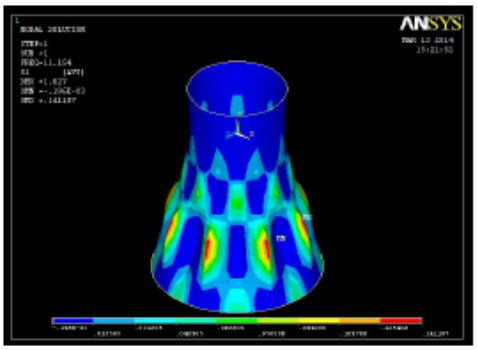

***Figure 96**: Maximum principal stress (Mode 1) for cooling tower 1* (Kulkarni & Kulkarni, 2014)

Sl no	Description	Symbols	Cooling tower 1 (CT 1)	Cooling tower 2 (CT 2)
1	Total height	H	143.50m	175.50m
2	Height of throat	Hthr	107.75m	131.60m
3	Diameter at top	Dt	63.6m	82.00m
4	Diameter at bottom	Db	110m	122.00m
5	Diameter at throat level	Dthr	61.0m	68.750m
6	Column Height	Hc	9.20m	9.275m
7	(Hthr/H) ratio		0.750	0.749
8	(Dthr/D) ratio		0.554	0.563

***Table 6**: Cooling towers geometry details* (Kulkarni & Kulkarni, 2014)

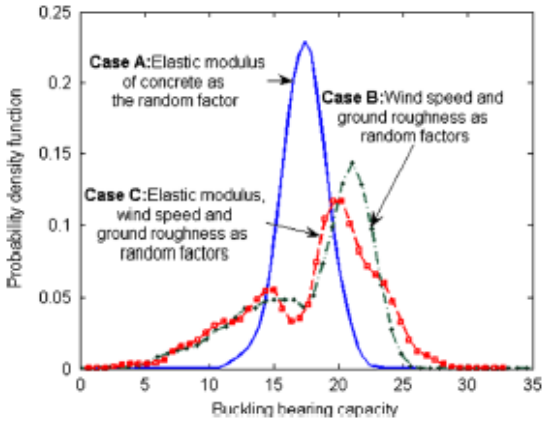

***Figure 95**: Comparison of probability density functions of the buckling bearing capacity with different random factors* (Xu & Bai, 2013)

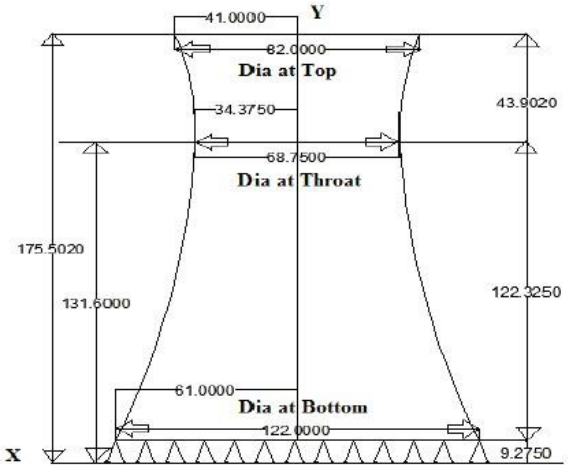

***Figure 97**: Geometry of existing cooling tower* (Kulkarni & Kulkarni, 2014)

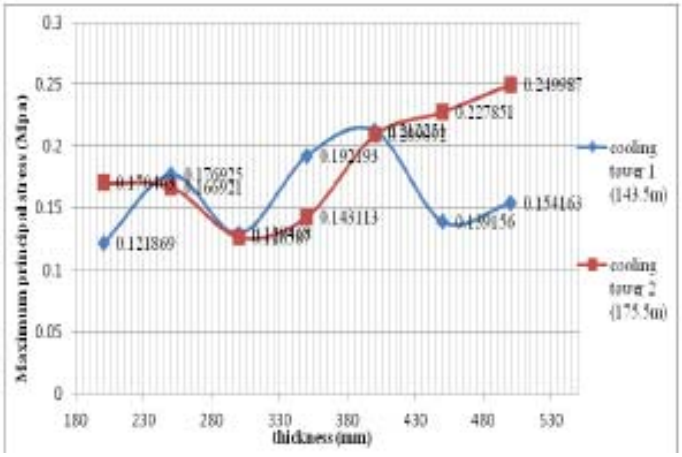

***Figure 98**: Meridional variation with shell thickness for CT1 and CT2* (Kulkarni & Kulkarni, 2014)

From the graphs and tables, it was observed that this parametric study's results are cluttered. No significant key findings can be deciphered from the results. This was also observed from the research's summary and conclusions. The results and presentation obtained from this study provide a classical example of how not to perform a parametric study. The parameters thickness, height, diameters should at least be represented as ratios in order to study the change in behaviour as the cooling tower's geometric aspect ratios are varied. The natural frequencies could at least be presented in relation to the change in thickness per each mode for the two different cooling towers. This approach is the focus of the current study.

2.3.3 Experimental and field studies

(Jullien, *et al.*, 1994) conducted field observations and measurements coupled with finite element modelling and analysis of hyperbolic cooling towers in order to determine the cause(s) of deformed shapes in cooling towers. They were interested in establishing that not only the damage and deterioration of concrete leads to the collapse of cooling

towers, but also the structural damage corresponding to the pre-buckling process arising from the cooling tower shell slenderness (diameter, height, thickness).

They conducted field exploratory observations and measurements of 4 in-situ cooling towers in France built in the 1960's. The observations were to record the deformed shapes and crack progression and distribution. The study was performed by mapping of the cooling towers using photogrammetry. Crack width and length measurements were taken (see *Figure 99*). Parametric finite element calculations were performed to establish the cause(s) and influence of the structural damages that were frequently encountered.

Afterwards, they performed elastic buckling calculations considering self-weight, wind and thermal loading in order to check the relationship/correspondence between the observed deformed cooling tower shapes and their pre-critical behaviour. They considered two types of defects in order to determine the sensitivity of the cooling tower on geometrical defects: (1) simple defects initiated under self-weight during construction and representing an instantly constructed cooling tower. (2) multi-modal defects arising from the superposition of several modes representing real defects formed by the appearance of different several modes during construction of the cooling tower. Some of the results are shown in *Figure 100* and *Figure 101*.

They concluded that all the four in-situ cooling towers displayed a significant difference between their current shape and the theoretical shape. The maximum discrepancy amplitude (geometrical defects) was about three or four times the thickness of the shell. The deformed shapes displayed modal shapes along the meridional and circumferential directions with the length of the wave in the circumferential direction being the smaller of the two and hence showing significant wrinkles along the circumferential direction. The inspected cracks were all parallel to the meridional direction. This similarity on all the four cooling towers led to the authors to postulate the assumption that there must be an inherent structural deformation other than accidental effects in the cooling towers. The calculated buckling mode corresponding to self-weight showed a correlation with the real deformed shape.

In addition, they concluded that, the simple defects analysis showed that the cooling tower is very sensitive to the modes that form during the first stages of construction. The multimodal defects analysis showed that the overall state of stresses is modified and bending was induced. By observing the meridional cracks, the authors concluded that the shell undergoes deterioration in the circumferential direction significantly compared to the meridional direction. The self-weight loading is the cause of the deformed shapes in cooling towers. The shape deformation is initiated during the construction phase. Meridional geometrical defects causes local reduction of shell stiffness in its circumferential direction. The shape deformation causes cracking by initiation of bending in the circumferential direction which causes the meridional cracking. The study showed that any realistic approach to the determination of the buckling safety must take into account the geometrical defects and the damaging behaviour of concrete.

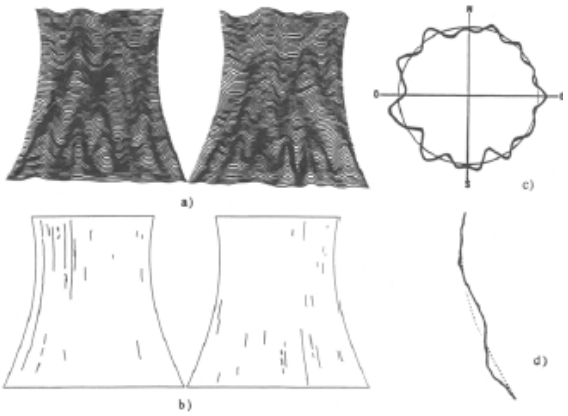

***Figure 99**: Cooling tower (a) actual deformed shape; (b) crack distribution; (c) horizontal section; (d) vertical section* (Jullien, *et al*., 1994)

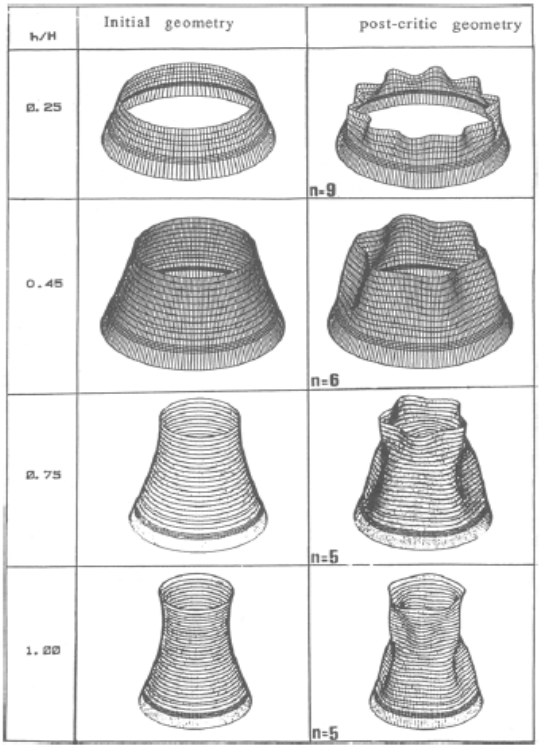

***Figure 100**: Buckling modes calculated under self-weight for different cooling tower elevations* (Jullien, *et al*., 1994)

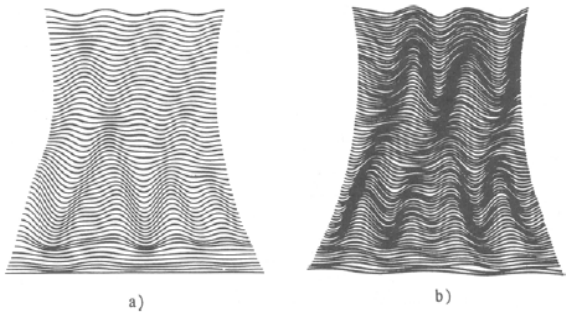

***Figure 101**: (a) Initial imperfection obtained by calculation; (b) Actual deformed shape for modes 5, 6 and 9* (Jullien, *et al*., 1994)

A year later, (Kaluza & Gigiel, 1995) conducted an experimental investigation into the influence of cooling tower base displacements on its buckling stability by using models. Four different load arrangements were tested on the cooling tower models:

- concentrated vertical edge load;
- edge vertical load plus lateral surface load;
- concentrated vertical edge load plus an imposed deformation of the lower ring;
- edge vertical load plus lateral surface load plus an imposed deformation of the lower ring.

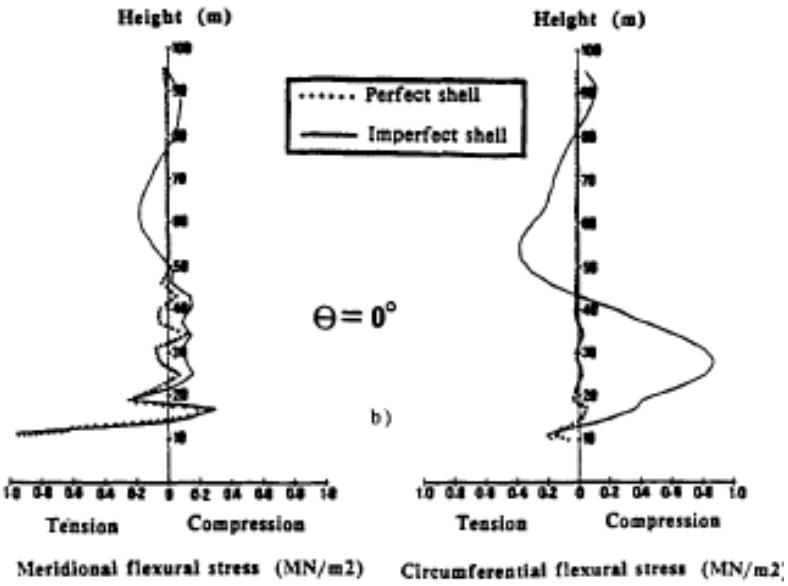

***Figure 102**: Stress distribution in perfect and imperfect cooling tower shell under self-weight* (Kaluza & Gigiel, 1995)

The smooth shell models were firstly analysed with an un-deformed lower ring and secondly with a deformed lower ring according to the formula indicated below. The critical loads corresponding to the critical meridional and circumferential stresses were then determined. They obtained the distribution of flexural stresses shown in *Figure 102*.

$u_v = \Delta_v \cos 2\beta$ and $u_v = \Delta_v \cos 4\beta$.....[42]

The authors reported that the influence of the imposed displacements of the lower cooling tower ring on its stability was insignificant. They noted that introducing stiffening ribs of different rigidity and spacing only increased the upper shell critical load. The lower shell critical load was not affected. They therefore concluded that the introduction of circumferential ribs results only in the increase of the local stiffness of the shell in its circumferential direction. This does not significantly increase the local or global meridional shell stiffness. They derived a formula to compute the critical loads using the results from the experiment. The formulas derived by the authors can be used in the design practice to check cooling tower shell stability when influenced by base displacements.

2.4 DYNAMIC RESPONSE – Free Vibrations

2.4.1 Theoretical studies

(Wen-da & Shi-qiao, 1987) performed a theoretical analysis of the natural frequencies of a hyperbolic cooling tower shell considering geometric imperfections by using the perturbation method. The geometric imperfections were first considered as initial displacements to obtain the additional element stiffness matrix caused by meridional geometric imperfections. The fundamental equations governing the free vibration of the cooling tower considering the geometric imperfections was then derived and are shown in the equations below including the frequencies of the imperfect shell. The frequencies and modes of the hyperbolic cooling tower shell were then calculated for a 90m high cooling tower with a throat height of 72m, using the derived perturbation equations.

$$[M_k]\{\ddot{a}\} + [K_k]\{a\} + [\Delta K_k]\{a\} = 0 \quad \text{.....[43]}$$

$$C_{mn} = -\omega_m^2 \Delta k_{nm} / \bar{k}_m / (\omega_m^2 - \omega_n^2) \ (n \neq m) \quad \text{.....[44]}$$

The authors found that the geometric imperfections increased the frequencies of the cooling tower. They also observed that the larger the range of imperfections, the more the frequencies were increased.

About a decade later (Kaiser, *et al*., 1995) introduced the total Lagrangian formulation for axisymmetric solids in their earlier paper (1993) and later investigated in more detail its application to a series of sample structures (cylinders, pipes and cooling towers). Their formulation uses a cylindrical reference system to define the geometry, a Cartesian reference system for the displacement field. The displacement field in the circumferential direction was described by a Fourier decomposition. The authors performed analyses on several sample structures (spherical cap, cooling tower, cylindrical shell and a pipe in bending) to compare the formulation with Fourier decomposition shell models with conventional finite element formulations. The transformed displacements were related to the Cartesian system and the transformations expressed in a matrix form.

Analysis of a cooling tower was done with the Cartesian formulation of the Harmonic Lagrangian Tubular (HLT) element (a solid axisymmetric element using common polynomial functions in the axisymmetric plane for geometry and displacements). Two loading cases were considered: external uniform pressure and wind loading pressure as had been performed by Chan and Trbojevic (1976) with the vertical wind pressure distribution assumed to be a constant. The cooling tower shown in *Figure 103* was analysed. Some of the results obtained are shown in *Figure 104* and *Figure 105*.

They concluded that the lowest collapse mode occurred in the ninth harmonic at a pressure of 10kN/m^2 as compared to the seventh harmonic obtained by Chan and Trbojevic (1978). Despite improving the number of solutions from eight to 10 harmonics, their results were significantly different from those obtained by Chan and Trbojevic (1976). The load-displacement curves start to compare well but the difference became significant as the deformations increased.

The HLT element employed by the authors brought with it less computational effort devoted to the geometrical representation of the structure and more focused on the structural behaviour as compared to the general three dimensional finite elements. The difference in the author's results from those of others indicated that the cooling tower dynamic problem had not been answered in detail.

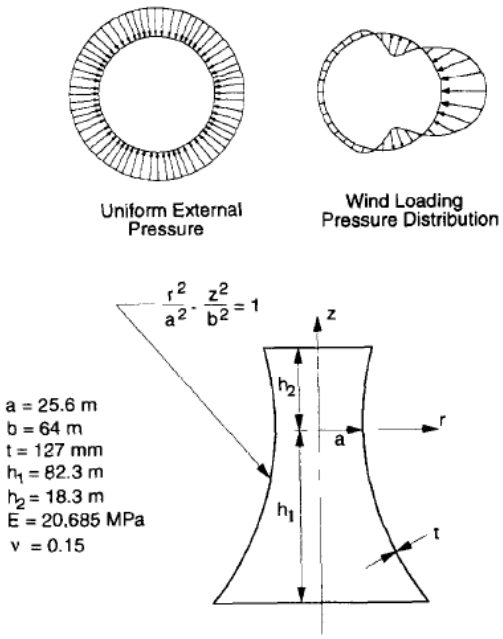

***Figure 103**: Full size cooling tower model with two load cases* (Kaiser, *et al*., 1995)

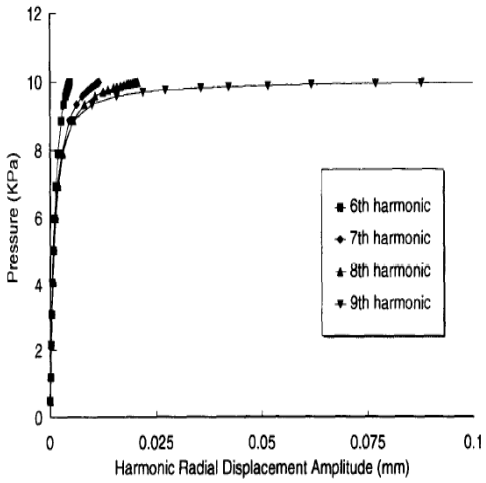

***Figure 104**: Load-radial displacement amplitude response for the cooling tower under external pressure* (Kaiser, *et al*., 1995)

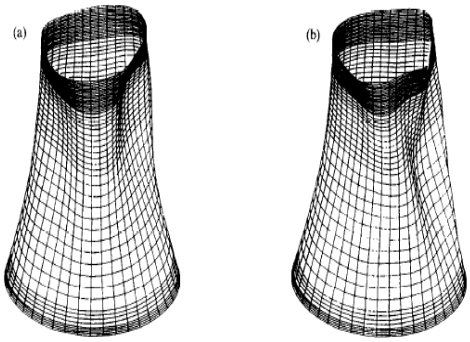

***Figure 105**: Deformed shapes for cooling tower (a) initial deformation; (b) advanced deformation mode* (Kaiser, *et al*., 1995)

Seven years later, (Busch, *et al*., 2002) summarised all the structural design aspects of the largest cooling tower at the time (using the Niederaussem cooling tower in Germany) as shown in *Figure 106*. They had considered that at a height of 200m, such a cooling tower can never be merely designed as an enlargement of the smaller ones, but would require careful and innovative design. The tower's geometry was optimised to account for thermal design radius at the shell bottom, unperturbed steam flow radius at the top, practical bottom angle inclination and cost of reinforcement. Openings in the shell for flue gas pipes were also considered in the design. Requirements to extend the cooling tower durability for a 55 year life time, limiting cracking and acid ingress into the concrete were considered by using an advanced high performance concrete (Acid Resistant High Performance Concrete: ARHPC). *Figure 107*, *Figure 108* and *Figure 109* show the analysis results performed on the cooling tower.

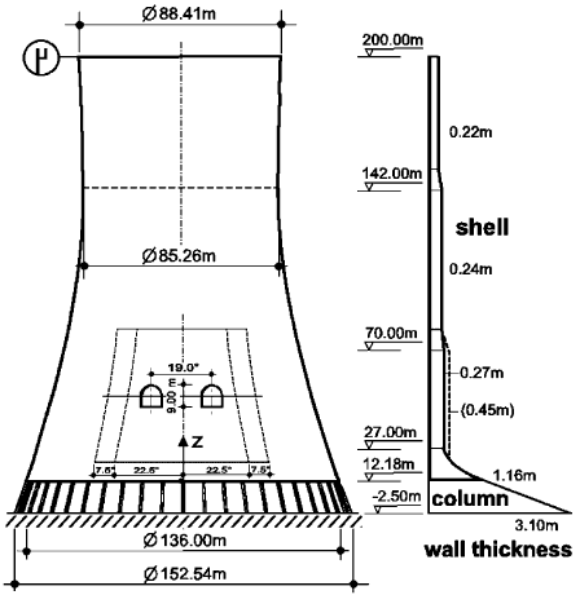

***Figure 106**: Overview of the cooling tower geometry* (Busch, *et al*., 2002)

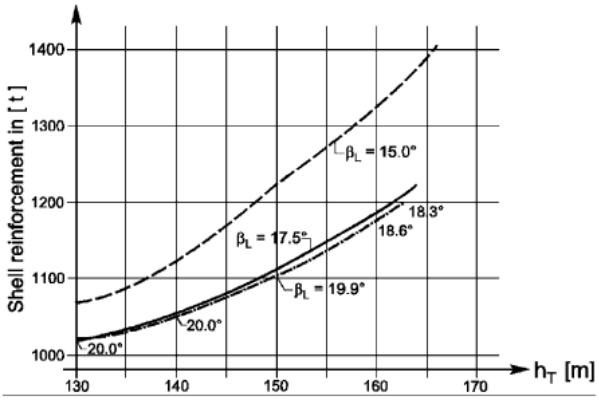

***Figure 107**: Shape-finding process: dependence of shell reinforcement on shell thickness* (Busch, *et al*., 2002)

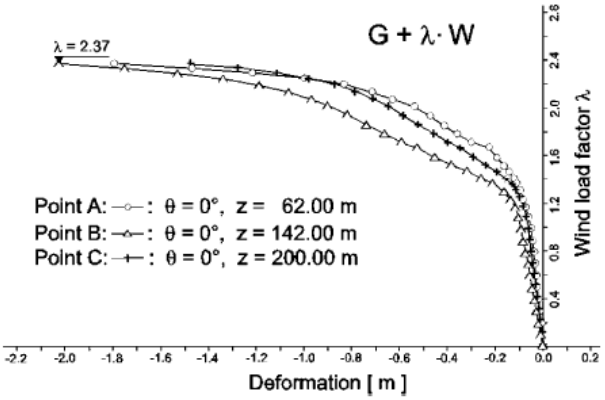

***Figure 108**: Load -displacement plots for G+λW* (Busch, *et al*., 2002)

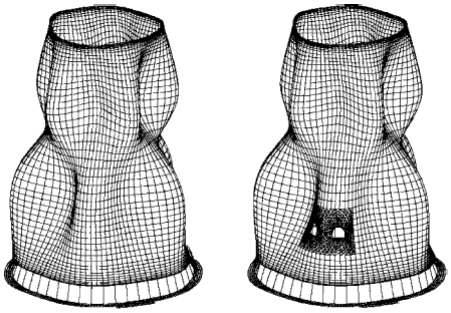

***Figure 109**: Comparison of lowest natural modes of vibration with/without flue gas inlets* (Busch, *et al*., 2002)

They found out that the lowest natural vibration modes and frequency with and without the flue gas openings were similar (see *Figure 109*). The reinforcement was designed with the meridional reinforcement spacing ranging from 92mm in the bottom shell to 190mm towards the top and the splicing staggered at regular intervals. The circumferential reinforcement spacing was ranging from 82mm to 200mm positioned closer to the outer and inner surfaces in order to limit initiation of vertical cracks. The load displacement curve for the load case self-weight + wind load was found to be as shown in Figure 108. Cracking of concrete was noted to start at about 1.2W with cracks widths limited to 0,05mm. The design considerations presented by the authors offer a practical method of stretching the size limit in the design of cooling towers.

Three years later, (Kang & Leissa, 2005) presented a three dimensional method of analysis to determine free vibration frequencies and modes for thick hyperbolic shells of revolution. They based their analysis method on 3-D dynamic equations of elasticity. The radial (U_r), circumferential (U_o) and axial (U_z) displacements were considered as sinusoidal with respect to time (period θ) and are presented in the equations below. The Raleigh-Ritz method was used to solve the eigenvalue problem of the strain and kinetic energy equations. The hyperbolic shell of revolution geometry considered is shown in *Figure 110* below. The accuracy of the frequencies was obtained by conducting a convergence study to determine the number of terms required in the displacement algebraic power series equations. A parametric study was

conducted by varying the geometrical parameters of the shell (b/a, H_b/a, H_t/H_b, and h/a) and producing the frequency of the shell for various modes (n).

$$U_r(\varphi,\zeta) = \eta_r(\varphi,\zeta)\sum_{k=0}^{K}\sum_{l=0}^{L} A_{ij}\varphi^i\zeta^j$$

$$U_\theta(\varphi,\zeta) = \eta_\theta(\varphi,\zeta)\sum_{k=0}^{K}\sum_{l=0}^{L} B_{kl}\varphi^k\zeta^l$$

$$U_z(\varphi,\zeta) = \eta_z(\varphi,\zeta)\sum_{m=0}^{M}\sum_{n=0}^{N} C_{mn}\varphi^m\zeta^n$$

.....[45]

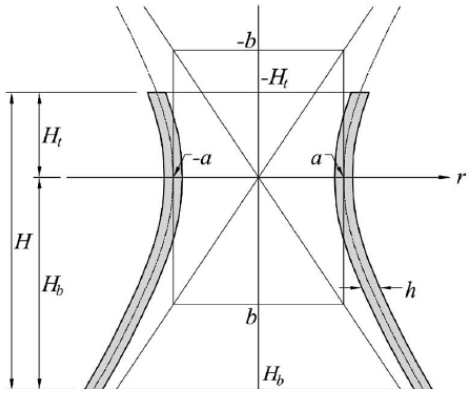

***Figure 110**: A representative hyperboloidal cooling tower shell with cylindrical coordinate system* (Kang & Leissa, 2005)

They found that the bending modes for n = 2 were noted to be the most significant. When the shell thickness ratio h/a was increased all the frequencies increased, except for the first and second torsional modes. When the shell curvature was increased (b/a became smaller), most of the frequencies decreased. When the curvature was reduced (b/a became larger) and the shell thickness simultaneously increased, the torsional and bending modes for n = 1 became more significant. The results obtained can serve as a benchmark against which other studies and approximate methods of analysis can be performed.

A year later, (Tornabene & Viola, 2006) studied the dynamic behaviour of general parabolic shells of revolution using the first-order Shear Deformation Theory (FSDT) to analyse the shells. Their study was limited to homogeneous, isotropic material behaviour and thick shells. They used the Generalised Differential Quadrature (GDQ) numerical method leading to a generalised eigenvalue problem. Governing equations of motion were derived as a set of five bi-dimensional partial differential equations expressed in terms of the kinematic parameters. Free vibration analysis examples were performed using the derived equations and the results compared with those obtained from commercial software based on the same theory. A convergence and stability analysis of the natural frequencies derived from the equations was performed (see *Figure 111*).

The convergence rate of the natural frequencies was shown to be very fast. The stability of the proposed numerical method was therefore noted to be very good. The study's results were noted to be very close to those obtained from commercial software programmes that use the same theory. The same study can be performed for thin parabolic shells of revolution like the cooling tower shell.

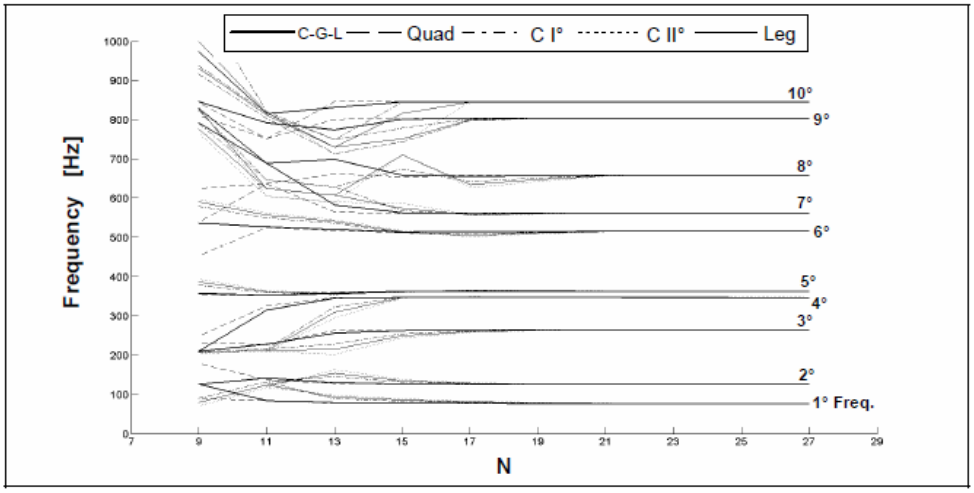

***Figure 111**: Convergence and stability of the first ten frequencies* (Tornabene & Viola, 2006)

Half a decade later, (Tornabene, 2011) demonstrated the efficiency and accuracy of the application of the Generalised Differential Quadrature (GDQ) approach when applied to the dynamic behaviour of laminated composite doubly-curved shells of revolution (cooling towers included). The study was two pronged in the following:

- Dynamic solutions were obtained using the GDQ numerical technique leading to a generalised eigenvalue problem. The solution of this problem was by generalised displacement components.
- Numerical results computed using commercial software programmes to compare and verify the accuracy of the GDQ method.

The governing equations of motion in terms of the stress resultants were expressed as kinematic, constitutive and equilibrium equations as shown in equations below and was combined into a complete equation of motion in terms of the displacements as shown. By considering two kinds of boundaries (fully clamped edge C and free edge F boundaries),

an analysis was performed using the above set of equations to determine the natural frequencies and modes of the hyperbolic shell of revolution.

The author noted that the results obtained using the GDQ method were very close to those obtained by the commercial software programmes. There was an excellent agreement. The analysis procedure showed a very quick convergence as seen in *Figure 114*. The study showed that the GDQ method can produce very accurate results with a computationally low cost and good convergence and numerical stability.

A year later, *(Ke, et al., 2012)* presented a new methodology for analysing equivalent static wind loads (ESWLs) on super large cooling towers. Their study considered analysing wind induced vibrations and corresponding ESWLs using a consistent coupling method (CCM) based on structural random vibration theory. The authors presented derivations of expressions for the ESWLs on super large cooling towers using the CCM to compensate for the coupled term between background and resonant responses. An aero-elastic model wind tunnel test (see *Figure 112*) was carried out for simultaneous pressure and vibration measurements in order to combine the wind tunnel and CCM results to determine the distribution characteristics of the ESWLs. A 215m high, 156m and 104m bottom and top diameter respectively, super large cooling tower was analysed. *Figure 113* and *Figure 116* show some of the response results obtained from the test.

$$[M]\{\ddot{y}(t)\} + [C]\{\dot{y}(t)\} + [K]\{y(t)\} = \{p(t)\} \quad [46]$$

The authors noted that the coupling effects between the resonant modes and the cross term between background and resonant component were significant. They concluded that the CCM was effective in calculating the ESWLs on super large cooling towers. The mean loads played a dominant role when considering the total wind loads. The wind vibration coefficients first increased and then decreased as the height increased. In addition, the authors also concluded that the usual method of using a single wind vibration coefficient has potential safety shortfalls. They instead suggested treatment of the wind vibration coefficient in sub-sections e.g. bottom, middle, throat and top regions of the super large cooling tower. The resonant component was noted to be the dominant in the fluctuating response. The coupling component values and distribution were noted to be similar to those of the background component. The findings by the authors are important for design engineers when considering the wind vibration coefficients along the height of super large cooling towers.

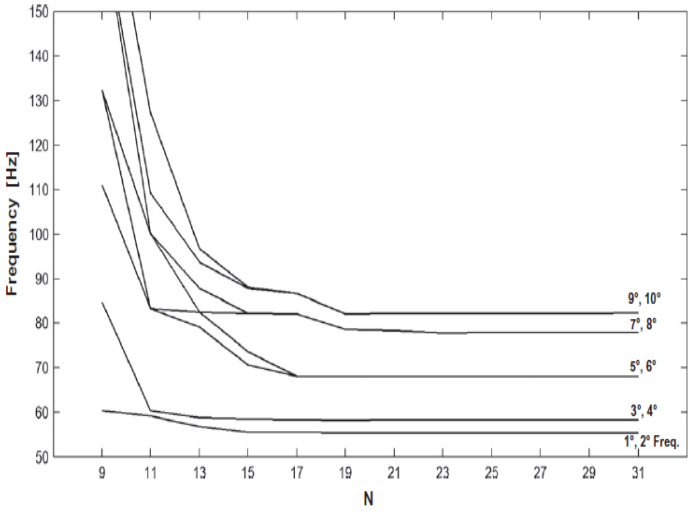

***Figure 112**: Convergence and stability characteristics of the first 10 frequencies* (Tornabene, 2011)

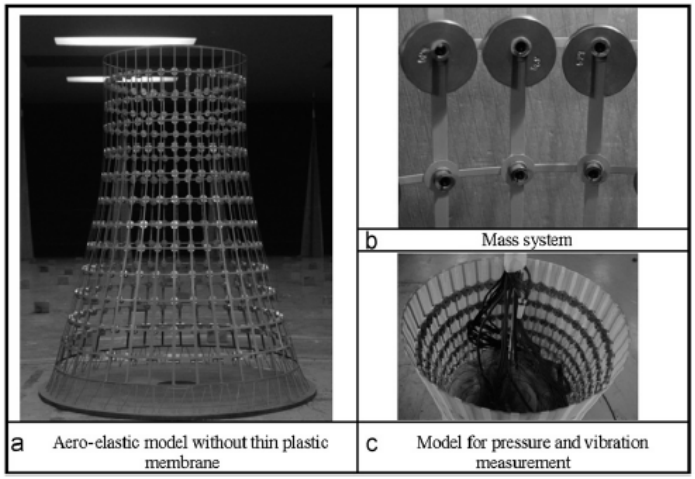

***Figure 113**: Aero-elastic model for simultaneous pressure and vibration measurements* (Ke, *et al.*, 2012)

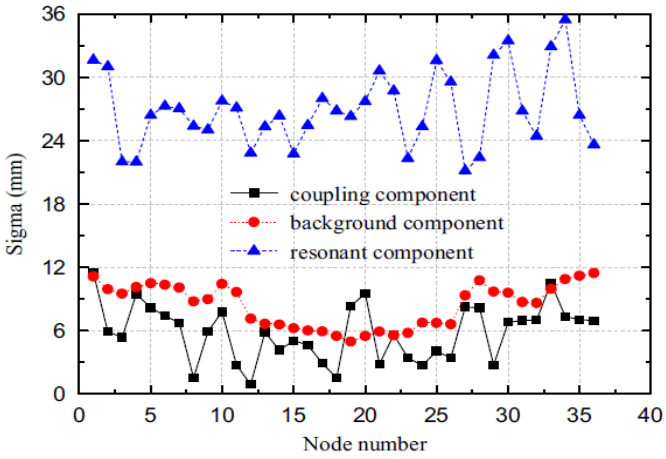

***Figure 114**: Fluctuating components of response by CCM* (Ke, *et al.*, 2012)

Three years later, (Kim, *et al*., 2015) studied the p-version two-node mixed finite element for the prediction of free vibration frequencies and mode shapes of an isotropic shell of revolution, the cooling tower included. The two-node p-version mixed finite element was proposed for the free vibration analysis.

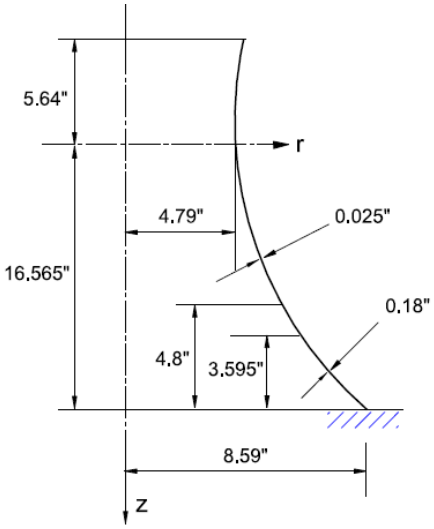

***Figure 115**: A scale model of hyperbolic cooling tower (Kim, et al., 2015)*

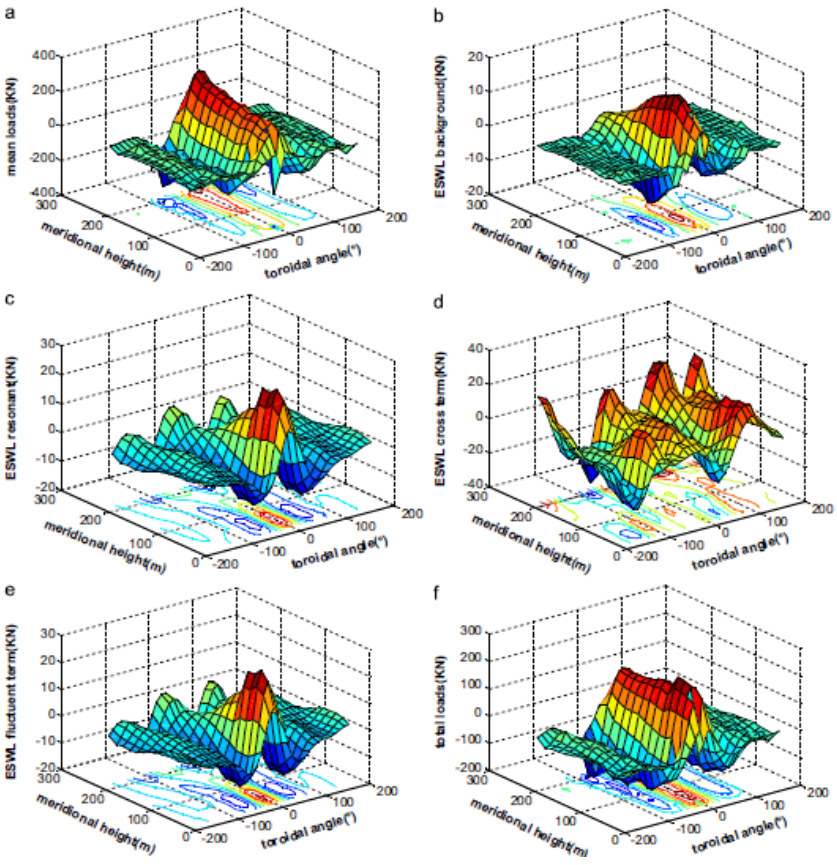

***Figure 116**: Distribution curve of fluctuating ESWLs of different components. (a) mean term; (b) background term; (c) resonant term; (d) cross term; (e) fluctuant term and (f) total ESWLs (Ke, et al., 2012)*

Then the numerical performance of the mixed element was evaluated using several shells of revolution examples including the hyperbolic cooling tower shell of revolution. The cooling tower shown in *Figure 115* had been studied previously by Sen and Gould (1974). The shell was assumed to be fixed at the base and free at the top and all non-uniform variations in thickness were considered. In their approach, the authors adopted the Hellinger-Reissner variational principal and the first-order Reissner-Mindlin shear deformation shell theory to solve the shell free vibrations equations. Some of the results of their study are shown in *Figure 117* and *Table 7*.

They concluded that their study showed that the mixed element/s convergence and accuracy in the free vibration of shells of revolution was satisfactory. There was a good agreement between the results obtained by the authors and those by Sen and Gould (1974). The study confirmed that the mixed element finite element proposed can be applied credibly to practical shells of revolution with a very rapid convergence rate of the natural frequencies for the modes considered.

In the same year, (Hara, 2015) evaluated the dynamic properties of a cooling tower under earthquake loading by considering a different column support system (I-column and V-column systems). The author introduced the numerical scheme under parallel processing to perform the dynamic evaluation of the cooling tower under seismic loading. The cooling tower displacement field was solved by treating the dynamic equilibrium equation shown below. The cooling tower considered was a 175m high shell with 16 equally spaced I or V-column systems.

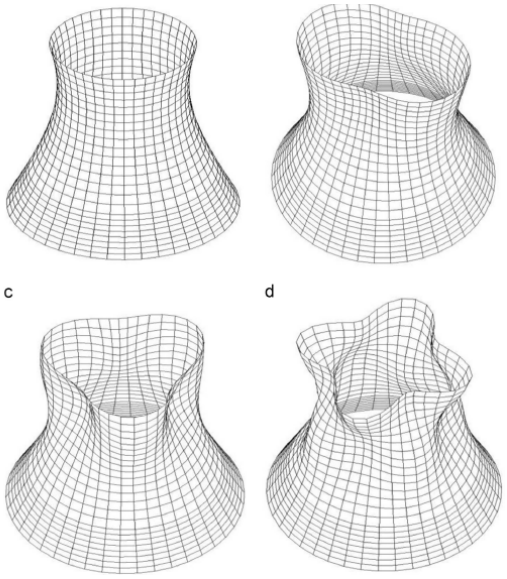

***Figure 117**: The first vibration mode shapes of the hyperbolic cooling tower (Kim, et al., 2015)*

Harmonic number *n*	Natural frequencies (Hz)			
	Experiment [31]	Sen [29]	Present (m=2) [10 elements]	Present (m=2) [15 elements]
3	188	168	167.58	167.56
4	130	130	129.94	129.71
5	–	122	122.31	122.21
6	157	143	143.56	142.82
7	177	161	161.95	161.40

***Table 7**: Natural frequencies of the clamped-free hyperbolic cooling tower shell (Kim, et al., 2015)*

$$M\Delta\ddot{y} + C\Delta\dot{y} + K\Delta y = -MI\Delta\ddot{y}_0 \quad [47]$$

With I-column supports, the cooling tower shell showed local deformation around the junction between the columns and the shell lintel under dynamic loading. Small deformations were observed for the shell structure. With V-column supports, the cooling tower shell showed cantilever-type global small deformations under dynamic loading. The total structural dynamic responses with either of the support columns was observed to be different from a conventional pin-supported ideal shell, suggesting that the precise supporting structures must be modelled in the analyses of cooling towers. The higher stress concentrations were observed to be due to the I-columns (at their junction with the shell) than those of the V-column supports. The author noted that the presented numerical scheme would be applicable to practical analysis of cooling towers under seismic loading. The findings of the study led to the conclusion by the author that additional reinforcements around the column supports/shell junction should be considered to arrest seismic excitation effects.

2.4.2 Numerical studies

(Yang & Kapania, 1983) investigated various shell elements for the column support cooling tower in order to achieve on optimum finite element modelling for seismic response. Their intention was to understand the distribution of the dominating bending and membrane stresses as well as the vulnerable shell-column region of the shell by using the discrete column elements and the quadrilateral shell elements in the finite element model. A family of finite elements was chosen as shown in *Figure 118* and described as follows:

- a 16 DOF column discrete element;
- a 48 DOF doubly curved general quadrilateral shell element (see Figure 120);
- a 42 DOF doubly curved quadrilateral general-membrane transition element;
- a 21 DOF and a 39 DOF doubly curved triangular filler element;
- a 28 DOF doubly curved quadrilateral membrane element.

The investigation considered cooling tower examples to evaluate single types, combined types and the whole set of the finite element types.

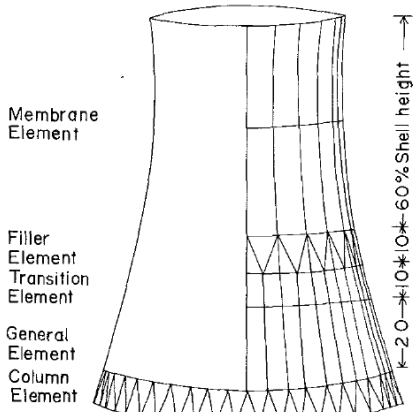

***Figure 118**: An efficient modelling for a column-supported cooling tower using a family of finite elements* (Yang & Kapania, 1983)

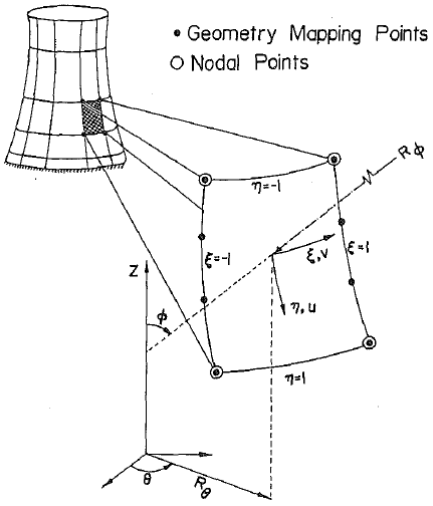

***Figure 120**: 48 DOF doubly-curved quadrilateral general shell element* (Yang & Kapania, 1983)

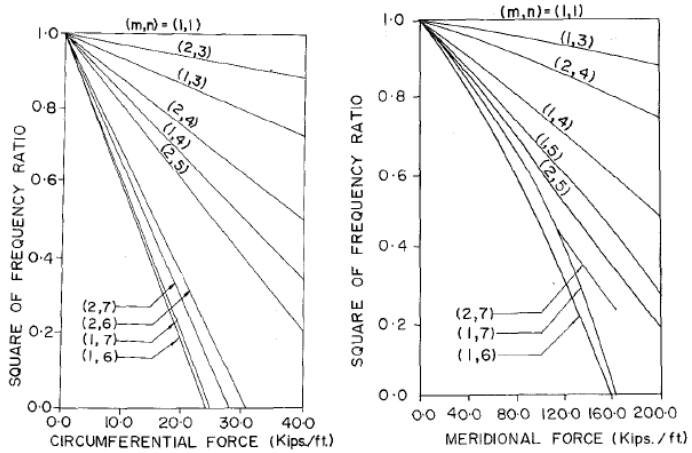

***Figure 119**: Effect of uniform circumferential and meridional force on frequency ratio for a fixed base cooling tower for various modes* (Yang & Kapania, 1983)

All the results obtained were noted to be in agreement with alternative finite element solutions. On each mode of vibration the square of frequency ratio $(w/w_0)^2$ was observed to vary linearly with the uniform circumferential stress, suggesting that the mode shapes do not change as the circumferential stress increases. On the other hand $(w/w_0)^2$ varies non-linearly with the uniform meridional stress, suggesting that each mode changes its shape as the meridional stress increases (see *Figure 119*). On investigating the effect of self-weight, the authors found that the natural frequencies obtained considering the cooling tower self-weight changed slightly and insignificantly.

It was observed that the triangular elements were efficient for use as filler elements in combination with other types of elements. The authors noted that the study could be extended to include material nonlinearity. The findings of this

study opened up possibilities of research in the nonlinear stress distribution of a cooling tower under seismic disturbances.

A year later, (Yang & Kapania, 1984) presented a finite element formulation and Gaussian quadrature procedure that uses direct complex matrix inversion and modal superposition to study the stationary random response of a cooling tower shell. By the time of their study, the authors noted that the application of finite element methods to stationary random response problems had only been performed on structures like trusses, beams, plates and application to shell elements was still outstanding. They used a 48 degree-of-freedom quadrilateral shell element with bi-cubic Hermitian polynomial interpolation displacement shape functions forming a matrix of cross-spectral densities of nodal forces. The displacement shape functions were used to formulate work-equivalent generalised nodal loads from the random distributed pressures. Gaussian quadrature was then used to allow the use of the spectral density function in its original form. This procedure was used to analyse a cooling tower shell subjected to random wind loads with three different velocities. The authors obtained the cross-spectral density function of the distributed wind pressure. They neglected the loads acting in the directions tangential to the shell surface.

***Figure 121**: Auto spectral density of normal displacement at top and throat for three different wind speeds* (Yang & Kapania, 1984)

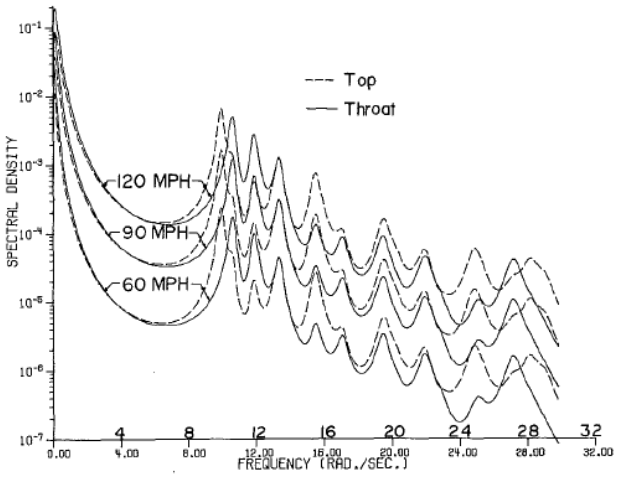

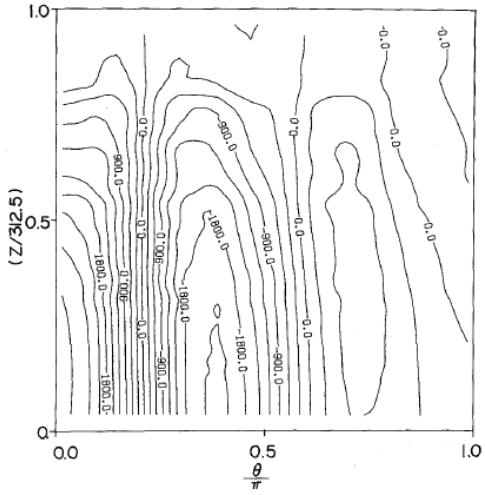

***Figure 122**: Contours of mean meridional stress resultant of the cooling tower due to wind speed of 120mph at throat* (Yang & Kapania, 1984)

The characteristics of the spectral density of pressures closely resembled those of the wind velocity in the vicinity of the most wind ward position ($\theta = 0°$) and the resemblance deteriorated gradually as θ increased. The procedure and formulation developed by the authors can be used by practicing engineers in checking the stationery random response analysis of the cooling tower shell.

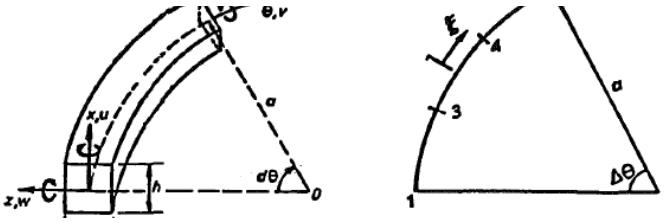

***Figure 123**: Curved beam element dimensions, coordinate system and description* (Bhimaraddi, *et al.*, 1991)

Eight years later, (Bhimaraddi, *et al.*, 1991) studied the free-vibration response of a column-supported cooling tower with ring stiffeners. They observed that this treatment had been performed for plates, cylinders, conical shells and spherical shells, but had not been extended to cooling towers. In their approach, they modelled the cooling tower using anisoparametric 64-DOF quadrilateral shell-of-revolution elements for the hyperbolic shell (see *Figure 125*) and isoparametric three-dimensional curved beam elements (see *Figure 123*) for the stiffener rings and columns. The effects of the ring stiffeners and column supports were incorporated into the cooling tower finite element analysis by coordinate transformation. The equation of motion of the entire system in terms of the shell element degrees of freedom was derived. Three rings were added along the height of the cooling tower. Firstly, one ring was added and the effect of the sub-sequent rings was observed by keeping one ring position constant (at throat level) and varying the other two. Thus 4 cases were obtained with:

- Case1 : L_1 = 27m; L_2 =52.618m
- Case 2: L_1 = 37m; L_2 = 51.618m
- Case 3: L_1 = 27m; L_2 = 56.618m
- Case 4 : L_1 = 37m; L_2 = 56.618m

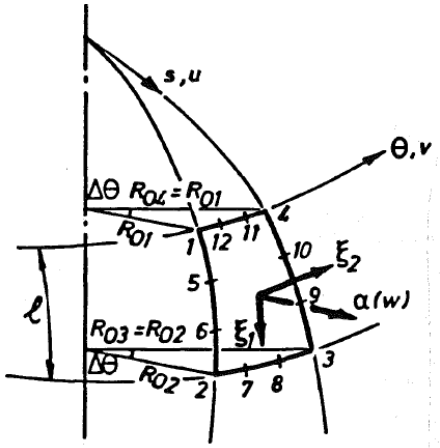

***Figure 125**: Shell of revolution finite element description* (Bhimaraddi, *et al.*, 1991)

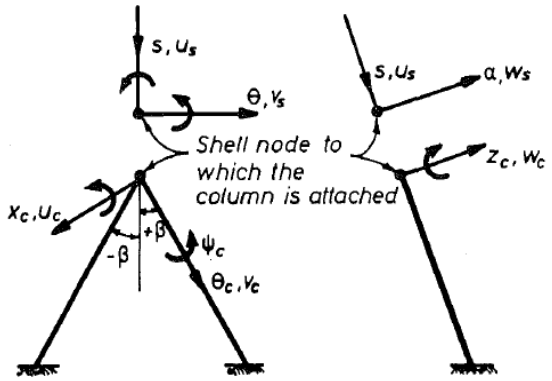

***Figure 124**: Shell and supporting columns orientation of coordinate system* (Bhimaraddi, *et al.*, 1991)

Meridional mode number (m) (1)	Basu and Gould (1979) (Hz) (2)	Yang and Kapania (1983) (Hz) (3)	Present, thin (Hz) (4)	Present, thick (Hz) (5)
1	2.336	2.333	2.3123	2.3085
2	4.119	4.156	3.9239	3.9236
3	7.056	6.952	7.2482	7.2450
4	—	—	8.2491	8.2474

***Table 8**: Lowest natural frequencies of column-supported cooling tower* (Bhimaraddi, *et al.*, 1991)

Table 8 and *Figure 126* show some of the analysis results obtained. On comparing their results to those by Basu and Gould (1979) and Yang and Kapania (1983), the authors noted that there was good agreement between the results. There was no significant difference between the thick-shell and thin-shell results. This was noted to be due to the fact that both wall thicknesses were very small compared to the radii of curvatures. An increase in the frequency for the higher circumferential wave numbers (n > 3) and a decrease in the same for the lower circumferential wave numbers (n = 1, 2) was observed.

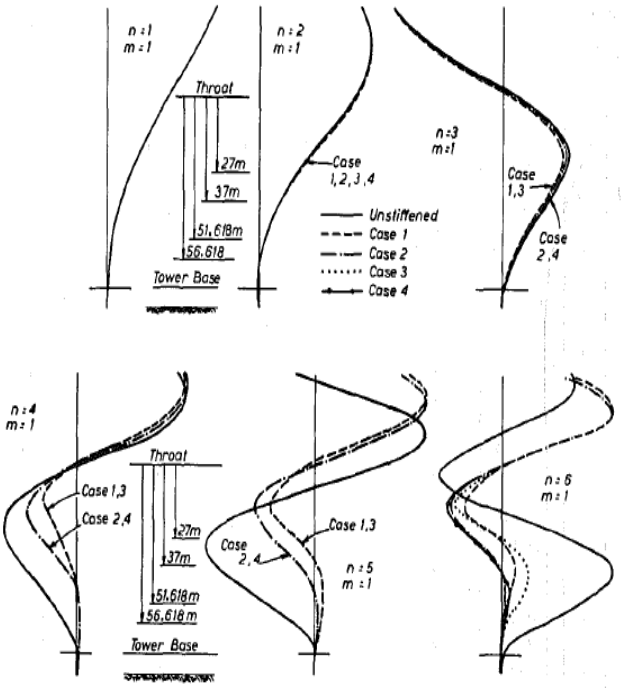

***Figure 126**: Shapes of first meridional mode for different circumferential half-wave numbers* (Bhimaraddi, *et al.*, 1991)

This was caused by the addition of stiffener rings altering the modal characteristics of the cooling tower. The modes (n > 3) are important for wind disturbances. The addition of the ring stiffeners increases the frequency in these mode shapes and ultimately increases the load-carrying capacity of the cooling tower shell under wind loading. On the other hand, the stiffening rings have no significant effect on the modal characteristics of the modes with lower circumferential waves (n=1, 2) which are seismic excitation sensitive modes. The authors concluded that the provision of stiffening rings may not help increase the resistance of the cooling tower shell to seismic loads. The findings by the authors eliminated the premise that stiffening rings can be used to increase the load carrying capacity of cooling towers under seismic excitation.

Four years later, (Lee, *et al.*, 1995) presented an efficient numerical method to analyse the eigenvalue problem of large structural systems with multiple or close eigenvalues including the cooling tower. Their objective was to improve the numerical stability and increase the convergence rate in the free vibration analyses of these structures. They presented the generalised eigenvalue problem in dynamic analysis as shown in the equation below, from which an algorithm for solving the eigenvectors was derived. The algorithm was noted to rapidly converge using the Newton-Raphson method. Various numerical examples were presented including a 100m high cooling tower consisting of 408 four-node shell elements with 2448 degrees of freedom and a 201 mean half-bandwidth stiffness and mass matrices.

$$A\bar{x}_i = \lambda_i B\bar{x}_i \quad (i = 1, 2, 3, \ldots, n) \qquad [48]$$

They concluded that the solution time to convergence of this method was found to be 51.1 minutes whilst the accelerated subspace iteration method took 2.02 times the time. They noted that the proposed method can identify eigen

pairs of a structure efficiently without any numerical stability problems. The method will not be affected by previously calculated eigen pairs because of the independence of the eigen pairs.

Half a decade later, (Koohestani, 2010) presented an efficient and alternative method for the free vibration analysis of cyclically symmetric finite element models including the cooling tower. The decomposition of generalised eigen problems into eigen sub-problems with smaller dimensions was the study's interest in solving the natural frequencies and mode shapes of structures with cyclic symmetry. The mass and stiffness matrices were observed to display a special pattern called the block circulant matrix (see *Table 11*). As such, the decomposition of the eigen problems was obtained by block diagonalisation of this block circulant matrix using similarity transformations and Kronecker products. The analysis was performed on various types of cylindrically symmetric structures (including the cooling tower) and the results compared to those obtained using the Fourier method and Group theoretic methods. The analysis was performed on a 60m high cooling tower model. *Table 9* and *Table 10* including *Figure 127* show some of the results obtained from the analysis.

$$K = \begin{bmatrix} k_{11} & k_{12} & & & k_{21} \\ k_{21} & k_{11} & k_{12} & & \\ & . & . & . & \\ & & k_{21} & k_{11} & k_{12} \\ k_{12} & & & k_{21} & k_{11} \end{bmatrix}$$

$$M = \begin{bmatrix} m_{11} & m_{12} & & & m_{21} \\ m_{21} & m_{11} & m_{12} & & \\ & . & . & . & \\ & & m_{21} & m_{11} & m_{12} \\ m_{12} & & & m_{21} & m_{11} \end{bmatrix}$$

***Table 11**: Block circulant stiffness and mass matrices* (Koohestani, 2010)

	Simply-Supported Plane(ratio)		Cooling Tower(ratio)
	Multiple	Close	
Proposed Method	172.39 (1.00)	177.41 (1.00)	3067.71 (1.00)
Acc. Subspace Iteration Method	274.60 (1.59)	291.85 (1.65)	6182.49 (2.02)
Determinant Search Method	1118.60 (6.49)	832.09 (4.69)	-

***Table 9**: Computer solution times in seconds* (Koohestani, 2010)

	Mode 1	Mode 2	Mode 3	Mode 4	Mode 5	Mode 6	Mode 7	Mode 8
Period (PM)	0.28578	0.28578	0.26096	0.26096	0.23307	0.23307	0.21871	0.21871
Period (SAP)	0.28605	0.28605	0.26125	0.26125	0.23329	0.23329	0.21886	0.21886
Error (%)	0.09404	0.09404	0.11215	0.11215	0.09430	0.09430	0.06899	0.06899

***Table 10**: Periods of cooling tower obtained from the proposed method by* (Koohestani, 2010)

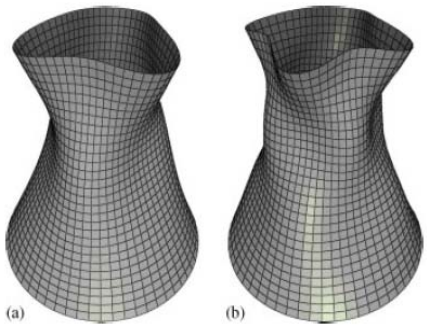

***Figure 127**: Cooling tower mode shapes* (Koohestani, 2010)

The author noted that the natural frequency results obtained completely agreed with other alternative methods. The precise natural frequencies and mode shapes were obtained with minimum computational effort. The presented method can be extended to the stability analysis of cylindrically symmetric finite element models by replacing the mass matrix with the geometric stiffness matrix.

A year later, (Kaveh & Nemati, 2011) presented an efficient eigen solution for calculating the free vibration natural frequencies of rotationally (cyclic) symmetric shell structures including cooling towers. Their method was primarily based on the decomposition of a Block Tri-diagonal matrix with corner blocks (block circulant matrix) which is a matrix associated with a rotationally repetitive structure. The large eigenvalue problem was transformed into smaller eigenvalue problems by the decomposition of the rotationally repetitive shell structures into subsystems. Both the stiffness and mass matrices were generated efficiently and the characteristic equation solved by block diagonalisation to obtain the eigenvalues and eigenvectors. The first six maximum natural periods of a cooling tower shell were calculated using this method and the classic methods and the results compared.

$$|[K] - \omega^2[M]| = 0 \quad \text{.....[49]}$$

They concluded that a considerable reduction in computational time was observed using the presented method. The results obtained with the presented method agreed very well with the classic method results. There was no necessity to generate the entire cooling tower stiffness and mass matrices since this could be done partly, leading to a significant reduction in time and computer memory required. The saving in time and computer memory was attributed to:

- calculating the mass and elastic stiffness matrices of a subsystem;
- calculating *n*-times, the eigenvalues and eigenvectors of a problem in dimensions of active DOFs in a subsystem instead of calculating the eigenvalues and eigenvector of a structure with an enormous number of DOFs.

Three years later, (Asadzadeh, *et al*., 2014) studied the effects of the type and inclination of supporting columns of a cooling tower shell on its dynamic characteristics. The study analysed the cooling tower shell as an assembly of layered non-linear shell elements comprising of different "reinforcement and concrete layers,"(see *Figure 128*). A modal analysis

of the hyperbolic cooling tower was performed using the Ritz vector analysis. A non-linear time history analysis method was applied to study the column support type and inclination effects on the cooling tower shell's dynamic characteristics. Two types of columns were considered: the I-type column and the Λ-type column. Different angles of inclination for the two column types were considered as follows:

- I-90° = zero inclination for the I-type column;
- I-85°= 5° Inclination to the vertical;
- I-80°=10° inclination to the vertical;
- I-75°=15° inclination to the vertical;
- Λ-85°=5° Inclination to the vertical;
- Λ-80°=10° inclination to the vertical;
- Λ-75°=15° inclination to the vertical.

Figure 129 and *Figure 130* show some of the results obtained from the analysis.

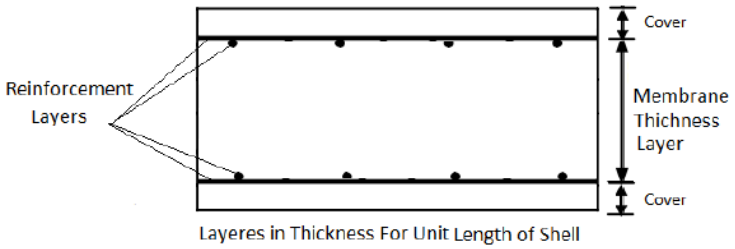

***Figure 128**: Layered shell element modelling the different layers of concrete and reinforcement* (Asadzadeh, *et al.*, 2014)

They concluded that, for the I-type column, the cooling tower supported by vertical columns (I-90°) is flexible than when it is supported by inclined column supports. The structure's stiffness increases as the degree of inclination increases. The opposite was true for the Λ-type columns: the flexibility of the whole cooling tower structure increases with a decrease in the degree of inclination of the column supports.

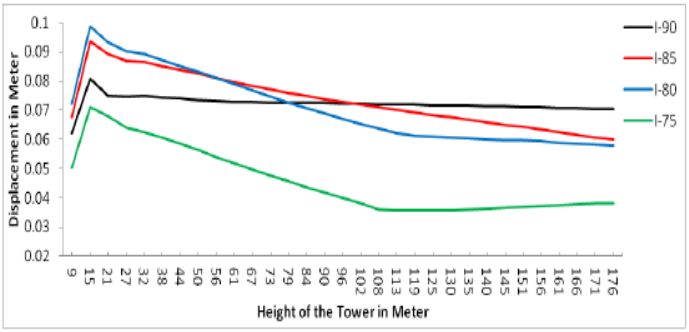

***Figure 129**: Maximum radial displacements along the tower height at $\theta = 0^0$ for I-type column supports* (Asadzadeh, *et al.*, 2014)

At higher inclination angles, the period of vibration increases and the frequency decreases. With an increase in frequency (lower inclination angles), the load carrying capacity of the cooling tower against wind became higher. The cooling towers supported by I-75° and Λ-75° will be more efficient under wind loading. For the I-type column supports, the tower shell is flexible at the bottom and stiffer at higher levels. An increase in the inclination angle causes an increase in the shell stiffness at higher levels.

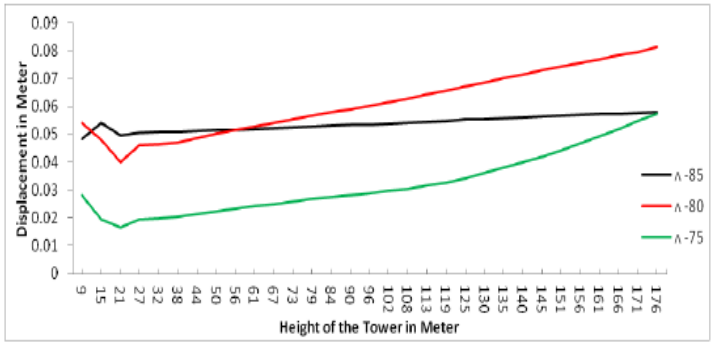

***Figure 130**: Maximum radial displacements along the tower height at $\theta = 0^0$ for Λ -type column supports* (Asadzadeh, *et al.*, 2014)

By comparing the above figures, the authors concluded that using column pairs (Λ-type columns) instead of single columns (I-type columns) of the same cross sectional area and reinforcement density results in a cooling tower structure that is more resistant to seismic loading (minimum displacement and minimum period of vibration). The location of the maximum displacement for the I-type column were observed to be at the bottom where as for the Λ-type columns they were noted to occur at the top. The base reactions were noted to be very sensitive to the change of column support inclination but inconsistent with the increase in the inclination. The findings of this study were noted to be of immense significance to the safe design of cooling towers against seismic excitations.

2.4.3 Experimental and field studies

(Shu & Wen-da, 1990) studied the dynamic properties of a cooling tower shell by considering the dynamic model of the shell and an infinite supporting soil system. Two methods of investigation were performed:

- A finite element analysis of a cooling tower shell of revolution represented by high precision rotational finite elements, discrete column supports, and a soil medium represented by a dynamic boundary system (see *Figure 131*).
- An experimental investigation of a three part model consisting of a finite soil volume, a standard viscous boundary and an analytical energy absorbing boundary (see *Figure 132*).

They concluded that the results from the two investigation methods were noted to be in agreement. The elasticity of the soil system was noted to reduce the natural frequency of the cooling tower. This reduction was noted to depend on the soil system stiffness i.e. the harder the soil, the smaller the reduction, the softer the soil, the larger the reduction. The authors established that the cooling tower shell structure - soil interaction must be considered in order to determine the true dynamic characteristics of the system. The FEM and the dynamic soil model were noted to be feasible and credible tests that can be depended on.

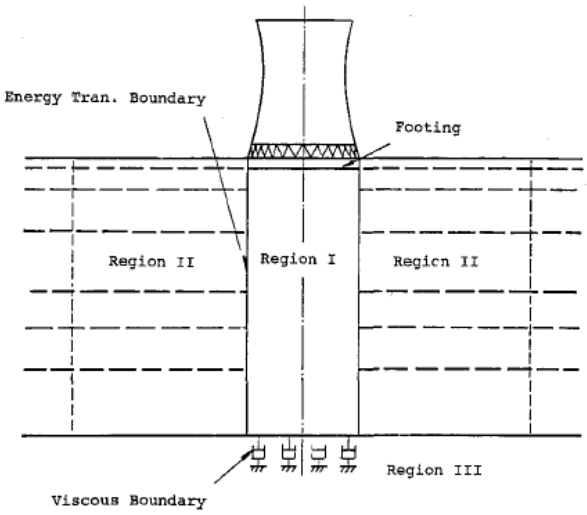

***Figure 131**: Regions of soil and structure model* (Shu & Wen-da, 1990)

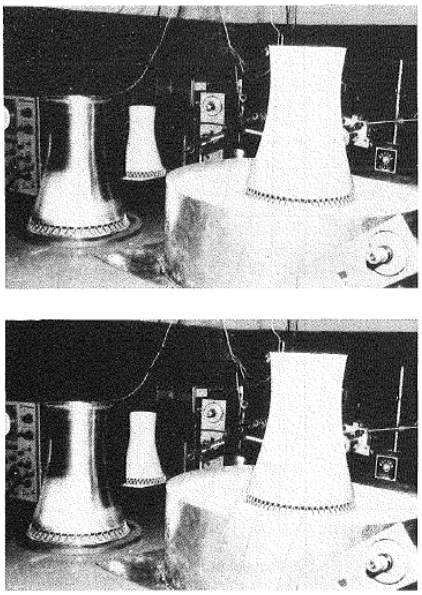

FIG. 2. Experimental Setup of Cooling Tower

***Figure 132**: Experimental model setup of cooling tower* (Shu & Wen-da, 1990)

2.5 DYNAMIC RESPONSE - Forced Vibrations

2.5.1 Theoretical studies

(Norton & Weingarten, n.d.) used a linear computer programme to evaluate the seismic response of different cooling towers with various asymmetric imperfections. They were concerned with the results of investigations by Weingarten *et al* (1973) and Schnobrich (1972) which had revealed that a significant response in higher circumferential wave numbers "did not exist." Their study used a computer programme to model one-half of the hyperbolic shell. Geometric imperfections were factored into the analysis considering various thicknesses of the shell.

The study found out that the maximum membrane stresses occurred at an excitation frequency of 1.606 Hz which was the first beam bending mode. The maximum bending moment occurred at an excitation frequency of 1.017Hz. The authors concluded that the achieved bending stresses were not a result of altering the beam bending modes but rather a result of modes other than the beam bending modes being excited. This meant that the cooling tower could have high bending stresses compared to membrane stresses when excited with an earthquake with a strong frequency of 1.017Hz. The study's findings raised an awareness for the need to increase reinforcement in regions of imperfections to allow for bending stresses that are higher than membrane stresses at certain seismic frequencies.

(Yang, *et al*., n.d.) studied the seismic response of the Paradise cooling tower in Kentucky (USA) using 3-D orthotropic quadrilateral flat plate finite elements. 3-D beam finite elements were used to model the top ring beam and bottom supporting columns. 3-D orthotropic quadrilateral and triangular plate finite elements were used to model the cooling tower shell as shown in Figure 134. Natural frequencies and normal vibration modes were found. Then the method of modal superposition was used to compute time history responses of 30 seconds of the 1940 EI Centro earthquake's North & South component. *Figure 134* and *Figure 135* show some of the results obtained.

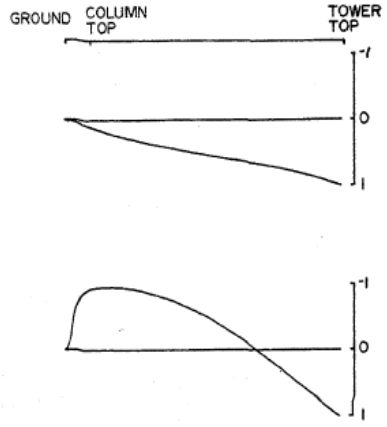

***Figure 134**: First two meridional mode shapes with one circumferential wave* (Yang, *et al*., n.d.)

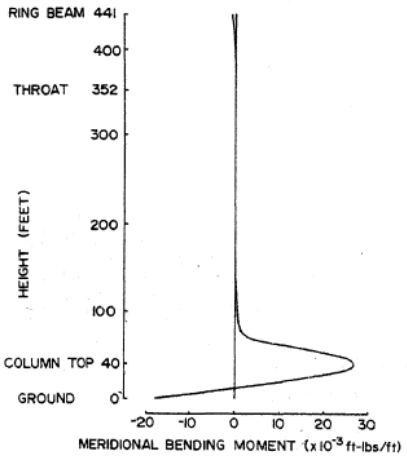

***Figure 135**: Meridional bending moment at $\theta = 0^0$* (Yang, *et al*., n.d.)

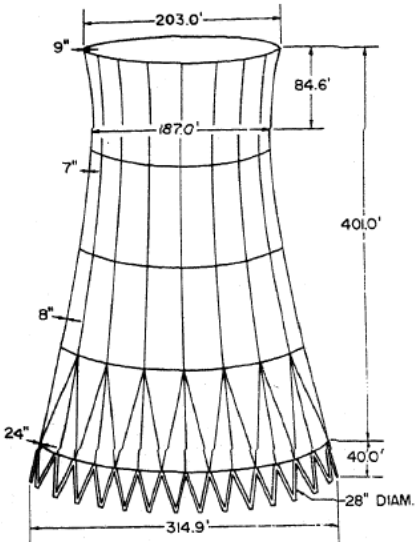

***Figure 133**: Finite element mesh model adopted for the Kentucky cooling tower* (Yang, *et al*., n.d.)

When comparing the fixed base versus column supported cooling tower, the authors found that the column supports reduced the natural frequencies of the cooling tower. This was in agreement with the observations by Gould *et al* (1974). The column top was observed to deflect significantly during seismic excitation. The study concluded that the fixed base assumption was therefore inadequate.

(Nasir, *et al*., 2002) performed a parametric study by treating the free vibration and seismic response of axisymmetric hyperbolic shell structures and examining the influence of thickness height and curvature on this dynamic response. Finite element modelling, analysis and verification was performed using the Stanwell Power Station (Australia) cooling tower of 121.5m height. The hyperbolic shell of revolution surface generating equation was used and the curvature parameter represented as shown in the equations below. The finite element model was verified with results done by others before and found to be in very good agreement. After the model verification, a parametric study was performed on the same cooling tower to investigate the free vibration response effect of the three parameters (shell thickness, height and meridional curvature). The three separate cases were treated with one parameter varied at a time whilst keeping the rest constant. *Table 12* and *Figure 136*, *Figure 137* and *Figure 138* show some of the results obtained.

$$\frac{r^2}{a^2} - \frac{H^2}{b^2} = 1\,,\; K = k^2 = \left(1 + \frac{a^2}{b^2}\right) \quad \text{.....[50]}$$

Mode		Shell Thickness (mm)				
Circumferential Modes		180	210	240	270	300
Mode 1	Period (s)	0.790	0.753	0.723	0.693	0.664
Mode 2	Period (s)	0.782	0.722	0.668	0.660	0.653
Mode 3	Period (s)	0.680	0.674	0.662	0.611	0.567
Mode 4	Period (s)	0.646	0.615	0.596	0.577	0.557
Mode 5	Period (s)	0.633	0.582	0.549	0.549	0.548
First Lateral Mode Period (s) (Mode number)		0.294 (28)	0.294 (24)	0.294 (21)	0.294 (19)	0.294 (17)

***Table 12**: Circumferential and lateral periods of vibration of hyperbolic axisymmetric shell structure of same height and curvature with shell thickness variation (Nasir, et al., 2002)*

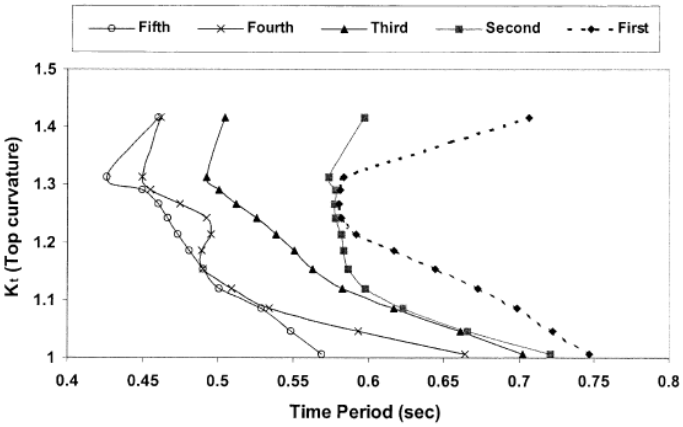

***Figure 137**: Effect of curvature on the response on the response of highest period of vibration (Nasir, et al., 2002)*

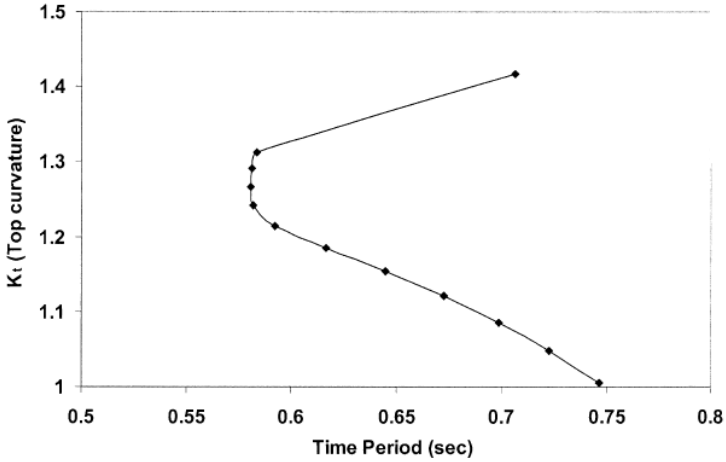

***Figure 138**: Effect of curvature on the response of the first five circumferential vibration periods (Nasir, et al., 2002)*

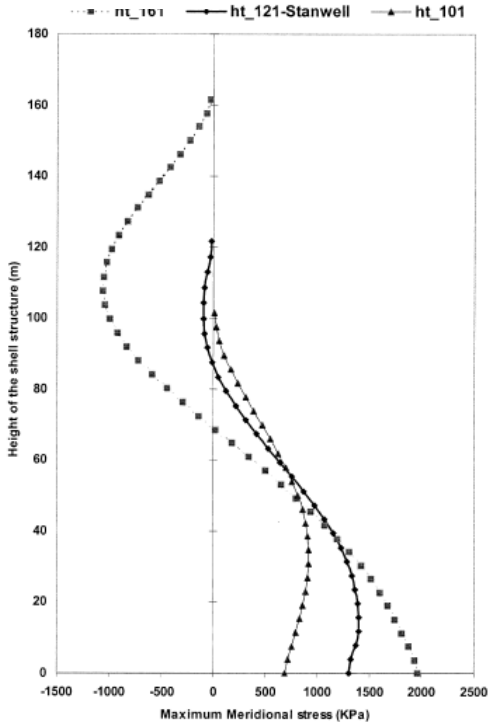

***Figure 136**: Maximum meridional stress response of three different height of hyperbolic axisymmetric shell (Nasir, et al., 2002)*

They found out that all the early modes were circumferential and the lateral modes occurred very much later beyond the 10th mode. The highest period of vibration was observed to vary approximately linearly with change in thickness and height for the thickness and height ranges studied. The period of vibration of the first lateral mode was found to be unaffected by the change in shell thickness and it occurred earliest in the thickest shell. The periods of vibration of the first lateral mode was found to increase with height and occurred earliest in the tallest cooling tower shell. The period of vibration and mode shape vibration with cooling tower meridional curvature was observed to be "interesting". The highest (fundamental) period was observed to decrease with increasing upper curvature almost linearly up to a curvature corresponding to the throat radius and thereafter reversing to increase with increase in the curvature.

The study concluded the evidence that the first lateral mode of vibration was earliest in the tallest and thickest shell with the highest curvature. The tallest cooling tower was noted to experience some of the largest deflections and stresses. The higher stress resultants in models of the same height were observed in the thicker wall shells. The cooling tower shell was observed to be very sensitive to curvature by examining the significant changes in the meridional stress as the

curvature was increased. The results from the study confirmed that the first five circumferential modes of vibration and the first lateral mode all lie within the critical band of the dominant periods of most earthquakes. This finding can therefore be conveniently used to optimise the geometry of the hyperbolic cooling tower shell when designing for these structures in seismic areas.

A decade later, (Kopenetz & Catarig, 2011) presented an efficient and simple free vibration analysis procedure for large cooling towers using bar type finite elements with inner nodes. They proposed that the cooling tower shell can be discretised as shown in *Figure 140* and *Figure 141*. The potential energy of the system due to bending and shear deformations was presented as shown in the equations below including the equilibrium condition. From these equations, the element stiffness matrix was obtained and a global analysis performed at the structural level. The obtained non-linear equilibrium equations were solved using the Newton-Raphson method. The column supported cooling tower studied by Gould *et al* (1974) was treated in this study as well. *Figure 139* shows the hoop stress response of the three different shell heights.

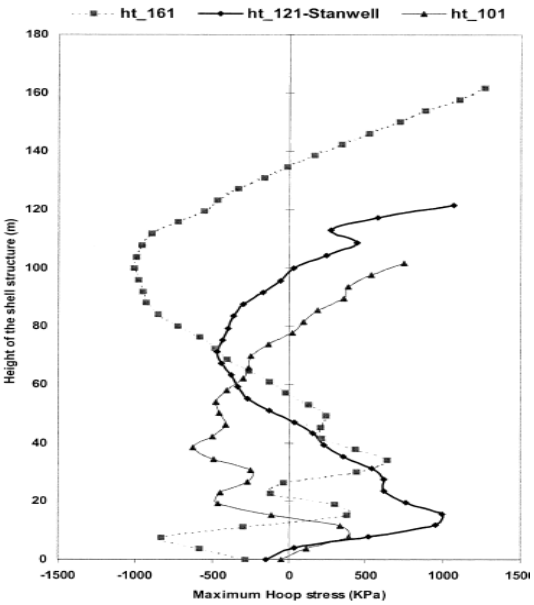

***Figure 139**: Maximum hoop stress response of three different heights of hyperbolic axisymmetric shell under earthquake loading* (Nasir, *et al*., 2002)

$$\pi = \frac{1}{2}\int_0^H E_t I_t \left(\frac{d\beta}{dx}\right)^2 dx + \frac{1}{2}\int_0^H k_t G_t A_t \left(\frac{dy}{dx} - \beta\right)^2 dx$$

$$\int_0^H E_t I_t \left(\frac{d\beta}{dx}\right)^2 \delta\left(\frac{d\beta}{dx}\right) dx + \int_0^H k_t G_t A_t \left(\frac{dy}{dx} - \beta\right) \delta\left(\frac{dy}{dx} - \beta\right) dx = 0 \quad \text{.....[51]}$$

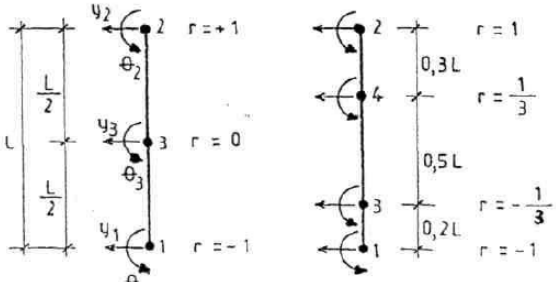

***Figure 140**: Cooling tower shell discretisation* (Kopenetz & Catarig, 2011)

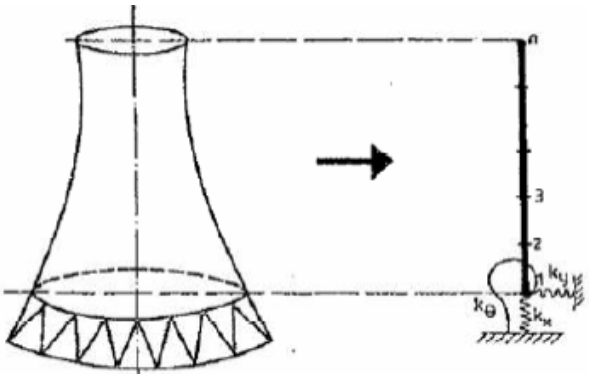

***Figure 141**: Cooling tower structural model* (Kopenetz & Catarig, 2011)

They noted that the frequency of the transverse vibrations was obtained as 2.472Hz and compared very well to those obtained by Gould *et al* (2.296Hz) with a difference of about 7.7%. The study confirmed that the free vibration analysis of cooling towers can be efficiently performed to a high degree of accuracy with a simple but practical bar type finite element idealisation of the cooling tower shell.

2.5.2 Numerical studies

(Julian, *et al*., 1983) acknowledged the earlier studies' (Albasiny and Martin, 1967; Ford, 1969) results that had showed that axisymmetric vertical flexibility of foundations reduces the cooling tower's capacity to carry wind loads by meridional membrane stresses thereby enhancing the development of circumferential bending moments along the whole height of the tower. Their study extended this finding to include the practical case of non-axisymmetric foundation stiffness. In their treatment they:

- developed a method of analysing cooling towers supported on foundations with arbitrary non-axisymmetric stiffness in either the vertical or meridional direction;
- investigated the behaviour of towers on axisymmetric flexible foundations;
- investigated the effect of non-uniform foundation stiffness on the behaviour of two typical cooling towers: (a) the 107m high Ardeer Tower and (b) the 150m high Trojan Tower.

The meridional/vertical foundation stiffness was represented by axisymmetric springs and numerically as shown in the equation below. *Figure 142* shows some of the results obtained from the analysis and *Figure 143* and *Figure 144* shows the shell displacements adopted and stiffness coefficients adopted respectively.

$$K_f(\theta) = K_{f0} + \sum_{j=1}^{j=n_f-1}\left(K_{fj}^{s}\cos j\theta + K_{fj}^{a}\sin j\theta\right) \quad \text{.....[52]}$$

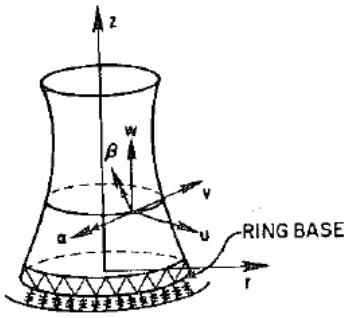

***Figure 143**: Shell displacements* (Julian, *et al.*, 1983)

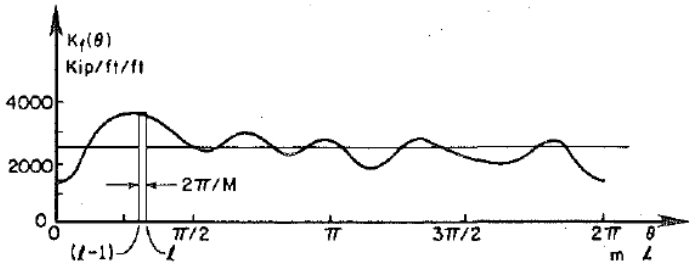

***Figure 142**: Vertical stiffness variation* (Julian, *et al.*, 1983)

The authors concluded that the vertical flexibility of the foundation plays a significant role in the cooling tower behaviour and cannot be ignored in the design. For the dead load case, it is the variation of stiffness that influences the tower stresses (circumferential moments). The magnitude of this effect is controlled by the ratio of the stiffness differential to the average stiffness. For the wind loading case, the magnitude of the average foundation stiffness controls the stress distribution compared to the stiffness variation. The response of the cooling tower was observed to depend upon two factors:

- The average foundation stiffness: the larger the ratio of the stiffness differential to the average stiffness, the larger the stresses induced into the tower shell by the foundation stiffness non-uniformity;
- The harmonic numbers: there is a specific harmonic for which the response is a maximum for each specific tower and foundation stiffness (given as a superposition of harmonic layers). This harmonic number corresponds to the harmonics for which the tower stiffness coefficient is in the same range as the foundation stiffness.

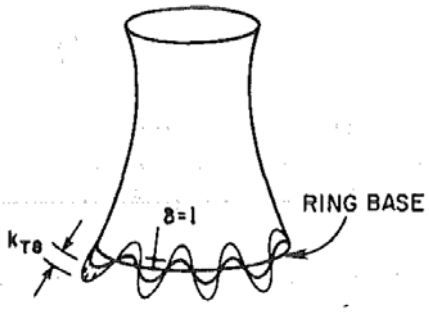

***Figure 144**: Meaning of stiffness coefficients* (Julian, *et al.*, 1983)

The results confirmed that the foundation boundary conditions should be carefully established in cooling tower design, including cases where the foundation stiffness can be variable and non-axisymmetric.

In the same year, (Reed & Scanlan, 1983) presented and discussed transfer function models that relate wind velocity to wind pressure differences at three circumferential regions around a cooling tower. The intention of the study was to use time series methods to characterise certain full-scale measured data and compare with the results from previous studies. Two cooling towers were used to perform experimental field measurements of wind velocity using anemometers or transducers located at specific points of the shell: Martin's Creek cooling tower (USA), Schenhausen cooling tower in Germany (see *Figure 145*). The time series wind velocity data was characterised into a set of wind pressure differences around the circumference of the cooling tower by using an "Autoregressive Integrated Moving Average (ARIMA)" model.

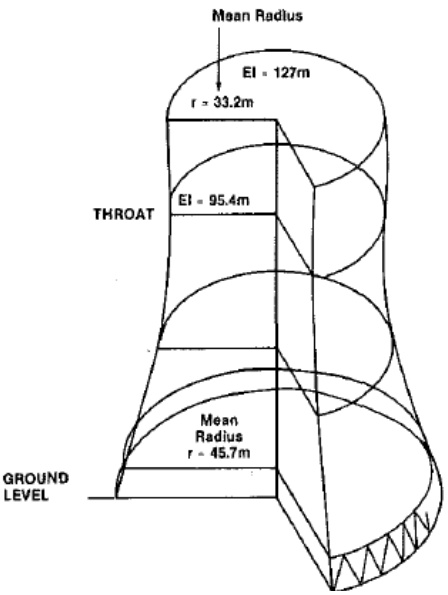

***Figure 145**: Martin Creek's cooling tower geometry* (Reed & Scanlan, 1983)

They confirmed that the study resulted in the delineation of three circumferential regions for wind flow around the cooling tower:

- Windward zone $0° \leq \theta \leq 100°$;
- Transition Zone $100° \leq \theta \leq 140°$;
- Leeward zone $140° \leq \theta \leq 180°$.

Figure 146 shows the mean and fluctuating pressure coefficient obtained.

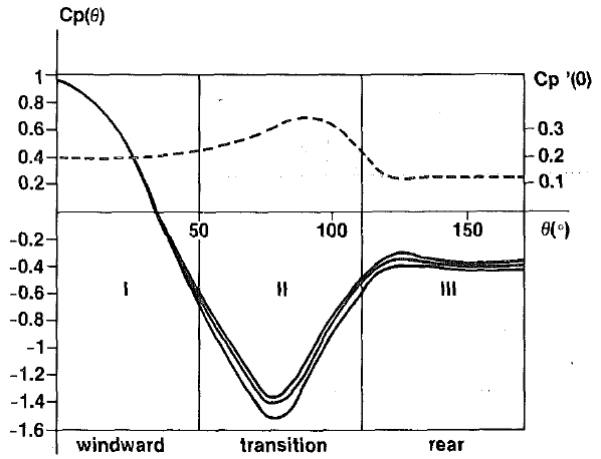

***Figure 147**: Mean and fluctuating pressure coefficient* (Reed & Scanlan, 1983)

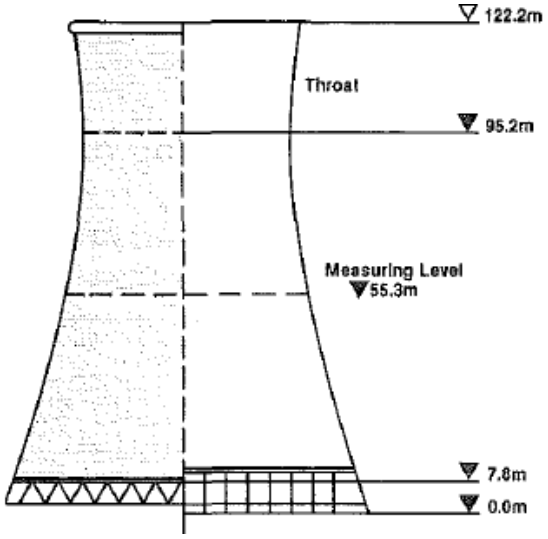

***Figure 146**: Martin Creek's cooling tower geometry* (Reed & Scanlan, 1983)

The location of the transition zone was found to be variable and dependent on the cooling tower surface roughness. The effect of the wind velocity was observed to disappear after approximately 15 seconds for the windward pressure. The ARIMA model showed that the wind pressure-difference at a time was not only affected by the velocity at time t, but also by a weighted sum of the previous wind velocities. The flow of wind gets distorted around the cooling tower shell by the geometry and the surface roughness.

Over two decades later, (Sabhouri-Ghomi, *et al*., 2006) investigated a cooling tower's dynamic behaviour under seismic excitation using realistic horizontal and vertical ground acceleration data from recent earthquakes. The Tabas, Naghan, and Bam (Iran) earthquakes' vertical and horizontal ground accelerations were used to perform a linear and non-linear dynamic analysis of the 134m high Shazand thermal power generating facility (Iran) cooling tower shown in Figure 149. A dynamic linear finite element analysis using elastic elements was first undertaken, followed by a dynamic non-linear finite element analysis with the long 15m X-type columns represented in the model. Geometric imperfections were excluded in the analysis. Some of the results of the analysis are shown in *Figure 151* and *Figure 152*.

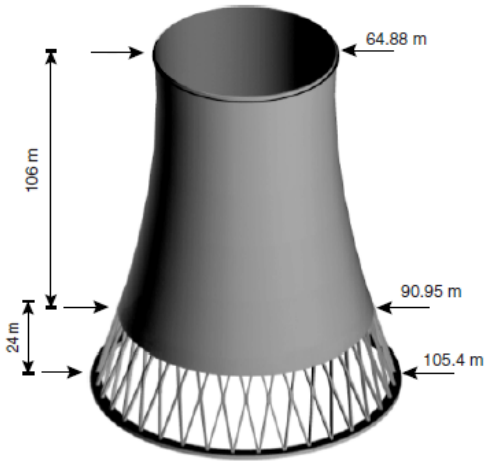

***Figure 149**: Representation of the Shazand cooling tower shell* (Sabhouri-Ghomi, *et al*., 2006)

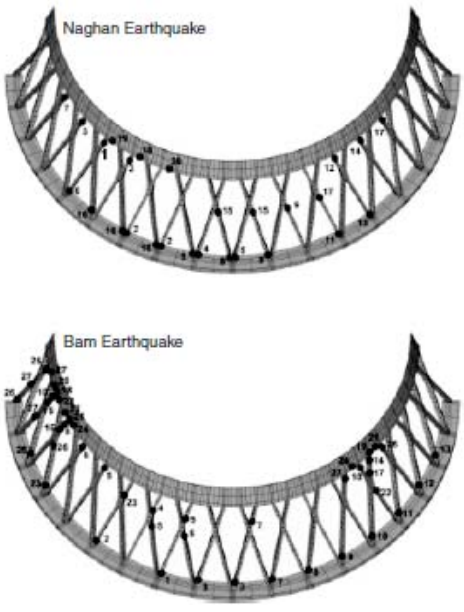

***Figure 148**: Sequential formation of plastic hinges under earthquake excitation* (Sabhouri-Ghomi, *et al*., 2006)

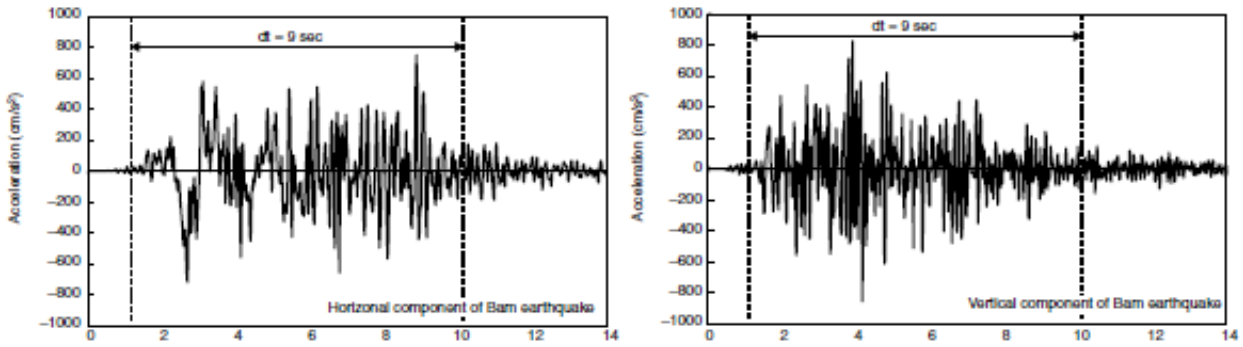

***Figure 150**: Some of the earthquake acceleration records* (Sabhouri-Ghomi, *et al*., 2006)

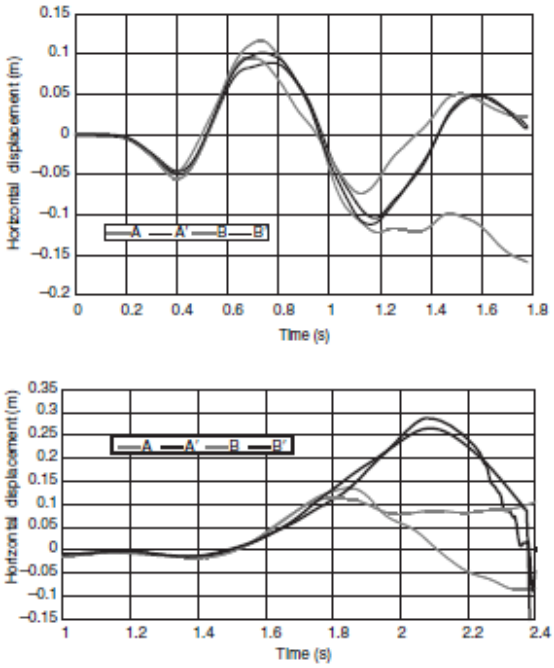

***Figure 151**: Horizontal displacements of key locations for two of the three earthquakes* (Sabhouri-Ghomi, *et al*., 2006)

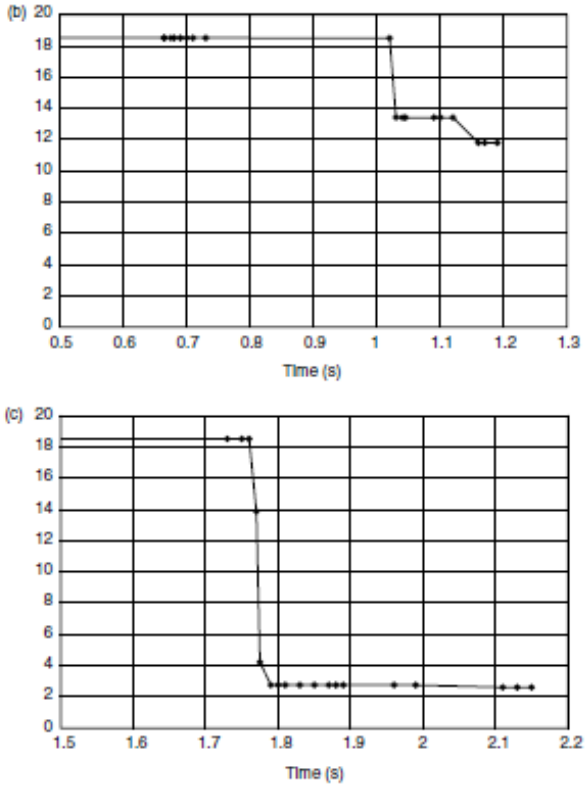

***Figure 152**: Degradation of buckling load factor with time for two of the earthquakes* (Sabhouri-Ghomi, *et al.*, 2006)

They concluded that the plastic hinges form mainly in the columns at junctions with other members where there are high stress concentrations as shown in *Figure 148*. The plastic hinges in the shell were the last hinges to form. The hinge formation sequence depends on the nature of the earthquake. The inelastic dynamic response due to the plastic hinge formation reduces the stiffness of the cooling tower structure, reduced the applied base shear and increased the displacements. After the plastic hinges formation in the columns, the cooling tower would collapse under gravity loading in the Tabas and Bam earthquakes before even the excitation had completed. On analysing the buckling load factor during the earthquake, it was observed to progressively decrease under self-weight and gets eroded significantly. The findings confirmed the need for further research in this area especially to account for the effects for simultaneous dynamic, gravity and stability analysis during seismic excitation.

Seven years later (Nangshineh, *et al*., 2013) investigated the behaviour of cooling towers under seismic excitation by finding suitable support solutions that reduce earthquake effects. An iso-parametric solid element was used for the finite element modelling of the cooling tower. A time-integration dynamic analysis was performed on the 115m high cooling tower. The investigation then focused on: (a) the cooling tower analysis with the hyperbolic cooling tower supported on either column supports on an annular raft on a fixed base and (b) the effects of a ring beam support on the overall response of the cooling tower.

They concluded that in the ring beam supported cooling towers, stresses at the base level significantly decrease while the high compressive stress effects caused buckling in the columns supporting the cooling towers. The ring beam system was therefore proposed as an alternative support system for cooling towers in high risk areas of seismicity.

At the same time, (Sahana & Sulaiman, 2013) performed a finite element static and dynamic analysis of a 125m high cooling tower by considering the influence of the shell thickness and size of opening in the shell on its behaviour. Three cases of the same geometry of the cooling tower were considered with the following parametric variations: (a) shell thickness at throat as 125mm, 175mm and 225mm and (b) shell opening size as 125mm, 1800mm and 2000mm respectively. The static maximum principal stresses under self-weight were found to decrease with increase with shell thickness.

In the same year, *(Veena, et al*., 2013) performed a static and dynamic finite element analysis of a 125m high cooling tower shell considering its behaviour under wind when supported by A-frame and H-frame columns. The finite element analysis was performed with all geometric and material properties of the cooling tower remaining constant except for the two cases where the shell was supported on: (a) A-frame columns and (b) H-frame columns. The study concluded that the principal static stresses and maximum deflections under self-weight were greater for the A-frame than for the H-frame column supports. The free vibration principal stress for the first mode and the principal stress due to the wind loading were greater for the H-frame than for the A-frame column supports. The maximum deflection due to wind load and seismic load was greater for the H-frame than for the A-frame column supports.

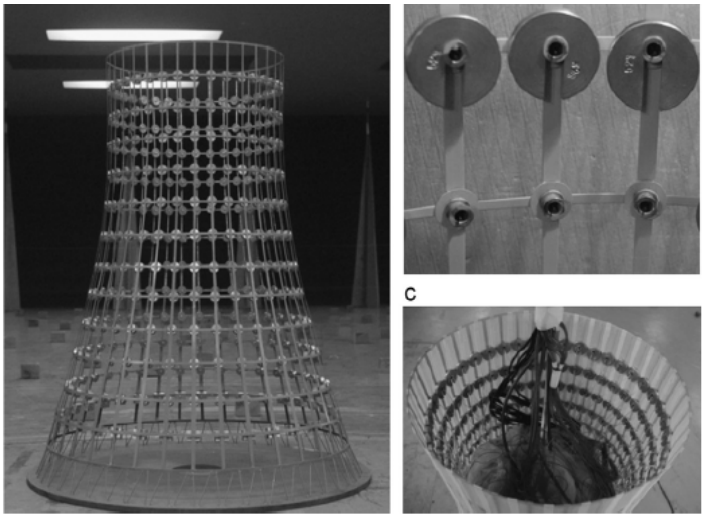

***Figure 154**: An aero-elastic cooling tower shell model for simultaneous pressure and vibration measurements* (Ke & Ge, 2014)

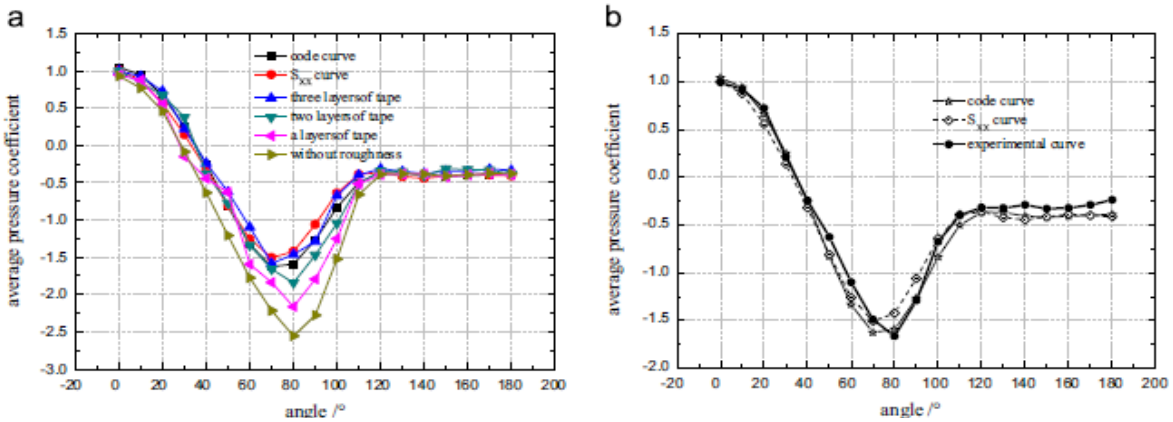

***Figure 153**: External wind pressure distribution for cooling towers: (a) rigid model without self-excited force; (b) aero-elastic model with self-excited force* (Ke & Ge, 2014)

A year later, (Ke & Ge, 2014) noted that earlier research conducted on wind loads and their effects on super-large cooling towers had technically ignored the effects of self-excited forces induced by the interaction of the cooling tower structure and the airflow. Their study concentrated on the effects of self-excited force on the distribution characteristics of external mean and fluctuating wind pressures as well as the characteristics of the spectral density of displacement responses.

A Chinese 215m high super-large cooling tower was used as an example and wind tunnel tests of the cooling tower aero-elastic model pressure and vibration measurements were performed (see *Figure 154*). External wind pressures of the cooling tower were obtained with the presence of a self-excited force. Wind tunnel responses of the super-large cooling tower were computed for the two cases of wind tunnel tests with and without the self-excited force using refined frequency domain algorithm of wind-induced responses. After this, the self-excited force effects on wind-induced responses and Gust Response factors of the super-large cooling towers were presented. The wind pressure distributions for the various cases are shown in Figure 155. Figure 157 shows a 3-D distribution of the various components of the fluctuating response.

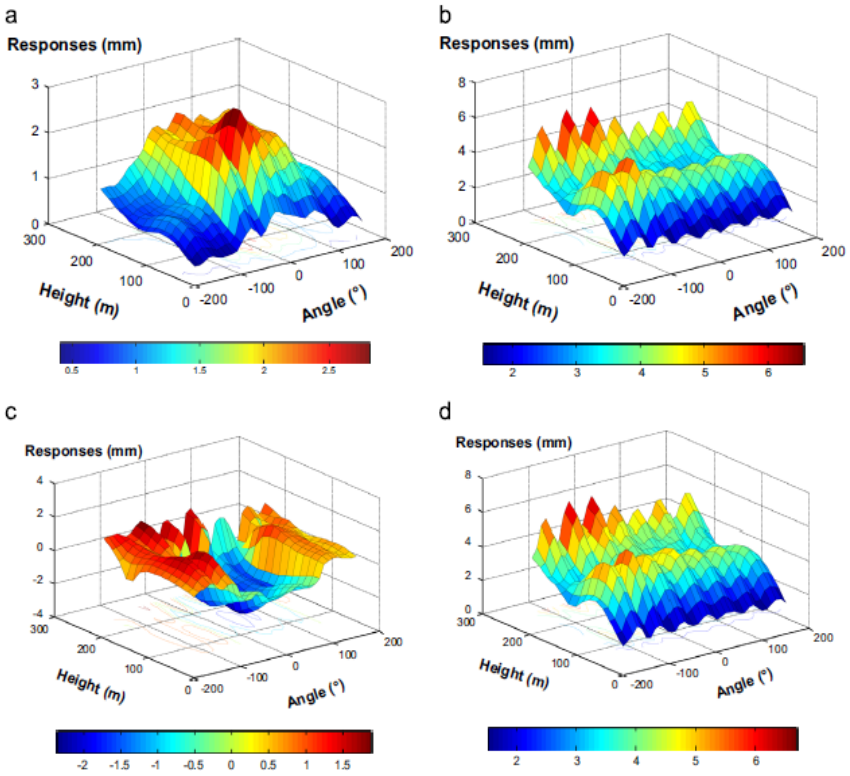

***Figure 155**: 3D distribution of different components of the fluctuating response on super-large cooling towers with self-excited force: (a) background response; (b) resonance response; (c) coupling response and (d) total fluctuating response* (Ke & Ge, 2014)

The authors concluded that the external mean wind pressure distribution showed good symmetry in the absence of the self-excited force. The consideration of the self-excited force completely destroyed the symmetry of the fluctuating wind pressures. The effect of the self-excited force on the displacement response spectrum was found to be negligible. The effect of the self-excited force on the Gust Response factors is a reduction in the lower region and an increase in the upper and top areas of the super-large cooling tower, but was however small and negligible. In the displacement response power spectra of the two model cases, the resonant response was found to have a dominant role and the background component was less than the resonant component. The study managed to allay any worries practicing engineers may have on the influence of self-excited forces on the distribution characteristics of external mean and fluctuating wind pressures on super-large cooling towers.

In the same year, (Li, *et al*., 2014) studied the modes and mechanisms of collapse of super-large cooling towers when subjected to accidental loads like vehicle collision, airplane impact, localised explosion and missile attack. A 235m high cooling tower was adopted as an example in which the four accidental loading cases were taken into account. A finite element modelling analysis was performed and verified with a physical 1:100 scaled model subjected to the same loads and the modes of failure compared. After verification of the finite element model, simulations of the four accidental loads were performed. Some of the results of the comparison are shown in *Figure 156*, *Figure 157* and *Figure 158*.

***Figure 156**: Comparison between tested collapse modes and calculated collapse modes* (Li, *et al*., 2014)

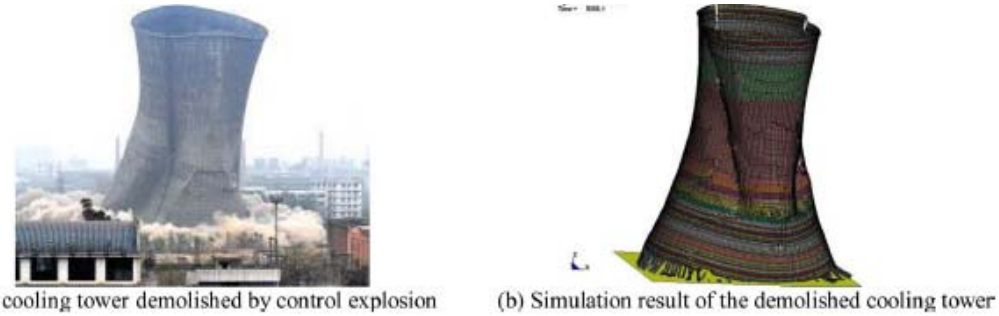

(a) A cooling tower demolished by control explosion (b) Simulation result of the demolished cooling tower

***Figure 157**: Comparison of collapse modes of a cooling tower demolished by controlled explosion* (Li, *et al.*, 2014)

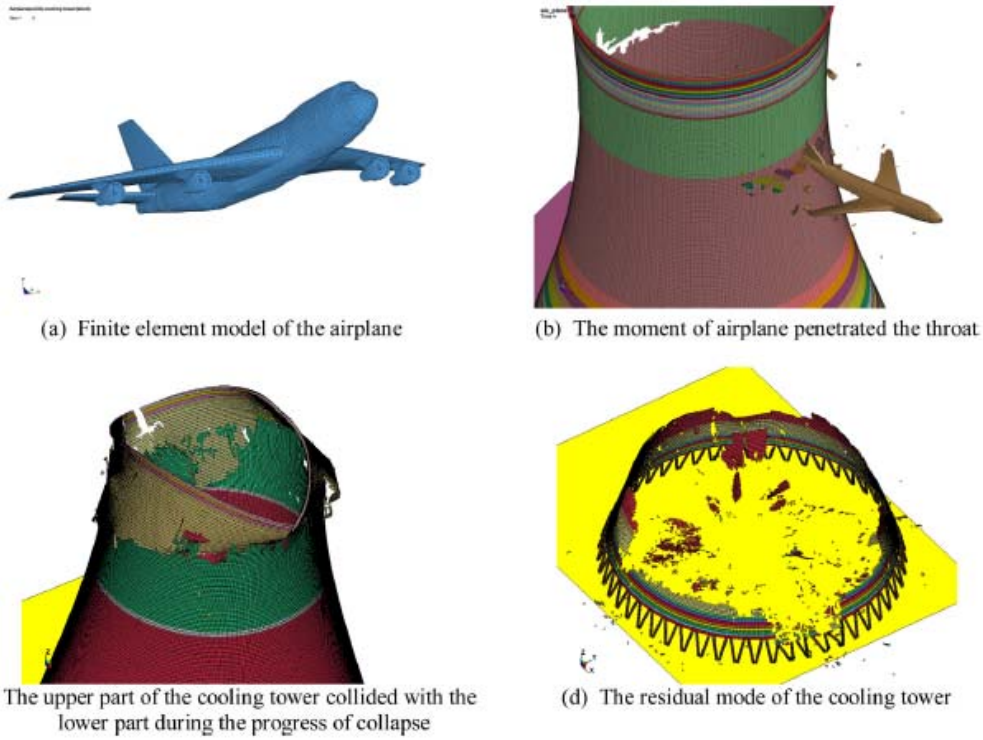

(a) Finite element model of the airplane (b) The moment of airplane penetrated the throat

(c) The upper part of the cooling tower collided with the lower part during the progress of collapse (d) The residual mode of the cooling tower

***Figure 158**: The collapse progress of the tower subjected to airplane impact* (Li, *et al.*, 2014)

The study concluded that only local damage occurred when the inclined columns suffered the truck collision, or a 200kg or less TNT equivalent mass explosion and the tower was still stable. Progressive collapse and different collapse modes were observed when the super-large cooling tower was subjected to large TNT equivalent mass explosions of 2000kg and 4500kg as well as an airplane impact. With the large TNT equivalent mass explosions, the inclined columns were severely demolished causing the entire structure to fall down. With the airplane impact, localised failure of the shell was induced causing the upper cooling tower shell to collide with the lower part due to gravity. The results obtained can be used to understand the collapse modes of super-large cooling towers when exposed to such accidental loads.

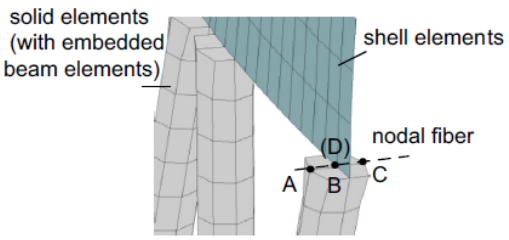

***Figure 159**: Connection of shell elements to solid elements* (Lin, *et al.*, 2014)

Still in the same year, (Lin, et al., 2014) predicted ground motion accelerations caused by the collapse of a large-scale cooling tower under a strong earthquake. They developed a cooling tower-soil model on the basis of a falling weight - soil model verified by weight tests as depicted in *Figure 160*. They then simulated the cooling tower collapse process using the proposed model to assess the collapse-induced ground accelerations. After this, the overall combined ground motion consisting of the earthquake-induced (primary) ground motion and the collapse-induced (secondary) ground motion was estimated using the principle of wave superposition. A 215m high cooling tower was modelled and analysed as a three-dimensional finite element model with layered shell elements. The soil model was also modelled as a 1000m x 1000m x 35m deep finite element model depicting strongly weathered sandy slate properties. Six types of real earthquake characteristics (peak ground acceleration, PGA, duration and spectrum characteristics) were chosen and

applied to the finite element model. *Figure 159* shows the adopted shell elements/solid elements connection whilst *Figure 161* shows the contour map of the collapse induced ground movement distribution. *Figure 162* and *Figure 163* show some of the analysis results obtained.

The authors concluded that the large-scale cooling tower may collapse under strong earthquakes with horizontal PGAs ranging from 0.35g to 0.45g. Moderate collapse induced ground vibrations may occur at horizontal PGAs ranging from 0.011g to 0.080g at 350m from the cooling tower. These vibrations were observed to attenuate with increased distance from the cooling tower. The combined ground motion (earthquake-induced + collapse-induced) was estimated at horizontal PGAs of 1.17 times the earthquake-induced PGAs. The collapse modes and site geology were noted to significantly affect the collapse-induced ground motion. The collapse modes for all the six earthquakes were found to be similar. The results obtained from this study showed that the effects of collapse-induced ground vibrations should be seriously considered in the safety evaluation and planning of critical plants like nuclear power plants and related facilities.

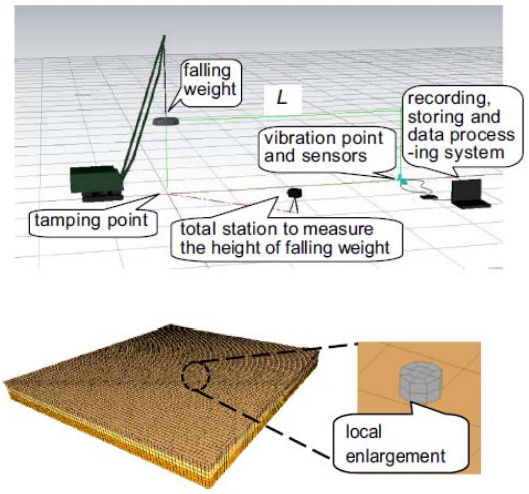

***Figure 160**: The falling weight-soil model* (Lin, *et al*., 2014)

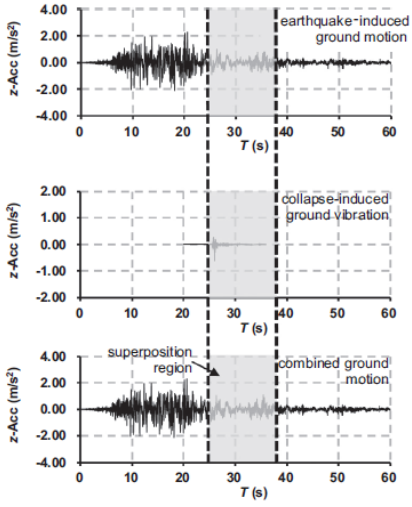

***Figure 162**: The superposition process of ground vibration/motion at a distance of 350m* (Lin, *et al*., 2014)

***Figure 163**: Collapse mode with "collapse in fragments" for another cooling tower under the Tabas earthquake* (Lin, *et al*., 2014)

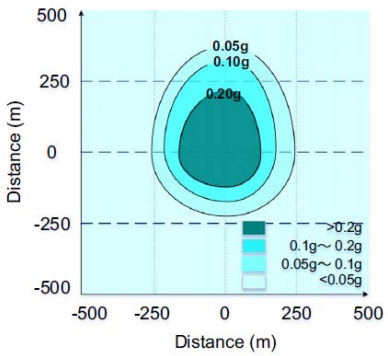

***Figure 161**: The contour map of collapse-induced peak ground acceleration distribution under earthquake excitation* (Lin, *et al*., 2014)

In the same year, (Kulkarni & Kulkarni, 2014) performed static, dynamic and buckling analysis on five different cooling towers with variable geometry under self-weight, wind and seismic loads. Two 144m and 176m high cooling towers with variable geometry (five cases) were modelled as three-dimensional finite element models and analysed to assess the maximum principal stresses, deflections and buckling modes. They observed that the free vibration principal stresses for the first mode at the cooling tower top increases as the shell thickness is increased and the converse is true in the region from the throat to the shell bottom. Under wind loading, the deflection and maximum principal stress decreased as the thickness was increased.

2.5.3 Experimental and field studies

(Weingarten, *et al*., n.d.) studied the effect of gravity loading on the seismic response of cooling towers. Their study performed free vibration analysis (natural frequencies and mode shapes) and forced vibration analysis of various size cooling towers using analytical and experimental methods. A cooling tower model was subjected to a harmonic loading applied through a rigid plate fixed to the shell. Analytical free vibration equations were derived to compute the natural frequencies and mode shapes. These were found to be in good agreement with the experimental results and the equations were solved using a finite element analysis method. *Figure 165* shows the effect of dead loads on the natural frequencies of the shell.

They concluded that the natural frequencies obtained from the experimental investigation compared very well with those obtained from the finite element analysis. The dead load was noted to have a significant effect on the natural frequencies of the tallest cooling tower compared to the shorter ones. The deflections were noted to be much larger for cases were dead load is considered than for those cases that excluded dead load. The study confirmed with authority the influence of dead loads on the free vibration properties especially of taller cooling towers.

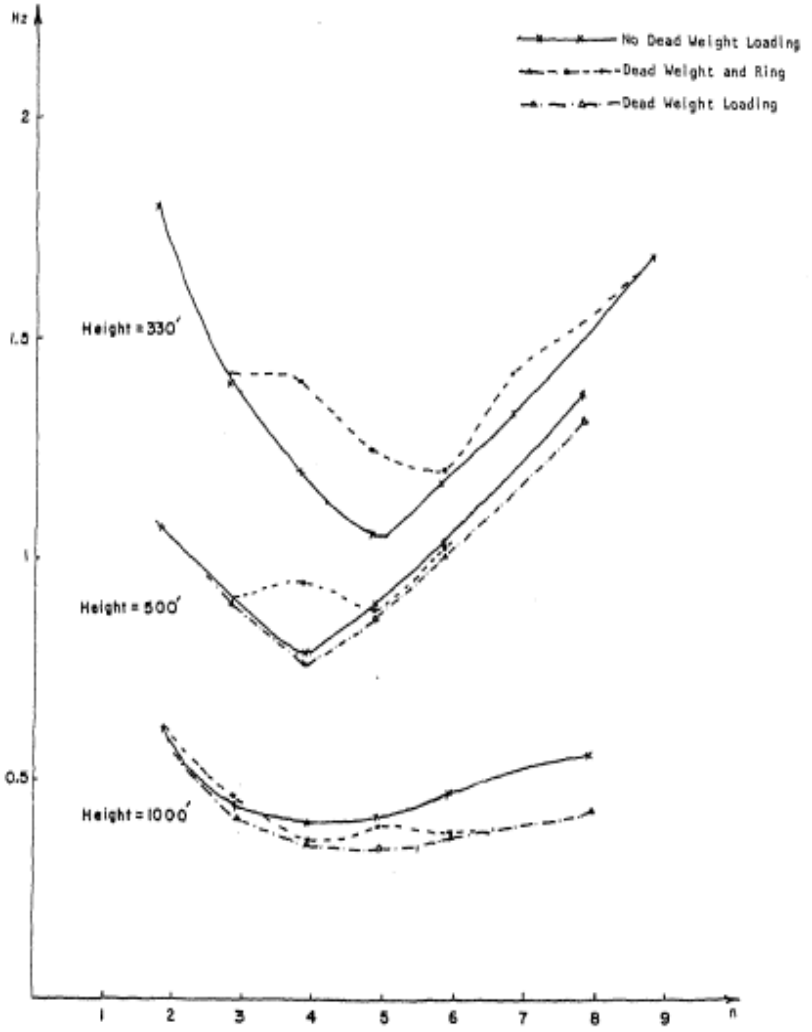

***Figure 165**: Effects of deadweight loading on natural frequencies of hyperboloidal shells* (Weingarten, *et al*., n.d.)

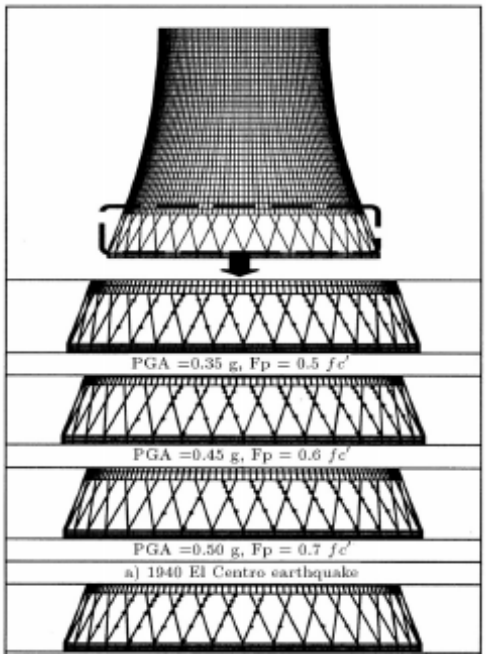

***Figure 164**: Plastic hinges formed in the finite element model* (Sabhouri-Ghomi & Kharrazi, 2005)

(Sabhouri-Ghomi & Kharrazi, 2005) presented an analysis of the stability, non-linear behaviour and the state of stresses of a hyperbolic cooling tower under seismic loading. An existing 119m high cooling tower in Ishafa (Iran) with long X-shaped supporting columns was studied for its seismic behaviour. A non-linear finite element analysis was performed for the cooling tower under two types of earthquakes, namely the El Centro earthquake (1940) and the Tabas earthquake (1978). A non-linear time history finite element analysis was performed for the cooling tower under the two earthquake records followed by a non-linear buckling analysis to determine the buckling factors.

The outcome of their analysis showed that there were no significant plastic deformations within the cooling tower shell elements. The first plastic hinges formed in the columns around the following regions:

- shell to column connections;
- column to foundation connections and
- column to column intersections as shown in *Figure 164*.

An unstable condition for the high risk seismic regions did not exist since the buckling factors were shown to be higher than the design provisions of five of the different combinations of loads and material properties. They established that the design of the supporting columns of a hyperbolic cooling tower requires careful attention in order to minimise plastic hinge formation and shear deformations in these columns. They established that the buckling safety factor of the shell is not a concern under seismic excitation.

2.6 COOLING TOWER GROUP EFFECTS

2.6.1 Experimental and field studies

For his PhD thesis, (Orlando, 2001) carried out experimental wind tunnel tests on two adjacent rigid model cooling towers to measure the interference effect of the towers on the wind pressure against the towers as compared to an isolated tower. Boundary Layer Wind Tunnel (BLWT) tests were first performed on a single rigid model and the results were verified against the Niemann's curve with very good agreement (see *Figure 167*). The same test was then performed on two adjacent rigid models with varying distances apart and varying wind directions. The distance between the two models was varied from 1 to 3 times the cooling tower base diameter. The wind direction was varied from 0° to 30° and one test at 90° (side by side arrangement) as depicted in *Figure 168*. Ignoring resonance, the structural response of the cooling towers was evaluated taking linear elastic behaviour of the material into account and the wind loads as qausi-static. Interference factors were computed for the structural response to compare the group results to those of the isolated cooling tower. The studied model is shown in *Figure 166*.

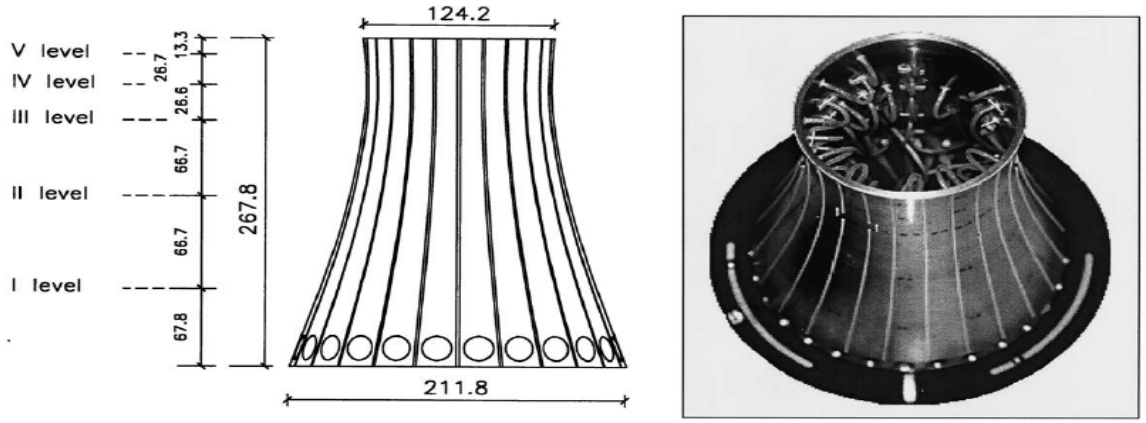

***Figure 166**: Model dimensions* (Orlando, 2001)*)*

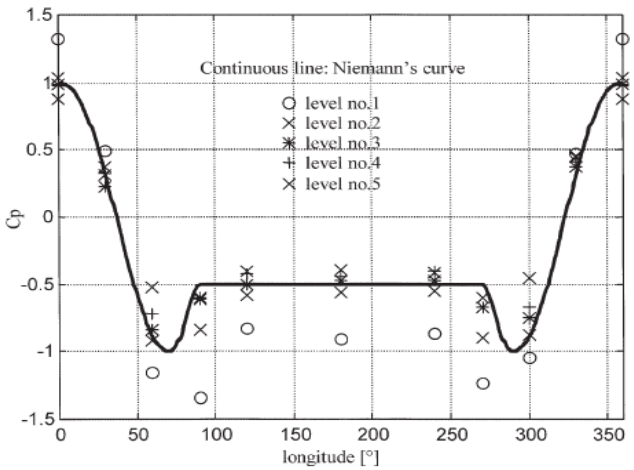

***Figure 167**: Comparison of experimental values with Niemann's theoretical curve* (Orlando, 2001)

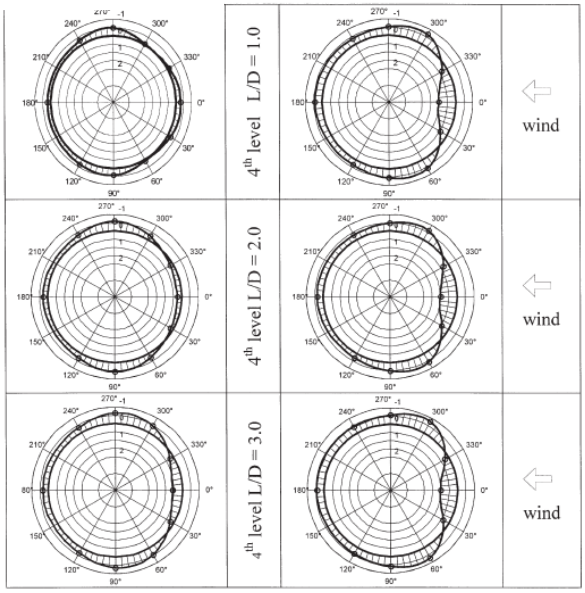

***Figure 168**: Polar diagrams of the mean pressure coefficients at the throat of the tower "in tandem"* (Orlando, 2001)

For the wind direction 0° (in tandem arrangement) the wind pressure measurements were found to be similar to those on the isolated tower. For the staggered wind direction ($0° < \theta < 30°$) the wind pressure pattern for the upwind cooling tower was similar to that of the isolated cooling tower, but was however asymmetrical. For the side by side arrangement ($\theta = 90°$) the pressure distribution reflected that of the isolated case but the maximum suction was asymmetrical when compared to the wind flow direction. For all the wind direction arrangements it was observed that the highest interference affected the lowest levels of the cooling towers. The interference at the highest levels of the cooling tower was less pronounced because

- of the longer distance between the towers at the top;
- of the less turbulence intensity at the top and
- of the flow over the top of the towers.

3-D interference factor representation was presented for the maximum and mean pressures, mean meridional force, mean hoop bending moment, maximum hoop stress and maximum meridional stress. The results obtained agreed with those of other researchers *Figure 169*, *Figure 170*, *Figure 171* and *Figure 172* show some of the results obtained from the experiment. The procedure presented is therefore a suitable method for studying wind group interference effects of adjacent cooling towers.

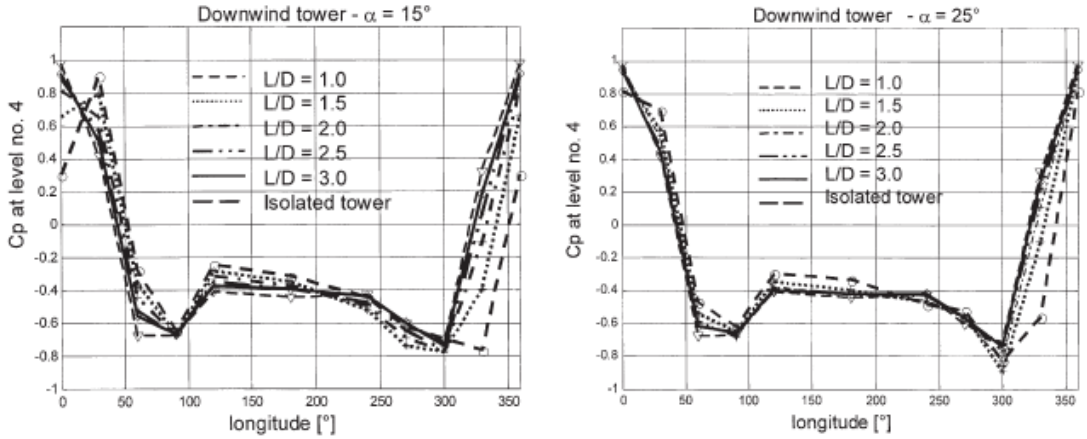

***Figure 169**: Downwind tower: mean pressure coefficients at the throat for a= 15^0 and a= 25^0* (Orlando, 2001)

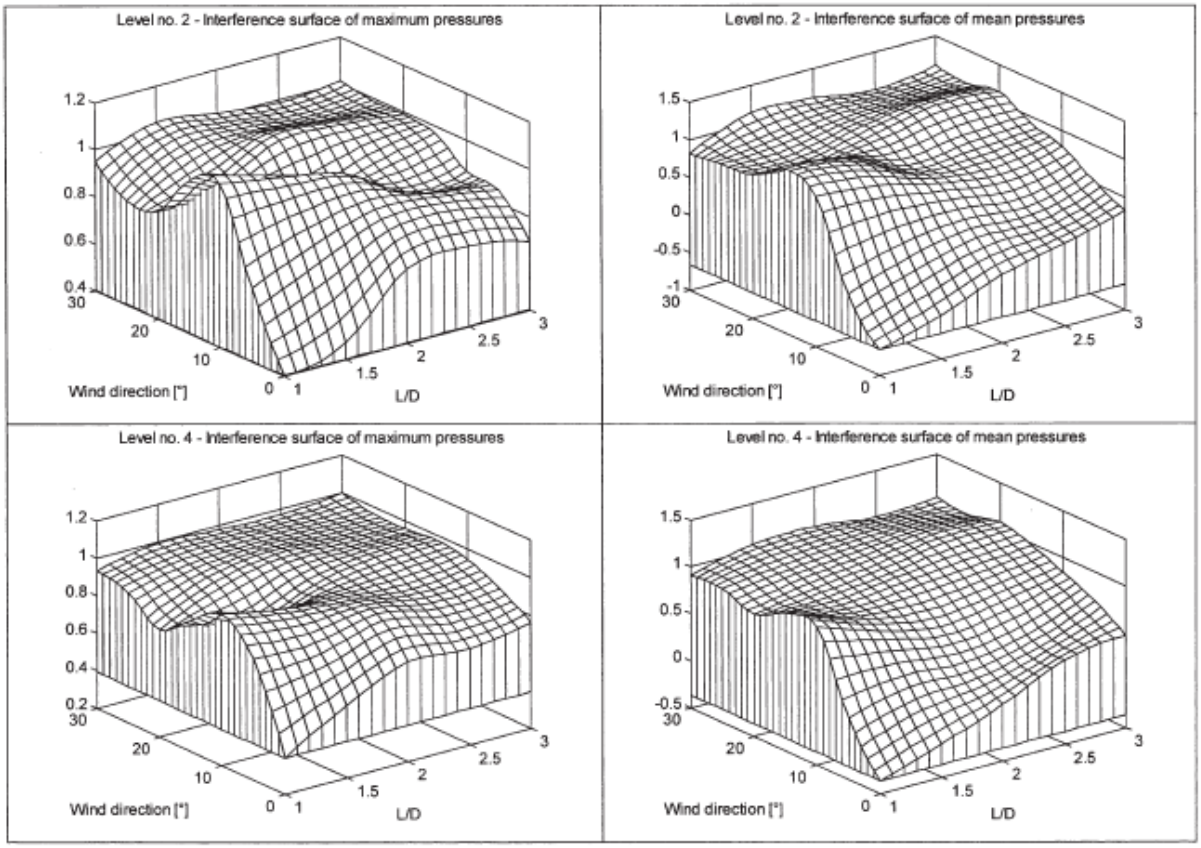

***Figure 170**: Downwind tower interference surfaces of the maximum and mean pressure coefficients at the second and fourth levels* (Orlando, 2001)

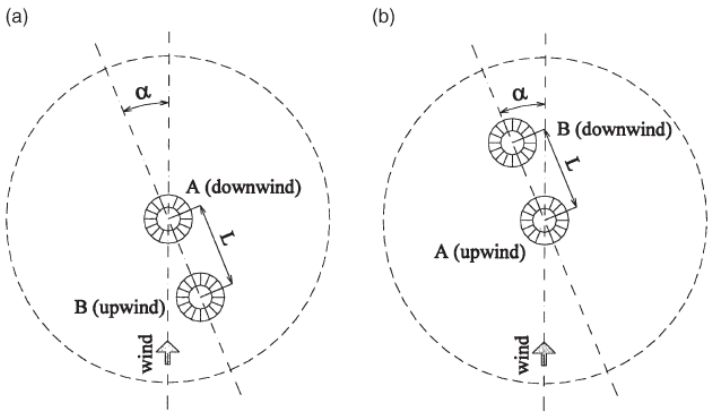

***Figure 171**: Positions of the two models in relationship to the wind directions* (Orlando, 2001)

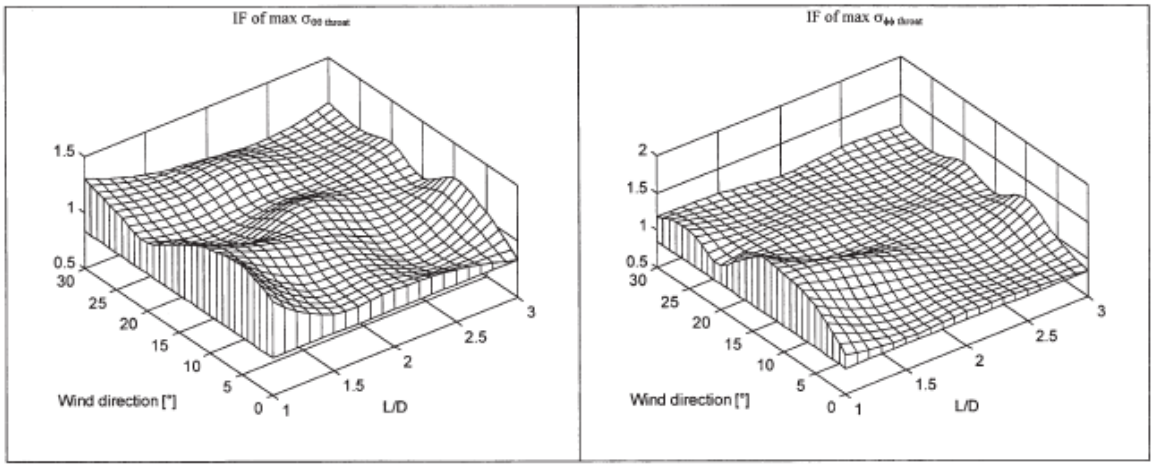

***Figure 172**: Interference factors of the maximum hoop normal stresses and maximum meridional normal stresses at the throat* (Orlando, 2001)

2.7 CONCLUSION OF THE LITERATURE REVIEW

The literature review has been categorised into studies done on cooling towers in respect of their quasi static behaviour, stability behaviour, dynamic response and group effects when subjected to wind loading, seismic excitation and under self-weight.

The main findings of the studies performed on cooling towers in respect of their quasi static behaviour have revealed that the use of ring elements in finite element analysis is efficient. It has been shown that openings and cut-outs introduce significant stress distribution patterns in the shell. Ultimate failure of the shell under quasi static loads has been shown to be by crack propagation, load carrying capacity increase, reinforcement yielding and followed by failure. The stability behaviour studies have revealed that geometric construction imperfections require a critical consideration when considering the buckling behaviour of cooling towers. The self-weight loading causes early deformed shapes that cause local reduction in circumferential shell stiffness and initial circumferential bending leading to meridional cracking - hence buckling safety must take into account geometrical defects. The provision of ring stiffeners results in more significant gain in buckling safety factors as opposed to a gradual thickening of the shell. The circumferential buckling of the shell around the throat leads to failure, as opposed to meridional reinforcement yielding under wind loads. It was revealed that the use of combined membrane and flexural stresses as opposed to a pure membrane stress approach can improve general design methods of the shells. Unlike with buckling, the studies on dynamic response have revealed that openings and cut outs do not influence the lower natural frequencies and modes of the shell. A number of finite element models have been studied to obtain efficient converging models for the dynamic analysis of cooling tower shells subjected to wind loading. Addition of stiffening rings does not assist the seismic resistance of cooling tower shells. The modelling of the columns, foundations and soil-structure interaction plays a significant role in the results of finite element results on wind and seismic dynamic response of the cooling towers. Finally, the studies on the group effects of cooling towers have revealed that interference of wind effects on a group of cooling towers is more significant at the bottom of the shell than at the top. However, it was observed that not much research has been done in this area.

The main focus of the studies has been on the buckling of cooling tower shells as compared to their vibration behaviour and dynamic response to loading. It was observed that generally equal attention has been focused on both wind induced vibration of cooling towers and their dynamic response to seismic excitation. However, less attention was observed on the form finding and geometrical parametric analyses. The most recent research trends were observed to focus on the seismic response of cooling towers as compared to wind induced vibration. In addition, more attention is being given to the concrete deterioration, durability and repair methods of cooling towers.

Further attention should be focused on the vibration analysis of cooling towers when subjected to wind loading. There is need to understand the vibration behaviour of cooling towers as their geometry is changed. In addition, there is need for studies focusing on the geometrical form finding of the cooling tower shell with respect to its buckling and vibration behaviour. Similarly, more focus is required on cooling tower group effects under wind loading. It is apparent that the gaps in the understanding of cooling tower behaviour are particularly on the effect of changing the shell geometry on the buckling behaviour and vibration response as well as finding shell forms that satisfy pre-determined buckling safety factors and vibration response. In the light of the gaps, this research will focus on investigating the buckling behaviour of cooling towers in response to changes in shell geometry when the shell is subjected to increasing wind speed. It will also focus on investigating the free and forced vibration behaviour of cooling towers in response to shell geometry changes when the shell is subjected to increasing wind frequencies of the same speed.

3 RESEARCH METHODOLOGY

3.1 RESEARCH NEEDS, AIMS, OBJECTIVES AND KEY QUESTIONS

An enormous amount of research has been conducted on cooling towers over the last sixty years. A fair amount of this research has concentrated on the stability behaviour and dynamic response of cooling towers. A huge amount of research papers have been presented worldwide. Most of these are with the American Society of Civil Engineers (ASCE) as observed during the literature review in this research. Even so, the understanding of the stability behaviour and dynamic response of cooling towers remains of paramount importance due to the continued growth of economies, industries and power generation plants.

With the increasing capacity of power generation plants, it will always be necessary to consider increasing both the height and diameter of the cooling tower shell. Similarly, it may be necessary to alter the geometrical proportion of the shell dimensions to optimise the thermal properties of the cooling tower. Consequently, understanding the stability behaviour and dynamic response of the cooling tower shell becomes more important. There will always be a need to establish an understanding of the stability behaviour and dynamic response patterns of the cooling tower shell as the geometry of the shell is altered. With the advent of high speed computer hardware and software, the relationship between the change in geometry and the stability behaviour and dynamic response can be established. This research will focus on establishing the relationship between the stability behaviour and dynamic response of the cooling tower shell and its geometrical parameters. The aims and objectives of this research are presented below.

3.1.1 Aims and objectives

The *aim* of this research is to establish the relationship between the changing trends in stability behaviour and dynamic response of a cooling tower shell and its change in geometry (height, diameters and thickness).

The *objectives* of this research are:

- To determine the variation in the stability behaviour (critical buckling wind loads and modes) of the cooling tower shell with change in height, diameter and thickness of the shell;
- To determine the variation in the free vibration response (natural frequencies and modal shapes) of a cooling tower shell with change in height, diameter and thickness of the shell;
- To determine the variation in the cooling tower's forced vibration response (response frequencies) when subjected to wind loading with its change in height, diameter and thickness of the shell;
- To determine the optimum geometries of the cooling tower shell with respect to stability behaviour and dynamic response under wind load.

3.1.2 Key questions and expected outcomes

This research will attempt to answer the following *key question*: How would the cooling tower's stability behaviour (critical buckling wind loads and modes) and dynamic response (free vibration, modal shapes and forced wind vibration response) change as its shell geometry (height, diameter and thickness) is changed?

The research's expected outcomes are as follows:

- The critical buckling wind loads are expected to reduce with increasing height and increase with increasing thickness;
- The natural frequencies are expected to reduce with the increase in the height and diameter of the shell;
- The response frequencies are expected to reduce with the increase in the height and thickness.

3.2 RESEARCH METHODOLOGY

3.2.1 Parametric studies on cooling tower shell

A parametric study of the cooling tower's stability behaviour and dynamic response was performed. The following aspects were considered:

Stability behaviour analysis: A linear eigenvalue buckling analysis was performed for various categories of the cooling tower geometries. The cooling tower was subjected to an increasing wind pressure (corresponding to increasing wind velocity) in order to obtain the critical pressures/velocities at which the shell first buckled and the respective buckling modes. The cooling tower's geometrical parameters were changed in a systematic manner in order to obtain the relationship between critical wind velocities associated with the first mode of buckling and the cooling tower's geometrical parameters. In order to cover a wider range of the geometrical parameters, ratios of the cooling tower's dimensions were considered. At least twenty (20) cooling towers were considered for each set of parameters in order to obtain a wider range of representative samples of the analysed cooling towers.

The following geometrical parameters were investigated to obtain their variation with the critical wind velocity:

- Height *(H)* of the cooling tower;
- Throat height position using throat height to total height *(H_t/H)* ratio of the cooling tower;
- Cooling tower height to diameter ratios represented by the height to top edge/bottom edge/throat diameters *(H/D_{top}, H/D_{bot}, H/D_{thr})*;
- Top edge and bottom edge diameter to throat diameter ratios *(D_{top}/D_{thr}, D_{bot}/D_{thr})* of the cooling tower;
- Bottom edge to top edge diameter ratios (D_{bot}/D_{top}) of the cooling tower;
- Cooling tower shell thickness.

Free and forced vibration analysis: A linear eigenvalue vibration analysis was performed to obtain the first ten (10) different natural frequencies and mode shapes for each cooling tower under a group of geometrical parameters as for the stability behaviour analysis. The natural frequencies were recorded for modes 1, 3, 5, …, 17 and 19 being the odd numbered modes because the even numbered modes have the same natural frequencies and were observed to be the same modes but in a different orthogonal direction since the cooling tower shape is axi-symmetric. The natural frequencies were computed into a tabular format and plotted graphically against the various geometrical parameters. The mode shapes were also tabulated for selected geometries. Afterwards, the same cooling towers were subjected to constant wind gusts of the same speed with variable periods (2-, 5-, 10-, 20- and 30-second wind gusts) and therefore variable forcing frequencies to obtain the response frequencies and mode shapes. The response periods of vibration at the cooling tower's top edge in the windward direction were read and converted into response frequencies. These were tabulated and plotted graphically against the various geometrical parameters. This analysis was systematically repeated to obtain the relationship between these vibration responses and the geometrical parameters indicated below. The following geometrical parameters were investigated to obtain their variation with the natural frequencies, mode shapes and response frequencies:

- Height *(H)* of the cooling tower;
- Cooling tower height to top edge diameter ratio *(H/D_{top});*
- Top edge diameter to throat diameter ratio *(D_{top}/D_{thr})* of the cooling tower;
- Bottom edge diameter to top edge diameter ratios *(D_{bot}/D_{top})* of the cooling tower;
- Cooling tower shell thickness.

3.2.2 Shell geometric and material properties

The cooling tower geometry was derived by rotating the meridian through a 360 degree angle around an arbitrary vertical axis as is the case for all shells of revolution. The meridian profile was derived from the hyperbolic equation:

$$\frac{x^2}{a^2} - \frac{y^2}{b^2} = 1,$$

where

x = cooling tower radius at any given height position;
y = cooling tower height measured from the throat and is positive in an upward direction;
a = throat radius;
b = curvature constant;

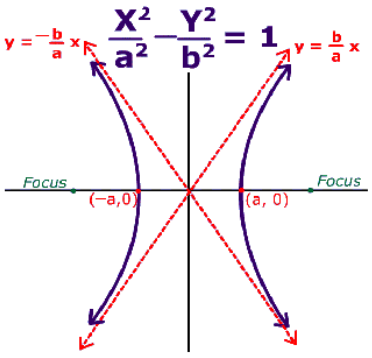

Figure 173: *Graphical representation of the hyperbolic equation adopted from http://astarmathsandphysics.com/a-level-maths-notes/194-fp2/3457-hyperbolae.html*

hence the famous *hyperbolic shell of revolution* name for the cooling tower geometry. This equation is usually referred to as the canonical form of the hyperbolic equation and is a transformation of the simpler form:

$$y = \frac{k}{x},$$

as can be seen in *Figure 173*. The geometrical properties of the cooling towers were systematically changed in order to obtain a representative range of cooling tower geometries for the parametric study. The following geometrical parameter ranges were considered:

- Height range = 60m to 250m;
- Diameters range = 33m to 200m;
- Thickness range = 20mm to 500mm.

An example of one cooling tower's geometrical parameters and meridional profile is shown in the Figure below. The figure shows the cooling tower's height, diameters, throat height to total height ratio, height to diameter ratios, top edge, bottom edge and throat diameter ratios. In addition, the figure shows the variation of the cooling tower's radius with height as well as the variation of the curvature of the meridian with height. The node number, radius and height obtained in the manner shown in the Figure above were copied into the software model in order to obtain the profile of the meridian for each cooling tower that was analysed for the parametric study.

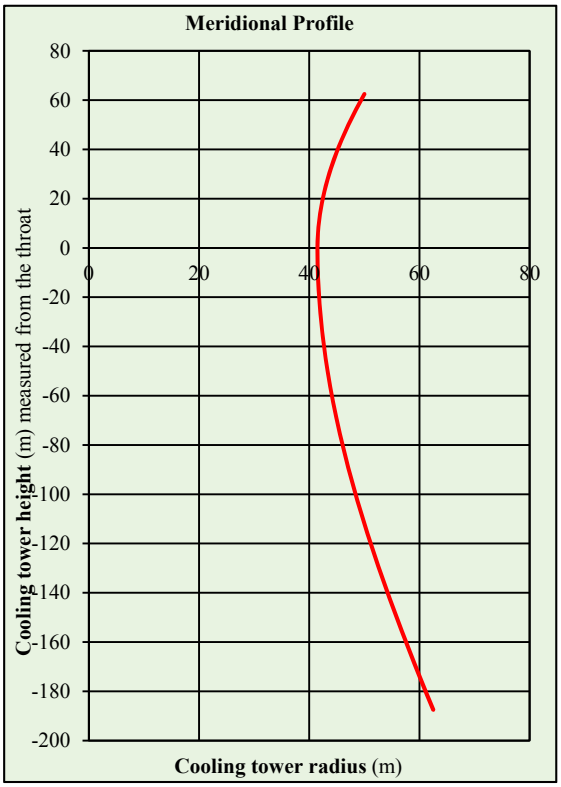

GEOMETRICAL PARAMETERS			
Total Height (m)	250	Throat Height/ Total Height ratio	0.75
Top Diameter (m)	100	Top Thickness (mm)	150
Throat Diameter (m)	83	Throat Thickness (mm)	175
Bottom diameter (m)	125	Base Thickness (mm)	200
GEOMETRICAL RATIOS			
Height/Top Diameter ratio	2.500	Top Diameter/ Throat Diameter ratio	1.205
Height/Throat Diameter ratio	3.012	Bottom Diameter/ Throat Diameter ratio	1.506
Height/Bottom Diameter ratio	2.000	Bottom Diameter/ Top Diameter ratio	1.250

FEM Node	Cooling Tower Radius (m)	Simillar to X	Cooling Tower Height (m)	Shell Curvature (m)
Node	X	Y	Z	b
1	50.000	0.000	62.500	93.005
2	48.500	0.000	56.250	93.005
3	47.117	0.000	50.000	93.005
4	45.862	0.000	43.750	93.005
5	44.746	0.000	37.500	93.005
6	43.780	0.000	31.250	93.005
7	42.973	0.000	25.000	93.005
8	42.335	0.000	18.750	93.005
9	41.873	0.000	12.500	93.005
10	41.594	0.000	6.250	93.005
11	41.500	0.000	0.000	93.005
12	41.529	0.000	-6.250	166.503
13	41.617	0.000	-12.500	166.503
14	41.762	0.000	-18.750	166.503
15	41.965	0.000	-25.000	166.503
16	42.225	0.000	-31.250	166.503
17	42.540	0.000	-37.500	166.503
18	42.909	0.000	-43.750	166.503
19	43.331	0.000	-50.000	166.503
20	43.804	0.000	-56.250	166.503
21	44.327	0.000	-62.500	166.503
22	44.899	0.000	-68.750	166.503
23	45.516	0.000	-75.000	166.503
24	46.177	0.000	-81.250	166.503
25	46.882	0.000	-87.500	166.503
26	47.626	0.000	-93.750	166.503
27	48.409	0.000	-100.000	166.503
28	49.230	0.000	-106.250	166.503
29	50.085	0.000	-112.500	166.503
30	50.973	0.000	-118.750	166.503
31	51.893	0.000	-125.000	166.503
32	52.843	0.000	-131.250	166.503
33	53.822	0.000	-137.500	166.503
34	54.827	0.000	-143.750	166.503
35	55.857	0.000	-150.000	166.503
36	56.911	0.000	-156.250	166.503
37	57.989	0.000	-162.500	166.503
38	59.087	0.000	-168.750	166.503
39	60.206	0.000	-175.000	166.503
40	61.344	0.000	-181.250	166.503
41	62.500	0.000	-187.500	166.503

The *material properties* were considered to be constant throughout the whole spectrum of the parametric study. The following material properties were considered:

- Concrete grade = 40 MPa/19mm aggregate;
- Concrete Young's Modulus of Elasticity = 35 GPa;
- Poisson's ratio = 0.17;

- Density of concrete = 24 kN/m^3;
- Concrete coefficient of thermal expansion = 15 x 10^{-6} m/^{0}C.

3.2.3 Software modelling of cooling tower shell

The computer modelling of the cooling tower shell was done on ADINA software (900 nodes version 9.0.1 build 01.30.2014) using a 64 bit Windows 7 Professional operating system on an Intel® Core ™ i7 – 3537U CPU @ 2.00GHz processor.

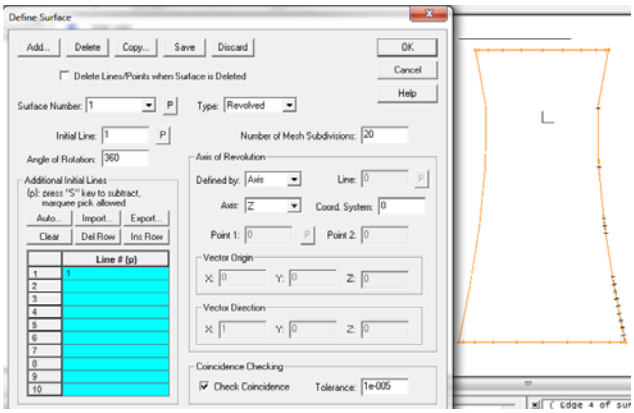

Figure 174: *ADINA software cooling tower shell surface definition*

Each cooling tower's geometrical parameters (height, radius and curvature) were arranged in Microsoft Excel in a tabular format and copied into ADINA's Point Coordinates section (*Figure 177*) to define the meridian of the cooling tower. The point coordinates were joined together to form a polyline using ADINA's line definition tool (*Figure 176*). To form the cooling tower shell surface, the polyline was rotated through 360^0 about an imaginary vertical axis using ADINA's surface definition tool (*Figure 174*). After this, the surface was meshed into specific 4-node shell elements using ADINA's meshing tool (*Figure 178*). Finally, the wind loading was applied using a combination of the spatial function tool and the load application tool (*Figure 175*).

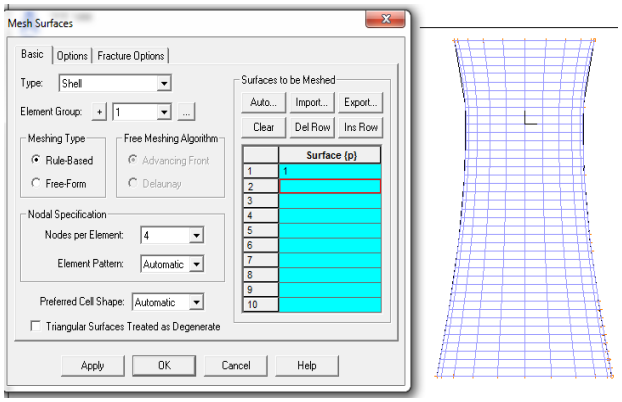

Figure 178: *ADINA software cooling tower shell meshing*

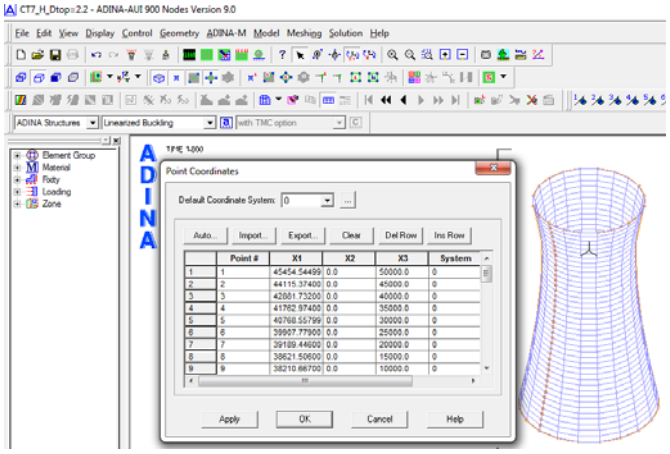

Figure 177: *ADINA software point coordinates of the cooling tower meridian*

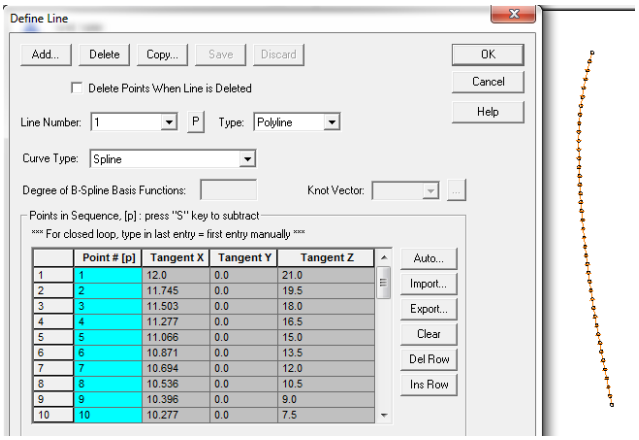

Figure 176: *ADINA software cooling tower meridian line definition*

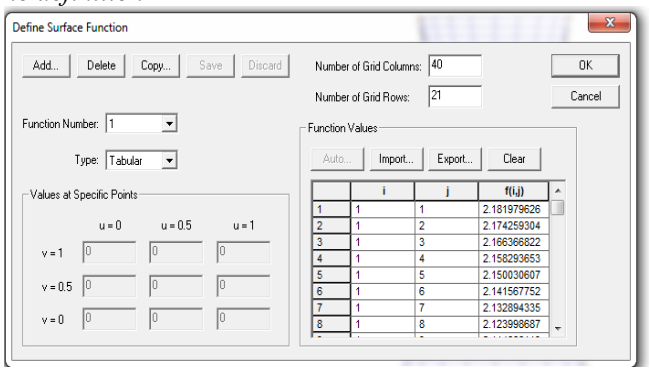

Figure 175: *ADINA software cooling tower shell surface loading using a spatial loading function*

The modelling of the cooling tower shell was checked for errors as indicated in section 3.2.5.

The shell's bottom edge was modelled as clamped (fixed) against vertical, lateral translations as well as rotational movement. The shell was considered to be complete with no cut-outs.

Shell Element Type

The shell element type used is a 4-node (degenerate) isoparametric single layered (non-composite) shell element and is shown in *Figure 179*. The element's nodes are in the mid-surface only. This element is a part of the quadrilateral group of shell elements.

The basic equations used in the formulation of this shell element are formulated treating the shell as a three dimensional continuum by using the two assumptions used in the Timoshenko beam theory and the Reissner / Mindlin plate theory:

1) Material particles that originally lie on a straight line "normal" to the middle surface of the structure remain on that straight line during the deformations;

2) The stress in the direction normal to the shell middle surface is zero.

The shell element has a high predictive capability and can therefore be used for effective analysis of thin and thick shells.

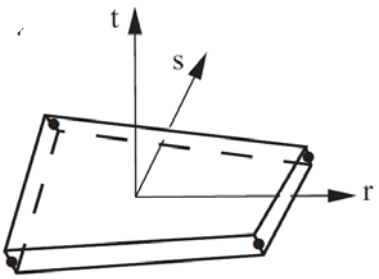

Figure 179: *4-node shell element*

3.2.4 Wind loading

The circumferential wind pressure distribution was considered to follow the following Fourier series summation as per the test results confirmed by other authors (Gaikwad, *et al.*, 2014):

$$\omega = \sum_{n=1}^{\infty} A_n \cos n\theta = A_1 \cos\theta + A_2 \cos 2\theta + A_3 \cos 3\theta + \cdots \ldots + A_n \cos n\theta$$

where

ω = wind pressure coefficient;
A_n = Fourier coefficient for the nth harmonic;
n = harmonic number;
θ = angle of point under consideration from the reference meridian in radians.

The summation of the Fourier series was considered up to a total of 9 harmonics beyond which the variation of the wind pressure coefficient was considered to be relatively converging. *Table 13* below shows the summation of the harmonic Fourier series and the adopted total summation as the wind pressure coefficient. Figure 188 shows a graphical variation of the wind pressure coefficient circumferentially around the cooling tower.

FOURIER COEFFICIENT An			-3.502	1.939	5.342	4.238	0.487	-1.095	0.011	0.514	0.066	
CIRCUMFERENTIAL ANGLE AND NODE POSITION			**FOURIER HARMONIC n**									
NODE	**ANGLE (°)**	**ANGLE (RAD)**	**0**	**1**	**2**	**3**	**4**	**5**	**6**	**7**	**8**	**TOTAL**
1	0	0.000	-3.002	2.439	5.842	4.738	0.987	-0.595	0.511	1.014	0.566	1.562
2	18	0.314	-3.002	2.344	4.822	2.991	0.650	0.500	0.497	0.198	0.447	1.181
3	36	0.628	-3.002	2.069	2.151	-0.810	0.106	1.595	0.491	0.341	0.520	0.433
4	54	0.942	-3.002	1.640	-1.151	-3.530	0.106	0.500	0.509	0.989	0.520	-0.427
5	72	1.257	-3.002	1.099	-3.822	-2.928	0.650	-0.595	0.503	0.084	0.447	-0.945
6	90	1.571	-3.002	0.500	-4.842	0.500	0.987	0.500	0.489	0.500	0.566	-0.475
7	108	1.885	-3.002	-0.099	-3.822	3.928	0.650	1.595	0.503	0.916	0.447	0.140
8	126	2.199	-3.002	-0.640	-1.151	4.530	0.106	0.500	0.509	0.011	0.520	0.173
9	144	2.513	-3.002	-1.069	2.151	1.810	0.106	-0.595	0.491	0.659	0.520	0.134
10	162	2.827	-3.002	-1.344	4.822	-1.991	0.650	0.500	0.497	0.802	0.447	0.173
11	180	3.142	-3.002	-1.439	5.842	-3.738	0.987	1.595	0.511	-0.014	0.566	0.163
12	198	3.456	-3.002	-1.344	4.822	-1.991	0.650	0.500	0.497	0.802	0.447	0.173
13	216	3.770	-3.002	-1.069	2.151	1.810	0.106	-0.595	0.491	0.659	0.520	0.134
14	234	4.084	-3.002	-0.640	-1.151	4.530	0.106	0.500	0.509	0.011	0.520	0.173
15	252	4.398	-3.002	-0.099	-3.822	3.928	0.650	1.595	0.503	0.916	0.447	0.140
16	270	4.712	-3.002	0.500	-4.842	0.500	0.987	0.500	0.489	0.500	0.566	-0.475
17	288	5.027	-3.002	1.099	-3.822	-2.928	0.650	-0.595	0.503	0.084	0.447	-0.945
18	306	5.341	-3.002	1.640	-1.151	-3.530	0.106	0.500	0.509	0.989	0.520	-0.427
19	324	5.655	-3.002	2.069	2.151	-0.810	0.106	1.595	0.491	0.341	0.520	0.433
20	342	5.969	-3.002	2.344	4.822	2.991	0.650	0.500	0.497	0.198	0.447	1.181
21	360	6.283	-3.002	2.439	5.842	4.738	0.987	-0.595	0.511	1.014	0.566	1.562

Table 13: *Wind pressure coefficient circumferential distribution derived from a Fourier series summation of nine (9) harmonics*

The vertical wind pressure distribution was determined in accordance with SANS 10160-3:2010 (Basis of structural design and actions for buildings and industrial structures: Part 3: Wind actions). The peak wind speed, at a height z, was determined from the following formula:

$v_p(z) = c_r(z)\, v_{b,peak}$;

where

$v_{b,peak}$ = $1.4\, v_b$;

v_b = is the basic wind speed defined at 10 m above ground in terrain category B determined in accordance with SANS 10160-3;

$c_r(z)$ = is the roughness factor calculated from the following equation:

$c_r(z) = 1.36 \left(\frac{z-z_0}{z_g-z_0}\right)^{\alpha}$;

where

z = the height above the ground level;

z_0 = is the height of the reference plane, as defined in table 1 of SANS 10160-3;

z_g = is the gradient height, as defined in table 1 of SANS 10160-3;

α = is the exponent as defined in table 1 of SANS 10160-3.

The peak wind pressure, at a height z, was then calculated from the following equation:

$$q_p(z) = \frac{1}{2}\, \rho \left(v_p(z)\right)^2;$$

where ρ is the air density, expressed as 1.2 kilograms per cubic metre (kg/m^3) at sea level. The calculated peak wind pressure variation with height is shown in *Figure 175* for a basic wind speed of 28m/s. The combined circumferential and meridional wind pressure distribution was copied from Microsoft Excel data into the software model as a spatial loading function that can be factored and changed at any interval. A graphical representation of the loading function when applied to the cooling tower is shown in *Figure 182*.

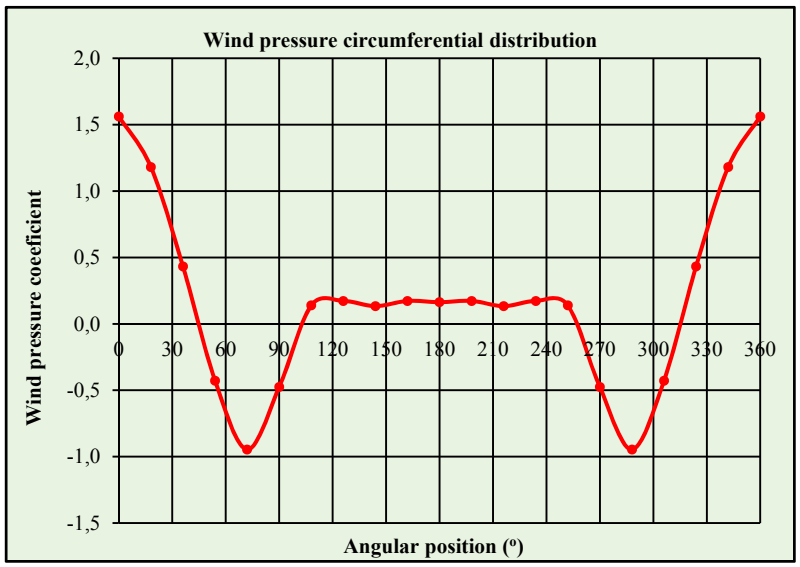

Figure 181: *Circumferential distribution of the wind pressure coefficient*

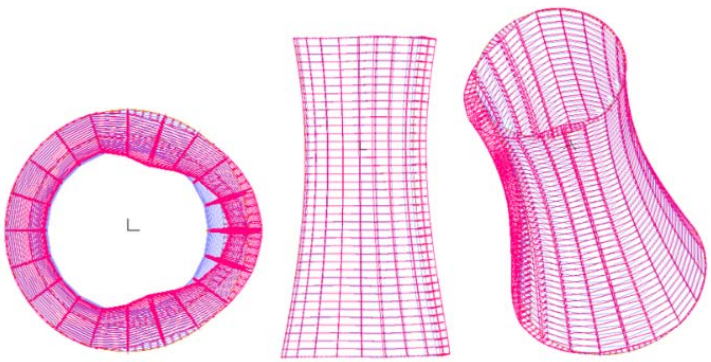

Figure 182: *A graphical representation of the wind loading around the cooling tower*

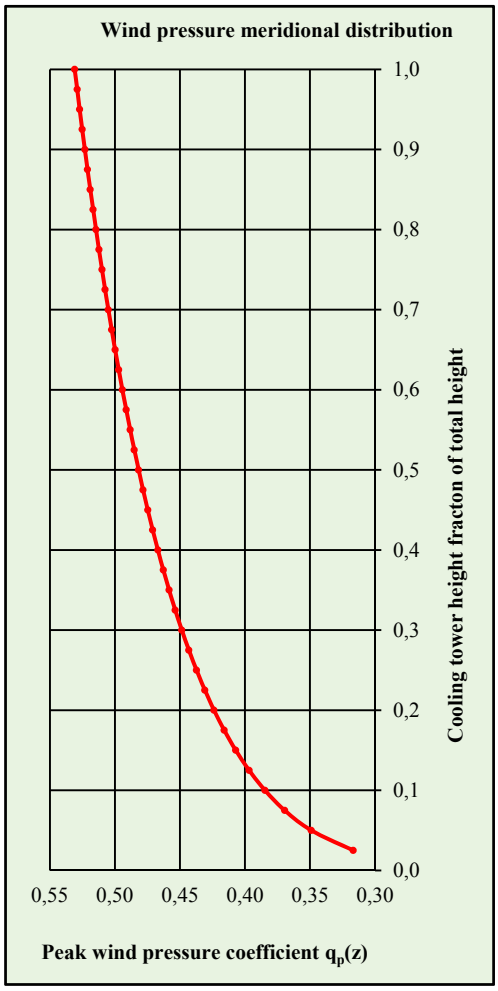

Figure 180: *Peak wind pressure variation with height (meridional wind pressure distribution)*

3.2.5 Software and model validation

The computer software used is not immune to errors. The best way to check any errors would be to test the computer software completely. However, this is impractical because a large number of test cases will need to be considered. This usually takes a lot of time, money, resources and usually ends up taking forever. It is for this reason that the validation and verification of any software becomes important before the results associated with the software can be adopted.

The following verification process was performed:

- A systematic *checking for error warnings* during and after the analysis of each group of models for the different geometrical parameters was performed. This was necessary so as to determine whether the software indicated any error warnings in the modelling or loading. An example of an error warning report obtained is indicated in Figure 183.

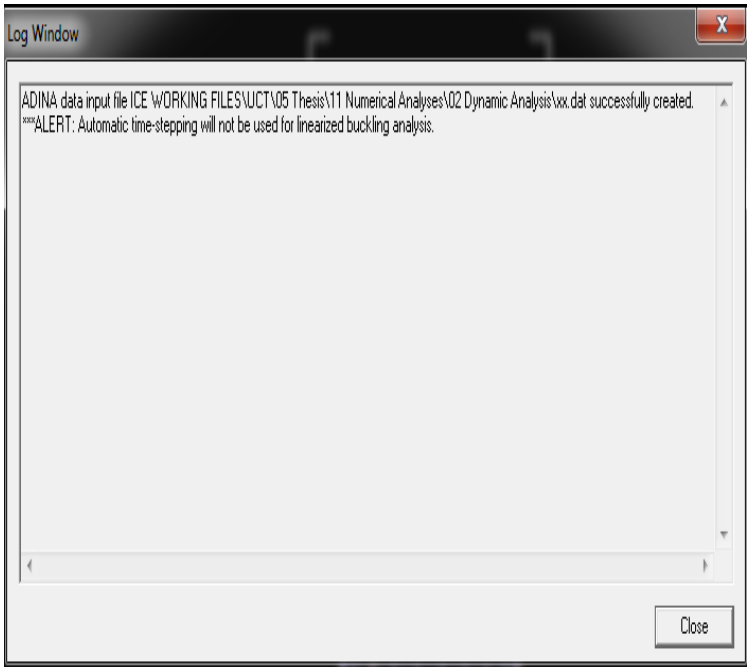

Figure 183: *Adina analysis log window showing alerts or warning of errors*

- An overall equilibrium check was performed to check the difference between the sum of all applied loads on the model in a particular direction P_x and the sum of the support reactions in that direction P_r. The difference P_x - P_r was found to be of the order of 10^{-12} which is insignificant. This meant that the model support reactions were in equilibrium with the applied external loads.
- The support reactions were systematically checked for each model to ensure that they have been placed at each node at the bottom edge of the model to avoid any omissions;
- A *qualitative analysis* of the output results was performed by observing the deformed shape and the distribution of the shell element stresses. These were found to conform to what was expected;
- A symmetrical wind loading around the cooling tower model was applied to check the behaviour of the deformations. It was found that the difference between deformations in opposite directions was zero.

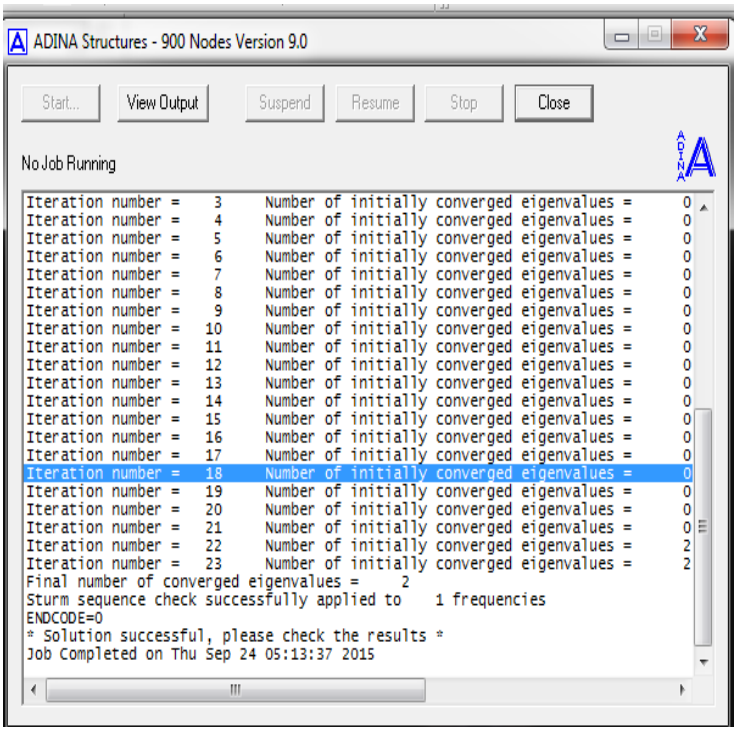

Figure 184*: Adina analysis output report*

Based on the above checks, the computer software and model were assumed to have been validated and the actual analyses could now be performed with reasonable comfort that the chances of errors or risks associated with the errors would have been diminished.

3.2.6 Analyses and reading of results

Stability behaviour analysis: The model was analysed in ADINA's *Linearized Eigenvalue Buckling* module and the results obtained from the Post Processing section of ADINA. The buckling load factors were read from this section and the buckling modes also observed from this section. Figure 186 below shows an example of one set of the linearised buckling analyses results. The results were copied into Microsoft Excel sheets next to the geometrical parameters in order to analyse their relationship with the cooling tower's geometry.

The buckling load factor was multiplied with the basic wind speed to obtain the critical wind speed at which the cooling tower shell would first buckle. The trends in the change of this critical wind speed with change in geometry were plotted to observe the behaviour. The change in the buckling modes were also observed and plotted for specific cooling tower geometries.

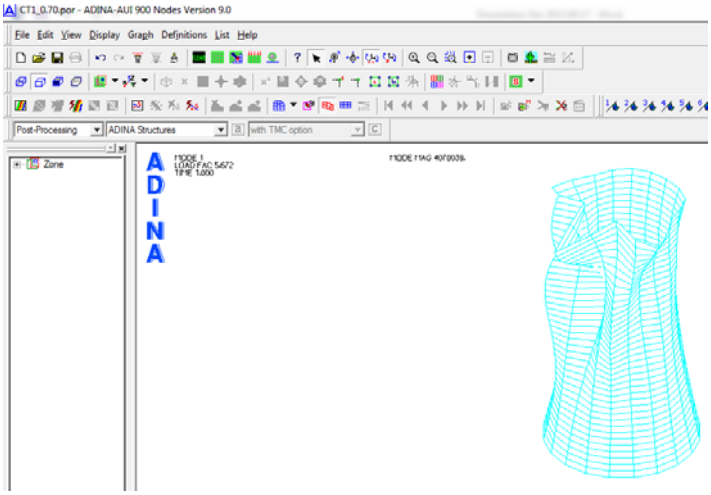

Figure 186: *Post processing results of the linearised buckling analysis*

Free vibration analysis: The model was analysed in ADINA's *Mode Superposition* module and the results obtained from the Post Processing section of ADINA. The natural frequencies were directly read from the List Zone for the first ten (10) different modes being the odd numbered modes: 1, 3, 5, …, 17, and 19. It was observed that the even numbered modes had the same natural frequencies and mode shapes as the odd numbered modes because they were the same modes of vibration but only in a different orthogonal direction.

The mode shapes were also read in a similar way by choosing the first mode and displaying subsequent mode shapes from the results section. Examples of the natural frequency and mode shapes charts are shown in *Figure 185* and *Figure 187*.

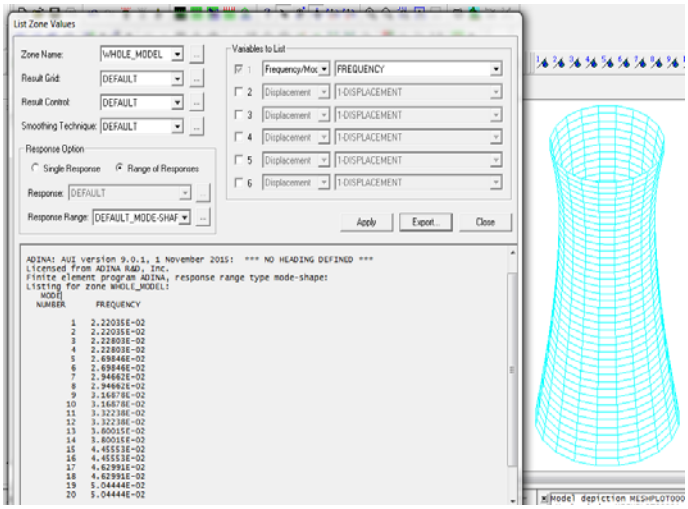

Figure 185: *Post processing results of the natural frequencies*

Forced vibration analysis: The model was analysed in ADINA's Mode superposition module and the results obtained from the Post Processing section of ADINA. The response frequencies were computed by creating a response graph of the displacement for the cooling tower's top edge for a node in the windward direction. Definition of the particular node is shown in Figure 188. The response graph was plotted as shown in *Figure 188* and *Figure 189* to obtain the period of vibration for the concerned node to go through a full cycle of vibration. This period was then translated into a response frequency.

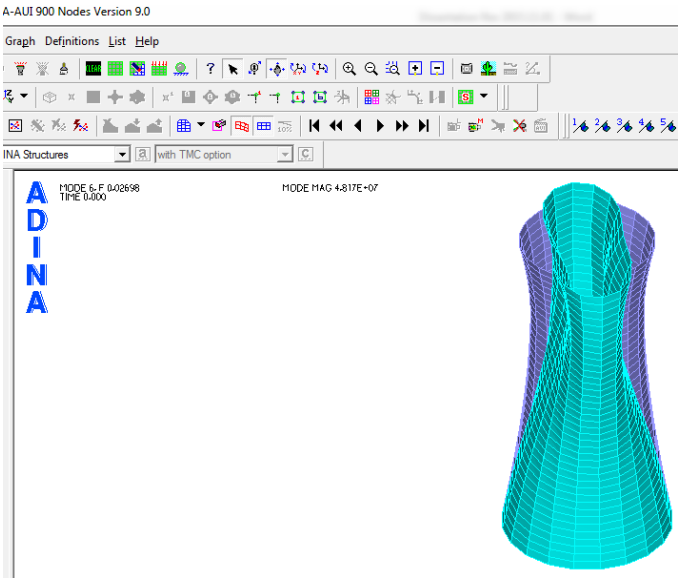

Figure 187: *Post processing results of the mode shapes*

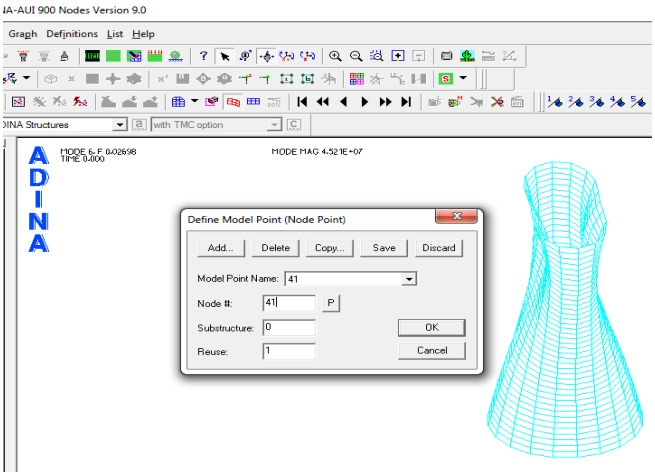

Figure 188: *Definition of the top edge node in the wind ward direction*

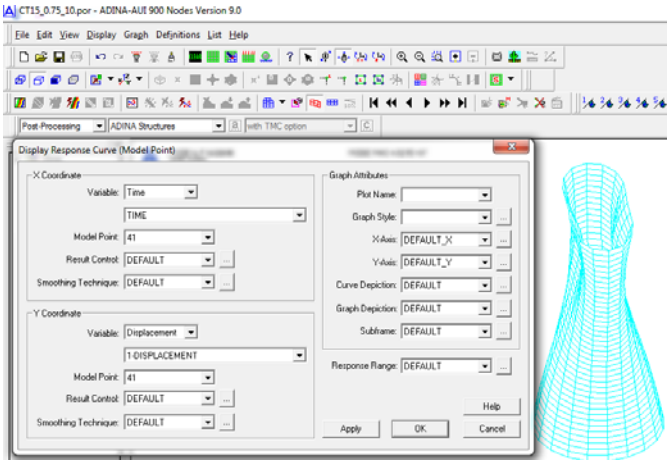

Figure 189: *Plotting of the displacement response graph of the top edge node in the windward direction*

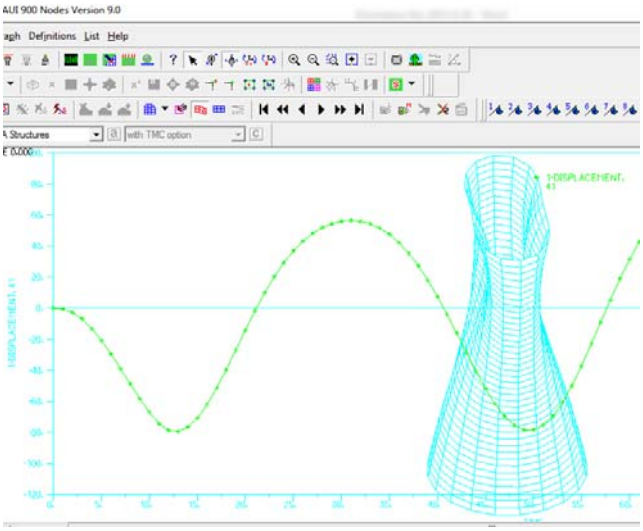

Figure 190: *Displacement response graph of the top edge node in the windward direction*

3.2.7 Work Programme

The following work programme shows the sequence of research tasks that were performed in the final year of research including interactions with the Supervisor.

UNIVERSITY OF CAPE TOWN: MSC THESIS WORK PROGRAMME

Stability behaviour and dynamic response of cooling towers subjected to wind loading by Grant T. Kucherera

ID	Task Name	Duration	Start	Finish	% Complete
1	**MSC THESIS WORK PROGRAMME OF ACTION**	**194 days**	**Fri 15 Feb 27**	**Wed 15 Nov 25**	100%
2	**RESEARCH PROPOSAL**	**45 days**	**Fri 15 Feb 27**	**Thu 15 Apr 30**	100%
3	Kick off meeting with supervisor	0 days	Fri 15 Feb 27	Fri 15 Feb 27	100%
4	Programme of action	10 days	Fri 15 Feb 27	Thu 15 Mar 12	100%
5	Dissertation structure/contents page	10 days	Fri 15 Feb 27	Thu 15 Mar 12	100%
6	Literature review and synthesis	45 days	Fri 15 Feb 27	Thu 15 Apr 30	100%
7	Define research questions and objectives	10 days	Fri 15 Mar 13	Thu 15 Mar 26	100%
8	Progress meeting with supervisor	0 days	Thu 15 Mar 26	Thu 15 Mar 26	100%
9	Compile research work methodoly	5 days	Fri 15 Mar 27	Thu 15 Apr 02	100%
10	Proposal write-up	10 days	Fri 15 Apr 03	Thu 15 Apr 16	100%
11	First draft presentation	0 days	Thu 15 Apr 16	Thu 15 Apr 16	100%
12	Review of draft by supervisor	5 days	Fri 15 Apr 17	Thu 15 Apr 23	100%
13	Final write-up	5 days	Fri 15 Apr 24	Thu 15 Apr 30	100%
14	Progress meeting with supervisor	0 days	Thu 15 Apr 30	Thu 15 Apr 30	100%
15	Research proposal submission	0 days	Thu 15 Apr 30	Thu 15 Apr 30	100%
16	**DISSERTATION**	**149 days**	**Fri 15 May 01**	**Wed 15 Nov 25**	100%
17	Literature review and synthesis	110 days	Fri 15 May 01	Thu 15 Oct 01	100%
18	Numerical modelling	20 days	Fri 15 May 01	Thu 15 May 28	100%
19	Progress meeting with supervisor	0 days	Thu 15 May 28	Thu 15 May 28	100%
20	Finite element analysis	20 days	Fri 15 May 29	Thu 15 Jun 25	100%
21	Progress meeting with supervisor	0 days	Thu 15 Jun 25	Thu 15 Jun 25	100%
22	Parametric studies	20 days	Fri 15 Jun 26	Thu 15 Jul 23	100%
23	Progress meeting with supervisor	0 days	Thu 15 Jul 23	Thu 15 Jul 23	100%
24	Data processing and analysis	10 days	Fri 15 Jun 26	Thu 15 Jul 09	100%
25	Dissertation write-up	46 days	Fri 15 Jun 26	Fri 15 Aug 28	100%
26	First draft presentation	0 days	Fri 15 Aug 28	Fri 15 Aug 28	100%
27	Review of draft by supervisor	10 days	Mon 15 Aug 31	Fri 15 Sep 11	100%
28	Progress meeting with supervisor	0 days	Fri 15 Sep 11	Fri 15 Sep 11	100%
29	Second draft write-up	20 days	Mon 15 Sep 14	Fri 15 Oct 09	100%
30	Comments on draft by supervisor	10 days	Mon 15 Oct 12	Fri 15 Oct 23	100%
31	Final draft write-up	23 days	Mon 15 Oct 26	Wed 15 Nov 25	100%
32	Dissertation submission	0 days	Wed 15 Nov 25	Wed 15 Nov 25	100%
33	**SEMC CONFERENCE PAPER (Two Papers)**	**47 days**	**Tue 15 Sep 22**	**Wed 15 Nov 25**	100%
34	Abstracts write up and approval	20 days	Tue 15 Sep 22	Mon 15 Oct 19	100%
35	Papers write up and First draft presentation	15 days	Tue 15 Oct 20	Mon 15 Nov 09	100%
36	Final write-up	12 days	Tue 15 Nov 10	Wed 15 Nov 25	100%
37	Conference paper submission	0 days	Wed 15 Nov 25	Wed 15 Nov 25	100%

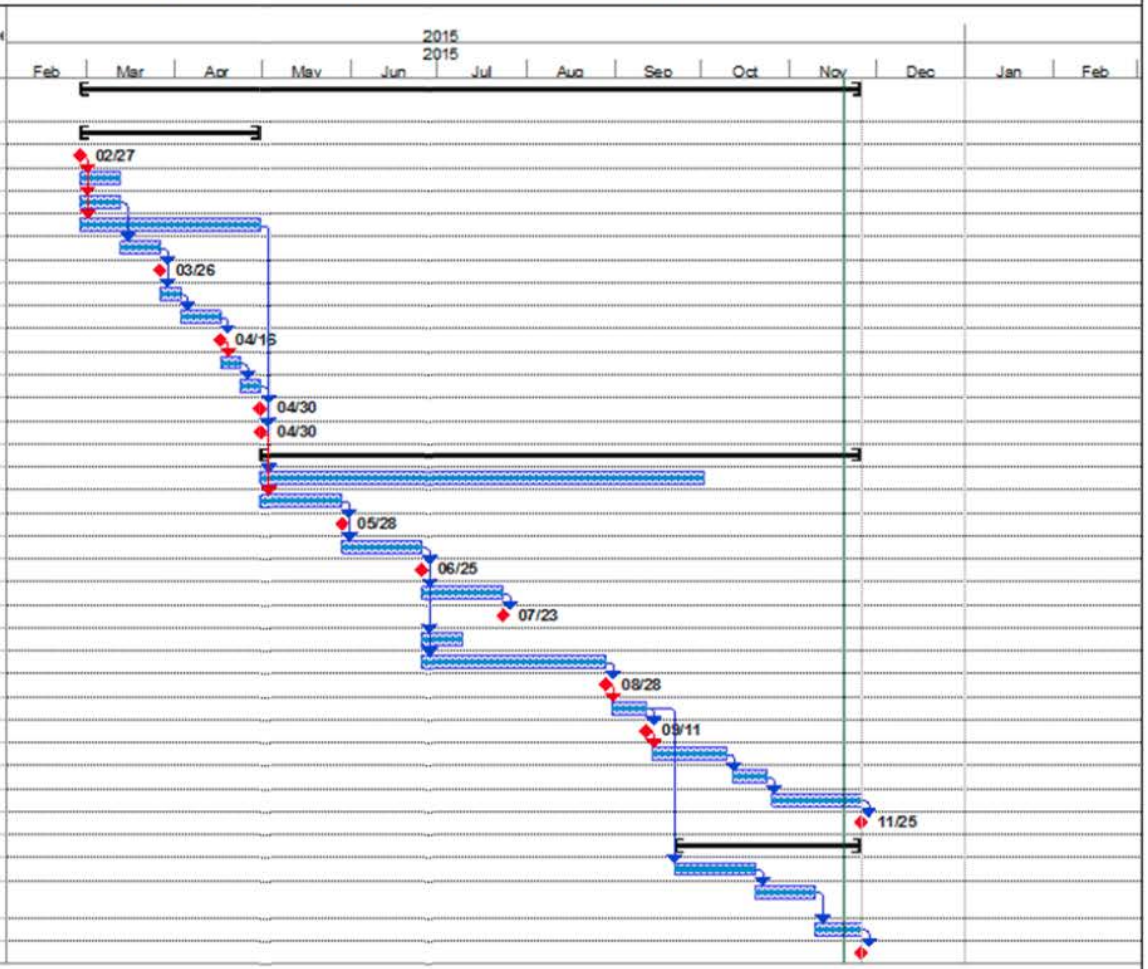

Task	External Tasks	Manual Task	Finish-only	Progress
Split	External Milestone	Duration-only	Deadline
Milestone	Inactive Task	Manual Summary Rollup	Critical
Summary	Inactive Milestone	Manual Summary	Critical Split
Project Summary	Inactive Summary	Start-only	Late

1

4 NUMERICAL PARAMETRIC STUDY RESULTS AND OBSERVATIONS

4.1 ON STABILITY BEHAVIOUR UNDER UNSYMMETRICAL WIND LOADING

The parametric study results for various geometrical parameters are included in the following sections. In each section, a summary of the critical wind speeds is indicated in a table for various cooling towers whose geometry is changed systematically in order to study the change in the buckling behaviour of the cooling tower. Followed by this is a series of graphs plotted to describe this behaviour. Particular buckling mode shapes of the cooling towers are added onto these graphs to describe the change in the buckling modes with variation in the cooling tower geometry. The study observations are recorded next to the plotted graphs.

The critical wind pressure load factors associated with the first mode of buckling are those factors by which the applied wind pressure corresponding to the applied wind speed of 28m/s should be multiplied with to obtain the wind pressure at which the cooling tower will start to buckle. Consequently, the critical wind speed equals the applied wind speed multiplied by the obtained load factors. The critical wind speed associated with the first mode of buckling is therefore the wind speed at which the cooling tower would start to buckle.

For each parametric study, the particular geometrical parameter (e.g. height) is changed systematically for at least twenty (20) cooling towers whilst keeping the rest of the other geometrical parameters (e.g. thickness, diameters etc.) constant in order to study the influence of a single parameter on the buckling behaviour of the cooling tower. The constant parameters are included at the bottom of each table of results. In order to cover a wider range of geometrical parameters, the study is tailored to investigate ratios of the geometrical parameters instead of looking into just the actual parameters.

The following parameters were investigated:

- *Height* of the cooling tower;
- *Throat height* position by analysing the influence of the position of the cooling tower compared to the total height (H_t/H);
- *Height to diameter ratio* represented by the height to top/bottom/throat diameters (H/D_{top}, H/D_{bot}, H/D_{thr});
- *Top diameter to throat diameter* and *bottom diameter to throat diameter ratios* (D_{top}/D_{thr}, D_{bot}/D_{thr});
- *Bottom diameter to top diameter ratio* (D_{bot}/D_{top});
- *Shell thickness* of the cooling tower.

4.1.1 Height influence on stability behaviour

Table 14 below shows the results of the parametric study of cooling towers whose height and throat height position were changed to observe the change in the critical wind speed.

COOLING TOWER	GEOMETRICAL PARAMETERS										LINEAR EIGENVALUE BUCKLING ANALYSIS RESULTS *(First Mode)*									
	Total Height	Throat Height/ Total Height					Top Diameter	Throat Diameter	Bottom Diameter		**Critical Wind Pressure LOAD FACTORS H_t/H** *(basic pressure corresponds to a wind speed of 28m/s and a model load multiplier of 5)*					**Critical Wind Velocity for H_t/H** *(m/s)*				
	H	H_t/H					D_{top}	D_{thr}	D_{bot}		*0.65*	*0.7*	*0.75*	*0.8*	*0.85*	*0.65*	*0.7*	*0.75*	*0.8*	*0.85*
	(m)						*(m)*	*(m)*	*(m)*											
CT1	60	0.65	0.70	0.75	0.80	0.85	24	20	30		77.78	85.42	87.61	84.52	81.25	552.2	578.7	586.0	575.6	564.4
CT2	70	0.65	0.70	0.75	0.80	0.85	28	23	35		53.25	58.83	60.49	58.53	55.53	456.9	480.2	487.0	479.0	466.6
CT3	80	0.65	0.70	0.75	0.80	0.85	32	27	40		38.52	42.79	44.02	42.41	39.94	388.6	409.6	415.4	407.7	395.7
CT4	90	0.65	0.70	0.75	0.80	0.85	36	30	45		29.05	32.44	33.40	32.01	29.90	337.5	356.6	361.8	354.2	342.4
CT5	100	0.65	0.70	0.75	0.80	0.85	40	33	50		22.64	25.41	26.18	24.96	23.14	297.9	315.6	320.4	312.8	301.2
CT6	110	0.65	0.70	0.75	0.80	0.85	44	37	55		18.11	20.42	21.06	20.00	18.41	266.4	282.9	287.3	280.0	268.6
CT7	120	0.65	0.70	0.75	0.80	0.85	48	40	60		14.81	16.78	17.31	16.37	14.99	240.9	256.5	260.5	253.3	242.4
CT8	130	0.65	0.70	0.75	0.80	0.85	52	43	65		12.33	14.03	14.49	13.67	12.47	219.8	234.5	238.3	231.5	221.1
CT9	140	0.65	0.70	0.75	0.80	0.85	56	47	70		10.43	11.92	12.33	11.62	10.61	202.2	216.2	219.8	213.4	203.9
CT10	150	0.65	0.70	0.75	0.80	0.85	60	50	75		8.94	10.26	10.64	10.06	8.86	187.2	200.5	204.2	198.6	186.4
CT11	160	0.65	0.70	0.75	0.80	0.85	64	53	80		7.75	8.94	9.32	8.56	7.63	174.3	187.2	191.1	183.2	172.9
CT12	170	0.65	0.70	0.75	0.80	0.85	68	57	85		6.79	7.88	8.28	7.50	6.65	163.1	175.8	180.2	171.5	161.5
CT13	180	0.65	0.70	0.75	0.80	0.85	72	60	90		6.00	7.02	7.17	6.63	5.85	153.4	165.9	167.6	161.2	151.4
CT14	190	0.65	0.70	0.75	0.80	0.85	76	63	95		5.35	6.32	6.40	5.90	5.18	144.8	157.4	158.4	152.1	142.5
CT15	200	0.65	0.70	0.75	0.80	0.85	80	67	100		4.81	5.56	5.76	5.30	4.63	137.3	147.6	150.3	144.1	134.7
CT16	210	0.65	0.70	0.75	0.80	0.85	84	70	105		4.35	5.03	5.22	4.78	4.16	130.6	140.4	143.0	136.9	127.7
CT17	220	0.65	0.70	0.75	0.80	0.85	88	73	110		3.97	4.57	4.75	4.35	3.77	124.7	133.8	136.5	130.6	121.6
CT18	230	0.65	0.70	0.75	0.80	0.85	92	77	115		3.65	4.18	4.35	3.97	3.45	119.6	128.0	130.6	124.7	116.3
CT19	240	0.65	0.70	0.75	0.80	0.85	96	80	120		3.38	3.83	4.00	3.65	3.19	115.1	122.5	125.2	119.6	111.8
CT20	250	0.65	0.70	0.75	0.80	0.85	100	83	125		2.99	3.53	3.70	3.38	2.99	108.3	117.6	120.4	115.1	108.3
CONSTANT PARAMETERS:																				
Top Thickness						=	150	mm			Height/Bottom Diameter ratio					=	2.0			
Throat Thickness						=	175	mm			Top Diameter/Throat Diameter ratio					=	1.2			
Base Thickness						=	200	mm			Bottom Diameter/Throat Diameter ratio					=	1.5			
Height/Top Diameter ratio						=	2.5				Bottom Diameter/Top Diameter ratio					=	1.3			
Height/Throat Diameter ratio						=	3.0													

***Table 14**: Parametric linear eigenvalue buckling analysis of cooling towers with variable height and throat height position*

Figure 191 shows the variation of the critical wind speed with the cooling tower height for the various throat height positions. *Figure 192* shows the variation of the critical wind speed with change in the throat height position for the various cooling tower heights. In addition, the buckled shapes of the cooling tower (for the first mode) are shown for a selected cooling towers to show the change in the buckling modes with respect to cooling tower height and throat height position.

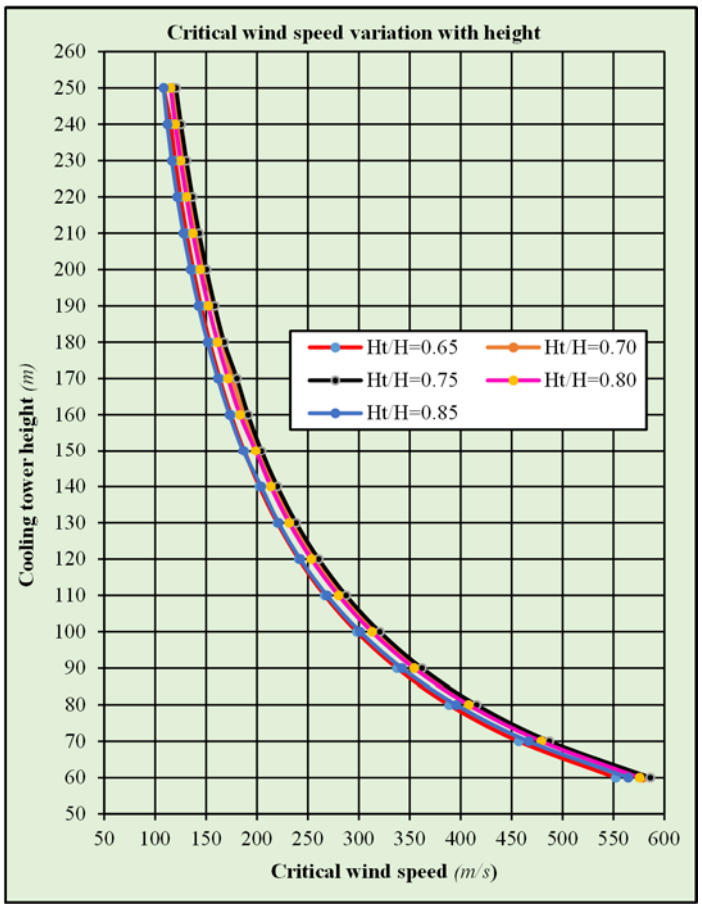

Figure 191: *Critical wind speed variation with cooling tower height*

Observations:
From *Figure 191*, it can be observed that:

- The variation of the critical wind speed is similar to the Euler buckling curve. This observation is correct and is so because the critical wind speeds/pressures are proportional to the buckling eigenvalues (load factors);
- As the height increases, the reduction rate of the critical wind speed reduces;
- The variation of the critical wind speed in relationship to the change in height is similar for all the throat height positions. The graphs for the various throat height positions follows the same shape and profile. This suggest that the change in critical speed with height is similar regardless of the position of the throat for the throat height to total height range considered.

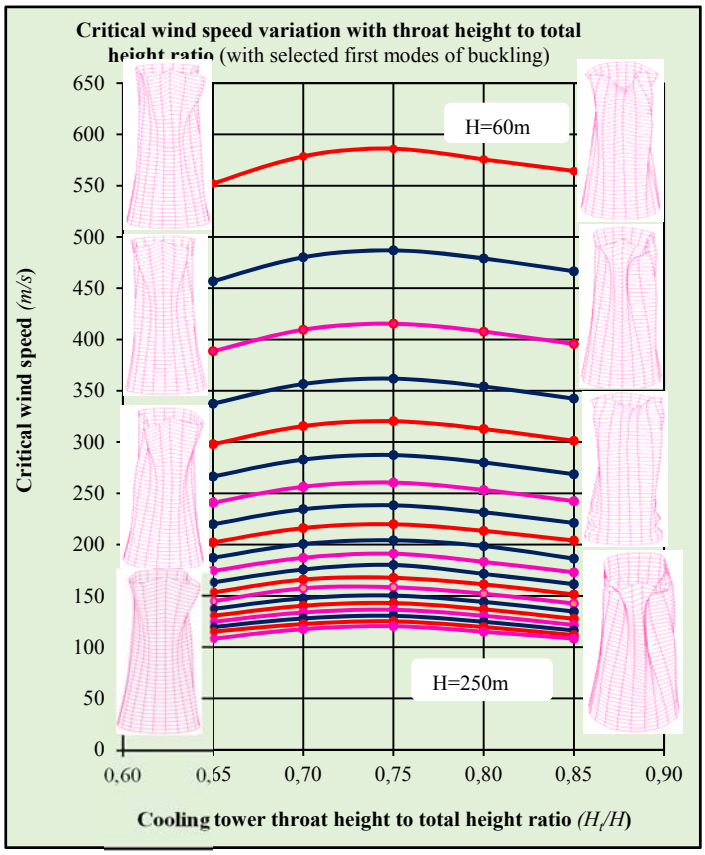

Figure 192: *Critical wind speed variation with cooling tower throat height position*

Observations:
From *Figure 192*, it can be observed that:

- There is a certain optimum throat height to total height ratio for any cooling tower at which the critical wind speed is maximum. This ratio is generally close to 0.75;
- The first mode of buckling for cooling towers of a lower throat height to total height ratio (0.65) are generally the same irrespective of the height and irrespective of the critical wind speed. For a higher throat height to total height, the first modes of buckling are different for various cooling tower heights;
- The change in critical wind speeds for cooling towers with throat to total height ratios of less than 0.75 is more rapid compared to that of cooling towers with throat to total height ratios of more than 0.75;
- There is a significant difference in critical wind speeds for shorter cooling towers when compared to higher cooling towers.

4.1.2 Height to diameter ratio influence on stability behaviour

Table 15 below shows the results of the parametric study of cooling towers whose height to diameter ratios were changed to observe the change in the critical wind speed whilst the total height, throat height to total height ratio, thickness and diameter ratios were kept constant.

COOLING TOWER	GEOMETRICAL PARAMETERS							LINEAR EIGENVALUE BUCKLING ANALYSIS RESULTS *(First Mode)*					
	Total Height	Top Diameter	Throat Diameter	Bottom Diameter	Height/ Top Diameter	Height/ Throat Diameter	Height/ Bottom Diameter	**Critical Wind Pressure LOAD FACTORS** *(basic pressure corresponds to a wind speed of 28m/s and a model load multiplier of 5)*			**Critical Wind Velocity** *(m/s)*		
	H	D_{top}	D_{thr}	D_{bot}	H/D_{top}	H/D_{thr}	H/D_{bot}	H/D_{top}	H/D_{thr}	H/D_{bot}	H/D_{top}	H/D_{thr}	H/D_{bot}
	(m)	*(m)*	*(m)*	*(m)*									
CT1	200	200	167	250	1.0	1.2	0.8	5.29	5.29	5.29	144.0	144.0	144.0
CT2	200	167	139	208	1.2	1.4	1.0	5.22	5.22	5.22	143.0	143.0	143.0
CT3	200	143	119	179	1.4	1.7	1.1	5.21	5.21	5.21	142.9	142.9	142.9
CT4	200	125	104	156	1.6	1.9	1.3	5.25	5.25	5.25	143.5	143.5	143.5
CT5	200	111	93	139	1.8	2.2	1.4	5.33	5.33	5.33	144.5	144.5	144.5
CT6	200	100	83	125	2.0	2.4	1.6	5.43	5.43	5.43	145.9	145.9	145.9
CT7	200	91	76	114	2.2	2.6	1.8	5.67	5.67	5.67	149.1	149.1	149.1
CT8	200	83	69	104	2.4	2.9	1.9	5.65	5.65	5.65	148.8	148.8	148.8
CT9	200	77	64	96	2.6	3.1	2.1	5.89	5.89	5.89	151.9	151.9	151.9
CT10	200	71	60	89	2.8	3.4	2.2	6.17	6.17	6.17	155.5	155.5	155.5
CT11	200	67	56	83	3.0	3.6	2.4	6.51	6.51	6.51	159.7	159.7	159.7
CT12	200	63	52	78	3.2	3.8	2.6	6.89	6.89	6.89	164.3	164.3	164.3
CT13	200	59	49	74	3.4	4.1	2.7	7.31	7.31	7.31	169.3	169.3	169.3
CT14	200	56	46	69	3.6	4.3	2.9	7.79	7.79	7.79	174.7	174.7	174.7
CT15	200	53	44	66	3.8	4.6	3.0	8.33	8.33	8.33	180.7	180.7	180.7
CT16	200	50	42	63	4.0	4.8	3.2	8.92	8.92	8.92	187.0	187.0	187.0
CT17	200	48	40	60	4.2	5.0	3.4	9.57	9.57	9.57	193.7	193.7	193.7
CT18	200	45	38	57	4.4	5.3	3.5	10.28	10.28	10.28	200.7	200.7	200.7
CT19	200	43	36	54	4.6	5.5	3.7	11.05	11.05	11.05	208.1	208.1	208.1
CT20	200	42	35	52	4.8	5.8	3.8	11.89	11.89	11.89	215.9	215.9	215.9
CT21	200	40	33	50	5.0	6.0	4.0	12.82	12.82	12.82	224.2	224.2	224.2

CONSTANT PARAMETERS:					
Throat Height/Total Height rat	=	0.75		Top Diameter/Throat Diameter ratio	= 1.200
Top Thickness	=	150	mm	Bottom Diameter/Throat Diameter ratio	= 1.500
Throat Thickness	=	175	mm	Bottom Diameter/Top Diameter ratio	= 1.250
Base Thickness	=	200	mm		

Table 15: *Parametric linear eigenvalue buckling analysis of cooling towers with variable height to diameter ratios: height to top edge diameter ratio (H/D_{top}); height to throat diameter ratio (H/D_{thr}); height to bottom edge diameter ratio (H/D_{bot})*

Figure 193 shows the variation of the critical wind speed with the cooling tower height to diameter ratios: height to top edge diameter ratio (H/D_{top}); height to throat diameter ratio (H/D_{thr}); height to bottom edge diameter ratio (H/D_{bot}). In addition, the buckled shapes of the cooling tower (for the first mode) are shown for selected cooling towers to show the change in the buckling modes with respect to the cooling tower height to diameter ratios.

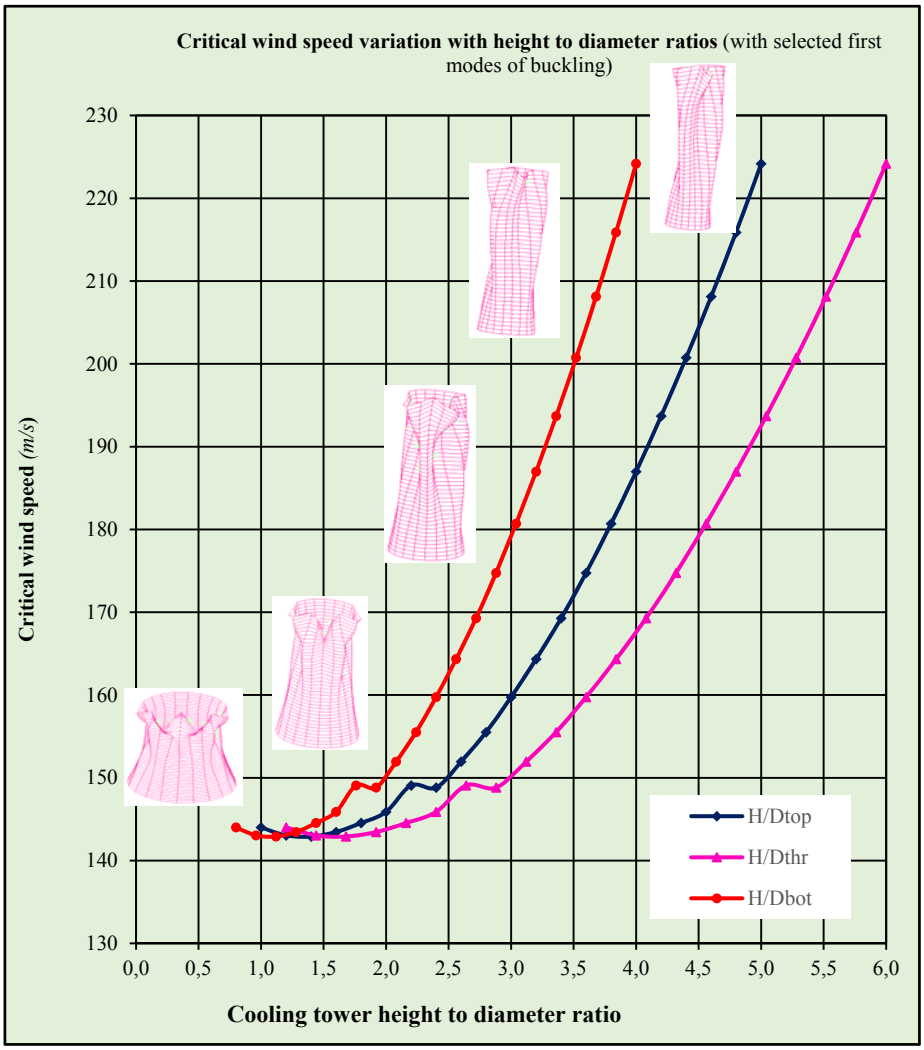

Figure 193: *Critical wind speed variation with cooling tower height to diameter ratios: height to top diameter ratio (H/D_{top}); height to throat diameter ratio (H/D_{thr}); height to bottom diameter ratio (H/D_{bot})*

Observations:
From *Figure 193*, it can be observed that:

- The critical wind speed generally increases non-linearly when the height to top edge/throat/bottom edge diameter are increased;
- For dwarf cooling towers, the rate of increase of the critical wind speed is small compared to that for long and thin cooling towers where the rate of increase of the critical wind speed is relatively rapid;
- The dwarf cooling towers buckle by displaying a series of meridional dimples along the full height of the cooling tower mostly around the windward face of the shell;
- The long/thinner cooling towers buckle at relatively high wind speeds. They display meridional buckling also for the full height of the tower but mostly around the entire circumference of the shell.

4.1.3 Top edge diameter and bottom edge diameter to throat diameter ratio influence on stability behaviour

Table 16 below shows the results of the parametric study of cooling towers whose top edge diameter and bottom edge diameter to throat diameter ratios were changed to observe the change in the critical wind speed whilst the total height, throat to total height ratio, thickness and height to diameter ratios were kept constant.

COOLING TOWER	GEOMETRICAL PARAMETERS										LINEAR EIGENVALUE BUCKLING ANALYSIS RESULTS *(First Mode)*			
	Total Height	Top Diameter	Throat Diameter	Bottom Diameter	Height/ Top Diameter	Height/ Throat Diameter	Height/ Bottom Diameter	Top Diameter/Throat Diameter	Bottom Diameter/Throat Diameter	Bottom Diameter/ Top Diameter	**Critical Wind Pressure LOAD FACTORS** *(basic pressure corresponds to a wind speed of 28m/s and a model load multiplier of 5)*		**Critical Wind Velocity** *(m/s)*	
	H	D_{top}	D_{thr}	D_{bot}	H/D_{top}	H/D_{thr}	H/D_{bot}	D_{top}/D_{thr}	D_{bot}/D_{thr}	D_{bot}/D_{top}	D_{top}/D_{thr}	D_{bot}/D_{thr}	D_{top}/D_{thr}	D_{bot}/D_{thr}
	(m)	*(m)*	*(m)*	*(m)*										
CT1	200	80	76	100	2.5	2.6	2.0	1.05	1.313	1.25	3.22	3.22	112.3	112.3
CT2	200	80	73	100	2.5	2.8	2.0	1.10	1.375	1.25	4.76	4.76	136.6	136.6
CT3	200	80	70	100	2.5	2.9	2.0	1.15	1.438	1.25	5.25	5.25	143.5	143.5
CT4	200	80	67	100	2.5	3.0	2.0	1.20	1.500	1.25	5.76	5.76	150.3	150.3
CT5	200	80	64	100	2.5	3.1	2.0	1.25	1.563	1.25	6.28	6.28	156.9	156.9
CT6	200	80	62	100	2.5	3.3	2.0	1.30	1.625	1.25	6.72	6.72	162.3	162.3
CT7	200	80	59	100	2.5	3.4	2.0	1.35	1.688	1.25	7.04	7.04	166.1	166.1
CT8	200	80	57	100	2.5	3.5	2.0	1.40	1.750	1.25	7.20	7.20	168.0	168.0
CT9	200	80	55	100	2.5	3.6	2.0	1.45	1.813	1.25	7.31	7.31	169.3	169.3
CT10	200	80	53	100	2.5	3.8	2.0	1.50	1.875	1.25	7.39	7.39	170.2	170.2
CT11	200	80	52	100	2.5	3.9	2.0	1.55	1.938	1.25	7.45	7.45	170.9	170.9
CT12	200	80	50	100	2.5	4.0	2.0	1.60	2.000	1.25	7.49	7.49	171.3	171.3
CT13	200	80	48	100	2.5	4.1	2.0	1.65	2.063	1.25	7.51	7.51	171.6	171.6
CT14	200	80	47	100	2.5	4.3	2.0	1.70	2.125	1.25	7.50	7.50	171.5	171.5
CT15	200	80	46	100	2.5	4.4	2.0	1.75	2.188	1.25	7.46	7.46	171.0	171.0
CT16	200	80	44	100	2.5	4.5	2.0	1.80	2.250	1.25	7.39	7.39	170.2	170.2
CT17	200	80	43	100	2.5	4.6	2.0	1.85	2.313	1.25	7.29	7.29	169.0	169.0
CT18	200	80	42	100	2.5	4.8	2.0	1.90	2.375	1.25	7.18	7.18	167.8	167.8
CT19	200	80	41	100	2.5	4.9	2.0	1.95	2.438	1.25	7.03	7.03	166.0	166.0
CT20	200	80	40	100	2.5	5.0	2.0	2.00	2.500	1.25	6.87	6.87	164.1	164.1
CT21	200	80	39	100	2.5	5.1	2.0	2.05	2.563	1.25	6.70	6.70	162.1	162.1
CONSTANT PARAMETERS:														
Throat Height/Total Height					=	0.75								
Top Thickness					=	150	mm							
Throat Thickness					=	175	mm							
Base Thickness					=	200	mm							

Table 16: *Parametric linear eigenvalue buckling analysis of cooling towers with variable top edge diameter and bottom edge diameter to throat diameter ratios: top edge diameter to throat diameter ratio (D_{top}/D_{thr}); bottom edge diameter to throat diameter ratio (D_{bot}/D_{thr})*

Figure 194 and *Figure 195* show the variation of the critical wind speed with the cooling tower top edge diameter to throat diameter ratios (D_{top}/D_{thr}) and bottom edge diameter to throat diameter ratios (D_{bot}/D_{thr}) respectively. In addition, the buckled shapes of the cooling tower (first mode) are shown for a selected cooling towers to show the change in the

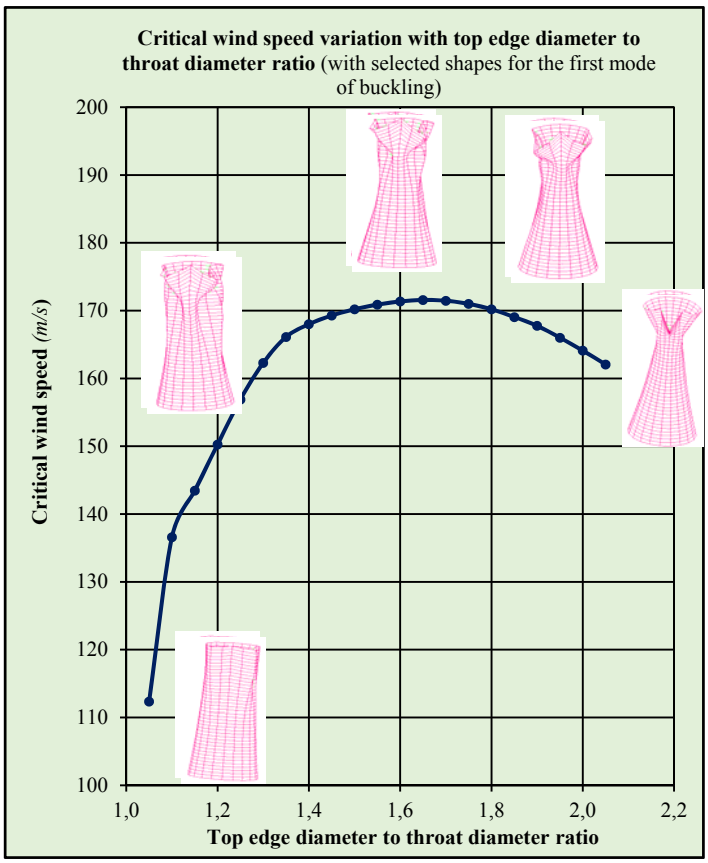

Figure 194: *Critical wind speed variation with cooling tower top edge diameter to throat diameter ratio (D_{top}/D_{thr})*

buckling modes with respect to the top edge diameter to throat diameter and bottom edge diameter to throat diameter ratios.

Observations:

From *Figure 194*, it can be observed that:

- The critical wind speed varies non-linearly with the top edge diameter to throat diameter ratio;
- As the top diameter to throat diameter ratio increases, the critical speed increases rapidly up to a state where the rate of increase reduces. The critical wind speed is a maximum at about a top edge diameter to throat diameter ratio of 1.65. From this state, the critical wind speed reduces gently as the top edge diameter to throat diameter ratio increases;
- As the throat diameter reduces relative to the top edge diameter, the stability of the portion of the shell below the throat improves up to a state where it does not display instability when the top edge diameter to throat diameter ratio is a maximum.

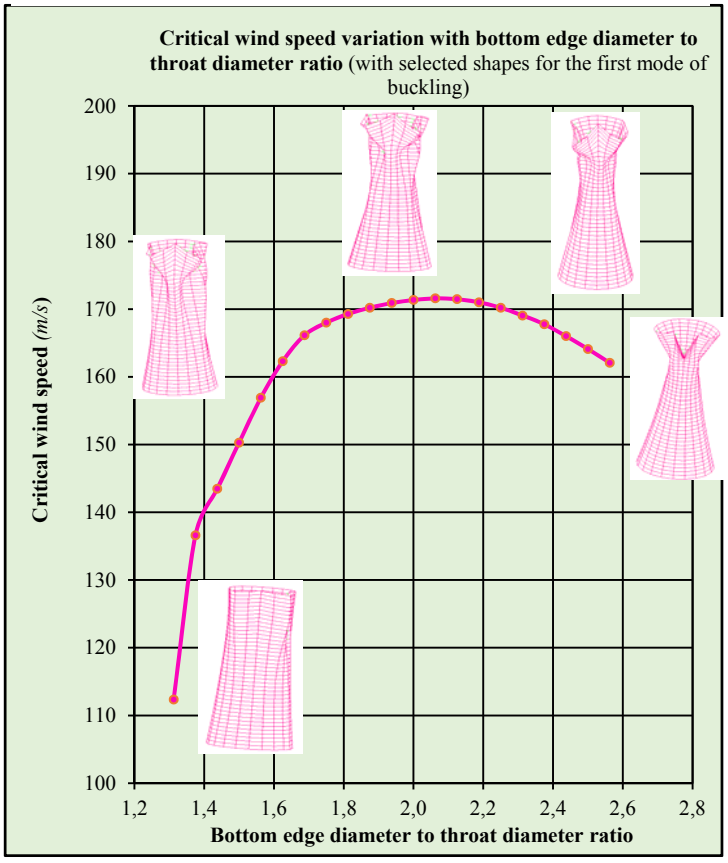

Figure 195*: Critical wind speed variation with cooling tower bottom edge diameter to throat diameter ratio (D_{bot}/D_{thr})*

Observations:

From *Figure 195*, it can be observed that:

- The critical wind speed varies non-linearly with the bottom edge diameter to throat diameter ratio;
- As the bottom edge diameter to throat diameter ratio increases, the critical speed increases rapidly up to a state where the rate of increase reduces. The critical wind speed is a maximum at about a bottom edge diameter to throat diameter ratio of 2.06. From this state, the critical wind speed reduces gently as the bottom edge diameter to throat diameter ratio increases;
- As the throat diameter reduces relative to the bottom edge diameter, the stability of the portion of the shell below the throat improves up to a state where it does not display instability when the bottom edge diameter to throat diameter ratio is a maximum.

4.1.4 Bottom edge diameter to top edge diameter ratio (bottom edge diameter fixed) influence on stability behaviour

Table 17 below shows the results of the parametric study of cooling towers whose bottom edge diameter to top edge diameter ratios were changed to observe the change in the critical wind speed by changing *only the top edge diameter* whilst the bottom edge diameter, the total height, throat to total height ratio, thickness and height to diameter ratios were kept constant. By default, the top edge diameter to throat diameter ratio becomes variable.

COOLING TOWER	GEOMETRICAL PARAMETERS									LINEAR EIGENVALUE BUCKLING ANALYSIS RESULTS (First Mode)	
	Total Height	Throat Height/ Total Height	Top Diameter	Throat Diameter	Bottom Diameter	Height/ Top Diameter	Top Diameter/Throat Diameter	Bottom Diameter/Throat Diameter	Bottom Diameter/ Top Diameter	**Critical Wind Pressure LOAD FACTORS** (basic pressure corresponds to a wind speed of 28m/s)	**Critical Wind Velocity** (m/s)
	H (m)		D_{top} (m)	D_{thr} (m)	D_{bot} (m)	H/D_{top}	D_{top}/D_{thr}	D_{bot}/D_{thr}	D_{bot}/D_{top}	D_{bot}/D_{top}	D_{bot}/D_{top}
CT1	200	0.75	100	67	100	2.00	1.500	1.500	1.000	5.33	144.5
CT2	200	0.75	98	67	100	2.05	1.463	1.500	1.025	5.43	145.9
CT3	200	0.75	95	67	100	2.10	1.429	1.500	1.050	5.33	144.5
CT4	200	0.75	93	67	100	2.15	1.395	1.500	1.075	5.40	145.5
CT5	200	0.75	91	67	100	2.20	1.364	1.500	1.100	5.46	146.3
CT6	200	0.75	89	67	100	2.25	1.333	1.500	1.125	5.53	147.2
CT7	200	0.75	87	67	100	2.30	1.304	1.500	1.150	5.59	148.0
CT8	200	0.75	85	67	100	2.35	1.277	1.500	1.175	5.64	148.7
CT9	200	0.75	83	67	100	2.40	1.250	1.500	1.200	5.69	149.3
CT10	200	0.75	82	67	100	2.45	1.224	1.500	1.225	5.73	149.9
CT11	200	0.75	80	67	100	2.50	1.200	1.500	1.250	5.76	150.3
CT12	200	0.75	78	67	100	2.55	1.176	1.500	1.275	5.77	150.4
CT13	200	0.75	77	67	100	2.60	1.154	1.500	1.300	5.75	150.1
CT14	200	0.75	75	67	100	2.65	1.132	1.500	1.325	5.67	149.1
CT15	200	0.75	74	67	100	2.70	1.111	1.500	1.350	5.46	146.3
CT16	200	0.75	73	67	100	2.75	1.091	1.500	1.375	5.09	141.3
CT17	200	0.75	71	67	100	2.80	1.071	1.500	1.400	4.62	134.6
CT18	200	0.75	70	67	100	2.85	1.053	1.500	1.425	4.16	127.7
CT19	200	0.75	69	67	100	2.90	1.034	1.500	1.450	3.75	121.2
CT20	200	0.75	68	67	100	2.95	1.017	1.500	1.475	3.40	115.4
CT21	200	0.75	67	67	100	3.00	1.000	1.500	1.500	3.12	110.6
CONSTANT PARAMETERS:											
Throat Height/Total Height ratio				=	0.75						
Top Thickness				=	150						
Throat Thickness				=	175						
Base Thickness				=	200						
Height/Throat Diameter ratio				=	3.0						
Height/Bottom Diameter ratio				=	2.0						

Table 17: *Parametric linear eigenvalue buckling analysis of cooling towers with variable bottom edge diameter to top edge diameter ratios (D_{bot}/D_{top}) and the top edge diameter to throat diameter ratio (D_{top}/D_{thr}) by default*

Figure 196 and *Figure 197* show the variation of the critical wind speed with the cooling tower bottom edge diameter to top edge diameter ratios (D_{bot}/D_{top}) and top edge diameter to throat diameter ratios (D_{top}/D_{thr}) respectively. In addition, the buckled shapes of the cooling tower (first mode) are shown for a selected cooling towers to show the change in the buckling modes with respect to the bottom edge diameter to top edge diameter ratios.

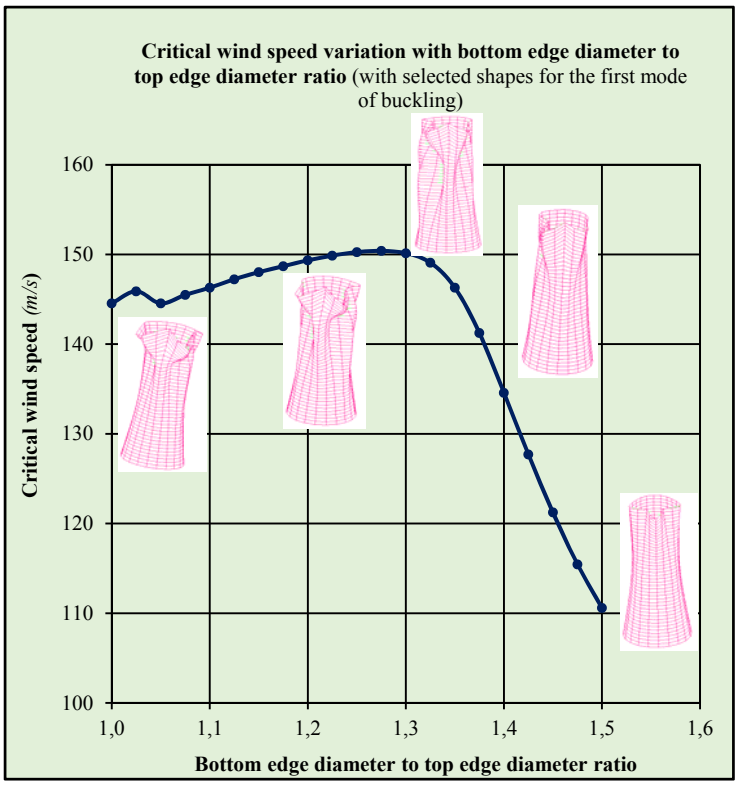

Figure 196: *Critical wind speed variation with cooling tower bottom edge diameter to top edge diameter ratios (D_{bot}/D_{top})*

Observations:

From *Figure 196*, it can be observed that:

- The critical wind speed varies non-linearly with the bottom edge diameter to top edge diameter ratios;
- As the bottom edge diameter to top edge diameter ratio increases, the critical wind speed increases at a marginally gentle rate until it reaches a maximum value close to a bottom edge diameter to top edge diameter ratio of 1.3. From this value, critical wind speed reduces rapidly as the bottom edge diameter to top edge diameter ratio is increased;
- The cooling tower shell displays different buckling modes with increasing bottom edge diameter to top edge diameter ratios.

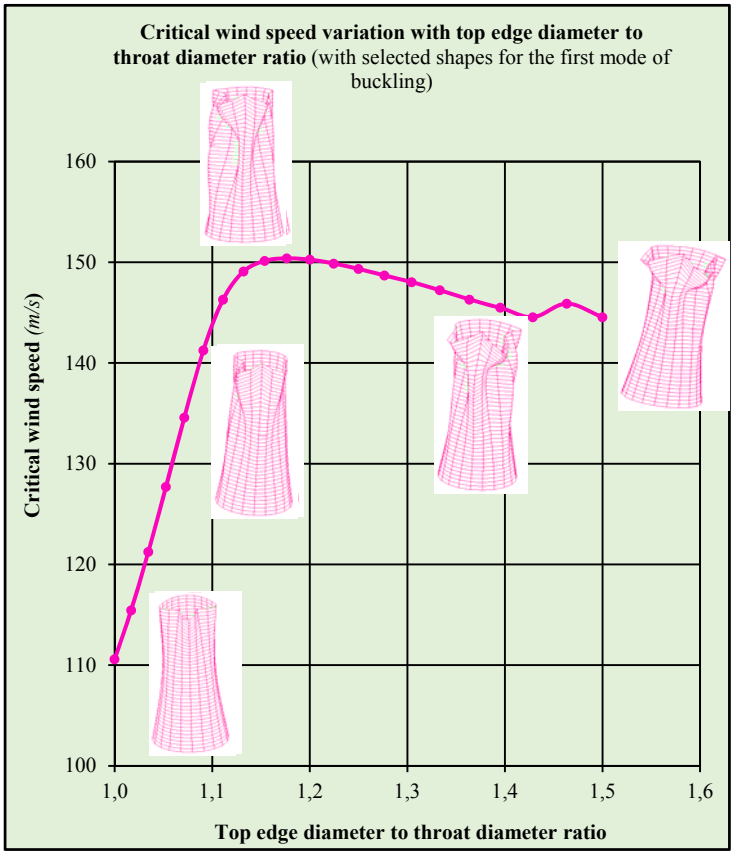

Figure 197: *Critical wind speed variation with cooling tower top edge diameter to throat diameter ratio (D_{top}/D_{thr})*

Observations:

From *Figure 197*, it can be observed that:

- The variation of the top edge diameter to throat diameter ratio with the critical wind speed is by default as indicated above;
- The critical wind speed varies non-linearly with the top edge diameter to throat diameter ratios;
- As the top edge diameter to throat diameter ratio increases, the critical wind speed increases at a marginal rate until it reaches a maximum value close to a top edge diameter to throat diameter ratio of 1.15. From this value, critical wind speed reduces rapidly as the top edge diameter to throat diameter ratio reduces;
- The cooling tower shell displays different buckling modes with increasing top edge diameter to throat diameter ratios.

4.1.5 Bottom edge diameter to top edge diameter ratio (top edge diameter fixed) influence on stability behaviour

Table 18 below shows the results of the parametric study of cooling towers whose bottom edge diameter to top edge diameter ratios were changed to observe the change in the critical wind speed by changing *only the bottom edge diameter* whilst the top edge diameter, the total height, throat to total height ratio, thickness and height to diameter ratios were kept constant. By default, the bottom edge diameter to throat diameter ratio becomes variable.

COOLING TOWER	GEOMETRICAL PARAMETERS									LINEAR EIGENVALUE BUCKLING ANALYSIS RESULTS (First Mode)	
	Total Height	Throat Height/ Total Height	Top Diameter	Throat Diameter	Bottom Diameter	Height/ Bottom Diameter	Top Diameter/ Throat Diameter	Bottom Diameter/ Throat Diameter	Bottom Diameter/ Top Diameter	**Critical Wind Pressure LOAD FACTORS** (basic pressure corresponds to a wind speed of 28m/s)	**Critical Wind Velocity** (m/s)
	H (m)		D_{top} (m)	D_{thr} (m)	D_{bot} (m)	H/D_{bot}	D_{top}/D_{thr}	D_{bot}/D_{thr}	D_{bot}/D_{top}	D_{bot}/D_{top}	D_{bot}/D_{top}
CT1	200	0.75	110	67	110	1.8	1.650	1.650	1.000	5.75	150.1
CT2	200	0.75	110	67	113	1.8	1.650	1.691	1.025	5.90	152.1
CT3	200	0.75	110	67	116	1.7	1.650	1.733	1.050	6.02	153.6
CT4	200	0.75	110	67	118	1.7	1.650	1.774	1.075	6.11	154.8
CT5	200	0.75	110	67	121	1.7	1.650	1.815	1.100	6.18	155.6
CT6	200	0.75	110	67	124	1.6	1.650	1.856	1.125	6.25	156.5
CT7	200	0.75	110	67	127	1.6	1.650	1.898	1.150	6.30	157.1
CT8	200	0.75	110	67	129	1.5	1.650	1.939	1.175	6.35	157.8
CT9	200	0.75	110	67	132	1.5	1.650	1.980	1.200	6.40	158.4
CT10	200	0.75	110	67	135	1.5	1.650	2.021	1.225	6.44	158.9
CT11	200	0.75	110	67	138	1.5	1.650	2.063	1.250	6.49	159.5
CT12	200	0.75	110	67	140	1.4	1.650	2.104	1.275	6.53	160.0
CT13	200	0.75	110	67	143	1.4	1.650	2.145	1.300	6.57	160.5
CT14	200	0.75	110	67	146	1.4	1.650	2.186	1.325	6.61	161.0
CT15	200	0.75	110	67	149	1.3	1.650	2.228	1.350	6.65	161.5
CT16	200	0.75	110	67	151	1.3	1.650	2.269	1.375	6.69	161.9
CT17	200	0.75	110	67	154	1.3	1.650	2.310	1.400	6.73	162.4
CT18	200	0.75	110	67	157	1.3	1.650	2.351	1.425	6.77	162.9
CT19	200	0.75	110	67	160	1.3	1.650	2.393	1.450	6.81	163.4
CT20	200	0.75	110	67	162	1.2	1.650	2.434	1.475	6.84	163.7
CT21	200	0.75	110	67	165	1.2	1.650	2.475	1.500	6.86	164.0
CONSTANT PARAMETERS:											
Throat Height/Total Height ratio				=	0.75						
Top Thickness				=	150						
Throat Thickness				=	175						
Base Thickness				=	200						
Height/Top Diameter ratio				=	1.82						

Table 18: *Parametric linear eigenvalue buckling analysis of cooling towers with variable bottom edge diameter to top edge diameter ratios (D_{bot}/D_{top}) and the bottom edge diameter to throat diameter ratio (D_{bot}/D_{thr}) by default*

Figure 198 and *Figure 199* show the variation of the critical wind speed with the cooling tower bottom edge diameter to top edge diameter ratios (D_{bot}/D_{top}) and bottom edge diameter to throat diameter ratios (D_{bot}/D_{thr}) respectively. In addition, the buckled shapes of the cooling tower (first mode) are shown for selected cooling towers to show the change in the buckling modes with respect to the bottom edge diameter to top edge diameter ratios.

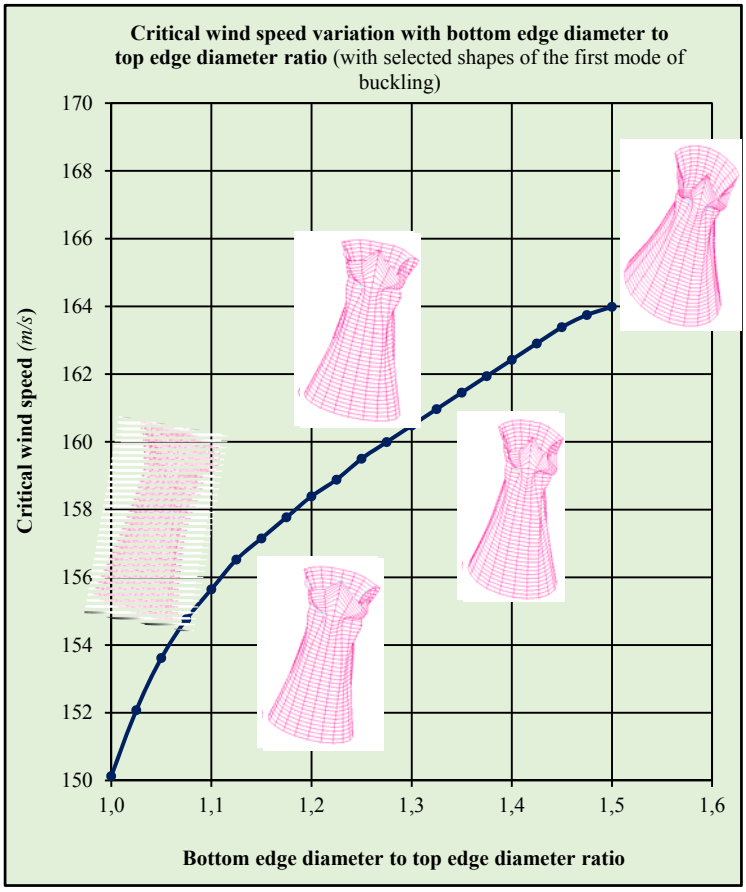

Figure 198: *Critical wind speed variation with cooling tower bottom edge diameter to top edge diameter ratio (D_{bot}/D_{top})*

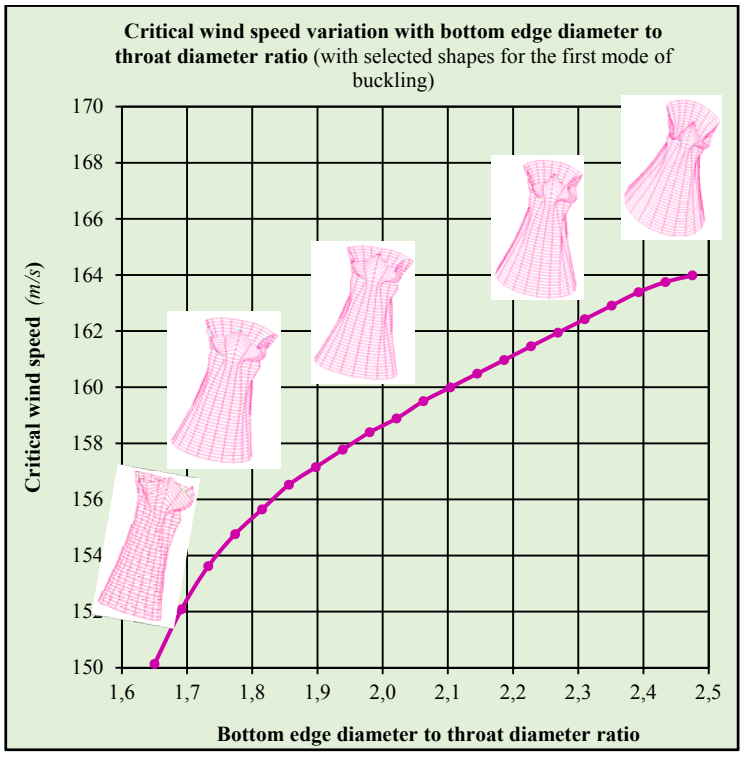

Figure 199: *Critical wind speed variation with cooling tower bottom edge diameter to throat diameter ratio (D_{bot}/D_{thr})*

Observations:

From *Figure 198*, it can be observed that:

- For smaller bottom edge diameter to top diameter ratio (1.0 to 1.1), the critical wind speed varies non-linearly with the bottom edge diameter to top edge diameter ratios. This relationship changes to a linear relationship for larger bottom edge diameter to top edge diameter ratios (1.1 to 1.45);
- The lower the bottom edge diameter to top edge diameter ratio, the lower the critical wind speed and vice versa: When the shell bottom edge diameter and top edge diameters are equal or of more or less the same size, the critical wind speed is lower; the shell buckles at lower wind speeds (150 m/s). When the top edge diameter is small compared to the bottom edge diameter, the shell buckles at higher wind speed (164 m/s). However, the difference in the critical wind speed is only 9.3%;
- The cooling tower shell buckles in a similar fashion by displaying meridional dimples around and above the throat for both lower and higher bottom edge diameter to top edge diameter ratios;
- By fixing the top edge diameter to a constant whilst the bottom edge diameter is changed, the modes of buckling are different for the same parameter of bottom edge diameter to top edge diameter ratio from the buckling modes when the bottom edge diameter is fixed to a constant and the top edge diameter changed as seen from section 4.1.4 above.

Observations:

From *Figure 199*, it can be observed that:

- For smaller bottom edge diameter to throat diameter ratio (1.6 to 1.9), the critical wind speed varies non-linearly with the bottom edge diameter to throat diameter ratios. This relationship changes to a linear relationship for larger bottom edge diameter to throat edge diameter ratios (1.9 to 2.5);
- The lower the bottom edge diameter to throat diameter ratio, the lower the critical wind speed and vice versa;
- The cooling tower shell buckles in a similar fashion by displaying meridional dimples around and above the throat for both lower and higher bottom edge diameter to throat diameter ratios.

4.1.6 Shell thickness influence on stability behaviour

Table 19 below shows the results of the parametric study of cooling towers whose shell thickness was changed to observe the change in the critical wind speed whilst the diameters, height, throat to total height ratio and height to diameter ratios were kept constant. A uniform thickness for the entire height and circumference of the shell was considered.

COOLING TOWER	GEOMETRICAL PARAMETERS						LINEAR EIGENVALUE BUCKLING ANALYSIS RESULTS *(First Mode)*	
	Total Height	Throat Height/ Total Height	Top Diameter	Throat Diameter	Bottom Diameter	Thickness	**Critical Wind Pressure LOAD FACTORS** *(basic pressure corresponds to a wind speed of 28m/s and a model load multiplier)*	**Critical Wind Velocity** *(m/s)*
	H	H_t/H	D_{top}	D_{thr}	D_{bot}	T		
	(m)		*(m)*	*(m)*	*(m)*	*(mm)*		
CT0.2	200	0.75	80	67	100	20	4.41	18.6
CT0.4	200	0.75	80	67	100	40	1.73	36.8
CT0.6	200	0.75	80	67	100	60	3.59	53.0
CT0.8	200	0.75	80	67	100	80	1.61	79.4
CT1	200	0.75	80	67	100	100	2.46	98.2
CT2	200	0.75	80	67	100	120	2.98	108.1
CT3	200	0.75	80	67	100	140	3.89	123.5
CT4	200	0.75	80	67	100	160	5.03	140.4
CT5	200	0.75	80	67	100	180	6.38	158.1
CT6	200	0.75	80	67	100	200	7.94	176.4
CT7	200	0.75	80	67	100	220	9.83	196.3
CT8	200	0.75	80	67	100	240	11.78	214.9
CT9	200	0.75	80	67	100	260	13.98	234.1
CT10	200	0.75	80	67	100	280	16.15	251.6
CT11	200	0.75	80	67	100	300	18.50	269.3
CT12	200	0.75	80	67	100	320	21.06	287.3
CT13	200	0.75	80	67	100	340	23.82	305.6
CT14	200	0.75	80	67	100	360	26.79	324.1
CT15	200	0.75	80	67	100	380	29.97	342.8
CT16	200	0.75	80	67	100	400	33.38	361.7
CT17	200	0.75	80	67	100	420	37.01	380.9
CT18	200	0.75	80	67	100	440	40.86	400.2
CT19	200	0.75	80	67	100	460	44.96	419.8
CT20	200	0.75	80	67	100	480	49.28	439.5
CT21	200	0.75	80	67	100	500	53.86	459.5
CONSTANT PARAMETERS:								
Throat Height/Total Height ratio					=	0.75		
Height/Top Diameter					=	2.50		
Height/Throat Diameter					=	3.00		
Height/Bottom Diameter					=	2.00		
Top Diameter/Throat Diameter					=	1.20		
Bottom Diameter/Throat Diameter					=	1.50		
Bottom Diameter/Top Diameter					=	1.25		

Table 19: *Parametric linear eigenvalue buckling analysis of cooling towers with variable thickness*

Figure 200 shows the variation of the critical wind speed with the cooling tower thickness. In addition, the buckled shapes of the cooling tower (first mode) are shown for a selected cooling tower thicknesses to show the change in the buckling modes with respect to the shell thickness.

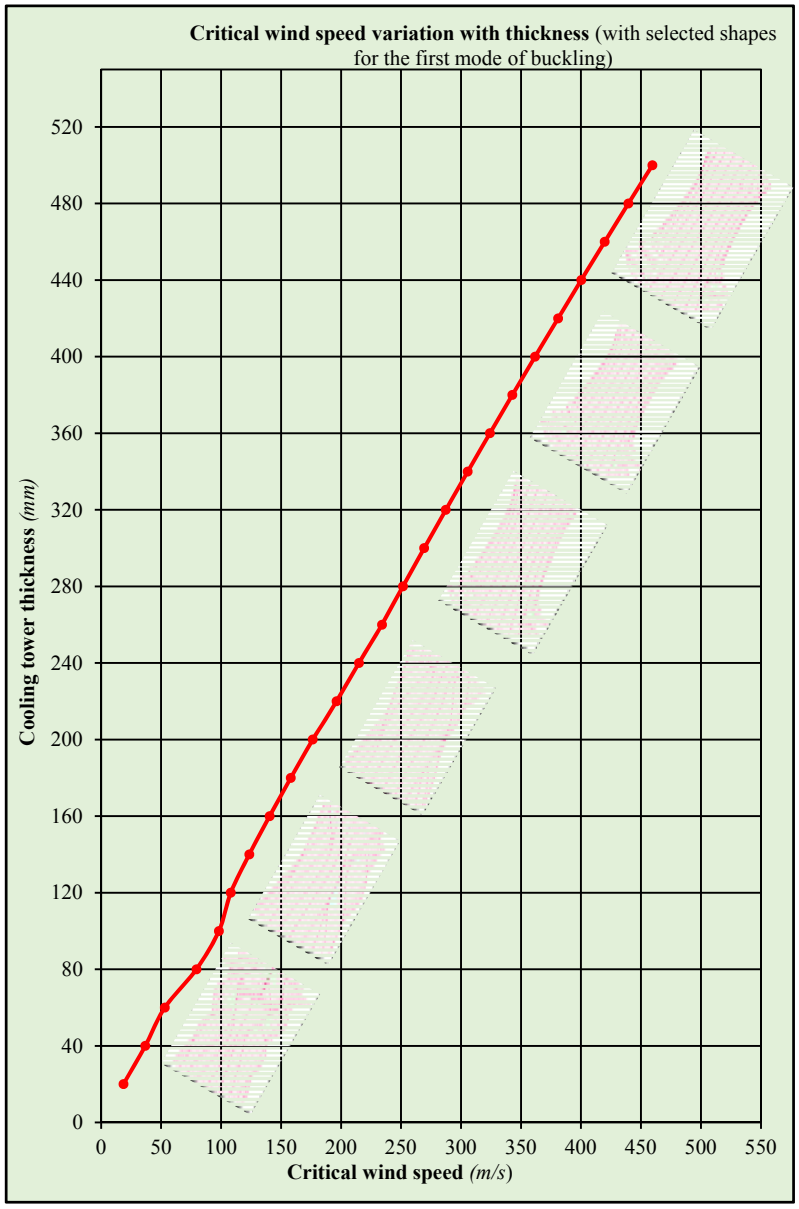

Figure 200: *Critical wind speed variation with cooling tower shell thickness*

Observations:

From *Figure 200*, it can be observed that:

- The critical wind speed varies linearly with the cooling tower thickness. The smaller the shell thickness, the lower the critical speed. Conversely, the thicker the shell, the higher the critical wind speed. The thinner shell buckles at lower wind pressures and wind speeds;
- For lower thicknesses, the cooling tower shell above the throat buckles in a similar fashion by displaying meridional dimples in the windward direction;
- In addition, the entire shell buckles for thinner cooling towers;
- For higher thicknesses, the cooling tower shell close to the bottom buckles in a similar fashion by displaying localised circumferential dimples at about 72 degrees to the windward direction on both sides of the shell;
- For thicker cooling tower shells, the top part of the cooling tower does not buckle;
- The bottom part of the thicker shell buckles in the regions where the wind suction pressure is highest.

4.2 ON FREE VIBRATION BEHAVIOUR

The parametric study results for various geometrical parameters are included in the following sections. In each section, a summary of the natural frequencies is indicated in a table for various cooling towers whose geometry is changed systematically in order to study the change in the vibration behaviour of the cooling tower. Followed by this is a table showing the mode shapes for the first ten (10) different modes for a selected geometrical parameters to cover the full spectrum of the considered parameter. Finally, the natural frequencies are plotted on a graph against the various geometrical parameters.

The first ten (10) different modes of vibration are analysed. Due to the axi-symmetry of the cooling tower shell geometry, it is observed that the even and odd numbered modes of vibration have the same natural frequencies and similar mode shapes but in different orthogonal directions. That is, mode 1 and mode 2 have the same natural frequencies and mode shapes but in different directions along the X and Z plane directions. Therefore, the modes presented in this study are the Odd numbered modes: *1, 3, 5,…, 17* and *19* which are of course the same as the *2, 4, 6, …, 18* and *20*.

For each parametric study, the particular geometrical parameter (e.g. height) is changed systematically for at least twenty (20) cooling towers whilst keeping the rest of the other geometrical parameters (e.g. thickness, diameters etc.) constant in order to study the influence of a single parameter on the free vibration behaviour of the cooling tower. The constant parameters are included at the bottom of each table of results. In order to cover a wider range of geometrical parameters, the study was tailored to investigate ratios of the geometrical parameters instead of looking into just the actual parameters.

The following parameters were investigated:

- *Height* of the cooling tower;
- *Height to top edge diameter ratio* (H/D_{top});
- Top edge diameter to throat diameter ratio (D_{top}/D_{thr});
- *Bottom edge diameter to top edge diameter ratio* (D_{bot}/D_{top});
- *Shell thickness* of the cooling tower.

4.2.1 Height influence on free vibration behaviour

Table 20 below shows the results of the parametric study of cooling towers whose height was changed from 60m to 250m whilst maintaining the throat height to total height ratio (0.75) in order to observe the change in the natural frequencies for the first ten (10) different modes of vibration.

COOLING TOWER	GEOMETRICAL PARAMETERS					LINEAR EIGENVALUE VIBRATION ANALYSIS RESULTS *(10 Modes)*									
	Total Height	Throat Height/ Total Height	Top Diameter	Throat Diameter	Bottom Diameter	**Natural Frequencies (Hz) and Mode Shapes** *(basic pressure corresponds to a wind speed of 28m/s)*									
	H		D_{top}	D_{thr}	D_{bot}	*Mode*									
	(m)		*(m)*	*(m)*	*(m)*	*1*	*3*	*5*	*7*	*9*	*11*	*13*	*15*	*17*	*19*
CT1	60	0.75	24	20	30	0.0931	0.1057	0.1440	0.1640	0.1680	0.1900	0.2250	0.2250	0.2710	0.2790
CT2	70	0.75	28	23	35	0.0790	0.0836	0.1190	0.1240	0.1440	0.1450	0.1840	0.1930	0.2030	0.2110
CT3	80	0.75	32	27	40	0.0687	0.0689	0.0974	0.1020	0.1160	0.1260	0.1580	0.1580	0.1660	0.1680
CT4	90	0.75	36	30	45	0.0585	0.0608	0.0791	0.0891	0.0961	0.1121	0.1264	0.1338	0.1340	0.1496
CT5	100	0.75	40	33	50	0.0508	0.0545	0.0659	0.0792	0.0816	0.1009	0.1037	0.1104	0.1182	0.1345
CT6	110	0.75	44	37	55	0.0449	0.0495	0.0561	0.0706	0.0713	0.0867	0.0917	0.0930	0.1058	0.1169
CT7	120	0.75	48	40	60	0.0403	0.0453	0.0486	0.0622	0.0649	0.0738	0.0795	0.0841	0.0958	0.1028
CT8	130	0.75	52	43	65	0.0365	0.0417	0.0426	0.0555	0.0596	0.0636	0.0690	0.0776	0.0876	0.0917
CT9	140	0.75	56	47	70	0.0334	0.0379	0.0387	0.0501	0.0551	0.0555	0.0606	0.0721	0.0807	0.0827
CT10	150	0.75	60	50	75	0.0308	0.0340	0.0361	0.0457	0.0490	0.0512	0.0537	0.0673	0.0748	0.0754
CT11	160	0.75	64	53	80	0.0286	0.0308	0.0338	0.0420	0.0436	0.0479	0.0481	0.0631	0.0675	0.0692
CT12	170	0.75	68	57	85	0.0266	0.0282	0.0318	0.0388	0.0392	0.0434	0.0450	0.0594	0.0603	0.0627
CT13	180	0.75	72	60	90	0.0250	0.0259	0.0300	0.0354	0.0361	0.0395	0.0424	0.0542	0.0560	0.0563
CT14	190	0.75	76	63	95	0.0235	0.0240	0.0284	0.0322	0.0337	0.0361	0.0401	0.0490	0.0509	0.0531
CT15	200	0.75	80	67	100	0.0222	0.0223	0.0270	0.0295	0.0317	0.0332	0.0380	0.0446	0.0463	0.0504
CT16	210	0.75	84	70	105	0.0208	0.0210	0.0257	0.0271	0.0299	0.0307	0.0361	0.0407	0.0423	0.0480
CT17	220	0.75	88	73	110	0.0195	0.0200	0.0245	0.0251	0.0283	0.0286	0.0345	0.0374	0.0388	0.0459
CT18	230	0.75	92	77	115	0.0184	0.0191	0.0233	0.0234	0.0267	0.0268	0.0329	0.0344	0.0358	0.0439
CT19	240	0.75	96	80	120	0.0174	0.0182	0.0217	0.0225	0.0250	0.0255	0.0315	0.0319	0.0331	0.0420
CT20	250	0.75	100	83	125	0.0165	0.0174	0.0203	0.0216	0.0235	0.0243	0.0296	0.0302	0.0307	0.0401

CONSTANT PARAMETERS:							
Top Thickness	=	150	mm	Height/Bottom Diameter ratio	=	2.0	
Throat Thickness	=	175	mm	Top Diameter/Throat Diameter ratio	=	1.2	
Base Thickness	=	200	mm	Bottom Diameter/Throat Diameter ratio	=	1.5	
Height/Top Diameter ratio	=	2.5		Bottom Diameter/Top Diameter ratio	=	1.3	
Height/Throat Diameter rati	=	3.0					

Table 20: *Parametric linear eigenvalue vibration analysis of cooling towers with variable heights and constant throat height to total height ratio of 0.75*

Figure 201 shows the variation of the natural frequencies with the change in cooling tower height and *Table 21* shows the various mode shapes (first 10 different modes) for selected cooling tower heights.

Table 21: *Vibration mode shapes for the first 10 different modes for selected cooling tower heights*

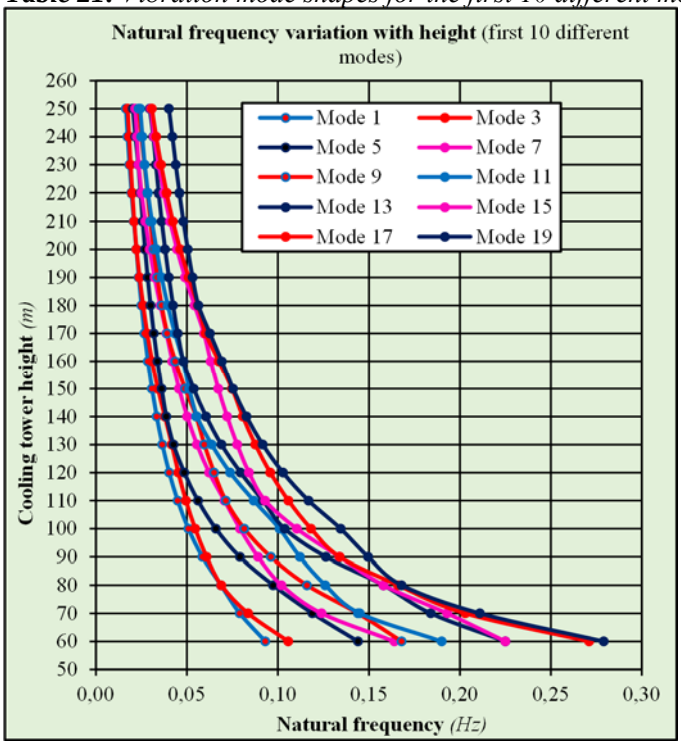

Observations:

From *Figure 201*, it can be observed that:

- The natural frequency reduces non-linearly with increase in height for all modes;
- The natural frequency bandwidth reduces as the height increases. The natural frequency band width for the first 10 different modes of vibration for a 60m high cooling tower is greater at (0.19Hz) compared to that of a 250m high cooling tower which is at 0.024Hz.

From *Table 21*, it can be observed that:

- The order of the mode shape changes from the lower to higher natural frequencies becomes different for each cooling tower height;
- For all heights, the vibration of the shell is by meridional dimpling of the shell inwards and outwards around the line of axi-symmetry;
- All modes of vibration display buckling inwards and outwards except for the global rigid body mode.

Figure 201: *Natural frequency variation with cooling tower height*

4.2.2 Height to diameter ratio influence on free vibration behaviour

Table 22 below shows the results of the parametric study of cooling towers whose height to diameter ratios were changed from 1 to 5 in order to observe the change in the natural frequencies for the first ten (10) different modes of vibration whilst the total height, throat height to total height ratio, thickness and diameter ratios were kept constant.

COOLING TOWER	GEOMETRICAL PARAMETERS							LINEAR EIGENVALUE VIBRATION ANALYSIS RESULTS (10 Modes)									
	Total Height	Top Diameter	Throat Diameter	Bottom Diameter	Height/ Top Diameter	Height/ Throat Diameter	Height/ Bottom Diameter	Natural Frequencies (Hz) and Mode Shapes for various H/D_{top} (basic pressure corresponds to a wind speed of 28m/s)									
	H	D_{top}	D_{thr}	D_{bot}	$H/Dtop$	$H/Dthr$	$H/Dbot$	Mode									
	(m)	(m)	(m)	(m)				1	3	5	7	9	11	13	15	17	19
CT1	200	200	167	250	1.0	1.2	0.8	0.0266	0.0288	0.0306	0.0321	0.0334	0.0347	0.0362	0.0365	0.0423	0.0433
CT2	200	167	139	208	1.2	1.4	1.0	0.0277	0.0278	0.0290	0.0307	0.0314	0.0343	0.0353	0.0364	0.0388	0.0453
CT3	200	143	119	179	1.4	1.7	1.1	0.0266	0.0275	0.0284	0.0294	0.0304	0.0325	0.0348	0.0366	0.0424	0.0435
CT4	200	125	104	156	1.6	1.9	1.3	0.0251	0.0260	0.0281	0.0296	0.0310	0.0313	0.0349	0.0393	0.0395	0.0402
CT5	200	111	93	139	1.8	2.2	1.4	0.0242	0.0246	0.0285	0.0300	0.0301	0.0313	0.0358	0.0370	0.0409	0.0457
CT6	200	100	83	125	2.0	2.4	1.6	0.0229	0.0249	0.0262	0.0300	0.0327	0.0330	0.0343	0.0349	0.0440	0.0482
CT7	200	91	76	114	2.2	2.6	1.8	0.0223	0.0243	0.0262	0.0302	0.0307	0.0332	0.0371	0.0384	0.0414	0.0547
CT8	200	83	69	104	2.4	2.9	1.9	0.0221	0.0228	0.0280	0.0282	0.0321	0.0322	0.0391	0.0419	0.0440	0.0519
CT9	200	77	64	96	2.6	3.1	2.1	0.0217	0.0226	0.0261	0.0309	0.0314	0.0344	0.0370	0.0474	0.0491	0.0492
CT10	200	71	60	89	2.8	3.4	2.2	0.0209	0.0235	0.0244	0.0313	0.0342	0.0352	0.0373	0.0465	0.0516	0.0518
CT11	200	67	56	83	3.0	3.6	2.4	0.0204	0.0230	0.0248	0.0317	0.0337	0.0379	0.0406	0.0441	0.0498	0.0526
CT12	200	63	52	78	3.2	3.8	2.6	0.0202	0.0217	0.0265	0.0324	0.0326	0.0419	0.0421	0.0444	0.0485	0.0544
CT13	200	59	49	74	3.4	4.1	2.7	0.0203	0.0206	0.0286	0.0314	0.0341	0.0399	0.0465	0.0477	0.0485	0.0556
CT14	200	56	46	69	3.6	4.3	2.9	0.0197	0.0207	0.0306	0.0309	0.0359	0.0381	0.0473	0.0512	0.0527	0.0534
CT15	200	53	44	66	3.8	4.6	3.0	0.0189	0.0213	0.0301	0.0335	0.0364	0.0382	0.0473	0.0514	0.0561	0.0570
CT16	200	50	42	63	4.0	4.8	3.2	0.0182	0.0221	0.0298	0.0349	0.0362	0.0409	0.0477	0.0495	0.0610	0.0612
CT17	200	48	40	60	4.2	5.0	3.4	0.0177	0.0232	0.0297	0.0334	0.0391	0.0440	0.0477	0.0486	0.0595	0.0659
CT18	200	45	38	57	4.4	5.3	3.5	0.0172	0.0245	0.0299	0.0321	0.0422	0.0461	0.0474	0.0498	0.0580	0.0707
CT19	200	43	36	54	4.6	5.5	3.7	0.0168	0.0259	0.0303	0.0309	0.0446	0.0455	0.0511	0.0515	0.0568	0.0748
CT20	200	42	35	52	4.8	5.8	3.8	0.0166	0.0275	0.0297	0.0309	0.0432	0.0488	0.0535	0.0551	0.0557	0.0755
CT21	200	40	33	50	5.0	6.0	4.0	0.0164	0.0286	0.0293	0.0317	0.0419	0.0523	0.0549	0.0559	0.0593	0.0766
Throat Height/Total Hei				=	0.75			Top Diameter/Throat Diameter ratio						=			1.200
Top Thickness				=	150	mm		Bottom Diameter/Throat Diameter ratio						=			1.500
Throat Thickness				=	175	mm		Bottom Diameter/Top Diameter ratio						=			1.250

Table 22: *Parametric linear eigenvalue vibration analysis of cooling towers with variable height to diameter ratios and a constant throat height to total height ratio of 0.75*

Figure 202 shows the variation of the natural frequencies with the change in cooling tower height to diameter ratios and *Table 23* shows the various mode shapes (first 10 different modes) for selected cooling tower heights to diameter ratios.

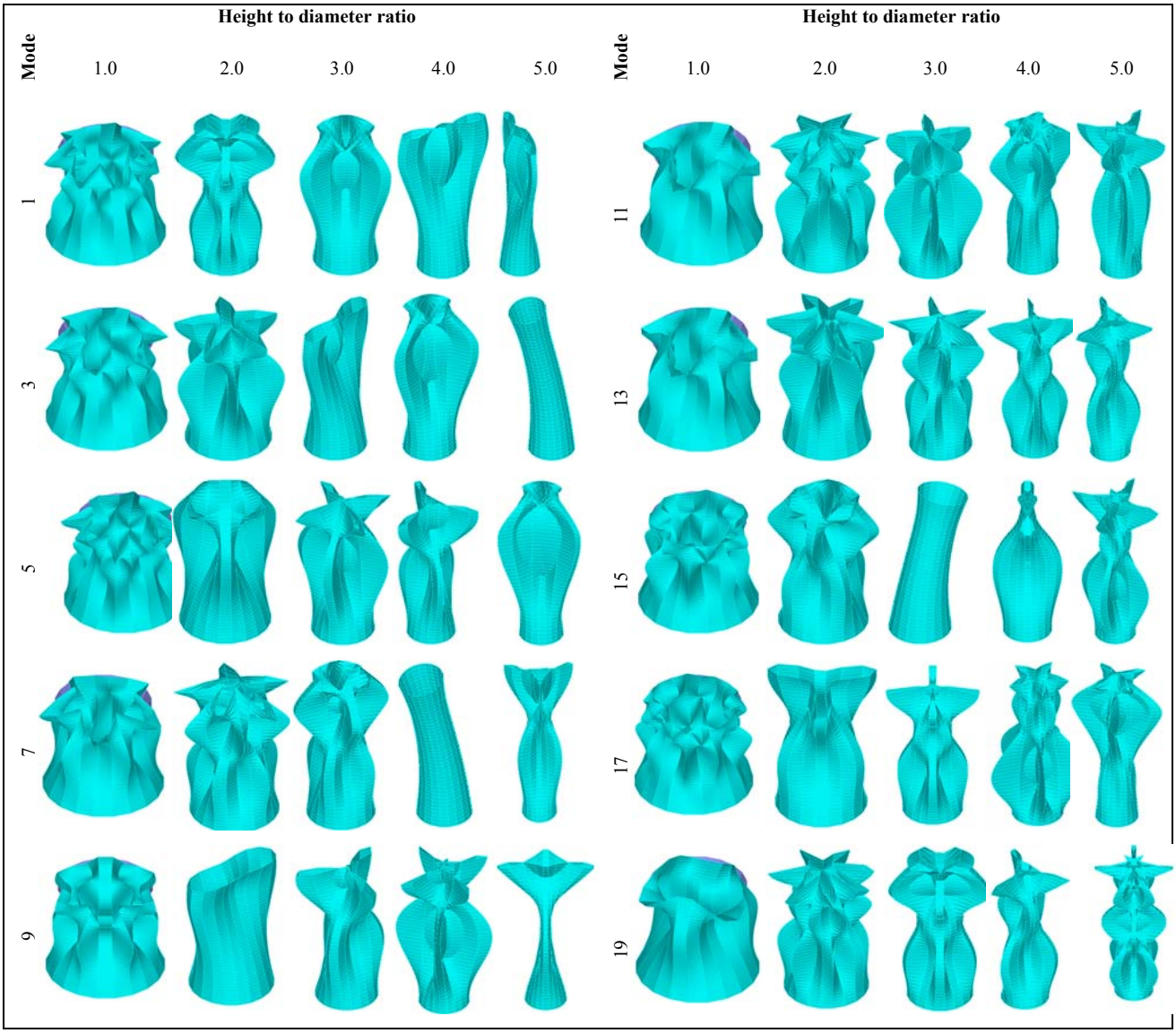

Table 23 *Vibration mode shapes for the first 10 different modes for selected cooling tower height to diameter ratios*

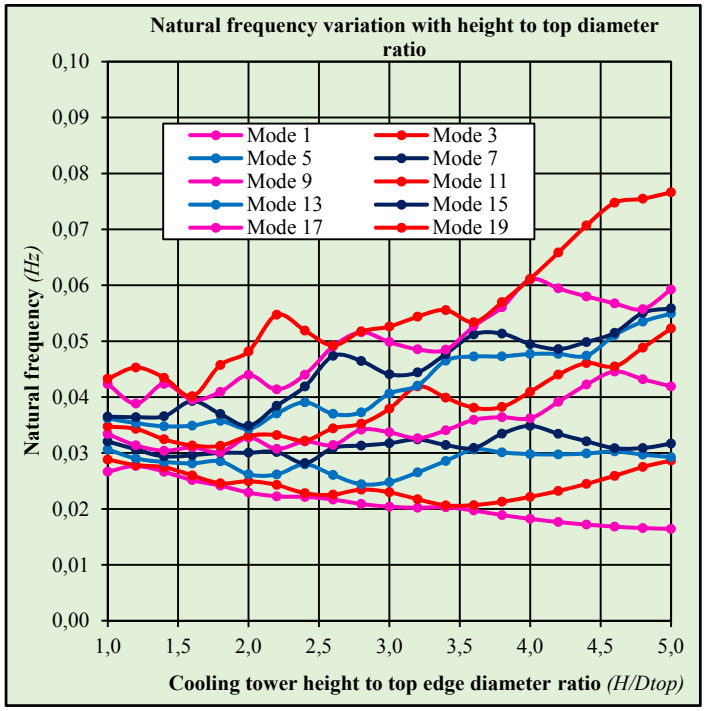

Figure 202: *Natural frequency variation with cooling tower height to top edge diameter ratio*

Observations:

From *Figure 202*, it can be observed that:

- The natural frequency reduces with increase in height to top diameter ratio for mode shapes 1 and 3. The opposite is true for mode shape 19, but the increase is jaggered. In between modes 3 and 19, the natural frequency trends are not predictable;
- The natural frequencies band width increases with increase in height to top edge diameter ratio. The dwarf cooling towers have a narrow natural frequency band width whilst the slender cooling towers have a wider natural frequency band width.

From *Table 23*, it can be observed that:

- All the mode shapes for the dwarf cooling towers are generally similar;
- The change of mode shapes for the various height to diameter ratios is in no particular order.

4.2.3 Top edge diameter to throat diameter ratio influence on free vibration behaviour

Table 24 below shows the results of the parametric study of cooling towers whose top edge diameter to throat diameter ratios were changed to observe the change in the natural frequencies for the first ten (10) different modes of vibration.

COOLING TOWER	GEOMETRICAL PARAMETERS							LINEAR EIGENVALUE VIBRATION ANALYSIS RESULTS (10 Modes)									
	Total Height	Throat Diameter	Bottom Diameter	Height/ Throat Diameter	Top Diameter/Throat	Bottom Diameter/Throat	Bottom Diameter/	**Natural Frequencies (Hz) and Mode Shapes** (for varioustop dia to throat diameter ratios and the basic pressure corresponds to a wind speed of 28m/s)									
	H	D_{thr}	D_{bot}	H/D_{thr}	D_{top}/D_{thr}	D_{bot}/D_{thr}	D_{bot}/D_{top}	*Mode Shape*									
	(m)	*(m)*	*(m)*					*1*	*3*	*5*	*7*	*9*	*11*	*13*	*15*	*17*	*19*
CT1	200	76	100	2.6	1.05	1.313	1.25	0.0167	0.0177	0.0234	0.0246	0.0252	0.0253	0.0363	0.0382	0.0387	0.0466
CT2	200	73	100	2.8	1.10	1.375	1.25	0.0188	0.0201	0.0246	0.0261	0.0264	0.0295	0.0375	0.0395	0.0430	0.0452
CT3	200	70	100	2.9	1.15	1.438	1.25	0.0206	0.0214	0.0258	0.0277	0.0291	0.0325	0.0374	0.0426	0.0443	0.0470
CT4	200	67	100	3.0	1.20	1.500	1.25	0.0222	0.0223	0.0270	0.0295	0.0317	0.0223	0.0380	0.0446	0.0463	0.0504
CT5	200	64	100	3.1	1.25	1.563	1.25	0.0230	0.0233	0.0282	0.0314	0.0330	0.0330	0.0393	0.0457	0.0494	0.0502
CT6	200	62	100	3.3	1.30	1.625	1.25	0.0238	0.0239	0.0294	0.0328	0.0328	0.0336	0.0412	0.0470	0.0499	0.0520
CT7	200	59	100	3.4	1.35	1.688	1.25	0.0242	0.0247	0.0306	0.0319	0.0328	0.0358	0.0431	0.0486	0.0495	0.0536
CT8	200	57	100	3.5	1.40	1.750	1.25	0.0242	0.0256	0.0308	0.0318	0.0330	0.0380	0.0446	0.0491	0.0503	0.0534
CT9	200	55	100	3.6	1.45	1.813	1.25	0.0242	0.0264	0.0299	0.0328	0.0335	0.0403	0.0452	0.0487	0.0521	0.0521
CT10	200	53	100	3.8	1.50	1.875	1.25	0.0241	0.0271	0.0294	0.0338	0.0341	0.0424	0.0449	0.0483	0.0513	0.0539
CT11	200	52	100	3.9	1.55	1.938	1.25	0.0239	0.0271	0.0298	0.0346	0.0349	0.0440	0.0442	0.0479	0.0512	0.0556
CT12	200	50	100	4.0	1.60	2.000	1.25	0.0238	0.0268	0.0308	0.0352	0.0358	0.0427	0.0452	0.0474	0.0520	0.0565
CT13	200	48	100	4.1	1.65	2.063	1.25	0.0237	0.0264	0.0320	0.0356	0.0368	0.0414	0.0454	0.0469	0.0537	0.0572
CT14	200	47	100	4.3	1.70	2.125	1.25	0.0235	0.0261	0.0333	0.0357	0.0378	0.0401	0.0454	0.0465	0.0560	0.0578
CT15	200	46	100	4.4	1.75	2.188	1.25	0.0234	0.0259	0.0346	0.0356	0.0388	0.0389	0.0453	0.0460	0.0568	0.0583
CT16	200	44	100	4.5	1.80	2.250	1.25	0.0233	0.0258	0.0353	0.0359	0.0377	0.0400	0.0452	0.0455	0.0555	0.0586
CT17	200	43	100	4.6	1.85	2.313	1.25	0.0231	0.0258	0.0347	0.0368	0.0372	0.0409	0.0450	0.0451	0.0544	0.0585
CT18	200	42	100	4.8	1.90	2.375	1.25	0.0230	0.0259	0.0341	0.0359	0.0384	0.0417	0.0446	0.0453	0.0535	0.0582
CT19	200	41	100	4.9	1.95	2.438	1.25	0.0228	0.0260	0.0333	0.0352	0.0396	0.0423	0.0441	0.0456	0.0527	0.0578
CT20	200	40	100	5.0	2.00	2.500	1.25	0.0226	0.0261	0.0325	0.0347	0.0407	0.0426	0.0436	0.0460	0.0522	0.0573
CT21	200	39	100	5.1	2.05	2.563	1.25	0.0238	0.0263	0.0317	0.0343	0.0415	0.0427	0.0432	0.0466	0.0520	0.0568

CONSTANT PARAMETERS:							
Throat Height/Total H	=	0.75		Height/ Bottom diameter	=	2.00	
Top Thickness	=	150	mm	Height/ Top diameter	=	2.50	
Throat Thickness	=	175	mm				

Table 24: *Parametric linear eigenvalue vibration analysis of cooling towers with variable top edge diameter to throat diameter ratios and a constant throat height to total height ratio of 0.75*

Figure 203 shows the variation of the natural frequencies with the change in cooling tower top edge diameter to throat diameter ratios and *Table 25* shows the various mode shapes (first 10 different modes) for selected cooling tower top edge diameter to throat diameter ratios.

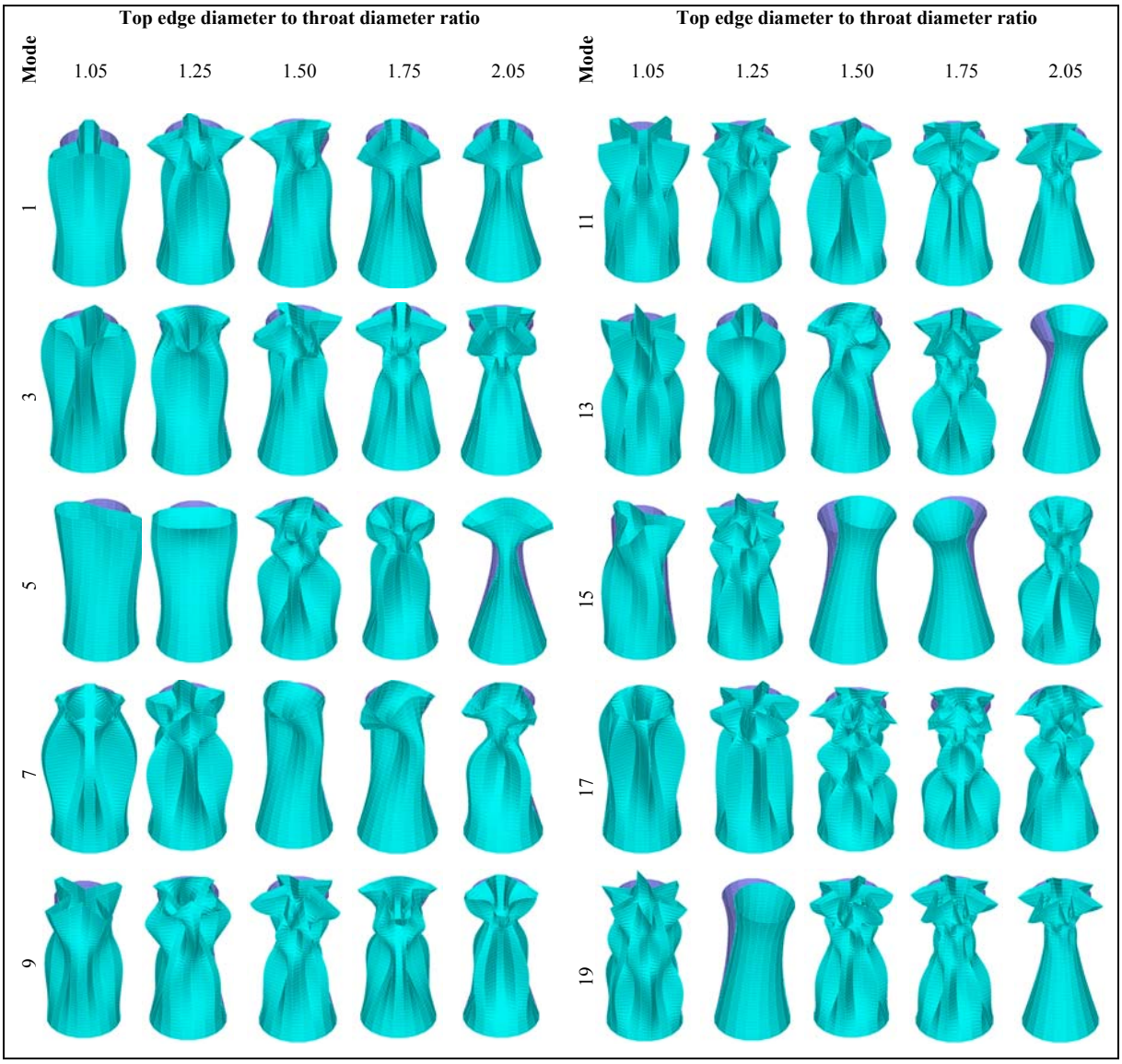

Table 25: *Vibration mode shapes for the first 10 different modes for selected cooling tower top edge diameter to throat diameter ratios*

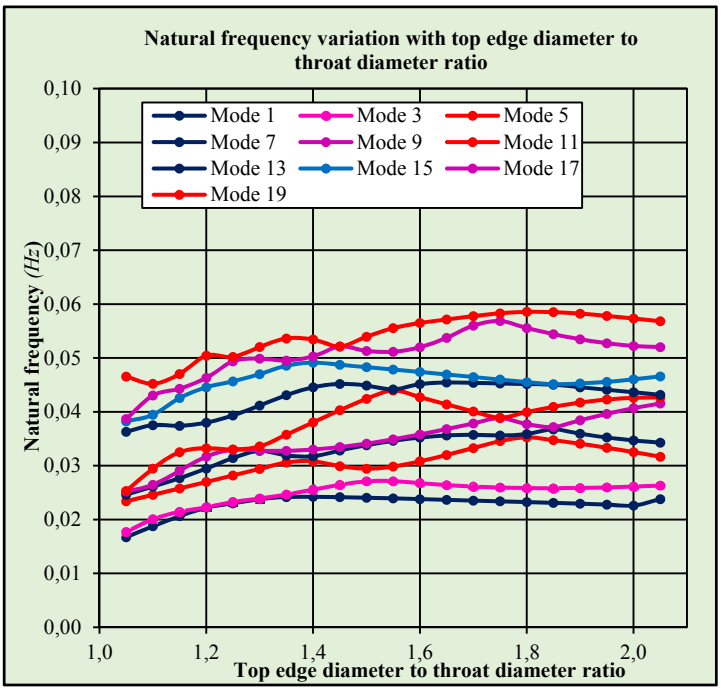

Figure 203: *Natural frequency variation with cooling tower top edge diameter to throat diameter ratio*

Observations:

From Figure 203, it can be observed that:

- The natural frequency has a marginally slight increase with increase in top edge diameter to throat diameter ratio;
- The natural frequency bandwidth is generally relatively constant with increase in the top edge diameter to throat diameter ratio;

From *Table 25*, it can be observed that:

- The order of the mode shapes changes from the lower to higher natural frequencies are different as the top edge diameter to throat diameter is changed;
- Most of the mode shapes display meridional dimpling of the shell inwards and outwards around the line of axi-symmetry.

4.2.4 Bottom edge diameter to top edge diameter ratio (top edge diameter fixed) influence on free vibration behaviour

Table 26 below shows the results of the parametric study of cooling towers whose bottom edge diameter to top edge diameter ratios were changed to observe the change in the natural frequencies for the first ten (10) different modes of vibration by changing *only the bottom edge diameter* whilst the top edge diameter, the total height, throat to total height ratio, thickness and height to diameter ratios were kept constant. By default, the bottom edge diameter to throat diameter ratio becomes variable.

COOLING TOWER	GEOMETRICAL PARAMETERS							LINEAR EIGENVALUE VIBRATION ANALYSIS RESULTS (10 Modes)									
	Total Height	Top Diameter	Bottom Diameter	Height/ Bottom Diameter	Top Diameter/ Throat Diameter	Bottom Diameter/ Throat Diameter	Bottom Diameter/ Top Diameter	**Natural Frequencies (Hz) and Mode Shapes** (for various bot to top dia ratios and the basic pressure corresponds to a wind speed of 28m/s)									
	H	D_{top}	D_{bot}	H/D_{bot}	D_{top}/D_{thr}	D_{bot}/D_{thr}	D_{bot}/D_{top}	*Mode Shape*									
	(m)	*(m)*	*(m)*					*1*	*3*	*5*	*7*	*9*	*11*	*13*	*15*	*17*	*19*
CT1	200	110	110	1.8	1.65	1.650	1.000	0.0194	0.0197	0.0247	0.0279	0.0322	0.0343	0.0391	0.0470	0.0471	0.0487
CT2	200	110	113	1.8	1.65	1.691	1.025	0.0200	0.0204	0.0248	0.0280	0.0329	0.0354	0.0391	0.0464	0.0470	0.0493
CT3	200	110	116	1.7	1.65	1.733	1.050	0.0207	0.0211	0.0249	0.0281	0.0338	0.0364	0.0391	0.0458	0.0470	0.0487
CT4	200	110	118	1.7	1.65	1.774	1.075	0.0213	0.0218	0.0250	0.0283	0.0347	0.0375	0.0391	0.0451	0.0471	0.0482
CT5	200	110	121	1.7	1.65	1.815	1.100	0.0219	0.0226	0.0251	0.0286	0.0357	0.0386	0.0391	0.0445	0.0471	0.0476
CT6	200	110	124	1.6	1.65	1.856	1.125	0.0225	0.0233	0.0251	0.0289	0.0367	0.0392	0.0396	0.0439	0.0471	0.0471
CT7	200	110	127	1.6	1.65	1.898	1.150	0.0230	0.0240	0.0252	0.0294	0.0378	0.0392	0.0406	0.0434	0.0465	0.0472
CT8	200	110	129	1.5	1.65	1.939	1.175	0.0234	0.0247	0.0253	0.0299	0.0389	0.0392	0.0416	0.0429	0.0460	0.0472
CT9	200	110	132	1.5	1.65	1.980	1.200	0.0238	0.0254	0.0254	0.0305	0.0392	0.0400	0.0424	0.0426	0.0455	0.0472
CT10	200	110	135	1.5	1.65	2.021	1.225	0.0241	0.0255	0.0260	0.0312	0.0393	0.0412	0.0419	0.0435	0.0450	0.0473
CT11	200	110	138	1.5	1.65	2.063	1.250	0.0244	0.0256	0.0267	0.0319	0.0393	0.0415	0.0424	0.0444	0.0446	0.0473
CT12	200	110	140	1.4	1.65	2.104	1.275	0.0246	0.0257	0.0274	0.0327	0.0392	0.0412	0.0435	0.0443	0.0453	0.0473
CT13	200	110	143	1.4	1.65	2.145	1.300	0.0248	0.0259	0.0280	0.0335	0.0391	0.0410	0.0435	0.0451	0.0461	0.0474
CT14	200	110	146	1.4	1.65	2.186	1.325	0.0250	0.0260	0.0286	0.0343	0.0388	0.0409	0.0431	0.0463	0.0469	0.0474
CT15	200	110	149	1.3	1.65	2.228	1.350	0.0252	0.0261	0.0293	0.0352	0.0386	0.0409	0.0427	0.0474	0.0476	0.0477
CT16	200	110	151	1.3	1.65	2.269	1.375	0.0254	0.0263	0.0299	0.0361	0.0382	0.0409	0.0423	0.0474	0.0484	0.0489
CT17	200	110	154	1.3	1.65	2.310	1.400	0.0255	0.0264	0.0309	0.0370	0.0379	0.0410	0.0418	0.0475	0.0491	0.0499
CT18	200	110	157	1.3	1.65	2.351	1.425	0.0256	0.0265	0.0310	0.0375	0.0378	0.0411	0.0414	0.0475	0.0493	0.0497
CT19	200	110	160	1.3	1.65	2.393	1.450	0.0258	0.0267	0.0316	0.0371	0.0387	0.0410	0.0413	0.0475	0.0486	0.0503
CT20	200	110	162	1.2	1.65	2.434	1.475	0.0259	0.0268	0.0321	0.0368	0.0396	0.0407	0.0415	0.0475	0.0480	0.0508
CT21	200	110	165	1.2	1.65	2.475	1.500	0.0260	0.0270	0.0326	0.0364	0.0403	0.0405	0.0416	0.0474	0.0475	0.0513
CONSTANT PARAMETERS:																	
Throat Height/Total Height ratio							=	0.75									
Top Thickness							=	150	mm								
Throat Thickness							=	175	mm								
Base Thickness							=	200	mm								
Height/Top Diameter ratio							=	1.82									

Table 26: *Parametric linear eigenvalue vibration analysis of cooling towers with variable bottom edge diameter to top edge diameter ratios*

Figure 204 shows the variation of the natural frequencies with the change in cooling tower bottom edge diameter to top edge diameter ratios and *Table 27* shows the various mode shapes (first 10 different modes) for selected cooling tower bottom edge to top edge diameter ratios.

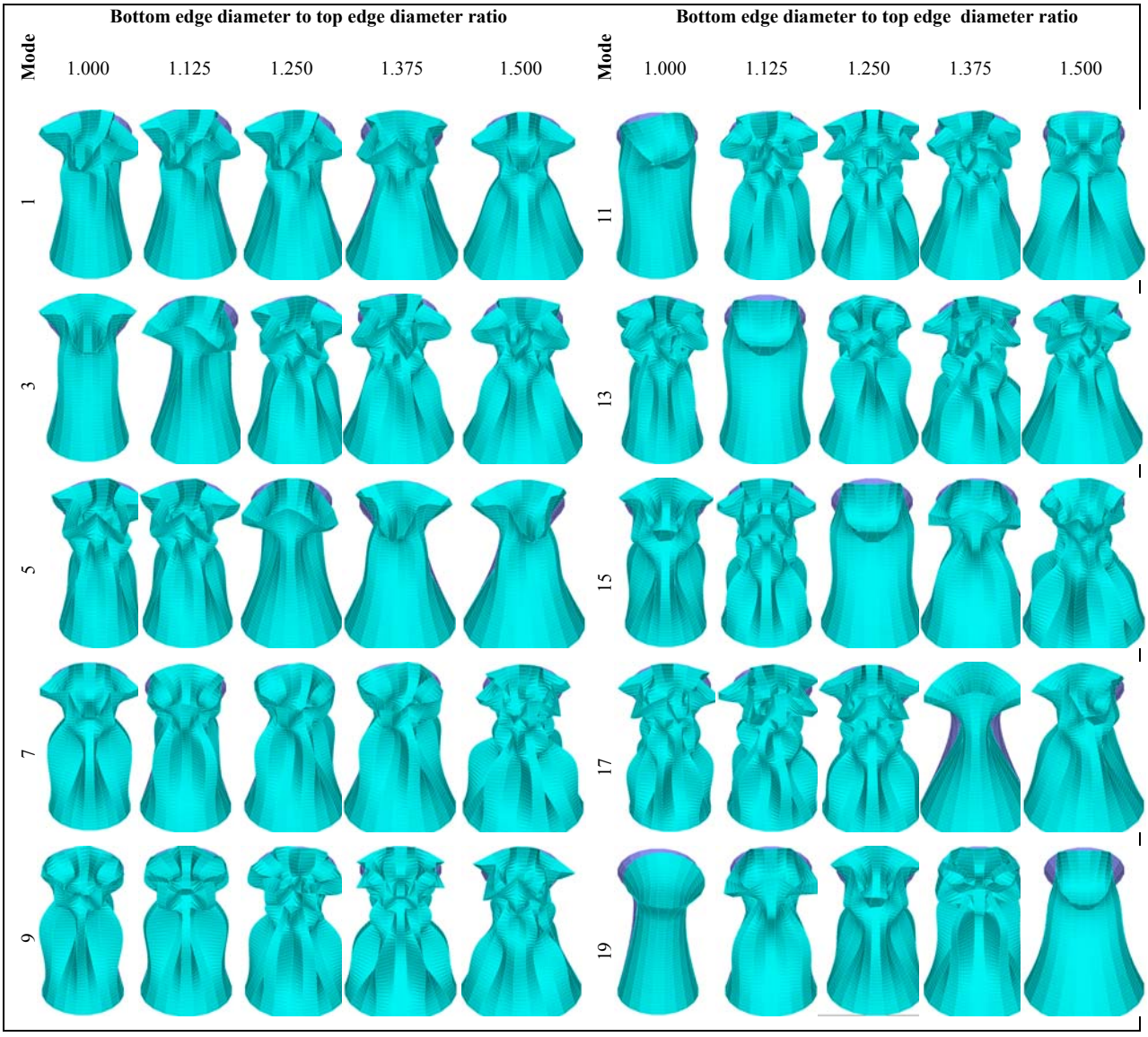

Table 27: *Vibration mode shapes for the first 10 different modes for selected cooling tower bottom edge to top edge diameter ratios*

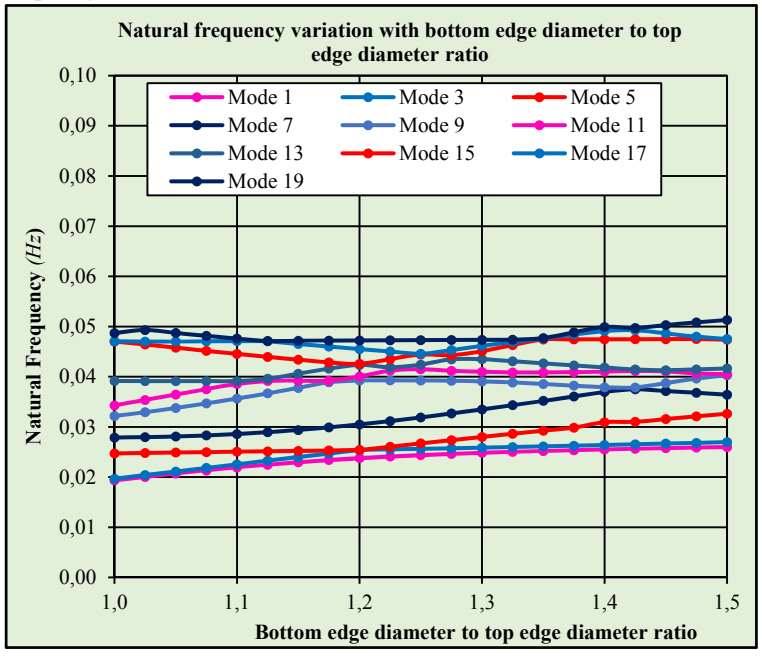

Observations:

From *Figure 204*, it can be observed that:

- The natural frequency has a marginally slight increase with increase in the bottom edge diameter to top edge diameter ratio;
- The natural frequency bandwidth is generally relatively constant with increase in the bottom edge diameter to top edge diameter.

From *Table 27*, it can be observed that:

- The order of the mode shapes changes from the lower to higher natural frequencies are different as the bottom edge diameter to top edge diameter ratio is changed;
- Most of the mode shapes display meridional dimpling of the shell inwards and outwards around the line of axi-symmetry.

Figure 204: *Natural frequency variation with cooling tower bottom edge diameter to top edge diameter ratio*

4.2.5 Shell thickness influence on free vibration behaviour

Table 28 below shows the results of the parametric study of cooling towers whose shell thickness was changed to observe the change in the natural frequencies for the first ten (10) different modes of vibration whilst the diameters, height, throat to total height ratio and height to diameter ratios were kept constant. A uniform thickness for the entire height and circumference of the shell was considered.

COOLING TOWER	GEOMETRICAL PARAMETERS						LINEAR EIGENVALUE VIBRATION ANALYSIS RESULTS (10 Modes)									
	Total Height	Throat Height/ Total Height	Top Diameter	Throat Diameter	Bottom Diameter	Thickness	**Natural Frequencies (Hz) and Mode Shapes** (for various thicknesses and the basic pressure corresponds to a wind speed of 28m/s)									
	H	H_t/H	D_{top}	D_{thr}	D_{bot}	T	*Mode Shape*									
	(m)		*(m)*	*(m)*	*(m)*	*(mm)*	*1*	*3*	*5*	*7*	*9*	*11*	*13*	*15*	*17*	*19*
CT 0.4	200	0.75	80	67	100	40	0.0158	0.0166	0.0173	0.0185	0.0200	0.0206	0.0207	0.0242	0.0252	0.0271
CT 0.6	200	0.75	80	67	100	60	0.0171	0.0172	0.0201	0.0206	0.0218	0.0220	0.0252	0.0274	0.0279	0.0317
CT 0.8	200	0.75	80	67	100	80	0.0176	0.0189	0.0202	0.0234	0.0244	0.0252	0.0262	0.0278	0.0354	0.0359
CT 1	200	0.75	80	67	100	100	0.0183	0.0204	0.0209	0.0252	0.0252	0.0283	0.0285	0.0307	0.0360	0.0426
CT 2	200	0.75	80	67	100	120	0.0192	0.0206	0.0230	0.0252	0.0274	0.0290	0.0327	0.0354	0.0361	0.0469
CT 3	200	0.75	80	67	100	140	0.0201	0.0208	0.0252	0.0253	0.0296	0.0297	0.0362	0.0370	0.0402	0.0469
CT 4	200	0.75	80	67	100	160	0.0211	0.0211	0.0252	0.0277	0.0305	0.0321	0.0363	0.0412	0.0451	0.0469
CT 5	200	0.75	80	67	100	180	0.0214	0.0222	0.0253	0.0302	0.0314	0.0346	0.0365	0.0454	0.0469	0.0500
CT 6	200	0.75	80	67	100	200	0.0217	0.0234	0.0253	0.0324	0.0327	0.0366	0.0372	0.0469	0.0494	0.0545
CT 7	200	0.75	80	67	100	220	0.0221	0.0246	0.0253	0.0335	0.0352	0.0368	0.0399	0.0469	0.0535	0.0552
CT 8	200	0.75	80	67	100	240	0.0224	0.0254	0.0258	0.0346	0.0370	0.0378	0.0426	0.0469	0.0556	0.0574
CT 9	200	0.75	80	67	100	260	0.0228	0.0254	0.0271	0.0358	0.0372	0.0403	0.0454	0.0469	0.0561	0.0602
CT 10	200	0.75	80	67	100	280	0.0233	0.0255	0.0284	0.0370	0.0374	0.0429	0.0469	0.0482	0.0567	0.0623
CT 11	200	0.75	80	67	100	300	0.0237	0.0255	0.0297	0.0377	0.0383	0.0454	0.0469	0.0509	0.0573	0.0646
CT 12	200	0.75	80	67	100	320	0.0242	0.0255	0.0311	0.0379	0.0396	0.0469	0.0479	0.0537	0.0579	0.0648
CT 13	200	0.75	80	67	100	340	0.0247	0.0256	0.0325	0.0382	0.0410	0.0469	0.0504	0.0565	0.0585	0.0648
CT 14	200	0.75	80	67	100	360	0.0252	0.0256	0.0338	0.0385	0.0424	0.0469	0.0529	0.0592	0.0593	0.0649
CT 15	200	0.75	80	67	100	380	0.0257	0.0258	0.0352	0.0387	0.0439	0.0469	0.0553	0.0599	0.0621	0.0649
CT 16	200	0.75	80	67	100	400	0.0258	0.0263	0.0366	0.0391	0.0454	0.0469	0.0578	0.0606	0.0649	0.0649
CT 17	200	0.75	80	67	100	420	0.0258	0.0269	0.0380	0.0394	0.0469	0.0469	0.0602	0.0614	0.0649	0.0677
CT 18	200	0.75	80	67	100	440	0.0259	0.0275	0.0395	0.0397	0.0469	0.0484	0.0622	0.0625	0.0650	0.0705
CT 19	200	0.75	80	67	100	460	0.0259	0.0281	0.0401	0.0409	0.0469	0.0500	0.0630	0.0649	0.0650	0.0732
CT 20	200	0.75	80	67	100	480	0.0260	0.0287	0.0404	0.0423	0.0469	0.0516	0.0638	0.0650	0.0672	0.0760
CT 21	200	0.75	80	67	100	500	0.0261	0.0293	0.0408	0.0437	0.0469	0.0532	0.0647	0.0651	0.0696	0.0787
CONSTANT PARAMETERS:																
Throat Height/Total Height ratio							=	0.75								
Height/Top Diameter							=	2.50								
Height/Throat Diameter							=	3.00								
Height/Bottom Diameter							=	2.00								
Top Diameter/Throat Diameter							=	1.20								
Bottom Diameter/Throat Diameter							=	1.50								
Bottom Diameter/Top Diameter							=	1.25								

Table 28: *Parametric linear eigenvalue vibration analysis of cooling towers with variable shell thickness*

Figure 205 shows the variation of the natural frequencies with the change in cooling tower shell thickness and *Table 29* shows the various mode shapes (first 10 different modes) for selected cooling tower shell thicknesses.

Table 29: *Vibration mode shapes for the first 10 different modes for selected cooling tower shell thickness*

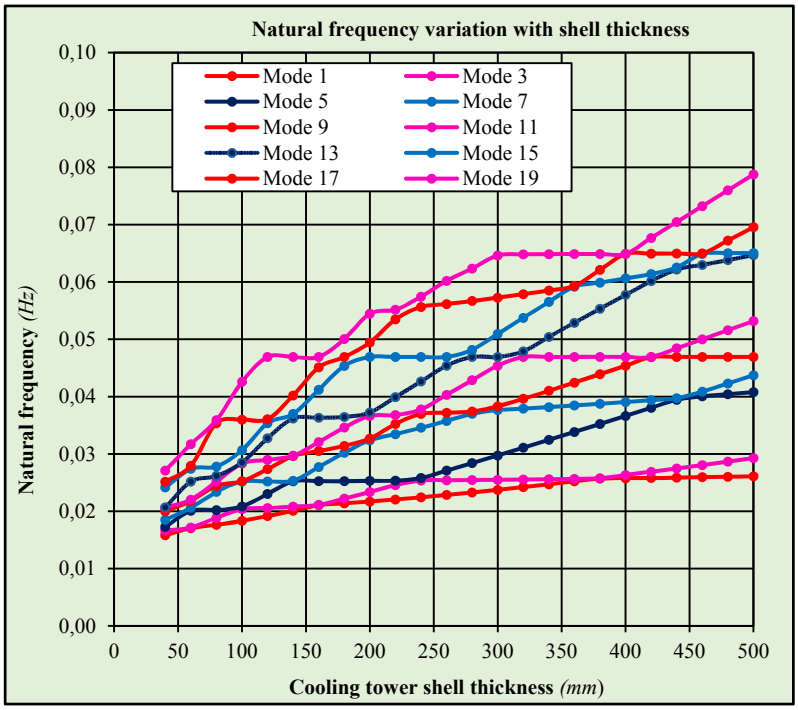

Figure 205: *Natural frequency variation with cooling tower shell thickness*

Observations:

From *Figure 205*, it can be observed that:

- The natural frequency increases non-linearly with increase in the shell thickness;
- The natural frequency bandwidth increases as the shell thickness increases. The natural frequency band width for the first 10 different modes of vibration for a 40mm thick cooling tower is smaller at (0.0113Hz) compared to that of a 500mm thick cooling tower which is at 0.0527Hz (more than 350% increase);

From *Table 29*, it can be observed that:

- The order of the mode shapes changes from the lower to higher natural frequencies are different as the shell thickness is changed;
- Most of the mode shapes display meridional dimpling of the shell inwards and outwards around the line of axi-symmetry.

4.3 ON FORCED VIBRATION BEHAVIOUR UNDER UNSYMMETRICAL WIND LOADING

The parametric study results for various geometrical parameters are included in the following sections. In each section, a summary of the response frequencies is indicated in a table for various cooling towers whose geometry is changed systematically in order to study the change in the forced vibration behaviour of the cooling tower. Followed by this is a series of graphs plotted to describe this behaviour. In addition, the ratio of the response frequency to the forcing frequency is computed and plotted to give a better comparison. The forcing frequencies are based on the applied wind gusts of 2s, 5s, 10, 20s and 30s.

The first ten (10) different modes of vibration are analysed. Due to the axi-symmetry of the cooling tower shell geometry, it is observed that the even and odd numbered modes of vibration have the same response frequencies and similar mode shapes but in different orthogonal directions. That is, mode 1 and mode 2 have the same response frequencies and mode shapes but in different directions along the X and X plane directions. Therefore, the modes presented in this study are the Odd numbered modes: *1, 3, 5,…, 17 and 19* which are of course the same as the *2, 4, 6, …, 18 and 20 modes*.

For each parametric study, the particular geometrical parameter (e.g. height) is changed systematically for at least twenty (20) cooling towers whilst keeping the rest of the other geometrical parameters (e.g. thickness, diameters etc.) constant in order to study the influence of a single parameter on the forced vibration behaviour of the cooling tower. The constant parameters are included at the bottom of each table of results. In order to cover a wider range of geometrical parameters, the study was tailored to investigate ratios of the geometrical parameters instead of looking into just the actual parameters.

The following parameters were investigated:

- *Height* of the cooling tower;
- *Height to top edge diameter* ratio (H/D_{top});
- *Top edge diameter to throat diameter* ratio (D_{top}/D_{thr});
- *Bottom edge diameter to top edge diameter* ratio (D_{bot}/D_{top});
- *Shell thickness* of the cooling tower.

4.3.1 Height influence on forced vibration behaviour

Table 30 below shows the results of the parametric study of cooling towers whose height was changed from 60m to 250m whilst maintaining the throat height to total height ratio (0.75) in order to observe the change in the response frequencies for the first ten (10) different modes of vibration when subjected to 2s-, 5s-, 10s-, 20s-, and 30s-wind gust.

COOLING TOWER	GEOMETRICAL PARAMETERS					FORCED RESPONSE									
	Total Height	Throat Height/ Total Height	Top Diameter	Throat Diameter	Bottom Diameter	Forced Frequency (Hz)					Response frequency to Forcing frequency ratio (f_r/f_f)				
	H		D_{top}	D_{thr}	D_{bot}	*Wind Gust Period (s)*					*Forcing frequency (Hz)*				
	(m)		*(m)*	*(m)*	*(m)*	*2*	*5*	*10*	*20*	*30*	*0.5*	*0.2*	*0.1*	*0.05*	*0.033*
CT1	60	0.75	24	20	30	0.0820	0.0750	0.0620	0.0470	0.0440	0.164	0.375	0.620	0.940	1.320
CT2	70	0.75	28	23	35	0.0800	0.0720	0.0560	0.0430	0.0377	0.160	0.360	0.560	0.860	1.131
CT3	80	0.75	32	27	40	0.0620	0.0560	0.0510	0.0400	0.0345	0.124	0.280	0.510	0.800	1.035
CT4	90	0.75	36	30	45	0.0548	0.0513	0.0465	0.0377	0.0315	0.110	0.257	0.465	0.754	0.945
CT5	100	0.75	40	33	50	0.0500	0.0465	0.0430	0.0339	0.0299	0.100	0.233	0.430	0.678	0.897
CT6	110	0.75	44	37	55	0.0460	0.0430	0.0396	0.0360	0.0282	0.092	0.215	0.396	0.721	0.845
CT7	120	0.75	48	40	60	0.0426	0.0400	0.0370	0.0328	0.0272	0.085	0.200	0.370	0.656	0.816
CT8	130	0.75	52	43	65	0.0400	0.0377	0.0348	0.0305	0.0261	0.080	0.189	0.348	0.611	0.783
CT9	140	0.75	56	47	70	0.0377	0.0357	0.0328	0.0290	0.0255	0.075	0.179	0.328	0.580	0.764
CT10	150	0.75	60	50	75	0.0351	0.0339	0.0313	0.0276	0.0253	0.070	0.169	0.313	0.552	0.760
CT11	160	0.75	64	53	80	0.0339	0.0323	0.0296	0.0261	0.0252	0.068	0.161	0.296	0.523	0.755
CT12	170	0.75	68	57	85	0.0318	0.0303	0.0282	0.0250	0.0206	0.064	0.152	0.282	0.500	0.619
CT13	180	0.75	72	60	90	0.0299	0.0290	0.0270	0.0241	0.0213	0.060	0.145	0.270	0.482	0.638
CT14	190	0.75	76	63	95	0.0286	0.0274	0.0256	0.0231	0.0208	0.057	0.137	0.256	0.462	0.625
CT15	200	0.75	80	67	100	0.0270	0.0261	0.0247	0.0222	0.0202	0.054	0.131	0.247	0.444	0.606
CT16	210	0.75	84	70	105	0.0258	0.0250	0.0235	0.0214	0.0196	0.052	0.125	0.235	0.428	0.588
CT17	220	0.75	88	73	110	0.0247	0.0238	0.0227	0.0206	0.0189	0.049	0.119	0.227	0.412	0.566
CT18	230	0.75	92	77	115	0.0235	0.0229	0.0217	0.0199	0.0183	0.047	0.114	0.217	0.398	0.550
CT19	240	0.75	96	80	120	0.0226	0.0220	0.0209	0.0192	0.0178	0.045	0.110	0.209	0.385	0.533
CT20	250	0.75	100	83	125	0.0225	0.0219	0.0207	0.0187	0.0169	0.045	0.109	0.207	0.374	0.506

CONSTANT PARAMETERS:							
Top Thickness	=	150	mm	Height/Bottom Diameter ratio	=	2.0	
Throat Thickness	=	175	mm	Top Diameter/Throat Diameter ratio	=	1.2	
Base Thickness	=	200	mm	Bottom Diameter/Throat Diameter ratio	=	1.5	
Height/Top Diameter ratio	=	2.5		Bottom Diameter/Top Diameter ratio	=	1.3	
Height/Throat Diameter rati	=	3.0					

Table 30: *Parametric forced vibration analysis of cooling towers with variable heights*

Figure 206 shows the variation of the response frequencies with the change in cooling tower height when subjected to 2s-, 5s-, 10s-, 20s-, and 30s-wind gusts of the same speed. The response frequency versus forcing period is also plotted to obtain a relationship between the response and the forcing frequencies for each cooling tower height. Finally, response frequency to forcing frequency ratio (f_r/f_f) is plotted against the cooling tower height to give a more representative behaviour of the response frequency compared to the forcing frequency for the height spectrum considered.

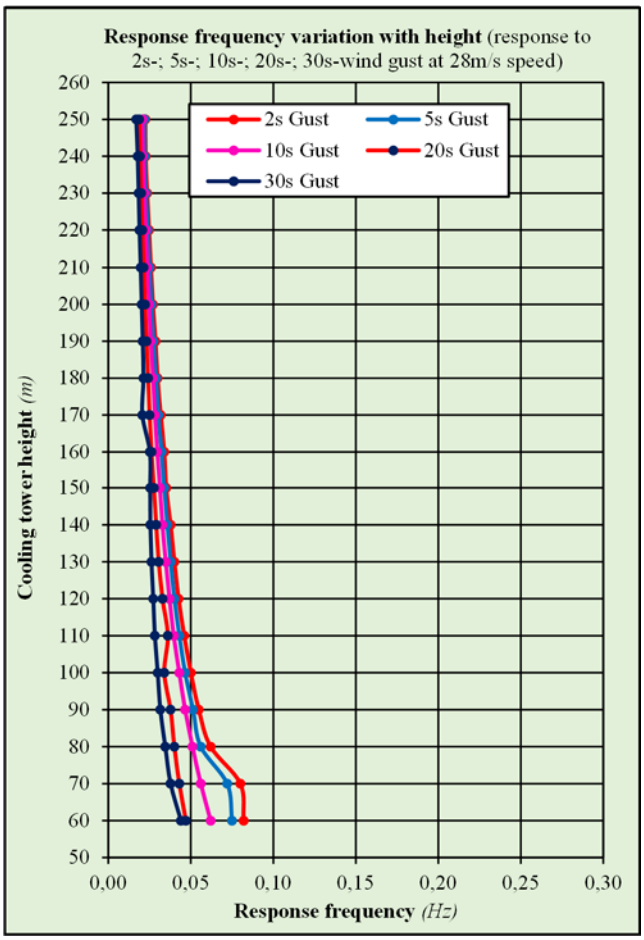

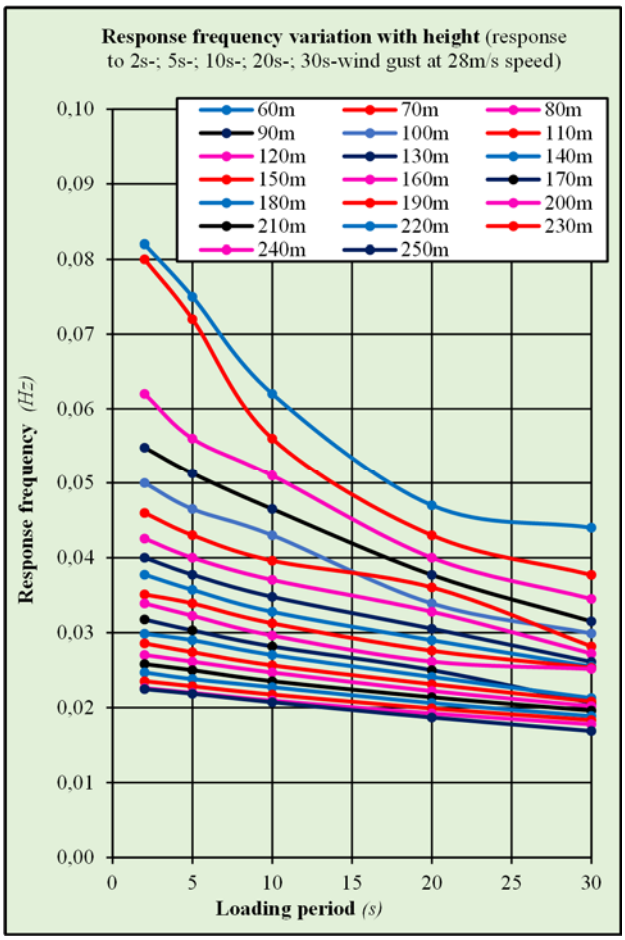

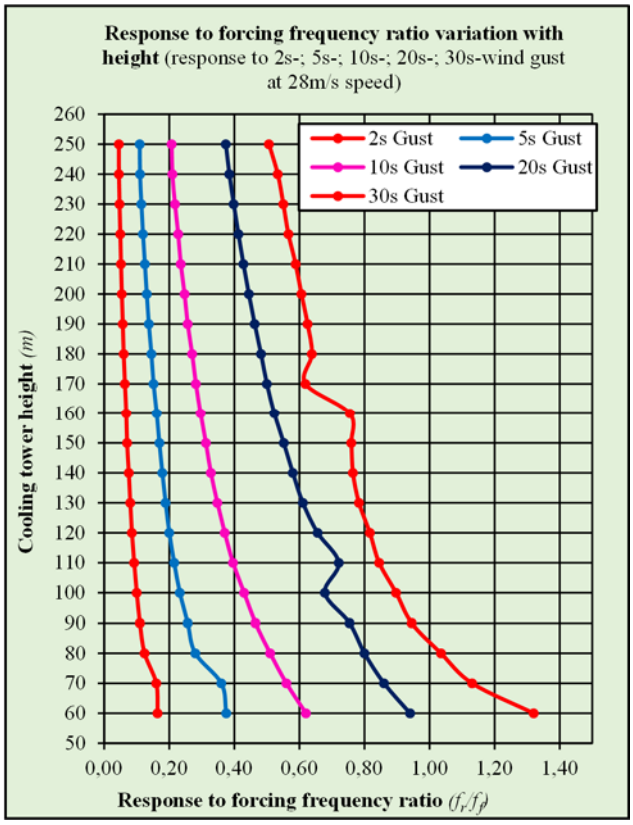

Figure 206: *Response frequency variation with height and loading period combined with response to forcing frequency ratio variation with cooling tower height*

Observations:

From *Figure 206*, it can be observed that:

- The response frequency reduces non-linearly with increase in height for all the loading frequencies;
- The response frequency bandwidth reduces as the height increases. The response frequency bandwidth for all the loading frequencies of 2s through to 30s wind gust for a 60m high cooling tower is greater at (0.038Hz) compared to that of a 250m high cooling tower which is at 0.0056Hz;
- The response frequency is higher when the loading frequency is higher (2s-gust) and lower when the loading frequency is lower (30s-gust);
- The response frequency generally reduces with reduction in loading frequency. This reduction is non-linear for dwarf cooling towers and changes to linear for slender cooling towers. The change in behaviour happens at a cooling tower height of about 170m;
- The response frequency bandwidth is wider for higher forcing frequencies and narrower for lower forcing frequencies;
- The response frequency to forcing frequency ratio for the entire loading frequency from 2s to 30s gusts generally decreases with increasing cooling tower height. For higher cooling towers, the range of this ratio is smaller compared to that of shorter cooling towers.

4.3.2 Height to diameter ratio influence on forced vibration behaviour

Table 31 below shows the results of the parametric study of cooling towers whose height to diameter ratios were changed to observe the change in the response frequencies for the first ten (10) different modes of vibration when subjected to 2s-, 5s-, 10s-, 20s-, and 30s-wind gust whilst the total height, throat height to total height ratio, thickness and diameter ratios were kept constant.

COOLING TOWER	GEOMETRICAL PARAMETERS							FORCED RESPONSE									
	Total Height	Top Diameter	Throat Diameter	Bottom Diameter	Height/ Top Diameter	Height/ Throat Diameter	Height/ Bottom Diameter	**Forced Frequency** (for various height to diameter ratios)					**Response frequency to Forcing frequency ratio** (f_r/f_f)				
	H	D_{top}	D_{thr}	D_{bot}	H/D_{top}	H/D_{thr}	H/D_{bot}	*Wind Gust Period (s)*					*Forcing frequency (Hz)*				
	(m)	*(m)*	*(m)*	*(m)*				*2*	*5*	*10*	*20*	*30*	*0.5*	*0.2*	*0.1*	*0.05*	*0.03*
CT1	200	200	167	250	1.0	1.2	0.8	0.0408	0.0388	0.0354	0.0310	0.0357	0.082	0.194	0.354	0.620	1.071
CT2	200	167	139	208	1.2	1.4	1.0	0.0377	0.0357	0.0330	0.0293	0.0333	0.075	0.179	0.330	0.585	1.000
CT3	200	143	119	179	1.4	1.7	1.1	0.0440	0.0412	0.0377	0.0351	0.0417	0.088	0.206	0.377	0.702	1.250
CT4	200	125	104	156	1.6	1.9	1.3	0.0392	0.0370	0.0339	0.0303	0.0357	0.078	0.185	0.339	0.606	1.071
CT5	200	111	93	139	1.8	2.2	1.4	0.0357	0.0341	0.0315	0.0278	0.0325	0.071	0.171	0.315	0.556	0.976
CT6	200	100	83	125	2.0	2.4	1.6	0.0334	0.0320	0.0296	0.0260	0.0313	0.067	0.160	0.296	0.519	0.938
CT7	200	91	76	114	2.2	2.6	1.8	0.0320	0.0296	0.0278	0.0244	0.0227	0.064	0.148	0.278	0.488	0.682
CT8	200	83	69	104	2.4	2.9	1.9	0.0280	0.0270	0.0255	0.0231	0.0213	0.056	0.135	0.255	0.462	0.638
CT9	200	77	64	96	2.6	3.1	2.1	0.0263	0.0253	0.0237	0.0211	0.0189	0.053	0.127	0.237	0.421	0.566
CT10	200	71	60	89	2.8	3.4	2.2	0.0244	0.0233	0.0216	0.0194	0.0180	0.049	0.116	0.216	0.388	0.541
CT11	200	67	56	83	3.0	3.6	2.4	0.0222	0.0215	0.0204	0.0187	0.0175	0.044	0.108	0.204	0.374	0.526
CT12	200	63	52	78	3.2	3.8	2.6	0.0211	0.0203	0.0195	0.0179	0.0168	0.042	0.102	0.195	0.357	0.504
CT13	200	59	49	74	3.4	4.1	2.7	0.0203	0.0198	0.0189	0.0172	0.0158	0.041	0.099	0.189	0.343	0.474
CT14	200	56	46	69	3.6	4.3	2.9	0.0194	0.0190	0.0179	0.0171	0.0160	0.039	0.095	0.179	0.342	0.480
CT15	200	53	44	66	3.8	4.6	3.0	0.0182	0.0177	0.0175	0.0172	0.0163	0.036	0.088	0.175	0.343	0.488
CT16	200	50	42	63	4.0	4.8	3.2	0.0178	0.0175	0.0175	0.0171	0.0163	0.036	0.088	0.175	0.342	0.490
CT17	200	48	40	60	4.2	5.0	3.4	0.0174	0.0174	0.0177	0.0175	0.0164	0.035	0.087	0.177	0.351	0.492
CT18	200	45	38	57	4.4	5.3	3.5	0.0168	0.0168	0.0179	0.0181	0.0168	0.034	0.084	0.179	0.362	0.504
CT19	200	43	36	54	4.6	5.5	3.7	0.0168	0.0172	0.0182	0.0188	0.0169	0.034	0.086	0.182	0.376	0.508
CT20	200	42	35	52	4.8	5.8	3.8	0.0167	0.0173	0.0190	0.0192	0.0171	0.033	0.087	0.190	0.385	0.513
CT21	200	40	33	50	5.0	6.0	4.0	0.0167	0.0175	0.0200	0.0196	0.0172	0.033	0.087	0.200	0.392	0.517

Throat Height/Total Height ratio	=	0.75		Top Diameter/Throat Diameter ratio	=	1.200
Top Thickness	=	150	mm	Bottom Diameter/Throat Diameter ratio	=	1.500
Throat Thickness	=	175	mm	Bottom Diameter/Top Diameter ratio	=	1.250
Base Thickness	=	200	mm			

Table 31: *Parametric forced vibration analysis of cooling towers with height to diameter ratios*

Figure 207 shows the variation of the response frequencies with the change in cooling tower height to diameter ratios when subjected to 2s-, 5s-, 10s-, 20s-, and 30s-wind gusts of the same speed. The response frequency versus forcing period is also plotted to obtain a relationship between the response and the forcing frequencies for each cooling tower height to diameter ratio. Finally, response frequency to forcing frequency ratio *(f_r/f_f)* is plotted against the cooling tower height to diameter ratio to give a more representative behaviour of the response frequency compared to the forcing frequency for the height to diameter ratio spectrum considered.

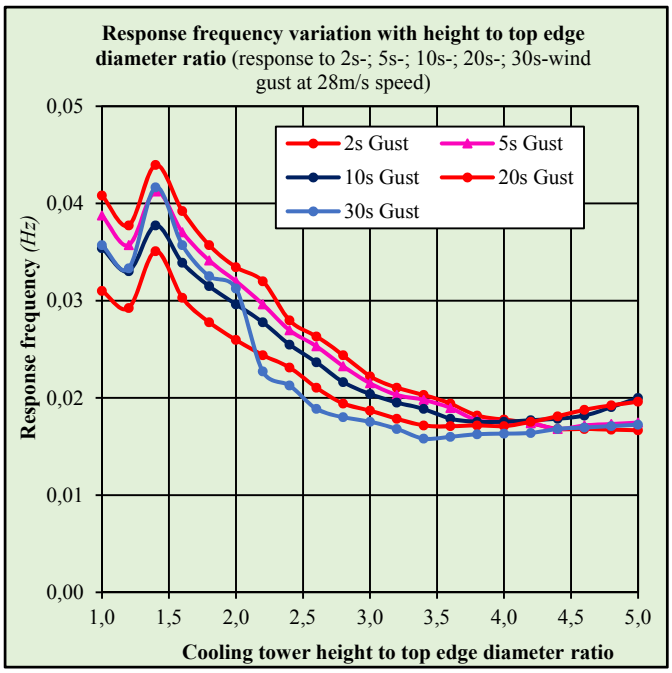

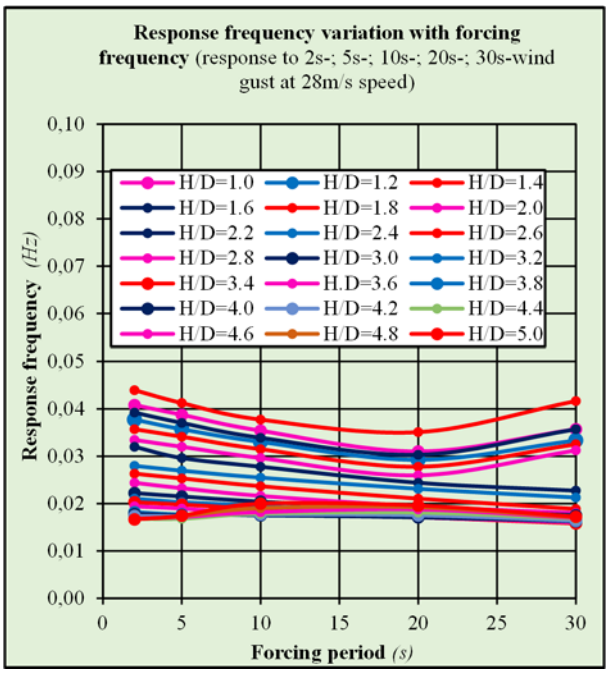

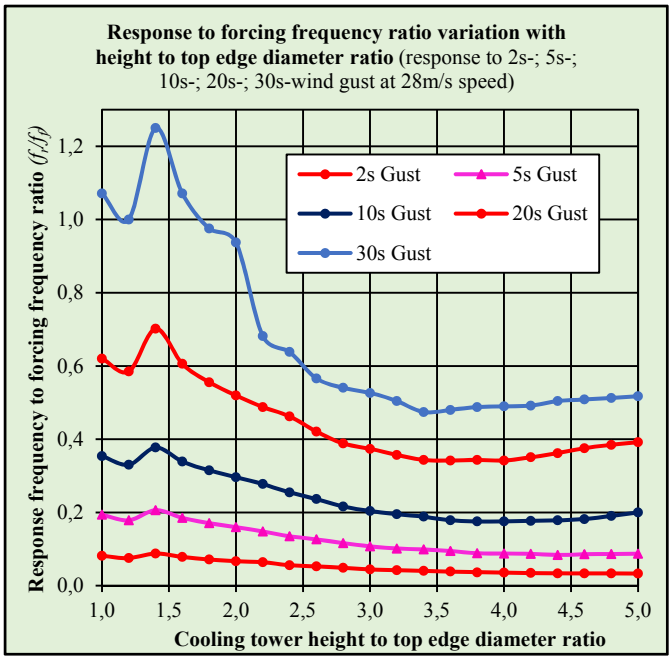

Figure 207: *Response frequency variation with height to diameter ratio and loading period combined with response to forcing frequency ratio variation with cooling tower height to diameter ratio*

Observations:

From *Figure 207*, it can be observed that:

- The response frequencies to the loading frequencies generally decrease with increasing height to diameter ratio. The slender cooling towers have lower response frequencies;
- The response frequency bandwidth generally reduces with increasing height to diameter ratio up to a height to top edge diameter ratio of about 4.0. Thereafter, it starts to increase again;
- For dwarf cooling towers with height to top edge diameter ratios of 1.0 to 2.0, there appears a minimum response frequency for all loading periods within the range of 2s to 30s. The minimum response frequency corresponds to a loading period of about 20s;
- For middle cooling towers with height to top edge diameter ratios of 2.0 to 4.0, the relationship between the response frequency and the loading frequency is generally linear. The response frequency reduces with reducing loading frequency;
- For slender cooling towers with height to top edge diameter ratios of 4.0 to 5.0, there appears a maximum response frequency for all loading periods within the range of 2s to 30s. The maximum response frequency corresponds to a loading period of about 20s;
- The response frequency to forcing frequency ratio generally decreases with increasing height to diameter ratio from a height to top edge diameter ratio of 1.0 to about 3.5. Thereafter the frequency ratio appears to be constant;
- The variation of response frequency to forcing frequency ratio with the height to top edge diameter ratio for the 2s and 5s gust is generally gentle whereas that for the 10s, 20s and 30s gusts is more rapid/steep for height to top edge diameter ratio of 1.0 to about 3.5.

4.3.3 Top edge diameter to throat diameter ratio influence on forced vibration behaviour

Table 32 below shows the results of the parametric study of cooling towers whose top edge diameter to throat diameter ratios were changed to observe the change in the response frequencies for the first ten (10) different modes of vibration when subjected to 2s-, 5s-, 10s-, 20s-, and 30s-wind gust whilst the total height, throat to total height ratio, thickness and height to diameter ratios were kept constant.

COOLING TOWER	GEOMETRICAL PARAMETERS								FORCED RESPONSE									
	Total Height	Top Diameter	Throat Diameter	Bottom Diameter	Height/ Throat Diameter	Top Diameter/Throat	Bottom Diameter/Throat	Bottom Diameter/ Top Diameter	**Forced Frequency** (for various top dia to throat dia ratios and forcing wind periods)					**Response frequency to Forcing frequency ratio** (f_r/f_f)				
	H	D_{top}	D_{thr}	D_{bot}	H/D_{thr}	D_{top}/D_{thr}	D_{bot}/D_{thr}	D_{bot}/D_{top}	*Wind Gust Period (s)*					*Forcing frequency (Hz)*				
	(m)	*(m)*	*(m)*	*(m)*					*2*	*5*	*10*	*20*	*30*	*0.5*	*0.2*	*0.1*	*0.05*	*0.03*
CT1	200	80	76	100	2.6	1.05	1.313	1.25	0.0199	0.0196	0.0196	0.0187	0.0164	0.040	0.098	0.196	0.374	0.492
CT2	200	80	73	100	2.8	1.10	1.375	1.25	0.0222	0.0220	0.0211	0.0194	0.0168	0.044	0.110	0.211	0.388	0.504
CT3	200	80	70	100	2.9	1.15	1.438	1.25	0.0247	0.0244	0.0227	0.0202	0.0175	0.049	0.122	0.227	0.404	0.526
CT4	200	80	67	100	3.0	1.20	1.500	1.25	0.0267	0.0260	0.0244	0.0219	0.0200	0.053	0.130	0.244	0.439	0.600
CT5	200	80	64	100	3.1	1.25	1.563	1.25	0.0328	0.0317	0.0294	0.0253	0.0222	0.066	0.159	0.294	0.506	0.667
CT6	200	80	62	100	3.3	1.30	1.625	1.25	0.0377	0.0370	0.0339	0.0294	0.0250	0.075	0.185	0.339	0.588	0.750
CT7	200	80	59	100	3.4	1.35	1.688	1.25	0.0213	0.0208	0.0202	0.0190	0.0172	0.043	0.104	0.202	0.381	0.517
CT8	200	80	57	100	3.5	1.40	1.750	1.25	0.0219	0.0215	0.0208	0.0192	0.0174	0.044	0.108	0.208	0.385	0.522
CT9	200	80	55	100	3.6	1.45	1.813	1.25	0.0233	0.0230	0.0220	0.0196	0.0173	0.047	0.115	0.220	0.392	0.519
CT10	200	80	53	100	3.8	1.50	1.875	1.25	0.0256	0.0253	0.0235	0.0198	0.0171	0.051	0.127	0.235	0.396	0.513
CT11	200	80	52	100	3.9	1.55	1.938	1.25	0.0270	0.0263	0.0244	0.0202	0.0168	0.054	0.132	0.244	0.404	0.504
CT12	200	80	50	100	4.0	1.60	2.000	1.25	0.0274	0.0267	0.0247	0.0208	0.0253	0.055	0.133	0.247	0.417	0.759
CT13	200	80	48	100	4.1	1.65	2.063	1.25	0.0278	0.0270	0.0250	0.0215	0.0256	0.056	0.135	0.250	0.430	0.769
CT14	200	80	47	100	4.3	1.70	2.125	1.25	0.0282	0.0274	0.0253	0.0220	0.0260	0.056	0.137	0.253	0.440	0.779
CT15	200	80	46	100	4.4	1.75	2.188	1.25	0.0444	0.0426	0.0377	0.0339	0.0345	0.089	0.213	0.377	0.678	1.034
CT16	200	80	44	100	4.5	1.80	2.250	1.25	0.0435	0.0417	0.0377	0.0345	0.0385	0.087	0.208	0.377	0.690	1.154
CT17	200	80	43	100	4.6	1.85	2.313	1.25	0.0417	0.0400	0.0357	0.0182	0.0187	0.083	0.200	0.357	0.364	0.561
CT18	200	80	42	100	4.8	1.90	2.375	1.25	0.0213	0.0208	0.0196	0.0182	0.0175	0.043	0.104	0.196	0.364	0.526
CT19	200	80	41	100	4.9	1.95	2.438	1.25	0.0211	0.0206	0.0196	0.0182	0.0171	0.042	0.103	0.196	0.364	0.513
CT20	200	80	40	100	5.0	2.00	2.500	1.25	0.0208	0.0204	0.0194	0.0182	0.0169	0.042	0.102	0.194	0.364	0.508
CT21	200	80	39	100	5.1	2.05	2.563	1.25	0.0206	0.0200	0.0192	0.0182	0.0169	0.041	0.100	0.192	0.364	0.508

CONSTANT PARAMETERS:						
Throat Height/Total Height	=	0.75		Height/ Bottom diameter	=	2.00
Top Thickness	=	150	mm	Height/ Top diameter	=	2.50
Throat Thickness	=	175	mm			
Base Thickness	=	200	mm			

Table 32: *Parametric forced vibration analysis of cooling towers with top edge diameter to throat diameter ratios*

Figure 208 shows the variation of the response frequencies with the change in cooling tower top edge diameter to throat diameter ratios when subjected to 2s-, 5s-, 10s-, 20s-, and 30s-wind gusts of the same speed. The response frequency versus forcing period is also plotted to obtain a relationship between the response and the forcing frequencies for each cooling tower top edge diameter to throat diameter ratio. Finally, response frequency to forcing frequency ratio *(f_r/f_f)* is plotted against the cooling tower top edge diameter to throat diameter ratio to give a more representative behaviour of the response frequency compared to the forcing frequency for the top edge diameter to throat diameter ratio spectrum considered.

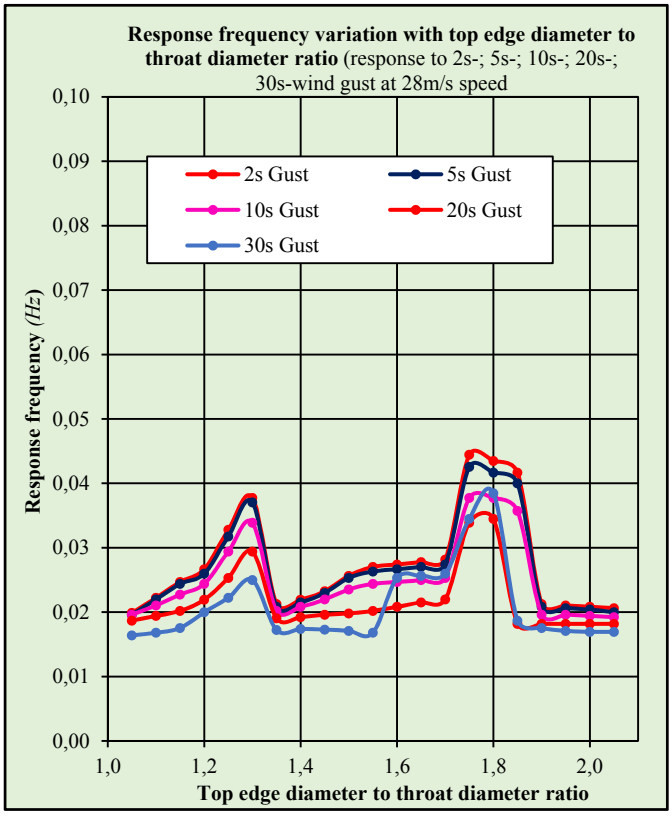

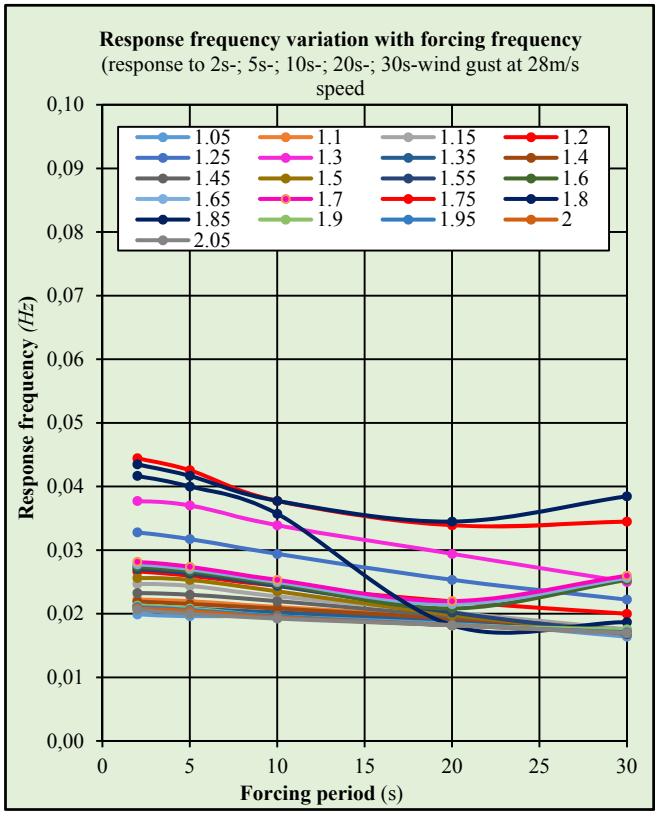

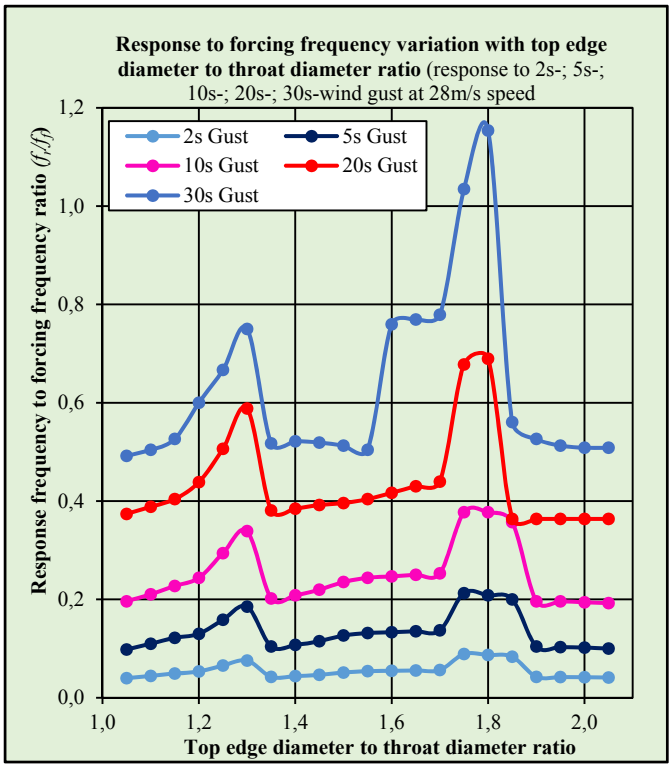

Figure 208: *Response frequency variation with top edge diameter to throat diameter ratio and loading period combined with response to forcing frequency ratio variation with cooling tower top edge diameter to throat diameter ratio*

Observations:

From *Figure 208*, it can be observed that:

- The response frequency is generally constant as the top edge diameter to throat diameter is increased except for two regions where it peaks to about double the generally constant response frequency. These two regions are for top edge diameter to throat diameter ratios of between 1.2 to 1.4 and 1.7 to 1.9;
- The response frequency bandwidth is generally relatively constant with increase in the top edge diameter to throat diameter ratio;
- The response frequency variation with the forcing frequency for various top edge diameter to throat diameter ratios is different. However, in global terms it is generally constant with the forcing frequency;
- The response frequency to forcing frequency ratio is generally constant as the top edge diameter to throat diameter is increased except for two regions where it peaks to about double the generally constant response frequency. These two regions are for top edge diameter to throat diameter ratios between 1.2 to 1.4 and 1.7 to 1.9.

4.3.4 Bottom edge diameter to top edge diameter ratio (top edge diameter fixed) influence on forced vibration behaviour

Table 33 below shows the results of the parametric study of cooling towers whose bottom edge diameter to top edge diameter ratios were changed to observe the change in the response frequencies for the first ten (10) different modes of vibration when subjected to 2s-, 5s-, 10s-, 20s-, and 30s-wind gusts by changing *only the bottom edge diameter* whilst the top edge diameter, the total height, throat to total height ratio, thickness and height to diameter ratios were kept constant. By default, the bottom edge diameter to throat diameter ratio becomes variable.

COOLING TOWER	GEOMETRICAL PARAMETERS							FORCED RESPONSE									
	Total Height	Top Diameter	Bottom Diameter	Height/ Bottom Diameter	Top Diameter/ Throat Diameter	Bottom Diameter/	Bottom Diameter/	**Forced Frequency** (for various bot to top dia ratios and forcing wind periods)					**Response frequency to Forcing frequency ratio** (f_r/f_f)				
	H	D_{top}	D_{bot}	H/D_{bot}	D_{top}/D_{thr}	D_{bot}/D_{thr}	D_{bot}/D_{top}	*Wind Gust Period (s)*					*Forcing frequency (Hz)*				
	(m)	*(m)*	*(m)*					*2*	*5*	*10*	*20*	*30*	*0.5*	*0.2*	*0.1*	*0.05*	*0.033*
CT1	200	110	110	1.8	1.65	1.650	1.000	0.0278	0.0270	0.0244	0.0161	0.0163	0.056	0.135	0.244	0.323	0.488
CT2	200	110	113	1.8	1.65	1.691	1.025	0.0270	0.0266	0.0241	0.0167	0.0164	0.054	0.133	0.241	0.333	0.492
CT3	200	110	116	1.7	1.65	1.733	1.050	0.0274	0.0267	0.0244	0.0171	0.0167	0.055	0.133	0.244	0.342	0.500
CT4	200	110	118	1.7	1.65	1.774	1.075	0.0278	0.0270	0.0244	0.0177	0.0169	0.056	0.135	0.244	0.354	0.508
CT5	200	110	121	1.7	1.65	1.815	1.100	0.0282	0.0270	0.0247	0.0182	0.0171	0.056	0.135	0.247	0.364	0.513
CT6	200	110	124	1.6	1.65	1.856	1.125	0.0282	0.0274	0.0250	0.0187	0.0174	0.056	0.137	0.250	0.373	0.522
CT7	200	110	127	1.6	1.65	1.898	1.150	0.0282	0.0274	0.0250	0.0192	0.0175	0.056	0.137	0.250	0.385	0.526
CT8	200	110	129	1.5	1.65	1.939	1.175	0.0282	0.0276	0.0250	0.0196	0.0177	0.056	0.138	0.250	0.392	0.531
CT9	200	110	132	1.5	1.65	1.980	1.200	0.0282	0.0276	0.0250	0.0200	0.0179	0.056	0.138	0.250	0.400	0.536
CT10	200	110	135	1.5	1.65	2.021	1.225	0.0282	0.0276	0.0250	0.0204	0.0180	0.056	0.138	0.250	0.408	0.541
CT11	200	110	138	1.5	1.65	2.063	1.250	0.0282	0.0270	0.0250	0.0207	0.0182	0.056	0.135	0.250	0.415	0.545
CT12	200	110	140	1.4	1.65	2.104	1.275	0.0278	0.0270	0.0247	0.0211	0.0183	0.056	0.135	0.247	0.421	0.550
CT13	200	110	143	1.4	1.65	2.145	1.300	0.0274	0.0267	0.0247	0.0213	0.0185	0.055	0.133	0.247	0.426	0.554
CT14	200	110	146	1.4	1.65	2.186	1.325	0.0270	0.0263	0.0244	0.0215	0.0187	0.054	0.132	0.244	0.430	0.560
CT15	200	110	149	1.3	1.65	2.228	1.350	0.0269	0.0262	0.0244	0.0216	0.0189	0.054	0.131	0.244	0.433	0.566
CT16	200	110	151	1.3	1.65	2.269	1.375	0.0267	0.0260	0.0244	0.0219	0.0213	0.053	0.130	0.244	0.439	0.638
CT17	200	110	154	1.3	1.65	2.310	1.400	0.0267	0.0260	0.0243	0.0220	0.0225	0.053	0.130	0.243	0.440	0.674
CT18	200	110	157	1.3	1.65	2.351	1.425	0.0267	0.0260	0.0243	0.0221	0.0230	0.053	0.130	0.243	0.442	0.690
CT19	200	110	160	1.3	1.65	2.393	1.450	0.0267	0.0260	0.0244	0.0222	0.0235	0.053	0.130	0.244	0.444	0.704
CT20	200	110	162	1.2	1.65	2.434	1.475	0.0267	0.0260	0.0244	0.0223	0.0238	0.053	0.130	0.244	0.446	0.714
CT21	200	110	165	1.2	1.65	2.475	1.500	0.0270	0.0262	0.0244	0.0225	0.0240	0.054	0.131	0.244	0.449	0.721

CONSTANT PARAMETERS:			
Throat Height/Total Height ratio	=	0.75	
Top Thickness	=	150	mm
Throat Thickness	=	175	mm
Base Thickness	=	200	mm
Height/Top Diameter ratio	=	1.82	
Height/Throat Diameter ratio	=	3.00	

Table 33: *Parametric forced vibration analysis of cooling towers with bottom edge diameter to top edge diameter ratios*

Figure 209 shows the variation of the response frequencies with the change in cooling tower bottom edge diameter to top edge diameter ratios when subjected to 2s-, 5s-, 10s-, 20s-, and 30s-wind gusts of the same speed. The response frequency versus forcing period is also plotted to obtain a relationship between the response and the forcing frequencies for each cooling tower bottom to top diameter ratio. Finally, response frequency to forcing frequency ratio *(f_r/f_f)* is plotted against the cooling tower bottom edge diameter to top edge diameter ratio to give a more representative behaviour of the

response frequency compared to the forcing frequency for the bottom edge diameter to top edge diameter ratio spectrum considered.

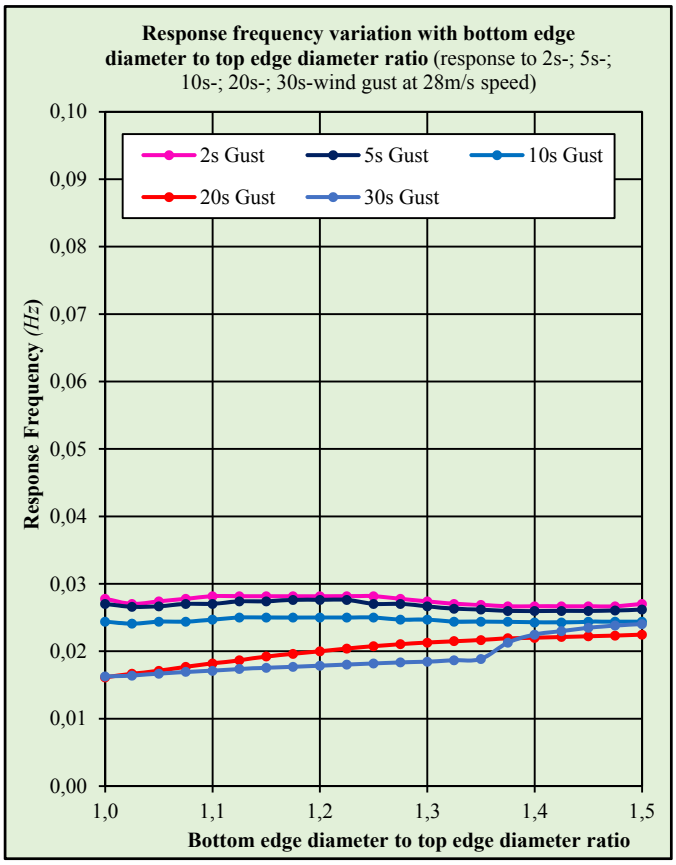

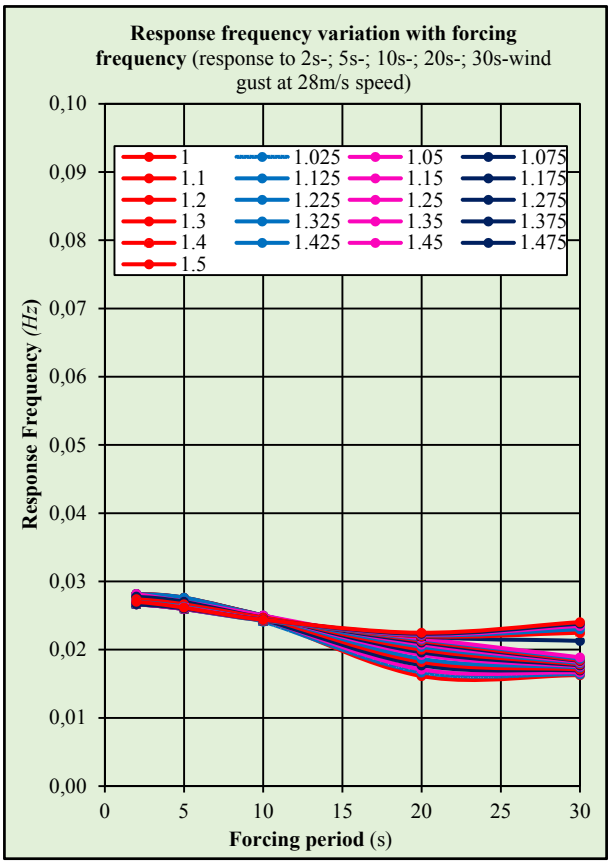

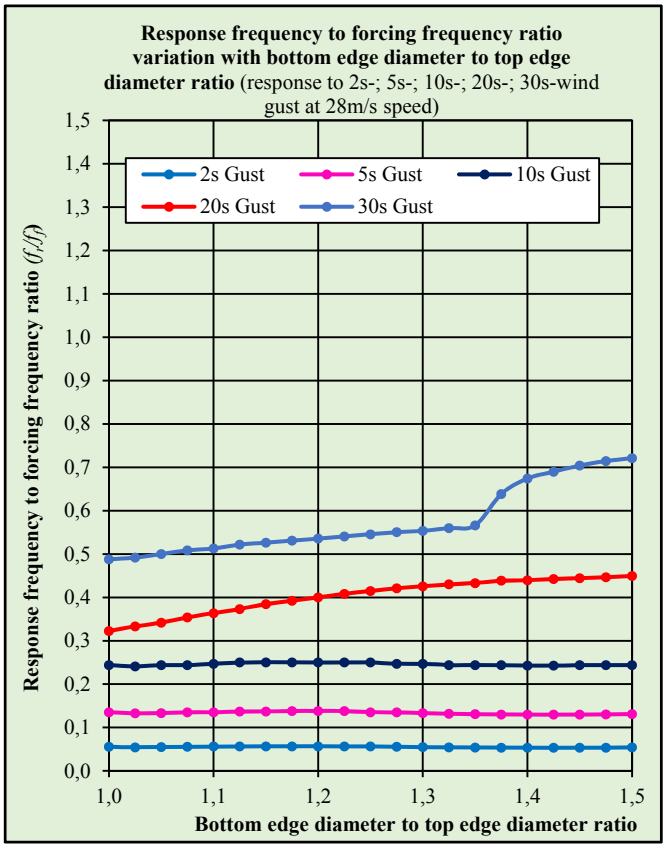

Figure 209: *Response frequency variation with bottom edge diameter to top edge diameter ratio and loading period combined with response to forcing frequency ratio variation with cooling tower bottom edge diameter to top edge diameter ratio*

Observations:

From *Figure 209*, it can be observed that:

- The response frequency is generally constant as the bottom edge diameter to top edge diameter ratio is increased;
- The response frequency bandwidth generally decreases with increase in the bottom edge diameter to top edge diameter ratio;
- The response frequency generally decreases with the decrease in between the forcing periods of (2s and 20s) and thereafter is constant up to the 30s forcing period. The response frequency bandwidth is close to zero for a forcing period of 2s and generally increases up to 0.008Hz for a forcing period of 20s;
- The response frequency to forcing frequency ratio is generally constant as the top edge diameter to throat diameter is increased for the 2s, 5s and 10s forcing periods. It however shows a marginal increase for the 20s and 30s forcing periods.

4.3.5 Shell thickness influence on forced vibration behaviour

Table 34 below shows the results of the parametric study of cooling towers whose shell thickness was changed to observe the change in the response frequencies for the first ten (10) different modes of vibration when subjected to 2s-, 5s-, 10s-, 20s-, and 30s-wind gusts whilst the diameters, height, throat to total height ratio and height to diameter ratios were kept constant. A uniform thickness for the entire height and circumference of the shell was considered.

COOLING TOWER	GEOMETRICAL PARAMETERS						FORCED RESPONSE									
	Total Height	Throat Height/ Total Height	Top Diameter	Throat Diameter	Bottom Diameter	Thickness	**Forced Frequency** (for various thicknesses and forcing wind periods)					**Response frequency to Forcing frequency ratio** (f_r/f_f)				
	H	H_t/H	D_{top}	D_{thr}	D_{bot}	T	*Wind Gust Period (s)*					*Forcing frequency (Hz)*				
	(m)		*(m)*	*(m)*	*(m)*	*(mm)*	*2*	*5*	*10*	*20*	*30*	*0.5*	*0.2*	*0.1*	*0.05*	*0.03*
CT0.4	200	0.75	80	67	100	40	0.0261	0.0250	0.0234	0.0217	0.0198	0.052	0.125	0.234	0.435	0.594
CT0.6	200	0.75	80	67	100	60	0.0260	0.0252	0.0225	0.0202	0.0187	0.052	0.126	0.225	0.404	0.561
CT0.8	200	0.75	80	67	100	80	0.0261	0.0253	0.0230	0.0196	0.0184	0.052	0.127	0.230	0.391	0.552
CT1	200	0.75	80	67	100	100	0.0256	0.0250	0.0233	0.0201	0.0194	0.051	0.125	0.233	0.402	0.583
CT2	200	0.75	80	67	100	120	0.0252	0.0244	0.0230	0.0203	0.0188	0.050	0.122	0.230	0.406	0.563
CT3	200	0.75	80	67	100	140	0.0238	0.0230	0.0241	0.0213	0.0212	0.048	0.115	0.241	0.426	0.635
CT4	200	0.75	80	67	100	160	0.0255	0.0245	0.0230	0.0205	0.0192	0.051	0.123	0.230	0.410	0.577
CT5	200	0.75	80	67	100	180	0.0255	0.0245	0.0230	0.0204	0.0189	0.051	0.123	0.230	0.408	0.566
CT6	200	0.75	80	67	100	200	0.0253	0.0244	0.0203	0.0223	0.0189	0.051	0.122	0.203	0.447	0.566
CT7	200	0.75	80	67	100	220	0.0253	0.0242	0.0227	0.0203	0.0189	0.051	0.121	0.227	0.406	0.566
CT8	200	0.75	80	67	100	240	0.0250	0.0241	0.0225	0.0202	0.0189	0.050	0.120	0.225	0.404	0.566
CT9	200	0.75	80	67	100	260	0.0247	0.0238	0.0223	0.0202	0.0189	0.049	0.119	0.223	0.404	0.566
CT10	200	0.75	80	67	100	280	0.0244	0.0235	0.0222	0.0202	0.0190	0.049	0.118	0.222	0.404	0.569
CT11	200	0.75	80	67	100	300	0.0244	0.0235	0.0222	0.0202	0.0189	0.049	0.118	0.222	0.404	0.566
CT12	200	0.75	80	67	100	320	0.0244	0.0235	0.0222	0.0201	0.0190	0.049	0.118	0.222	0.402	0.569
CT13	200	0.75	80	67	100	340	0.0244	0.0235	0.0222	0.0200	0.0189	0.049	0.118	0.222	0.400	0.566
CT14	200	0.75	80	67	100	360	0.0243	0.0235	0.0222	0.0200	0.0189	0.049	0.118	0.222	0.400	0.566
CT15	200	0.75	80	67	100	380	0.0242	0.0234	0.0226	0.0200	0.0187	0.048	0.117	0.226	0.400	0.561
CT16	200	0.75	80	67	100	400	0.0235	0.0230	0.0215	0.0198	0.0185	0.047	0.115	0.215	0.396	0.556
CT17	200	0.75	80	67	100	420	0.0235	0.0230	0.0215	0.0196	0.0185	0.047	0.115	0.215	0.392	0.554
CT18	200	0.75	80	67	100	440	0.0235	0.0230	0.0215	0.0196	0.0183	0.047	0.115	0.215	0.392	0.550
CT19	200	0.75	80	67	100	460	0.0234	0.0229	0.0215	0.0196	0.0185	0.047	0.115	0.215	0.392	0.554
CT20	200	0.75	80	67	100	480	0.0240	0.0231	0.0219	0.0199	0.0187	0.048	0.116	0.219	0.398	0.561
CT21	200	0.75	80	67	100	500	0.0238	0.0230	0.0219	0.0199	0.0187	0.048	0.115	0.219	0.398	0.561
CONSTANT PARAMETERS:																
Throat Height/Total Height ratio					=	0.75										
Height/Top Diameter					=	2.50										
Height/Throat Diameter					=	3.00										
Height/Bottom Diameter					=	2.00										
Top Diameter/Throat Diameter					=	1.20										
Bottom Diameter/Throat Diameter					=	1.50										
Bottom Diameter/Top Diameter					=	1.25										

Table 34: *Parametric forced vibration analysis of cooling towers with cooling tower shell thickness*

Figure 210 shows the variation of the response frequencies with the change in cooling shell thickness when subjected to 2s-, 5s-, 10s-, 20s-, and 30s-wind gusts of the same speeds. The response frequency versus forcing period is also plotted to obtain a relationship between the response and the forcing frequencies for each cooling tower shell thickness. Finally, response frequency to forcing frequency ratio *(f_r/f_f)* is plotted against the cooling tower shell thickness to give a

more representative behaviour of the response frequency compared to the forcing frequency for the shell thickness spectrum considered.

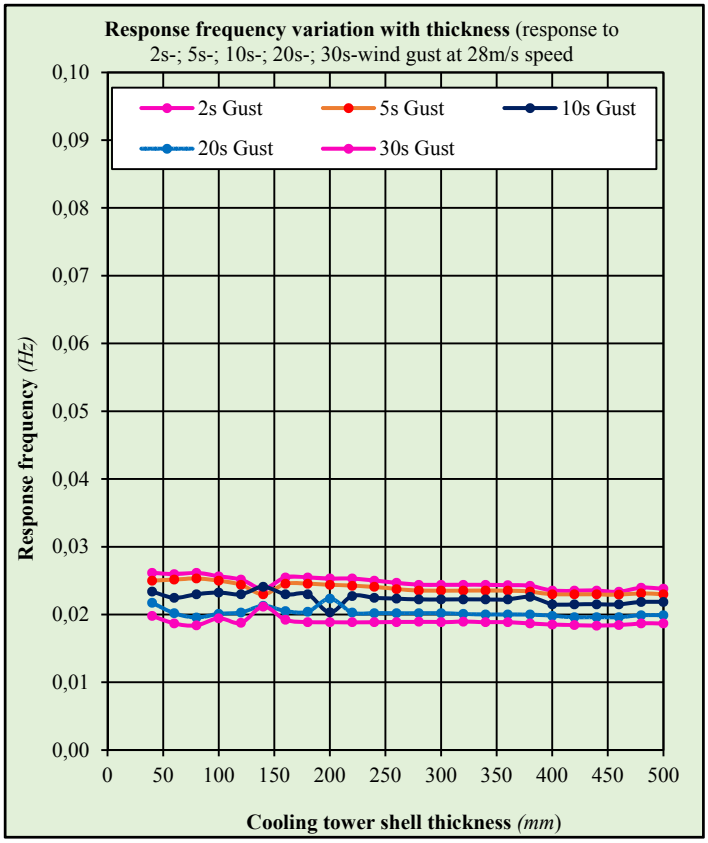

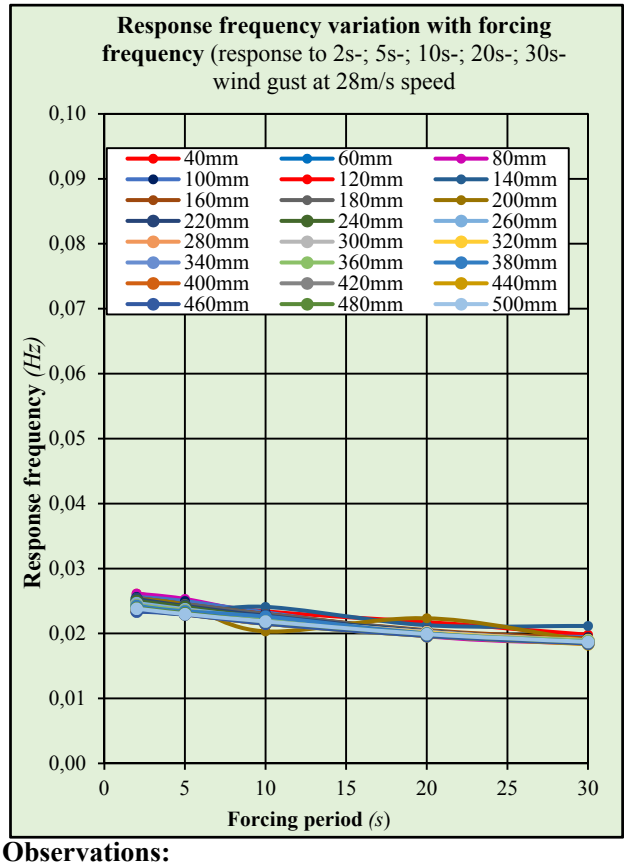

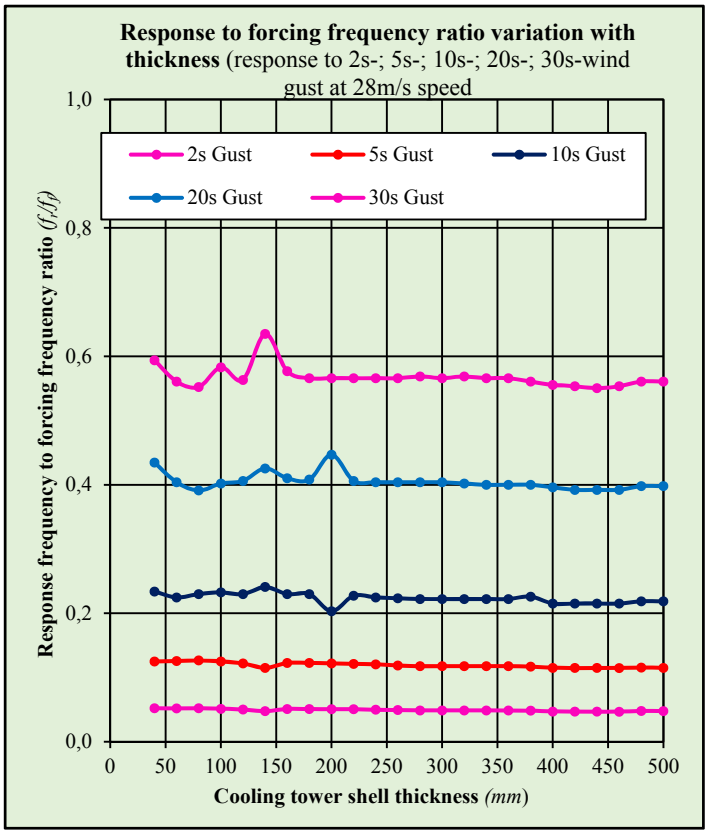

Figure 210: *Response frequency variation with shell thickness and loading period combined with response to forcing frequency ratio variation with cooling tower shell thickness*

Observations:

From *Figure 210*, it can be observed that:

- The response frequency is generally invariant with the shell thickness. The same response frequencies were observed for the 40mm thick shell through to the 500mm thick shell for the whole range of the applied loading frequencies;
- The response frequency bandwidth is generally constant for the entire range of the considered shell thicknesses;
- The response frequency is higher when the loading frequency is higher (2s-gust) and lower when the loading frequency is lower (30s-gust);
- The response frequency generally reduces with reduction in loading frequency. This reduction generally follows a linear relationship with the loading frequency;
- The response frequency to forcing frequency ratio for the entire forcing frequency range from 2s to 30s gust is generally constant for all shell thicknesses

5 DISCUSSION OF RESULTS

5.1 ON STABILITY BEHAVIOUR

The following sections discuss and summarise the stability parametric analysis results and observations in Section 4.1. The results are compared with other variables and other findings in other research. In some instances, the key findings are drawn and their meaning and implication spelt out.

Height *(influence on stability behaviour)*: The critical wind speed at which the cooling tower first buckles reduces with increase in the cooling tower height. This reduction follows a curve similar to the Euler buckling curve. This is to be expected since the buckling analysis performed is a linear eigenvalue problem which is similar to the Euler critical load derivation, itself also being a linear eigenvalue problem.

For cooling towers of the same height, the critical loads at which the shell first buckles are not very different. This is testimony to the fact that the order of magnitude of the critical wind speed at which cooling tower shells of the same height would first buckle is the same. This also verifies that when considering the height only, the height slenderness of the shell becomes the dominant factor that determines the critical loads and as such, the position of the throat height becomes a less dominant factor.

For shorter cooling towers, the change in critical wind speeds as the height is varied is more significant when compared to the same change for higher cooling towers. Again this testifies the similarity with the Euler buckling curve whose eigenvalue problem solution confirms that slender elements have lower critical buckling loads and the slenderness is the dominant factor that affects the critical buckling loads. The optimum throat height to total height ratio for which the cooling tower critical wind speed is always a maximum for any height is a very interesting result. It affords designers the opportunity to position the throat of the tower in a position (height wise) that optimises the buckling loads.

The buckling modes and variation with height are similar to the ones presented by (Mahmoud & Gupta, 1995) when they investigated the inelastic large displacement behaviour of various cooling tower heights. As such, the findings of this study are valid and can be used in the preparation of further research and design guidelines.

Height to diameter ratio *(influence on stability behaviour)*: As can be observed from the graphs, the dwarf cooling towers are not as sensitive to wind loads as the tall and thin cooling towers are. In other words, the rate of change in the critical wind speed for dwarf cooling towers is significantly smaller than that for the tall and thin cooling towers. In addition, it shows that the dwarf cooling towers buckle at relatively lower critical wind speeds than the tall and thin cooling towers. This is probably because the circumferential surface area for dwarf cooling towers is larger and meridional dimples are more easily developable than on the tall and thin cooling towers, whose circumferential surface area is smaller.

The variation of the critical wind speed with height to top edge diameter; height to throat diameter and height to bottom edge diameter ratios is similar. This is because the parametric study did not differentiate between the top edge, throat and bottom edge diameter variations. This differentiation is however performed under sections 4.1.3 and 4.1.4. The buckled shapes are similar to the ones obtained by (Jullien, et al., 1994) when they performed stability analysis on various cooling tower geometries. The findings under this particular section of the study show that designers need to carefully consider the buckling phenomena when changing the height to diameter ratios of cooling towers as the rate of change of critical wind speeds is higher for cooling towers with height to diameter ratios above 2.0.

Top edge diameter and bottom edge diameter to throat diameter ratio *(influence on stability behaviour)*: The top edge diameter to throat diameter ratio at which the critical wind speed is a maximum is 1.65. At ratios smaller or larger than this value, the critical wind speed starts to reduce. However, the rate of reduction of the critical wind speed is more rapid for cooling towers with top edge diameter to throat diameter ratios less than 1.65 than those whose same ratios are above this value. The variation of the critical wind speed with bottom edge diameter to throat diameter ratio is similar to that of the critical wind speed variation with top edge diameter to throat diameter ratio. This is mainly because the principal parameter that was changed was the throat diameter whilst the top edge and bottom edge diameters were kept constant. The buckled shape and results obtained show some similarities with the results obtained by (Tomas & Tovar, 2012) when they studied the influence of initial geometric imperfections on the buckling loads of various cooling tower geometries.

Bottom edge diameter to top edge diameter ratio (bottom edge diameter fixed) *(influence on stability behaviour)*: By changing the top edge diameter whilst the bottom edge diameter and the throat diameters are kept constant, it is shown that the critical wind speed slightly increases as the bottom edge diameter to top edge diameter ratio is increased up to a critical ratio of 1.3, after which the critical wind speed rapidly decreases. It can also be concluded that at bottom edge diameter to top edge diameter ratios of more than 1.3, the critical wind speed reduces rapidly and designers would need to pay extra attention to shells with geometries falling into this category. By default, the top edge diameter to throat diameter versus the critical wind speed graph follows the same shape and trends.

For cooling towers with larger top edge diameters (lower bottom edge diameter to top edge diameter ratios), the cooling tower buckling modes display dimples around the throat and top edge. This is probably because the large top

edge diameter is more sensitive to buckling under wind loads. However, for smaller top edge diameters (larger bottom edge diameter to top edge diameter ratios), the shell buckling modes only display dimples in the windward side with the rest of the top edge remaining stable.

Bottom edge diameter to top edge diameter ratio (top edge diameter fixed) *(influence on stability behaviour)*: The above study is repeated but now with the top edge diameter kept constant whilst the bottom edge diameter is changed. It is shown that the critical wind speed generally increases with increase in the bottom edge diameter to top edge diameter ratio. Unlike in the preceding section, there is no reduction of the critical wind speed for the diameter range considered in the study. This finding is of a key importance: It proves that changing the bottom edge diameter of the cooling tower alone whilst the other parameters are kept constant yields significantly different results compared to when the top edge diameter alone is changed whilst the rest of the other parameters are kept constant. Furthermore, it shows that the larger the bottom edge diameter, the higher the critical wind speed. This is however not so with the top edge diameter.

In addition, it is observed that the mode of buckling is the same for the entire range of bottom edge diameters considered i.e. buckling of the shell throat and the part above it with meridional dimples in the windward side of the shell. Although it is the same parameter (bottom edge diameter to top edge diameter ratio) that was considered in this section and the preceding section, it shows that changing the bottom edge diameter will most likely yield significant stability behaviour results (critical wind speeds) compared to changing the top edge diameter.

Shell thickness *(influence on stability behaviour)*: The variation of the critical wind speed with shell thickness is linear. The critical wind speed increases with the shell thickness increase. This is to be expected since the shell's stiffness is directly proportional to the thickness and the critical buckling loads are also proportional to the shell stiffness. It is observed that the thicker cooling tower shells buckle very differently from the thinner cooling tower shells. The thicker shells buckle only in the bottom part most likely due to wind suction whereas the thinner shell buckles everywhere.

The above finding can be easily combined with the other findings from other studies for example by (Zerna, *et al*., 1983) in which they observed the possibility of designing a "balanced" hyperbolic cooling tower having nearly the same buckling safety at every region to achieve economic use of materials. The change of the modes of buckling is significant. It allows designers to design for the correct mode of buckling for the chosen shell thickness at the particular or relevant cooling tower height.

5.2 ON FREE VIBRATION

The following sections discuss and summarise the free vibration parametric analysis results and observations in Section 4.2. The results are compared with other variables and other findings in other research. In some instances, the key findings are drawn and their meaning and implication spelt out.

Height *(influence on free vibration behaviour)*: Taller cooling towers have lower natural frequencies than shorter cooling towers. In addition, their natural frequency bandwidth is narrower than that of shorter cooling towers. This finding suggests that as the height is increased, the cooling tower tends to vibrate with different modes but at almost the same or close to the same natural frequencies. On the other hand, the shorter cooling towers would have significantly different natural frequencies for the different modes of vibration.

As the height of the cooling tower is increased, the mode shapes change in no particular order for the first ten (10) different modes. However, all the mode shapes are similar for the height spectrum considered. This suggest that the natural frequency trends obtained must be valid. The mode shapes obtained for the 100m and 150m high cooling towers are similar to those obtained by (Koohestani, 2010) when considering alternative methods for free vibration analysis of cooling towers.

Height to diameter ratio *(influence on free vibration behaviour)*: For the first modes of vibration (modes 1 and 3), the natural frequency reduces with increasing height to diameter ratio. Modes above these however show different natural frequency trends. In addition, the dwarf cooling towers have a narrow natural frequency bandwidth than the tall and thin cooling towers. This shows that the dwarf cooling towers would vibrate with different modes that have the same or close to the same natural frequencies. In addition, it can be concluded that as the height to diameter ratio reduces, (towards dwarf cooling towers), the modes of vibration tend to be similar and at almost the same natural frequencies as indicated above. On the other hand, the tall and thin cooling towers have a larger natural frequency bandwidth. Their modes of vibration will have significant natural frequency differences.

The dwarf cooling tower modes of vibration obtained are very similar to those obtained by (Kim, *et al*., 2015) when they were studying the prediction of free vibration frequencies and mode shapes of isotropic cooling towers. These results can be useful in determining the natural frequencies, bandwidths and mode shapes when considering applicable cooling tower heights relative to diameters during the conceptual design of cooling towers.

Top edge diameter to throat diameter ratio *(influence on free vibration behaviour)*: When considering the top edge diameter to throat diameter ratio, the natural frequency bandwidths are relatively constant with marginally slight increases for individual modes of vibration. This suggests that the top edge diameter and throat diameter variation does

not have any significant influence on the natural frequency behaviour of the cooling tower. As observed with other geometrical parameter variations, the change in the mode shapes as the top edge diameter to throat diameter ratio is varied is in no particular order, but the bandwidths remain relatively constant as recorded above. This key finding suggests that the throat diameter (being the primary variable parameter) does not have any significant influence on the natural frequency behaviour of the cooling tower shell. However, it influences the modes shapes but with no particular sequence as the throat diameter is changed.

Bottom edge diameter to top edge diameter ratio (top edge diameter fixed) *(influence on free vibration behaviour)*: When considering the bottom edge diameter to top edge diameter ratio, the natural frequency bandwidths are relatively constant with marginally slight increases for individual modes of vibration. This suggests that the bottom edge diameter variation does not have any significant influence on the natural frequency behaviour of the cooling tower. As observed with other geometrical parameter variations, the change in the mode shapes as the bottom edge diameter to top edge diameter ratio is varied is in no particular order, but the bandwidths remain relatively constant as recorded above. This key finding suggests that the bottom edge diameter (being the primary variable parameter) does not have any significant influence on the natural frequency behaviour of the cooling tower shell. However, it influences the modes shapes but with no particular sequence as the bottom diameter is changed.

Shell thickness *(influence on free vibration behaviour)*: The natural frequency increases as the shell thickness is increased. This finding should be valid since the shell stiffness (k) should increase as the shell thickness is increased. Although the shell mass (m) would inherently increase as well, it can be concluded that the stiffness/mass ratio increases and hence the natural frequency increases. In addition, the natural frequency bandwidth increases as the thicknesses increased. This implies that thinner shells would vibrate at different modes with the same or close to the same natural frequencies whereas the thicker shells would vibrate at different modes with significantly different natural frequencies.

Again as reported with the other geometrical parameters, the change in mode shapes as the thickness is varied is in no particular order. The natural frequency bandwidth observed can be very useful in considering cooling tower shell thicknesses during design, or for further research in optimising shell thicknesses and materials.

5.3 ON FORCED VIBRATION

The following sections discuss and summarise the forced vibration parametric analysis results and observations in Section 4.3. The results are compared with other variables and other findings in other research. In some instances, the key findings are drawn and their meaning and implication spelt out.

Height *(influence on forced vibration behaviour)*: As the height is increased, it takes the cooling tower more and more time (increasing response periods of vibration) to respond to the 2s-, 5s-, 10s-, 20s-, and 30s-wind gusts in a full cycle of revolution. That is, the response frequency of the cooling tower reduces as the height is increased. In addition, the response frequency bandwidth also reduces. The 30s-wind gusts result in lower response frequencies compared to the 2s-wind gusts and there is continuous reduction of the response frequency from 2s- to 30s-wind gusts.

A key finding observed from the forcing frequency variations is that the low forcing frequencies (30s-wind gusts) produce high response to forcing frequency ratio results for all cooling tower heights. Conversely, the high forcing frequencies (2s-wind gusts) produce low response to forcing frequency ratio results for all cooling tower heights. For cooling tower heights above 170m, the response frequency variation with height as well as with the forcing frequency itself is generally linear. This probably suggests that above this height, the height of the cooling tower becomes the dominant parameter affecting the vibration response of the cooling tower whereas below that height, other factors may be more or less equally dominant.

Height to diameter ratio *(influence on forced vibration behaviour)*: As the height to diameter ratio is increased, it takes the cooling tower more and more time (higher period of vibration) to respond to the 2s-, 5s-, 10s-, 20s-, and 30s-wind gusts in a full cycle of vibration. That is, the response frequency reduces. In addition, the response frequency bandwidth also reduces. The dwarf cooling towers have high response frequencies than the tall and thin cooling towers.

Again, it is observed that the low forcing frequencies (30s-wind gusts) produce high response to forcing frequency ratios for all cooling tower height to diameter ratios. The behaviour of the cooling tower shell in responding to the forcing frequencies changes between height to diameter ratios ranges of 1 to 2; 2 to 4 and 4 to 5. This observation is also consistent with the variation of the natural frequencies with the height to diameter ratios as shown in Figure 198 in which the natural frequency bandwidths can be said to be relatively constant within the height to diameter ratio ranges of 1 to 2; 2 to 4 and 4 to 5.

Top edge diameter to throat diameter ratio *(influence on forced vibration behaviour)*: There are two regions for which the response frequency becomes high as the top edge diameter to throat diameter is changed. These occur at the top edge diameter to throat diameter ratios of between 1.2 to 1.4 and 1.7 to 1.9. This finding is significant in that it allows designers to check these ratios for the design cooling tower geometries and allow for the response frequency variation in the design. As with other geometrical parameters, it is again observed that the low frequencies (30s-wind gusts) produce high response to forcing frequency ratios for all cooling tower top edge diameter to throat diameter ratios.

The fact that the response frequency bandwidth is generally constant for all the forcing frequencies should imply that the cooling towers respond to all the forcing frequencies with periods of vibration that are not far away from each other for all the top edge diameter to throat diameter ratios considered. Again as observed under the free vibration section, changing the throat diameter relative to the top edge diameter and bottom edge diameters does not have any significant influence on the response frequency bandwidths for all cooling tower top edge diameter to throat diameter ratios.

Bottom edge diameter to top edge diameter ratio (top edge diameter fixed) *(influence on forced vibration behaviour)*: Changing the bottom edge diameter whilst the top edge diameter is kept constant results in relatively constant response frequencies, suggesting that the bottom edge diameter variation has no significant influence on the shell's top edge response to 2s-, 5s-, 10s-, 20s- and 30s-wind gusts. It also appears that between the 20s- and 30s-wind gust forcing periods, the response frequencies are constant for all bottom edge diameter to top edge diameter ratios, suggesting that beyond the 20s-wind gust forcing period, the cooling tower shell's response does not change with respect to the bottom edge diameter to top edge diameter ratio. In other words, changing the bottom edge diameter will not result in a change of the response frequency if subjected to wind gusts of 20s and above. However, the results show that the response frequency bandwidth for forcing periods of 10s to 30s increases and is broader than that for the 2s and 5s wind gusts which is almost zero.

The above finding suggest that all cooling towers for all the bottom edge diameter to top edge diameter ratios considered would vibrate at the same response frequencies when subjected to 2s- and 5s-wind gusts. The opposite is evidently true for the same cooling towers when subjected to 10s-, 20s- and 30s-wind gusts. This finding is significant in that design engineers would need to differentiate between response frequencies behaviour when conceptualising bottom and top diameters by separating high frequency wind gusts (2s and 5s) from low frequency wind gusts (10s, 20s and 30s).

Shell thickness *(influence on forced vibration behaviour)*: The response frequency is constant/invariant with the shell thickness. Changing the cooling tower shell thickness does not in any way change the way the cooling tower shell would respond to all the considered forcing frequencies/periods. Similarly, the response frequency bandwidths are also constant/invariant with the shell thickness, implying that the response frequency differences for thinner shells would be the same as for thicker shells and everywhere else between these two extremes.

The higher forcing frequencies (2s-wind gusts) results in higher responses frequencies compared to the lower forcing frequencies, which in turn result in lower response frequencies. In-between these two extremes, the relationship is generally linear, implying that all or most of the cooling tower thicknesses would respond by vibrating cyclically with periods of vibration that are proportional to the forcing periods. As with the other geometrical parameters, the low forcing frequencies (30s-wind gusts) result in higher response to forcing frequency ratios and vice-versa.

6 CONCLUSIONS AND RECOMMENDATIONS

6.1 CONCLUDING REMARKS

A trace of the studies that have been performed on cooling towers in general has been presented. The studies have been categorised into four 4) broad categories being studies on:

- Static and quasi-static behaviour of cooling towers;
- Stability behaviour of cooling towers;
- Free vibration response of cooling towers and
- Forced vibration response of cooling towers.

Within each of the broad categories, the studies have been divided into theoretical, numerical and experimental/field studies. The literature review tables these studies in a chronologically dated order. These studies are referenced using the author date system.

A parametric study of the cooling tower's stability behaviour and dynamic response was performed. A linear eigenvalue buckling analysis was performed for various categories of the cooling tower geometries. The cooling tower was subjected to increasing wind pressures in order to obtain the critical pressures at which the shell first buckled and the respective buckling modes. The cooling tower's geometrical parameters were changed in a systematic manner in order to obtain the relationship between critical wind pressures associated with the first mode of buckling and the cooling tower's geometrical parameters. Ratios of the cooling tower's dimensions were considered to cover a wider geometrical spectrum.

The critical wind speed versus height curve is observed to be similar to the Euler buckling curve. There appears to be a certain optimum throat height to total height ratio (about 0.75) for any cooling tower at which the critical wind speed is maximum. For cooling towers of the same height, the critical loads at which the shell first buckles are not very different thereby confirming that the height slenderness of the shell becomes the dominant factor that determines the critical loads and as such, the position of the throat height becomes a less dominant factor. The buckling modes and variation with height are similar to the ones presented by (Mahmoud & Gupta, 1995). The critical wind speed varies linearly with the cooling tower thickness and non-linearly with all diameter ratios. The dwarf cooling towers are shown to buckle at relatively lower critical wind speeds than the tall and thin cooling towers. Although the same bottom edge diameter to top edge diameter ratio parameter was considered in two different analyses by changing the bottom edge diameter in one analysis and the top edge diameter in the other, it is shown that changing the bottom edge diameter will most likely yield significant stability behaviour results (critical wind speeds) compared to changing the top edge diameter. It shows that the larger the bottom edge diameter, the higher the critical wind speed. It is observed that the thicker cooling tower shells buckle very differently from the thinner cooling tower shells. The thicker shells buckle only in the bottom part most likely due to wind suction whereas the thinner shell buckles everywhere. These findings can be used as a basis for further research and establishment of conceptual design guidelines when considering stability behaviour of cooling towers.

A linear eigenvalue vibration analysis was performed to obtain the first ten (10) different natural frequencies and mode shapes for each cooling tower under a group of geometrical parameters as for the stability behaviour analysis. The natural frequencies and mode shapes were recorded for modes 1, 3, 5, …, 17 and 19 being the odd numbered modes as the even numbered modes have the same natural frequencies and were observed to possess the same shapes but in a different orthogonal direction since the cooling tower shape is axi-symmetric. The natural frequencies were computed into a tabular format and plotted graphically against the various geometrical parameters. Afterwards, the same cooling towers were subjected to a constant wind gusts of the same speed with variable periods (2-, 5-, 10-, 20- and 30-second wind gusts) and therefore variable forcing wind frequencies to obtain the response frequencies and mode shapes. The response periods of vibration at the cooling tower's top edge in the windward direction were read and converted into response frequencies. These were tabulated and plotted graphically against the various geometrical parameters. This analysis was systematically repeated to obtain the relationship between these vibration responses and the geometrical parameters.

The natural frequencies and their corresponding bandwidths for the first ten different modes reduce with increasing height and the natural frequency bandwidth for higher cooling towers is narrower than that of shorter cooling towers. The mode shapes obtained for the 100m and 150m high cooling towers are similar to those obtained by (Koohestani, 2010). For the first modes of vibration (modes 1 and 3), the natural frequency reduces with increasing height to diameter ratio whilst modes above these show different natural frequency trends. Dwarf cooling towers have a narrow natural frequency bandwidth than the tall and thin cooling towers. The dwarf cooling tower modes of vibration obtained are very similar to those obtained by (Kim, *et al.*, 2015). When considering the top edge diameter to throat diameter ratio, the natural frequency bandwidths are relatively constant with marginally slight increases for individual modes of vibration. The same finding was noted when considering the bottom edge diameter to top edge diameter ratio when the top edge diameter is kept constant. The natural frequency increases as the shell thickness is increased. In addition, the natural frequency bandwidth increases as the thicknesses increased. It is observed that for all geometrical parameters considered, the change in mode shapes as the geometry is varied is in no particular order.

The response frequency of the cooling tower reduces as the height is increased. In addition, the response frequency bandwidth also reduces. The 30s-wind gusts result in lower response frequencies compared to the 2s-wind gusts and there is continuous reduction of the response frequency from 2s- to 30s-wind gusts. The low forcing frequencies (30s-wind gusts) produce high response to forcing frequency ratio results for all cooling tower heights and the opposite is true for the high forcing frequencies (2s-wind gusts). For cooling tower heights above 170m, the response frequency variation with height as well as with the forcing frequency itself is generally linear. The response frequency is observed to reduce as the height to diameter ratio is increased. In addition, the response frequency bandwidth also reduces. The dwarf cooling towers have high response frequencies than the tall and thin cooling towers. The behaviour of the cooling tower shell in responding to the forcing frequencies is noted to change between height to diameter ratios ranges of 1 to 2; 2 to 4 and 4 to 5. When considering the top edge diameter to throat diameter ratio, it is observed that there are two regions for which the response frequency becomes high as the top edge diameter to throat diameter is changed. These occur at the top edge diameter to throat diameter ratios of between 1.2 to 1.4 and 1.7 to 1.9 and the response frequency bandwidth is generally constant for all the forcing frequencies. As observed under the free vibration section when considering the same parameter, changing the throat diameter relative to the top edge diameter and bottom edge diameters does not have any significant influence on the response frequency bandwidths for all cooling tower top edge diameter to throat diameter ratios.

Changing the bottom edge diameter whilst the top edge diameter is kept constant results in relatively constant response frequencies, suggesting that the bottom edge diameter variation has no significant influence on the shell's top edge response to 2s-, 5s-, 10s-, 20s- and 30s-wind gusts. Between the 20s- and 30s-wind gust forcing periods, the response frequencies are constant for all bottom edge diameter to top edge diameter ratios, suggesting that beyond the 20s-wind gust forcing period, the cooling tower shell's response does not change with respect to the bottom edge diameter to top edge diameter ratio. Thus, changing the bottom edge diameter will not result in a change of the response frequency if subjected to wind gusts of 20s and above. The response frequency and its corresponding bandwidth is observed to be constant/invariant with the shell thickness. Changing the cooling tower shell thickness does not change the way the cooling tower shell would respond to all the considered forcing frequencies. As expected, the higher forcing frequencies (2s-wind gusts) results in higher responses frequencies compared to the lower forcing frequencies, which in turn result in lower response frequencies. In-between these two extremes, the relationship is generally linear. Finally, it is observed that for all geometrical parameters considered, the low forcing frequencies (30s-wind gusts) produce high response to forcing frequency ratios for all cooling towers. These findings can be used as a basis for further research and establishment of conceptual design guidelines when considering cooling tower stability, free vibration and forced vibration response. As such, some recommendations can be drawn from these findings.

6.2 RECOMMENDATIONS

The following recommendations are made in the light of the research findings that have been tabled in chapters 4 and 5 above:

- A set of design guidelines can be developed for the conceptual design of cooling towers by a systematic creation of tables and charts that represent stability, free vibration and forced vibration behaviour when compared to a wide range of geometrical parameters as presented in this study;
- Since the forced vibration response was limited to the response at the top edge of the shell, further studies be done to create models that can obtain responses at the critical positions with maximum amplitudes and maximum stresses;
- Cooling tower designers should aim for optimum throat height to total height ratios of 0.75 in order to maximise on the cooling tower shell's critical buckling winds pressures/speeds;
- The shell thickness should be carefully chosen to avoid buckling of the lower part of the tower due to internal wind suction as well as avoid wasting of materials;
- A lower limit for height to diameter ratios be considered in design codes in order to avoid dwarf cooling towers which buckle at very low critical wind pressures/speeds;

6.3 ACKNOWLEDGEMENTS

The following parties immense contribution to the production of this dissertation has been acknowledged, for which without such, would have been compromised:

- Professor Alphose Zingoni: Research Supervisor for his guidance and supervisory role;
- KEON Consulting: Financial and printing assistance;
- GIBB (Pty) Ltd: Study leave assistance;
- ADINA R & D, Inc. for provision of the 900 node version ADINA software.

REFERENCES

[1] Alexandridis, A. & Gardner, N., 1992. Tolerance limits for geometric imperfections in hyperbolic cooling towers. *Journal of structural engineering,* 118(8), pp. 2082-2100.

[2] Andres, M. & Harte, R., 2006. Buckling of concrete shells: A simplified numerical approach. *Journal of international association for shell and spatial structures,* 47(3), pp. 1-13.

[3] Asadzadeh, E. & Alam, M., 2014. A survey on hyperbolic cooling towers. *International journal of civil, structural, construction and architectural engineering,* 8(10), pp. 1027-1039.

[4] Asadzadeh, E., Alam, M. & Asadzadeh , S., 2014. Dynamic response of layered hyperbolic cooling tower considering the effects of support inclinations. *Structural engineering and mechanics,* 50(6), pp. 797-816.

[5] Baillis, C., Jullien, J. & Limam, A., 2000. An enriched 2D modelling of cooling towers. Effects of real damage on the stability under self weight and on the strenght under wind pressure. *Engineering structures,* Volume 22, pp. 831-845.

[6] Bamu, P. & Zingoni, A., 2005. Damge, deterioration and the long-term structural performance of cooling-tower shells: A survey of developments over the last 50 years. *Engineering structures,* Volume 27, pp. 1794-1799.

[7] Bhimaraddi, A., Moss, P. & Carr, A., 1991. Free-vibration response of column-supported, ring-stiffened cooling tower. *Journal of engineering mechanics,* 117(4), pp. 770-788.

[8] Blocki, J., 1988. Stress states in cooling towers caused by thermal field. *Journal of structural engineering,* 114(12), pp. 2633-2651.

[9] Bosak, G. & Flaga, A., 1996. Probabilistic and deterministic aspects of combinations of wind, thermal and dead loads on cooling towers. *Journal of wind engineering and industrial aerodynamics,* Volume 65, pp. 107-119.

[10] Busch, D., Reinhard, H., Kratzih, W. & Montag, U., 2002. New natural draft cooling tower of 200m of height. *Engineering structures,* Volume 24, pp. 1509-1521.

[11] Choi, C.-K. & Noh, H.-C., 2000. Stochastic analysis of shape imperfection in rc cooling tower shells. *Journal of structural engineering,* 126(3), pp. 417-423.

[12] Croll, J., 2006. Stability in shells. *Nonlinear dynamics,* Volume 43, pp. 17-28.

[13] Don, Brush, O. & Almoth, B., 1975. *Buckling of bars, plates and shells.* s.l.:McGraw Hill.

[14] El Ansary, A., El Damatty, A. & Nassef, A., 2011. Optimum shape and design of cooling towers. *World academy of science, engineering and technology,* Volume 60, pp. 4-13.

[15] Flugge, W., 1973. *Stresses in shells.* 2nd ed. Berlin and Heildelberg, New York: Springer-Verlag.

[16] Gaikwad, T. et al., 2014. Effect of wind loading on analysis of natural draught hyperbolic cooling tower. *IJEAT. ISSN: 2249-8958,* 4(1), p. 38.

[17] Goudarzi, M., 2013. Proposing a new technique to enhance thermal performance and reduce structural design wind loads for natural draught cooling towers. *Energy,* Volume 62, pp. 164-171.

[18] Gould, P. & Kratzig, W., 1999. *Cooling tower structures.* Chen Wai-Fah Boca Raton: CRCC Press LLC.

[19] Gould, P., Ravichandran, R. & Sridharan, S., 1998. A local-global FE model for non-linear analysis of column-supported shells of revolution. *Thin-walled structures,* Volume 31, pp. 25-37.

[20] Hara, T., 2015. Dynamic response property of cooling tower structures. *Challenge journal of structural mechanics,* 1(1), pp. 38-41.

[21] Hara, T. & Gould, P., 2002. *Local-global analysis of cooling tower with cutouts.* s.l.:Unpublished.

[22] httk://en-wikipedia.org/wiki/Ferrybridge-power stations, n.d. [Online]
Available at: httk://en-wikipedia.org/wiki/Ferrybridge-power stations

[23] Ioannidis, C., Valani, A., Georgopoulos, A. & Tsiligiris, E., 2006. *3D model generation for deformation analysis using laser scanning data of a cooling tower.* Baden, 3RD iag/12th FIG Symposium.

[24] Jang, H. & Min, C., 2001. Design and inelastic behaviour of hyperbolic cooling towers. *KSCE Journal of civil engineering,* 5(4), pp. 309-318.

[25] Jia, X., 2013. Revisiting the failure mode of a RC hyperbolic cooling tower, considering changes of material and geometric properties. *Engineering structures,* Volume 47, pp. 148-153.

[26] Julian, A., Dumitrescu, A., Croll , J. & Billington , D., 1983. Cooling towers on flexible foundations. *Journal of structural engineering ,* 109(10), pp. 2248-2264.

[27] Jullien, J., Aflak, W. & L'Huby, Y., 1994. Cause of deformed shapes in cooling towers. *Journal of structural engineering ,* 120(5), pp. 1471-1488.

[28] Kaiser, T., Elwi, A. & Mioduchowski, A., 1995. Nonlinear harmonic analysis applied to axisymmetric structures. *Computers and structures,* Volume 55, pp. 1107-1118.

[29] Kaluza, R. & Gigiel, J., 1995. Experimental analysis of the influence of imposed displacements at the base of a cooling tower on its buckling stability. *Thin-walled structures,* Volume 23, pp. 367-378.

[30] Kang, J. & Leissa, A., 2005. Three-dimensional vibration analysis of thick hyperboloidal shells of revolution. *Journal of sound and vibration,* Volume 282, pp. 277-296.

[31] Kaveh, A. & Nemati, F., 2011. Efficient free vibration analysis of rotaionally symmetric shell structures. *International journal for numerical methods in biomedical engineering,* Volume 27, pp. 541-552.

[32] Ke, S. & Ge, Y., 2014. The influence of self-excited forces on wind loads and wind effects on super-large cooling towers. *Journal of wind engineering and industrial aerodynamics,* Volume 132, pp. 125-134.

[33] Ke, S., Ge, Y., Zhao, L. & Tamura, Y., 2012. Anew methodology for analysis of equivalent static wind loads on super-large cooling towers. *Journal of wind engineering and industrial aerodynamics,* Volume 111, pp. 30-38.

[34] Kim, J., Lee, J. & Yoon, H., 2015. Free vibration analysis for shells of revolution based on p-version mixed finite element formulation. *Finite elements in analysis and design,* Volume 95, pp. 12-19.

[35] Koohestani, K., 2010. On the decomposition of generalised eigenproblems for the free vibration analysis of cyclically symmetric finite element models. *International journal for numerical methods in engineering,* Volume 82, pp. 359-378.
[36] Kopenetz, L. & Catarig, A., 2011. Practically structural analysis of large cooling towers. *Journal of applied engineering sciences,* 1(14-4), pp. 39-44.
[37] Kulkarni, S. & Kulkarni, A., 2014. Static and dynamic analysis of hyperbolic cooling tower. *Journal of civil engineering technology and research,* 2(1), pp. 39-61.
[38] Kulkarni, S. & Kulkarni, A., 2014. *Wind and buckling analysis of natural draught cooling towers using ANSYS.* s.l., ISRASE.
[39] Lang, C., Meiswinkel, R. & Filippou, F., 2002. No-linear analysis of shells of revolution with ring elements. *Engineering structures,* Volume 24, pp. 163-176.
[40] Lang, C. & Straus, J., n.d. *Natural draft cooling tower design and construction in Germany - Past (since 1965), present and future.* s.l.:s.n.
[41] Lee, I., Jung, H. & Kim, M., 1995. *An efficient free vibration analysis of structures with multiple or close natural frequencies.* Hong Kong, s.n., pp. 119-124.
[42] Lin, F. et al., 2014. Prediction of ground motion due to the collapse of a large-scale cooling tower under strong earthquakes. *Soil dynamics and earthquakes engineering,* Volume 65, pp. 43-53.
[43] Li, Y., Lin, F., Gu, X. & Lu, X., 2014. Numerical research of a super-large cooling tower subjected to accidental loads. *Nuclear engineering and design,* Volume 269, pp. 184-192.
[44] Long-yuan, L. & Wen-da, L., 1987. Nonlinear buckling analysis of hyperbolic cooling tower shell with ring-stiffeners. *Applied mathematics and mechanics,* 10(2), pp. 113-118.
[45] Mahmoud, B. & Gupta, A., 1995. Inelastic large displacement behaviour and buckling of cooling towers. *Journal of structural engineering,* 121(6), pp. 961-965.
[46] Mang, H., Floegl, H., Trappel, F. & Walter , H., 1983. Wind-loaded reinforced-concrete cooling towers: buckling or ultimate load?. *Engineering structures,* Volume 5, pp. 163-179.
[47] Meschke, G., Mang, H. & Kosza, P., 1991. Finite element analysis of cracked cooling tower shell. *Journal of structural engineering,* 117(9), pp. 2620-2639.
[48] Min, C., 2004. Design and ultimate behaviour of RC plates and shells. *Nuclear engineering and design,* Volume 228, pp. 207-223.
[49] Min, C. & Gupta, A., 1993. Inelastic behaviour of hyperbolic cooling towers. *Journal of structural engineering,* 119(7), pp. 2235-2255.
[50] Murali, G., Vivek Vardhan, C. & Prasanth Kumar Reddy, B., 2012. Response of cooling towers to wind loads. *ARPN Journal of engineering and applied sciences,* 7(1), pp. 114-120.
[51] Nangshineh, A., Alavi, E. & Rezaee, M., 2013. To study the effect of seismic and wind loads on hyperbolic cooling tower of varying dimension and RCC shell thickness. *International journal of science and technology,* 1(3), pp. 1-9.
[52] Nasir, A., Thambiratnam, D., Butler, D. & Austin, P., 2002. Dynamics of axysymmetrichyperbolic shell structures. *Thin-walled structures,* Volume 40, pp. 665-690.
[53] Noh, H., 2006. Non-linear behaviour and ultimate load bearing capacity of reinforced concrete natural draught cooling tower shell. *Engieering structures,* Volume 28, pp. 399-409.
[54] Noorzaei, J. et al., 2006. Non-linear interactive analysis of cooling tower-foundation-soil interaction under unsymmetrical wind load. *Thin-walled structures,* Volume 44, pp. 997-1004.
[55] Norton, R. & Weingarten, V., n.d. The effect of asymmetric imperfections on the earthquake response of hyperbolic cooling towers. *Unpublished.*
[56] Novozhilov, V., 1970. *Thin shell theory.* s.l.:Wolters-Noordhoff Publishers.
[57] Orlando, M., 2001. Wind-induced interference effects on two adjacent cooling towers. *Engineering structures,* Volume 23, pp. 979-991.
[58] Orosz, A., 1980. *Research and development of reinforced concrete cooling towers,* Budapest: Department of Reinforced Concrete Structures, Technical University.
[59] Pieczara, J., 1999. Optimization of cooling tower shells using a simple genetic algorithm. *Springer-Verlag,* Volume 19, pp. 311-316.
[60] Prabhakar, N., 1990. *Structural design aspects of hyperbolic cooling towers.* Technical Session IV. Paper No. 9, National seminar on cooling towers: 18-20.
[61] Radwanska, M. & Waszczyszyn, Z., 1995. Buckling analysis of a cooling tower shell with measured and theoretically-modelled imperfections. *Thin-walled structures,* Volume 23, pp. 107-120.
[62] Rao, P. & Ramanjaneyulu, K., 1993. Stability of of cooling tower shell with modified wind pressure coefficients. *Journal of engineering mechanics,* 119(11), pp. 2207-2225.
[63] Reed, D. & Scanlan, R., 1983. Time series analysis of cooling tower wind loading. *Journal of structural engineering ,* 109(2), pp. 538-554.
[64] Sabhouri-Ghomi, S. & Kharrazi, M., 2005. Reinforced concrete column-supported hyperboloid cooling tower stability assessment for seismic loads. *Scientia Iranica,* 12(2), pp. 241-246.
[65] Sabhouri-Ghomi, S., Kharrazi, M. & Javidan, P., 2006. Effect of stiffening rings on buckling stability of RC hyperbolic cooling towers. *Thin-walled structures,* Volume 44, pp. 152-158.
[66] Sabhouri-Ghomi, S., Nik, F., Roufegarinejad, A. & Bradford, M., 2006. Numerical study of the nonlinear dynamic behaviour of reinforced concrete cooling towers under earthquake excitation. *Advances in structural engineering,* 9(3), pp. 1-9.

[67] Sahana, L. & Sulaiman, S., 2013. The effect of seismic and wind loads on cooling tower of varying RCC shell thickness and size of shell opening. *International journal of emerging trends in engineering and development,* 4(3), pp. 248-259.
[68] Shu, W. & Wen-da, L., 1990. Theoretical and experimental solutions of cooling-tower-soil system. *Journal of engineering mechanics,* 116(4), pp. 862-869.
[69] Sudret, B., Defaux, G. & Pendola, M., 2005. Time-variant finite element reliability analysis - application to the duarability of cooling towers. *Structural safety,* Volume 27, pp. 93-111.
[70] Tomas, A. & Tovar, J., 2012. The influence of initial geometric imperfections on the buckling load of single and double curvature concrete shells. *Computers and structures,* Volume 96-97, pp. 34-45.
[71] Tornabene, F., 2011. 2-D GDQ solution for free vibrations of anisotropic doubly-curved shells and panels of revolution. *Composite structures,* Volume 93, pp. 1854-1876.
[72] Tornabene, F. & Viola, E., 2006. *Differential quadrature solution for parabolicstructural shell elements.* Lisbon, Third europian conference on computational mechanics, solids, structures and coupled problems in engineering, pp. 1-20.
[73] University of Toronto, 1967. *Wind effects on buildings and structures.* s.l., s.n.
[74] Veena, N., Sulaiman, S. & Aswath, M., 2013. Comparative study of the effect of seismic and wind loads on cooling tower with A-Frame and H-Frame column supports. *International journal of science and technology,* 1(2), pp. 23-32.
[75] Viladkar, M., Godbole, P. & Krishna, P., 1997. Finite element analysis of column supported hyperbolic cooling towers using semi-loof shell and beam elements. *Engineering structures,* Volume 20, pp. 75-84.
[76] Viladkar, M., Karisiddappa, Bhargava, P. & Godbole, P., 2006. Static soil-structure interaction response of hyperbolic cooling towers to symmetrical wind loads. *Engineering structures,* Volume 28, pp. 1236-1250.
[77] Warburton, G., 1976. *The dynamic behaviour of structures.* s.l.:Pergamon Press.
[78] Waszczyszyn, Z., Pabisek, E., Pamin, J. & Radwanska, M., 2000. Nonlinear analysis of a RC cooling tower with geometrical imperfections and a technological cut-out. *Engineering structures,* Volume 22, pp. 480-489.
[79] Weingarten, V., Masri, S., Lashkari, M. & Kahyai, K., n.d. Effect of gravity loading on the earthquake response of cooling towers. *Unpublished.*
[80] Wen-da, L. & Shi-qiao, G., 1987. The effect of local geometrical imperfections of rotational shell on its natural frequencies and models. *Applied mathematics and mechanics,* 8(11), pp. 1013-1018.
[81] Xu, Y. & Bai, G., 2013. Random buckling bearing capacity of super-large cooling towers considering stochastic material properties and wind loads. *Probabilistic engineering mechanics,* Volume 33, pp. 18-25.
[82] Yang, T., Gran, C. & Lo, H., n.d. Theoretical study of earthquake response of a cooling tower. *Unpublished.*
[83] Yang, T. & Kapania, R., 1983. Shell elements for cooling tower analysis. *Journal of engineering mechanics,* 109(5), pp. 1270-1289.
[84] Yang, T. & Kapania, R., 1984. Finite element random response analysis of cooling tower. *Journal of engineering mechanics,* 110(4), pp. 589-609.
[85] Zerna, W., Mungan, I. & Steffen, W., 1983. Wind-buckling approach for RC cooling towers. *Journal of engineering mechanics,* 109(3), pp. 836-848.
[86] Zingoni, A., 1997. *Shell structures in civil and mechanical engineering.* s.l.:Thomas Telford Publishing.